SULPHUR SORBENT PARTICLE EFFECTS IN FLUIDISED COMBUSTION

James G. Petrie

September 1988

Submitted to the
University of Cape Town
in fulfilment of the requirements
for the degree of
Doctor of Philosophy

PREFACE

There is a classic problem in fluid dynamics called "the rain running problem" which poses the question of how fast a person should run through a rainstorm to minimise a soaking. The answer is of course a function of the assumptions used to define the problem - a thinly veiled muse. A parallel teaser could be posed by environmental lobbyists for engineers involved in power plant design. Entitled "the acid rain - running problem" it may well ask how much research needs to be done before the damage to vegetation, inland waterways, and ultimately to human life, caused by acid precipitation, be recognised for what it is - a technological problem firmly rooted in the use of fossil fuels. Engineers prepared to tackle this problem are faced with a further question - "how best do we steer our way through this 'storm' without further damaging our environment?". Unlike the first problem, this last is not open ended, and requires immediate sound and confident answers.

This thesis is an attempt to define the problem a little better, and to offer definite choices to engineers concerned with the design and operation of fluidised combustor power plant, specifically with regard to the selection of sorbents for the capture of sulphur dioxide released during coal combustion.

The work described in this dissertation was carried out in the Energy Research Institute, University of Cape Town, with financial support from the Foundation for Research Development, CSIR. I claim that this is my original and independent work, except where specifically referenced in the text, and that it has not been submitted in this, or any other form for a degree at any other university.

A number of people at the Energy Research Institute contributed meaningfully to this work. The construction of the laboratory units owes much to Kerry Motherwell, who, with Gareth Shaw, helped also in data collection. Thanks are due to Andrew Yates for his incisive comments on the direction of this work, and to Dr. Anton Eberhard for helping me to "draw the line".

The assistance of people outside the University of Cape Town needs also to be recognised. I am especially grateful to

Dr. Peter Harris at MINTEK, and Ms. Lorraine Keulerman of AECI Research Labs., for undertaking the porosimetry and B.E.T. measurements

Messrs Rob Rudman and John Spice of PPC Lime Ltd, and

Mr. Frank Schie of the Union Lime Co., who gave freely of their time trying to teach me something of the geology of carbonate rocks

The managements of Union Lime Co., Metalloys Ltd and the Piquetburg and Bredasdorp Limeworks for supplying large quantities of screened sorbent material, and

Mr. Brian North of the CSIR, who co-ordinated the pilot plant trials on the NFBC unit.

Finally, this work is dedicated to Brother Ray - I can now see the sky blue lining.

JAMES G.PETRIE

ABSTRACT

An overall process model is presented for the capture of sulphur dioxide by calcareous sorbents in a fluidised bed combustor for a feed of arbitrary size distribution. The description of sorbent sulphation kinetics, particle attrition and elutriation effects incorporated in this model is supported by experimental data for a wide range of South African sorbents.

The sulphation of sorbent particles is described by a simple, two-parameter, kinetic model. No loss in physical relevance is incurred when the decrease in reaction rate with time is given by a negative exponential term. Both sulphation rate and capacity are shown to be functions of sorbent type. The sulphation propensity of the 16 South African samples is correlated against their geologic description. Sorbent properties such as porosity, crystallinity and topography, which affect sulphation capacity directly, are functions of geologic age. It is possible to make a first order assessment of sorbent potential simply from this geologic data.

Sorbent attrition, caused by the continuous movement of particles within the combustor, is greatest for deep beds of soft friable material. Most of the attrition takes place in the distributor region where jetting action is important. The attrition model reflects an explicit dependence on fluidising velocity, bed depth, particle diameter, topography and structural strength. Measured values of attrition rate decrease with time to a steady state value, which, under normal FBC operating conditions, is attained after a time in the bed of 6 - 10 hours.

The elutriation model considers the effect of fines, generated by attrition, on the carryover of coarse particles from the bed.

The overall process model confirms that choice of sulphation kinetics exerts the greatest influence on attainable sulphur capture, although bed fluid dynamics, sorbent attrition and feed size distribution all play a role. The model is substantiated by extensive data from the performance of three dissimilar sorbents in a 10 MW_{th} FBC. The contribution of sorbent attrition to the solids loading of downstream gas cleaning equipment is highlighted.

CONTENTS

LIST OF SYMBOLS

$\underline{A}$	extent of attrition	%
A	fluid bed area	m^2
a	sorbent particle activity (eq. 2.25)	-
$a_{1,3}$	attrition regression constants (eq. 5.4)	
B	empirical parameter in sulphation model	s/m
C_a	bulk SO_2 concentration	$kmol/m^3$
C_{ao}	bulk SO_2 concentration prior to sorbent addition	$kmol/m^3$
C_b	bubble phase SO_2 concentration	$kmol/m^3$
$c_{1,3}$	exponents in attrition rate expressions	-
C_1	constants in Geldart elutriation model	-
C_p	particulate phase SO_2 concentration	$kmol/m^3$
C_s	concentration of SO_2 at pore mouth	$kmol/m^3$
d	general particle diameter	m
D_c	combustor diameter	m
D_e	effective gas diffusivity	m^2/s
D_{eo}	effective gas diffusiivity at X=0	m^2/s
$\underline{D}_e$	effective bubble diameter	cm
D_g	molecular diffusivity	m^2/s
D_K	Knudsen diffusion coefficient	m^2/s
D_o	overall diffusion coefficient equal to sum of Knudsen and molecular diffusivites	m^2/s
d_p	sorbent particle diameter	m
E	elutriation rate constant	$kg/m^2/s$
F	applied crushing force	N
f	asperity number related to surface topography	-
F_c	coal feed rate	kg/s
F_o	sorbent feed rate	kg/s
F_1	sorbent overflow rate	kg/s
F_2	sorbent elutriate flow rate	kg/s
$F'(d_p)$	attrition function defined by eq 5.13	
f_s	sorbent purity (% CaO)	-
G	dry flue gas molar flow	kmol/s
G_1	sulphation parameter (eq. 2.14)	-
H	fluid bed height	m
H_{mf}	bed height at minimum fluidisation	m

$k_{1,2}$	parameter in attrition rate expression = f(t)	
k	intrinsic rate constant for surface reaction	m/s
K	overall sulphation model parameter	-
k_d	deactivation rate constant	/s
k_g	physical mass transfer coefficient	m/s
K_s	effective surface rate constant (Fieldes nomenclature)	m/s
K_{so}	K_s at t=0	m/s
k_s	K_{so} (Zheng's nomenclature)	m/s
K_w	rate constant for diffusion and reaction within a particle	m/s
K_{wo}	K_w at t=0 (eq. 2.18)	m/s
K^*	elutriation velocity constant	/s
m_t	mass of sorbent at time t	kg
m_o	mass of sorbent at time t=0	kg
m_∞	mass of sorbent at time t=∞	kg
$\underline{M}$	molar CaO charge	kmol
M	total mass of bed solids	kg
M_{CO}	molar mass $CaCO_3$	kg
n	fractal dimension	-
$N(d_p)$	number of sorbent particles of mean size d_p	-
N_{We}	Weber number	-
p	system constant (eq. 5.6)	$m^{1/2}/s$
$p_o(d_p)$	feed number distribution function	
$p_1(d_p)$	overflow distribution function	
$p_2(d_p)$	elutriate distribution function	
$p_B(d_p)$	bed solids distribution function	
p'	attrition system constant (eq. 5.10)	-
P'_1	sulphation parameter	$m/s^{3/4}$
P'_2	sulphation parameter	$m/s^{5/4}$
Q	sulphation rate	kmol/s
Q_{avg}	average sulphation rate over all d_p	kmol/s
Q_o	initial sulphation rate	kmol/s
Q'	normalised sulphation rate	-
R	attrition rate	%/hr
r_c^*	dimensionless particle radius during calcination	-
$r(d_p)$	particle shrinkage rate	m/s
R_{CS}	calcium to sulphur molar ratio	-
R_{ss}	steady state attrition rate	%/hr
$\underline{S}$	sorption capacity (eq. 2.3)	g SO_3 / g CaO

S	particle surface area	m^2
S_o	BET surface area of particle	m^2
t	reaction time	s
t_s	sulphation time	s
t'	dimensionless sulphation time, t/t_s	-
T	fluid bed temperature	K
U	superficial velocity	m/s
U_{mf}	minimum fluidisation velocity	m/s
U_{si}	solid velocity of size d_{pi}	m/s
U_{ts}	terminal settling velocity	m/s
V	volumetric air flow	m^3/s
V'_{cc}	molar volume $CaCO_3$	cm^3/mol
V'_{co}	molar volume CaO	cm^3/mol
V'_{cs}	molar volume $CaSO_4$	cm^3/mol
V_p	particle pore volume	cm^3/g
W	mass of sorbent particles in fluid bed	kg
w_i	mass fraction in coal	-
	S=sulphur,C=carbon,H=hydrogen,N=nitrogen,O=oxygen,A=ash	
x	excess air ratio	-
X	conversion of oxide to sulphate	-
X_c	conversion of carbonate to oxide	-
X_m	maximum conversion	-
$\underline{X}$	crossflow exchange factor for fluid bed	-
y_o^*	base mole fraction of SO_2 in flue gas	-
y_o	mole fraction SO_2 in flue gas with sorbent	-
z_v	ratio of sulphate to oxide molar volumes	-
Z	moles calcium in a single particle	kmol

Greek Symbols

β	active bed flow area, fraction	-
Γ	coefficient of interparticle friction	-
ϵ_i	freeboard voidage	-
ϵ_{mf}	bed voidage at minimum fluidisation	-
ϵ_x	sorbent calcine porosity at conversion X	-
ϵ_o	sorbent calcine porosity at conversion X=0	-
ϵ_{Ls}	natural sorbent porosity	-
ρ_a	air density	kg/m^3

ρ_b	bulk density of bed solids	kg/m^3
ρ_{cc}	density of $CaCO_3$	kg/m^3
ρ_e	effective gas density	kg/m^3
ρ_g	gas density	kg/m^3
ρ_i	solids loading of particle size d_{pi}	kg/m^3
ρ_{LS}	natural sorbent density	kg/m^3
ρ_s	calcine density	kg/m^3
Π	efficiency of sulphur retention	-
μ	gas viscosity	Pa s
σ	structural strength of sorbent particles	N/m
τ	sorbent particle residence time	s
τ_{sf}	sulphation time constant (eq. B.7)	s

Abbreviations

BBM Bubbling bed model
CEGB Central Electricity Generating Board, U.K
CURL Coal Utilisation Research Laboratory, U.K
EPA Environmental Protection Agency, U.S.A
EPRI Electric Power Research Institute, U.S.A
FBC Fluid bed combustion
NCB National Coal Board, U.K.
NFBC National Fluidised Bed Combustor Demonstration Facility
NSPS New Source Performance Standards
TGA Thermo-gravimetric Analysis

CHAPTER 1 - INTRODUCTION

1.1 GENERAL

Interest in the application of fluidised bed technology to coal combustion has grown markedly since the early 1960's when the concept was effectively "rediscovered" by a team of researchers employed by the U.K.Central Electricity Generating Board. The enthusiasm with which the technology is currently pursued is a result of upheavals in world energy supply, specifically that of crude oil and natural gas. The growth of fluidised bed combustion (FBC) has been assisted by an increased environmental awareness of the hazards associated with fossil fuel combustion. The introduction of FBC at industrial scale has reached significant proportion, with, in 1984, a total installed capacity in excess of 15000 MW in over 25 different countries [Erlich, 1984]. Applications range from steam and electricity generation, to district heating, waste incineration, thermal fluid heat transfer and drying processes. There are now units in operation with a thermal rating of 250 MW, and economies of scale are such that the technology competes favourably with conventional pulverised coal combustion in many instances.

FBC offers distinct advantages over conventional combustion practices such as fixed bed (grate) or pulverised fuel firing. Principal among these are

* the ability to burn a wide variety of fuels, including low reactivity coal with a high mineral content
* low temperature operation, typically 1020 - 1170 K, which limits the vaporisation of potentially toxic elements from coal, eliminates clinker formation, and minimises fouling of heat transfer surfaces
* high volumetric heat release rates achieved by immersing heat transfer sufaces in-bed
* the potential for linking a fluidised combustor, operating at pressure, to a gas turbine, in a combined cycle configuration, with improved thermodynamic efficiency over a classic steam cycle

* the potential for in-situ control of acid gases such as sulphur dioxide by addition of calcareous sorbents such as limestone and dolomite, and of nitrogen oxides by staged combustion.

It is this ability to effectively control the emission of sulphur and nitrogen oxides in situ, rather than being forced to resort to costly flue gas treatment, which is perhaps the most significant attribute of the technology, and which is the focus of this work. The investigation is limited to an analysis of the reaction with sulphur dioxide.

1.2. SULPHUR DIOXIDE AS A POLLUTANT

The debate over the causative link between SO_2 emissions from fossil fuel power plant and acid precipitation damage is long standing. It is sufficient here to say that circumstantial evidence relating the two is overwhelming - the acidification of inland waterways in Scandinavia and Northern America, destruction of vegetation in these same areas, and the generalised attack on building structures, can all be attributed, in part, to the point source emission of SO_2 from large power plant [Uman (1983), Whitaker (1983), Chester (1986, 1987)]. The mechanism of acid gas precipitation is undoubtedly complex, and other chemicals, such as ozone, hydrocarbons, and NO_x, play major roles in atmospheric pollutant chemistry [Chester (1986), Ireland (1987)]. This, however, does not negate the significance of SO_2 as a contributor to acid precipitation damage, and the need to combat its emission from coal fired power plant remains.

Original strategies for the control of SO_2 were concerned simply with dispersion of the gas in the atmosphere. This was invariably achieved by the "tall stack" approach, which, in reality, serves only to exacerbate the problem [Crane and Cocks (1987)]. Further chemical reaction accompanies the transportation and mixing of SO_2 in the atmospheric boundary layer beyond the point at which the stack plume first contacts the ground. The potential exists for long range transport of SO_2 in gaseous form, and for its subsequent dry deposition at the surface, either directly, or through vegitation takeup. The dissolution of SO_2 in atmospheric moisture, and its subsequent oxidation to H_2SO_4 produces the well known "acid rain" during washout. In general, however, dry deposition is dominant.

The realisation that tall stacks are largely ineffective in abating SO_2 has prompted the implementation of absolute air quality standards (e.g. The U.S.A. Clean Air Act (1963, 1970, 1977)) as well as the creation of point source limits for SO_2 emission from coal combustion plant. The most severe limitations on SO_2 emissions stem from the Federal Republic of Germany (1984), where, for a coal combustion plant rated in excess of 400 MW_{th}, the maximum permissable SO_2 emission is 400 $mg.Nm^{-3}$. In addition, an 85% emission reduction efficiency is required. Similar absolute limits are enforced in the USA [E.P.A (1979)], and are under consideration in the U.K [Meethan (1981)]. Any new coal fired plant will require some form of SO_2 emission control in order to meet such severe statutory limits. The addition of calcareous sorbents to fluidised combustors is one way of achieving this required abatement in SO_2 emissions. Key features of this reaction are described below.

1.3 SULPHATION OF LIMESTONES / DOLOMITES

The general term "calcareous sorbents" applies to both limestones and dolomites and refers simply to their calcium content. Limestones are predominantly calcium carbonate whereas dolomites contain almost equal amounts of calcium and magnesium carbonates. Both may contain significant amounts of impurities (quartz, silicates and iron oxides predominantly). Their crystallographic structure distinguishes them from chalk and marble.

1.3.1 Thermodynamics

The reaction of calcareous sorbents with sulphur dioxide proceeds by the following steps:

1. At sufficiently high temperatures, both calcium and magnesium carbonates calcine to their respective oxides. Thus

$$CaCO_3(s) \longrightarrow CaO(s) + CO_2(g) \qquad 1.1$$

$$MgCO_3(s) \longrightarrow MgO(s) + CO_2(g) \qquad 1.2$$

2. The resulting oxides can then react with sulphur dioxide in the presence of oxygen, according to

$$CaO + SO_2 + 1/2\ O_2 \longrightarrow CaSO_4 \qquad 1.3$$

$$MgO + SO_2 + 1/2\ O_2 \longrightarrow MgSO_4 \qquad 1.4$$

The overall thermodynamic viability of the above four reactions is well documented [Fieldes (1979), Dennis (1985)]. At typical CO_2 concentrations in a combustor,

* $CaCO_3$ calcines at 1 atmosphere if T > 1030 K
* $MgCO_3$ calcines at 1 atmosphere if T > 610 K
* CaO is sulphated at 1 atmosphere if T < 1500 K
* MgO is sulphated at 1 atmosphere if T < 985 K

Normal operating temperatures in an FBC are in the range 1020 - 1175 K, and therefore the sulphation of MgO is unlikely to occur. The reaction of both limestones and dolomites is expected to proceed solely by the sulphation of the CaO component in each.

1.3.2 Aspects of the Sulphation Process

(i) On the basis of the respective molar volumes of $CaCO_3$, CaO, and $CaSO_4$, it can be shown that the conversion of CaO to $CaSO_4$ cannot reach 100%. Assuming that particle external dimension is unchanged on calcination, the total fractional unit pore volume available for sulphation is given simply by

$$\epsilon_o = 1 - V'_{co}/V'_{cc}$$

where V'_{co} and V'_{cc} are molar volumes of oxide and carbonate respectivley. Using molar volumes from Weast and Astle (1982), $\epsilon_o = 1 - 16.9/36.9 = 0.54$. As sulphation proceeds, the porosity decreases according to Dennis (1985)

$$\epsilon_x = 1 - \left[X\ V'_{cs} + (1-X)V'_{co}\right] / V'_{cc} \qquad 1.6$$

where X is the fractional conversion of CaO to $CaSO_4$. The maximum value

of X, i.e.X_∞, is found from eq.1.6 with ϵ_x=0. Noting that V'_{cs} = 52,2 cm^3/mol, X_∞ = 0,57 i.e. the maximum conversion of limestones is limited to 57%. This constraint does not apply to dolomites because MgO does not take part in the reaction, and therefore the pore volume generated by calcination of the $MgCO_3$ component is available for uptake by $CaSO_4$ product.

(ii) It has been shown by Ulerich et al (1977) and Dennis and Hayhurst (1986a) that fluid bed calcination of limestones and dolomites is rapid relative to their subsequent sulphation. In the development of this thesis, calcination will therefore be assumed to be instantaneous and to proceed to completion ahead of any sulphation.

(iii) It is expected that the sulphation capacity of a sorbent will be a function of particle size [Fieldes (1979)]. It is therefore important to identify those processes operating within a fluidised combustor which give rise to changes in the size distribution of sorbent particles. Here one thinks specifically of elutriation and attrition. Information is required on the rates of these processes relative to that of sulphation. The complexity of the overall sulphation process, and its relationship to coal combustion, can be seen in FIGURE 1.1. The interrelation between the various sub-processes is clearly apparent, and dictates the degree of sophistication required of any model which purports to describe sorbent sulphation accurately.

1.4 THE SOUTH AFRICAN POSITION

South Africa has extensive coal reserves, conservatively estimated at 58000 million tonnes economically recoverable [De Jager (1982)]. Current production of run-of-mine coal is 231 million tonnes per annum, with coal contributing between 80% and 90% to the country's primary energy supply. South African coals are generally low in sulphur (< 1%), which, historically, has contributed to the perception that SO_2 emissions pose no real threat to the environment. South Africa ranks fifth in world bituminous coal production, and fourth in total coal exports, with steam coal the principal export commodity [Krueger (1986)]. This latter market demands extensive beneficiation of raw coal prior to export. As a consequence of this upgrading, there is considerable accumulation of a discard fraction, high in both ash and sulphur. The sulphur content of

this discard stock can reach a high of 8 - 10%, but is typically in the range 2.5 - 4%. Much of the interest now shown in FBC technology stems from the desire to utilise this discard resource, which is accumulating at the rate of about 40 million tonnes per annum.

Environmental legislation in this country is applied rather loosely, and adheres to the principle of "best practical technology", rather than to the imposition of absolute levels, as a means of pollution control. SO_2 emission control is enforced on a "site - by - site" basis, but is generally poor. Over 94% of all coal used domestically is consumed by three industries (electricity, syn-fuels and steel), none of which employ technology for the abatement of SO_2. As an example of typical point source emissions, consider that of Matla Power Station, one of the new generation of pulverised fuel stations operated by ESKOM, the local utility company. This 3600 MW_e station burns roughly 500 kg of coal per second. Though the sulphur content of this coal is low (0.75-1 %), SO_2 emission levels from this unit are calculated to be in the range 2200 - 2975 mg/Nm^3 of flue gas. To fall in line with current absolute emission levels imposed elsewhere, e.g. in the Federal Republic of Germany, this "base" SO_2 level must be reduced by a factor of five. When this typical SO_2 level is scaled upwards for the higher sulphur discard coal, the situation becomes even more acute.

Ground level measurements of wet and dry sulphate loadings have been performed at discrete sites around South Africa. Bosman (1987) recorded high levels of wet SO_4^- in the Transvaal region (where most coal combustion occurs). Values as high as 54 kg ha^{-1} yr^{-1} were reported, which is nearly double the measured value in Pennsylvania, USA (25 - 39 kg ha^{-1} yr^{-1}). Dry SO_4^- levels were in the range 12 - 20 kg ha^{-1} yr^{-1}, which is comparable to the highest levels recorded in the USA. Bulk sulphate levels in ground regions close to major coal combustion plant were typically 60% higher than the maximum levels reported anywhere in the USA. These figures are disturbingly high, and lend further support to the need for some form of sulphur removal from combustor flue gas streams.

The call for utilisation of the coal discard resource has been amplified by the fact that many of the bituminous discard dumps have ignited spontaneously, and now burn uncontrollably with unrestrained SO_2

emission. FBC is seen as the most attractive method for discard coal combustion, not only because of the high sulphur content of this material, but because its high ash value (up to 50%) makes it particularly unreactive and therefore unsuited to pulverised fuel combustion.

An assessment of the potential demand for sulphur sorbents in this country requires some assumptions to be made. The cost of retrofitting existing power plant with SO_2 reduction equipment would be prohibitively expensive, and, for this reason, sorbent usage is expected to be limited to new coal fired plant. If the discard material alone (say with a sulphur content of 3%) is to be used in FBCs, and assuming, furthermore, that an 80% in base SO_2 levels is warranted, the annual sorbent requirement would be in the region of 10 million tonnes if limestone is used, and roughly double this quantity if dolomites are employed. These figures are comparable in magnitude to the total annual production of limestone and dolomite in this country [Martini (1987)]. There is thus an obvious need to optimise sorbent usage in FBC, and, where possible, to identify highly reactive sorbents. This requirement has provided one of the major driving forces for this work.

1.5 THESIS SCOPE AND LAYOUT

The selection of an ideal sulphur sorbent is a complex task, requiring a detailed knowledge of material physical and chemical properties, an intimate understanding of sorbent performance in the fluid bed combustor, and the ability to relate all these features to the plant environment. Ideally, the optimum sorbent would be one

> "which provides the lowest overall plant cost and meets all the constraints placed on plant reliability, technical performance and environmental impact"
>
> [O'Neill (1979)].

A flowsheet depicting the basic steps in the sorbent selection process is shown in FIGURE 1.2, due to O'Neill et al (1979). This figure shows clearly the interplay between sorbent properties, reaction phenomena and process plant features .

The overriding objective of this work is to provide an understanding of sorbent sulphation in FBCs, to describe the fundamental performance characteristics of sorbents in terms of their measurable properties, and to relate such performance to the physical processes operative in the combustor. This understanding should lead to the development of a simple mathematical description of the process, which has good predictive capability and can be used with confidence by both design engineers and operating personnel of FBC plant.

This thesis highlights two shortcomings of previous work. Little information is available on the performance of sorbents (whose sulphation kinetics have been measured by controlled experiments) at industrial scale. It is therefore difficult to assesss the predictive merit of process models derived on the basis of these laboratory experiments, even though the description of sulphation kinetics may be fundamentally based. This work overcomes this deficiency by analysing the performance of selected sorbents at both laboratory scale, and in a typical industrial - size FBC unit. Furthermore, most process models for sorbent sulphation ignore the contribution of particle attrition. This omission is rectified in the current work.

In parallel with the above objectives is the desire to assess the suitability of South African sorbents during FBC. Prior to this work, no information was available on the sulphation propensity of these materials. However, their use in other process industries is well defined, and desirable properties for these applications have been clearly identified. It is the intention of this work to relate sorbent performance to this existing property data base, with special reference to sorbent geology.

The dissertation layout is as follows:

* Chapter 2 reviews the literature for the sulphation of sorbents in FBCs, highlighting useful starting points for this work
* Chapter 3 examines the sulphation kinetics of a wide range of South African sorbents, and compares their performance to international standards. The validity of two simple kinetic models for sorbent sulphation is assessed. Chemical enhancement of sorbent performance is evaluated for one, low reactivity, dolomite.

* Chapter 4 describes the importance of sorbent physical properties in defining sulphation rate and capacity. Critical properties of the South African resource base are measured, and correlated with its geologic description. Sorbent performance is defined in terms of stone geology.
* Chapter 5 considers the significance of sorbent attrition in FBCs. A simple model that describes the contribution of major attrition mechanisms to continuous particle shrinkage is defined, and substantiated by experiment. Two elutriation correlations available in the literature are compared against measured data collected from a large laboratory FBC.
* Chapter 6 entails the development of an overall process model for sorbent sulphation in FBC. This model incorporates sulphation kinetics, attrition and elutriation, and examines their effect on sulphur capture, for a wide size distribution of sorbent particles. The model development is governed by the requirement that its solution be assured without resorting to further simplifications which entail a loss of physical accuracy.
* Chapter 7 provides a validation of the process model by sulphation data generated, for three representative South African sorbents, in a 10 MW_{th} atmospheric pressure fluidised boiler. The effect of sorbent selection on the design of downstream gas cleaning equipment is discussed.
* Chapter 8 summarises the salient points of the previous chapters and offers suggestions for further research activity in this field.

CHAPTER 2 - REVIEW OF SULPHATION MODELS

2.1 INTRODUCTION

The complexity of the sorbent selection process was outlined in Chapter 1. This current chapter reviews the published experimental understanding of the sulphation reaction and highlights attempts which have been made to characterise the performance of sorbents in fluidised combustors by both physical and mathematical models, identifying uncertainties and limitations inherent in both approaches. Thereafter, the need to provide a useful design tool for FBC practitioners, where sorbent performance can be assessed simply and with confidence, is addressed.

2.2 EXPERIMENTAL OBSERVATIONS OF THE SULPHATION PHENOMENON

Over the last twenty years there have been several substantive experimental investigations of the sulphation reaction. These range from the differential reactor studies of Borgwardt (1970), Borgwardt and Harvey (1972) and Hartman and Coughlin (1974, 1976), to the thermogravimetric measurements of Vogel (1977), Ulerich et al (1978 and 1980) and Dogu (1981), and the batch fluidised bed reactor studies of Fieldes (1979) and Zheng et al (1982). In some cases, a comparison was made between TGA and fluidised bed combustors [Spitsbergen (1981)]. In all the above mentioned fluid bed experiments, an attempt was made to measure sulphation kinetics of uncalcined sorbent particles in an atmosphere generated by coal combustion. The other techniques invariably measured kinetics of precalcined samples in a simulated flue gas environment. As addressed in Chapter 1, calcination is a necessary pre-requisite for sorbent sulphation. A brief review of this subject is given in APPENDIX A where fixed bed calcination studies of South African sorbents are described.

The range of sorbent types whose sulphation potential has been analysed is impressive. Both Borgwardt (1970) and Spitsbergen (1981) reported data on 11 (different) sorbents, whilst the Argonne data of Vogel (1977) concerned a further 10 samples. Potter (1969) had previously analysed the sulphation propensity of 86 different sorbents in a fixed bed

reactor.

A summary of the experimental conditions pertaining to each data set is given in TABLE 2.1. The data were generally in a form where specific reaction rate and conversion of sorbent particles could be determined as a function of time. In both the differential reactor and fluidised bed studies, this could be achieved directly - in the former case by chemically determining the sulphur uptake of the reactor charge over different time intervals, whilst in the latter case it was inferred from the change in flue gas SO_2 level with time. In the TGA studies, conversion was measured indirectly from rate of change of sample mass.

Fluidised bed studies offer the simplest, and most realistic, method of measuring the performance of particular sorbents, and the technique can be used under a wide range of process conditions spanning the complete operation of a fluidised bed combustor. In Chapter 3 results from these studies for a range of sorbents from different countries are compared with results from an array of South African sorbents.

A number of important conclusions can be drawn from this data bank of sulphation experiments. All correctly identified the decrease in reaction rate with time, the influence of calcination conditions (pore size distribution changing to larger pore sizes as temperature increased from 1023 K to 1223 K), and the significance of sorbent particle pore structure in determining sorbent conversion. Borgwardt and Harvey (1972) stressed the importance of sorbent geology in determining calcine structure. Scanning electron micrographs published by Ulerich et al (1979), showed that, in some cases, the total pore volume of CaO was permeated by SO2, whereas, for other sorbent types, sulphate deposition was constrained to a region in close proximity to the external surface of the particles. Dennis and Hayhurst (1985) presented electron micrographs for the more general case in which the dense deposition of sulphate product could be clearly seen near the external edge of particles. A concentration gradient in SO_2 was evident for particles of diameter greater than 0.5 mm [Hartman and Coughlin (1976)], whose size is typical of sorbent particles used in fluidised combustors. The resultant pore blockage and inaccessibility of internal surface area imply that maximal theoretical conversion is seldom attained.

The existence of a temperature optimum for sulphation at atmospheric pressure has been reported extensively. Maximal sorbent utility is achieved in the range 1100 K to 1150 K [Roberts et al (1975), Petrie (1983), Dennis (1985)] and is attributed to the interplay of calcination and sulphation. The pore volume generated during calcination is maximal at temperatures in the region of 1173 K. Extended exposure at this, or higher temperatures, whilst sulphation proceeds, leads to loss of pore volume by sintering [Ulerich et al (1977)].

It is evident from this experimental review that there are considerable variations in the ability of calcareous sorbents to absorb SO_2 during coal combustion. The variation in sulphation kinetics with sorbent type and process conditions points to the need for a predictive model to fully describe the sulphation phenomenon in a fluidised combustor, thereby minimising the amount of experimentation required to quantify the behaviour of a selected sorbent.

2.3 SULPHATION MODELS

A rigorous sulphation model must be capable of describing firstly the single sorbent particle behaviour during sulphation, and secondly, the influence of the fluidised bed process on the entire sorbent population, with all the attendant complexities of fluid dynamics, heat and mass transfer, and combustion. As a first stage, models which describe the sulphation of single, precalcined sorbent particles are reviewed. An extension of this class of models to fluidised combustors is discussed thereafter.

A comprehensive model for the sulphation of CaO must consider

a) mass transfer of gaseous reactants from fluidised bed bulk to the surface of reacting particles

b) diffusion of gaseous reactants through the porous network, and through the layer of sulphate product

c) chemical reaction at the interface between oxide and sulphate, with the added complexity that the available surface for reaction decreases with time as pores become blocked (due to the increased volume of

sulphate product)

d) decrease in reaction rate with conversion

2.3.1 Averaged Parametric Models

Discounting the models of Koppel (1970) and Keairns (1975), in which an average, time invariant, sulphation rate constant was derived from limited experimental data, the simplest such models are those based on calcine structure. Classically, these relate the attainable sorbent conversion, through a simple geometric relation, to such parameters as molar volumes of reactants and products, the inherent porosity of the raw sorbent, and true solid density. An example of such a model is that due to Hartman and Coughlin (1974), which assumes constant particle size, uniform sorbent interior, and $CaSO_4$ as the only product. Under these conditions, sorbent porosity is given as a function of the extent of calcination and sulphation by

$$\epsilon_x = 1 - (1 - \epsilon_{Ls})\,\rho_{Ls}\frac{f_s}{M_{cc}}\left[V'_{cc} - X_o(V'_{cc} - V'_{co} + X(V'_{cs} - V'_{co})\right] - (1 - \epsilon_{Ls})\left[1 - f_s\,\frac{\rho_{Ls}}{\rho_{cc}}\right] \qquad 2.1$$

This simple expression enables calcine porosities, prior to sulphation, to be determimed by setting X=0 in the above equation. In Chapter 4, the accuracy of this model in predicting calcine porosities from natural sorbent properties is assessed. Maximium sorbent utility, X_∞, is found by setting porosity ϵ_x=0.

Thus,

$$X_\infty = \frac{1}{V'_{cs} - V'_{co}}\left[\left[\frac{M_{cc}}{(1 - \epsilon_{Ls})\,\rho_{Ls} f_s}\left[1 - (1 - \epsilon_{Ls})\left[1 - f_s\,\frac{\rho_{Ls}}{\rho_{cc}}\right]\right]\right] + X_o\,(V'_{cc} - V'_{co}) - V'_{co}\right] \qquad 2.2$$

This expression shows the direct link between sorbent utility and inherent (natural) porosity and emphasises the need to be selective in choosing a sorbent which will guarantee a high conversion to sulphate. Substituting literature values for molar volumes of calcium oxide and calcium sulphate, eq. 2.2 reduces to [Hartman and Coughlin (1978)]

$$\underline{S} = 2.27\ V_p \qquad 2.3$$

where $\underline{S}$ is the mass of SO_2 adsorbed per unit mass of CaO. The authors found that eq 2.3 significantly overpredicted values of X_∞ for sorbent kinetics in a differential reactor. These same authors examined other data [Potter (1969), Mullins and Hatfield (1970), Borgwardt and Harvey (1972)] and found that the accuracy of this correlation was not improved. This is attributed to the fact that conditions are not uniform within the interior of a particle (as required of this model) and that pore blockage by sulphate prevents the attainment of a condition of zero porosity.

Classical gas-solid reaction models which have been used to take account of changing porosity during sulphation are of two types:

* those that model a sorbent particle as a collection of non porous grains within a spherical shell and consider the reaction to occur, according to a shrinking core mechanism, on the surface of these grains. The model effectively assumes that all pores are of uniform size. This model was first expounded by Szekely, Sohn and Evans (1976) and adapted for sulphation by Hartman and Coughlin (1976), and Ramachandran and Smith (1977).

* and those which view the reaction as occurring within single pores arranged in some from of pore network. The random pore model of Bhatia and Perlmutter (1981), the branched pore, "tree" network of Simons and Rawlins (1980), and the generalised pore model of Yu and Sotirchos (1987) offer elaborate treatments of the sulphation reaction.

2.3.2 Grain Theory Models

The grain theory model of Hartman and Coughlin (1976) assumed that
* external mass transfer resistance was negligible
* no intraparticle temperature gradients existed
* the sulphation reaction was first order in SO_2
* the pseudo-steady state hypothesis appled.

Gaseous diffusion was characterised by the Knudsen diffusion coefficient with a tortuosity factor of 1.5. The effective diffusivity was given

simply by $D_{eff} = D_k \epsilon_x$. As sulphation proceeds, the effective diffusivity decreased with porosity, ϵ_x according to eq. 2.1

This model successfully predicted the sulphate concentration profile through a sorbent particle. For large particles, the bulk of the deposit was constrained to their external surface. The significance of product layer diffusion was shown to increase with time. An important finding of this model, borne out by a series of experiments in a differential reactor, was the rapid fall-off in sulphation rate, with most of the reaction occurring in the first 15 minutes. The overall sorbent conversion increased only marginally even with prolonged (in the sense of hours) exposure to SO_2 rich flue gas. This has important implications for the design of fluidised combustors, in which sorbent particle residence times typically span several hours. A rapid loss of reactivity would necessitate a larger bed inventory. This opens the way for preserving high reaction rates by, for example, controlled attrition, where the external surface containing the sulphate layer is removed with time. Sorbent attrition is discussed in detail in Chapter 5.

The grain model predicted that product layer diffusion would dominate when conversion on the external particle surface reached a limiting value of 55%. This solid layer diffusional resistance limits the attainable conversion of large particles which are characteristic of fluidised combustor systems. The model did not explicitly state the effect of pore size distribution on sorbent utility.

In a later paper, Hartman and Coughlin (1978) confirmed the importance of natural sorbent porosity and calcination conditions on sorbent utility. It was postulated that an inherent porosity of 30% or greater in the raw (uncalcined) sorbent would ensure complete conversion to sulphate product. This is an important assertion, and of inestimable worth in the process of sorbent selection. This point is elaborated upon in a discussion of natural sorbent physical properties, and how these effect sorbent performance, in Chapter 4.

Ramachandran and Smith (1977) used a grain pellet model to develop criteria for pore closure based on the initial porosity of the calcined sorbent. The change in effective diffusion coefficient with changing porosity was ignored.

If

$$\epsilon_x > (z_v-1)/z_v \qquad 2.4$$

where z_v is the ratio of sulphate to oxide molar volumes, complete volumetric reaction is possible, otherwise pore closure occurs. This implies that complete conversion is attainable only if the initial calcine porosity exceeds 0.68. Hartman and Coughlin (1974) cite values in the range 0.515 - 0.531, assuming zero porosity in the parent stones. The porosity of calcines prepared by Borgwardt and Harvey (1972) at 1253 K over two hours spanned the range 0.08 - 0.535 (calculated here from the reported calcine pore volumes). These 11 sorbents covered the full range of geologic types, and included marble, limestones and dolomites. It would appear, then, that very few calcines attain the high base porosity required of the Ramachandran and Smith criterion. Thus the sulphation of calcined sorbent particles is generally limited by pore closure, which confirms the model findings of Hartman and Coughlin (1978). This analysis ignores the possibility of optimising calcination conditions in order to maximise calcine porosity.

Burdett (1983) proposed, via a grain-type model, that the rate limiting step in sulphation is the oxidation of SO_2 to SO_3 within the pores of a particle, and that the subsequent formation of sulphate product occurs at a rate dependent on the rate of SO_3 diffusion into the grains composing the particle. It was postulated that a high oxygen concentration in the interstitial gas would infer a high SO_3 presence at the edge of the sorbent particle, resulting in rapid pore blocking near the external surface. A good degree of correspondence was obtained between this model and sulphation data from CURL, Leatherhead, UK. This model was refuted by Dennis and Hayhurst (1986b) who concluded that it is an O_2 deficiency in the particulate phase, rather than SO_3 levels at grain boundaries, which dictates sulphation capacity. This was verified experimentally by monitoring the effect of temperature on the sulphation reaction. The fall-off in sulphur retention above 1150 K was attributed to the increased ability of volatiles to burn in the dense phase at these high temperatures. The initial reaction rate was shown to be independent of O_2, which further suggests that SO_3 is not a necessary intermediate.

2.3.3 Pore Network Models

Grain pellet models are unable to account for the wide pore size distribution of calcined sorbent particles or for its effect on sorbent utility. This limitation of the Hartman and Coughlin (1976) model was identified by Simons and Rawlins (1980) from a comparison of rate constants predicted by the former model and those measured by Borgwardt (1970). The latter values were in the region of 30 times slower. Two reasons were given for this disparity. Pore diffusion was characterised in the grain model by a Knudsen diffusion coefficient, whereas the range of pore volumes measured by Borgwardt would indicate that diffusion should be characterised by a continuum value. This, coupled to the fact that the model is based on pores of uniform size, reinforces the need to monitor the effect of pore size distribution on sorbent performance. Several models propounded in recent years attempt to do just this.

The idealised pore network model of Bhatia and Perlmutter (1981) allowed for a distribution of pore sizes (within a network of non-intersecting cylinders), and a reduction in local porosity by overlapping of product layers. High sorbent conversion was assured more readily in particles having a wide rather than a monodispersed pore size distribution. In sorbent selection, this points to a trade off between assuring high surface area through a preponderance of small pores, and their ready blocking by sulphate product. This model confirmed the importance of natural sorbent pore structure, insofar as it affects the porosity of the calcine, its surface area and pore size distribution. This model also confirmed, by manipulation of data generated by Hartman and Coughlin (1976), that the sulphation reaction is controlled by pore diffusion, with the kinetic resistance being small. Of interest is that this model predicted the rapid formation of a layer of sulphate product on pore walls, and that subsequent reaction appeared to be controlled by the solid state diffusion of activated complexes of SO_2 and O_2 through the impervious sulphate layer.

The importance of pore size distribution in relation to particle size was described by Yu and Sotirchos (1987). If a calcined sorbent particle develops a pore size distribution which results in pore blockage near the external surface of the particle, then smaller particles achieve a

higher overall conversion than do larger ones. For a particular sorbent with a bimodal size distribution, whose pores were blocked on sulphation, doubling the mean particle size from 0.5 mm to 1 mm resulted in a fall-off in conversion from 20 % to 10%. This has direct implications for fluidised combustion where sorbent particles are typically in this size range.

The branched pore network model of Simons, and its later extensions [Simons and Garman (1986), Simons, Garman and Boni (1987), and Simons (1988)] confirmed that

* when the effect of sulphate deposition is considered, deactivation occurs principally through the loss of internal surface as small pores are blocked

* the effect of particle size manifests itself in pore blocking of large particles near external surfaces

* product layer diffusion controls when product layer thickness is between 1 and 10 nm, which corresponds to the blockage of smallest pores

* small pore filling is dominant for 1-10 μm particles, whilst pore mouth clogging is dominant in particles whose diameter exceeds 100 μm. Product layer diffusion is more pronounced for thick layers in the pore mouths of large particles

* the explicit dependence of sorbent utility on particle size is less important than the implicit effect of size on porosity

* of greater significance than particle size is the interdependence of porosity and particle surface area. Simons (1988) suggested that increasing sorbent surface area beyond 40 m^2/g would not result in improved utility unless the porosity increased correspondingly. Such a constraint is of little practical use, however, as calcination of sorbents under conditions typical of fluidised combustor operation results in surface area values in the range 2 - 10 m^2/g (see Chapter 4 for discussion of sorbent surface area). It does, nevertheless, point to the superiority of sorbents with a high natural porosity.

Implicit in these model findings is the fact that altering pore size distribution, whilst maintaining porosity, has little influence on sorbent utility.

It may be generally concluded from all pore network models reviewed above that, for typically sized sorbent particles employed in fluidised combustion, deactivation is likely to occur by pore mouth blocking, and ultimate conversions will be low. The process of calcination ultimately affects sorbent performance by defining the porosity and pore size distribution of sorbent particles.

2.3.4 Sulphation Models: Extension to Fluidised Combustion: Part 1

The elaborate pore diffusion models described briefly above are, to a large extent, successful in predicting the salient features of sorbent particle sulphation. However, the complexity of the equations describing diffusion of SO_2 through the porous network and chemical reaction on pore walls, and the coupling of these equations through the local SO_2 concentration, necessitate the use of computer-based numerical methods to achieve a solution.

When sulphation in a real fluidised combustor is to be considered, the situation is complicated further by the size distribution of sorbent particles, the spread of residence times, attrition and elutriation, the release of SO_2 during combustion, and bed fluid dynamics.

The modelling literature on fluidised combustion is comprehensive and a review of its extent is outside the scope of this work. The reader is referred to the excellent review of La Nauze (1985) for detail of the physical and chemical mechanisms of combustion. Attempts to model the behaviour of coal particles in a real fluidised combustor [Bukur and Amundson (1980), Congalidis and Georgakis (1980), Rajan and Wen (1980)] resort to simplified assumptions regarding sulphation kinetics in order to achieve manageable solutions. Typically, sorbent particles are assumed to be of uniform size, constant with time, and the amount of sorbent required to effect a specified reduction in SO_2 emission levels is given by simple empirical correlations, an example of which is

$$\Pi = 0.223\ R_{cs} - 0.043 \quad (R_{cs} <= 4) \text{ [Burns \& Roe (1978)]} \qquad 2.5$$

where Π is the fractional reduction in flue gas SO_2 level, and R_{cs} is the Ca/S molar ratio. Sulphation is effectively decoupled from coal combustion, with SO_2 assumed to be released either entirely at the coal feed point (gas in plug flow), or uniformly throughout the bed (gas well mixed), and sulphation occurring at some average (constant) rate.

All these comprehensive fluidised combustor models stress the importance of knowing sorbent properties and how these affect the size distribution of sorbent particles in the combustor, yet make little effort to resolve their complexity. Any action within the combustor which changes this size distribution, e.g. sorbent attrition and fines elutriation, must be quantified before a complete picture of sorbent performance can be generated.

The need for a detailed yet tractable overall model of fluidised combustion, which incorporates sorbent action, is clear. The simplifications described above, which were required to achieve a solution to such a model, minimise the gains to be made from following the intricate pore diffusion model route. This approach invariably leads to an unwieldy model formulation, a solution to which can be assured only by simplifying its mathematical complexity, or by resorting to extensive and time consuming numerical methods. The value of such an approach to design engineers is minimal. A more rational and straightforward pursuit is to identify, through simple experiments, a minimum number of sorbent parameters which adequately characterise the sulphation reaction, and to incorporate these into an overall model with good predictive capability.

2.3.5 Kinetic Models

An example of such an approach was that taken by Fieldes (1979), who performed a series of experiments in which sorbent particles were added batch-wise to a fluidised combustor. These sorbent charges were subjected to either a simulated flue gas containing SO_2 or to an atmosphere generated by coal combustion. As mentioned in Section 2.2 the specific reaction rate and sorbent conversion were inferred from changes in the flue gas SO_2 level with time, according to the following development.

For a coal combustion experiment, the overall sorbent conversion was given by

$$X = Gy_o^*/\underline{M} \int (1 - y_o/y_o^*)\, dt \qquad 2.6$$

where G is the dry flue gas molar flow rate, y_o^* and y_o are the mole fractions of SO_2 in the flue gas prior to, and after, sorbent addition, and $\underline{M}$ is the molar CaO charge.

Defining the overall rate of reaction, Q, by

$$Q = K_s\, \pi\, d^2\, C_p \qquad 2.7$$

where C_p is the SO_2 concentration in the particulate phase, gives an expression for the specific reaction rate, K_s. The exact form of K_s is found from the bubbling bed model of Kunii and Levenspiel (1969). The pertinent assumptions of this model need not be repeated here (see Fieldes (1979)). For a coal combustion experiment, the expression for K_s reduces to:

$$y_o/y_o^* = (AU/K_sS).[1 - 1/\exp(AU/K_sS + 1/\underline{X})^{-1}] \qquad 2.8$$

where $\underline{X}$, the crossflow exchange factor between bubble and particulate phases, is equal to the number of times the contents of a gas bubble are replaced as it travels through the bed. Its magnitude is predicted by the correlation of Avedesian and Davidson (1973)

$$\underline{X} = \frac{6{,}34\ H_{mf}}{\underline{D}_e(g\underline{D}_e)^{1/2}} \left[U_{mf} + \frac{1{,}3\ \epsilon_{mf}\ D_g^{1/2} g^{1/4}}{(1 + \epsilon_{mf})\underline{D}_e^{1/4}} \right] \qquad 2.9$$

where U_{mf}, the minimum fluidisation velocity, is given by an empirical correlation [Kunii and Levelspiel (1969)], ϵ_{mf} is minimum fluidisation voidage, D_g is the molecular diffusion coefficient (Perry's Handbook values), and $\underline{D}_e$ is the effective bubble diameter, from Darton et al (1977).

Experimentally derived values of K_s were used by Dennis and Hayhurst (1986b) in a sulphation model where diffusion and reaction equations were solved analytically for a wedge shaped pore geometry. The model

assumes steady state operation, rapid calcination, negligible mass transfer resistance, first order rate dependence on SO_2 in an excess of O_2, and that the reaction is controlled by pore and product layer diffusion and reaction on the pore wall surfaces. Diffusion of SO_2 through pores and through the sulphate product layer is described in terms of an effective diffusion coefficient, D_{eo}, from the random pore model of Wakao and Smith (1962) -

$$D_{eo} = D_o \epsilon_o^2 \qquad 2.10$$

where the overall diffusion coefficent, D_o, is the sum of Knudsen and molecular contributions. The variation of this effective diffusion coefficient with time is given by

$$D_e = D_{eo} (\epsilon_x/\epsilon_o)^2 \qquad 2.11$$

according to Bhatia and Perlmutter (1981). This approach differs from that commonly taken [Dogu (1981)] where, with all other parameters uniquely determined, the magnitude of the effective diffusivity is allowed to vary in order to effect model closure.

The final form of the model expression for the specific rate constant is

$$K_s = P_1' \, t^{-1/4} - P_2' \, t^{1/4} \qquad 2.12$$

where the parameters P_1' and P_2' are determined from the physical properties of the sorbent and by simple batch experiment.

The basis of the model has been given in detail here purely to emphasise its robust nature, and its relative simplicity. The most significant findings of the model are that

* ultimate conversion increases with a decrease in solid state diffusivity
* the intrinsic rate constant has little effect on pore plugging time or ultimate conversion
* sorbent particles with a high effective surface area generally have a low utility because of associated blockage of small pores.
* external mass transfer has significance in the early phase of the

reaction

The model predicts the most salient features of the sulphation reaction. Little additional gain would be made by extending the model to the complicated pore networks described previously.

A similar conclusion was reached by Dennis and Fieldes (1986) using a simpler pore geometry (an irregular cylindrical pore network in a spherical particle) and assuming that Knudsen diffusion dominates (contested by Simons and Rawlins, 1980). Product layer formation and solid state diffusivity were given independently of position within a pore - the product layer thickness being equal to that at the pore mouth. The specific reaction rate was measured by the same set of batch experiments [Fieldes (1979)]. The overall reaction rate was related, at any time, to the dimensionless pore diameter available for sulphate deposition. This complicated time dependency on specific reaction rate was reduced to an empirical form characterised by one dimensionless parameter which describes the effect of product layer buildup at pore mouths. The exact value which this parameter takes for a specific sorbent depends on temperature, particle size, and calcine structure, the last being a function of the inherent porosity of the natural sorbent.

This model is used in Chapter 3 to discuss the performance of a wide range of South African sorbents, and its development is repeated below.

The overall rate of reaction, Q, is given by

$$Q = \pi\, d^2\, K_w\, C_s \qquad 2.13$$

where K_w, the rate constant for diffusion and reaction within a particle, at a given time, is defined in terms of the Thiele modulus $[d(kS_o/D_{eo})^{1/2}]$, where k is the surface rate constant, S_o is the B.E.T. surface area of the calcined, but unsulphated particle. C_s is the concentration of SO_2 at the pore mouth. The expression for Q was recast in a form with an explicit dependence on pore volume available for reaction. After considerable manipulation, an expression relating the change in pore radius with time was derived. Using numerical values for the various model parameters [defined by Dennis and Fieldes (1986)

equations 15-19] for a U.K.limestone, the dimensionless reaction rate, Q', reduces to

$$Q' = Q/Q_o = [1 + G_1/(1/t'-1)]^{-1} \qquad 2.14$$

where G_1 is a dimensionless system parameter, which, for a specific particle, is independent of time, and $t'=t/t_s$, where t_s is the time to pore closure.

When mass transfer to sorbent particles is considered, the reaction rate is rewritten as

$$Q = \pi\, d^2\, K_s\, C_p = \pi\, d^2\, k_g\, (C_p - C_s) \qquad 2.15$$

For the special case where K_s is independent of C_p (and thus C_s)

$$K_s = [1/k_g + 1/K_w]^{-1} \qquad 2.16$$

At t=0, $K_w=K_{wo}$ and therefore $K_{so} = [1/k_g + 1/K_{wo}]^{-1}$ 2.17

The theoretical value of K_w is relatively insensitve to C_s. Therefore, from eqs. 2.14, 2.15 and 2.16,

$$K_s = [1/k_g + 1/K_{wo}\,(1 + G_2/(1/t'- 1))]^{-1} \qquad 2.18$$

After some rearrangement, this leads to

$$K_s = (1 - t')/(1/K_{so} + Bt') \qquad 2.19$$

where $B = (G_2/K_{wo} - 1/K_{so})$, is constant with time for a given particle.

The final expression for the overall sulphation rate is therefore

$$Q = [(1-t')/(1/K_{so} + Bt')]\ \pi\, d^2\, C_p \qquad 2.20$$

Integration of this equation over time to pore closure gives the ultimate sorbent conversion.

The numerical values of the two sorbent specific parameters, t_s and B,

were found from the series of batch fluidised sulphation experiments already described.

It is encouraging to note that the above simple model predicts the sulphation behaviour of a specific U.K.limestone (Penrith) with reasonable accuracy. The fact that reaction rate time dependence is determined explicitly by a simple empirical relationhip prompts an investigation of other kinetic models where reaction rate is similarly defined, albeit in a different time dependent form. It has been observed experimentally that the reaction rate decreases almost exponentially with time [Ulerich et al (1980), Dogu (1981)]. Lee and Georgakis (1981) modelled sorbent sulphation accordingly. Two sorbent-specific parameters were defined; the first is a sulphation time constant which gives a measure of sorbent reactivity, and incorporates diffusional limitations which are very much a function of calcine geometry; the second is a pore plugging constant, which describes the ability of a sorbent particle to accommodate sulphate product, and as such is related to the pore size distribution of the particle. This model was substantiated by the TGA data from Argonne National Laboratory [Vogel (1977)] for 10 different sorbents. Although the model provided a good fit to this data, the values of initial specific rate constant so derived were considerably lower than those reported by Fieldes (1979). This comparison is discussed in greater detail in Chapter 3.

Chang and Thodos (1984) followed a similar approach, but cast the reaction rate as a direct function of sorbent conversion (with its implicit time dependence), and expressed this rate as the product of two negative exponential terms with two generalised constants. This form of the rate expression was an attempt to overcome the inability of the model of Lee and Georgakis (1981) to predict the reaction rate at conversions in excess of 50%. Such an embellishment is of relevance only to dolomites, where a theoretical conversion of 100% is attainable. The ultimate conversion was shown to be related to the total intergranular surface and pore size distribution of the calcined sorbent, although the exact physical significance of the generalised constants is unclear.

In another approach, Zheng, Yates and Rowe (1982) modelled the sulphation reaction analogously to a first order catalytic deactivation process. This, too, gave an expression for sulphation rate which

reflected an exponential decrease with time. The model was described by two rate sorbent specific parameters - an initial surface rate constant, k_s, and a deactivation rate constant, k_d, which takes into account pore and product layer diffusion resistances.

As in Fieldes' model, here too the reaction parameters are determined by a simple batch sulphation experiment in a fluidised combustor. This model could be easily extended to account for combustion and fluid dynamics, and is used in Chapter 3 to discuss the performance of South African sorbents. Its development is outined below.

If the overall reaction rate is given by

$$Q = k_s \, C_a \, S \qquad 2.21$$

where C_a is the bulk SO_2 concentration, S is the available sorbent surface for reaction, whose loss over time is given by

$$S = S_o \exp(-k_d \, t) \qquad 2.22$$

Assuming furthermore that both solids and gas in the fluidised combustor are well mixed, then

$$C_{ao} \, V = C_a \, V + k_s \, C_a \, S_o \exp(-k_d \, t) \qquad 2.23$$

where V is the air flow rate to the combustor, and Ca_o is the base SO_2 level. Further manipulation gives

$$(C_{ao}/C_a) - 1 = 1/V \; k_s \; S_o \exp(-k_d \, t) \qquad 2.24$$

For a specific set of operating conditions, k_s and k_d can be found from the linearised version of eq. 2.24, noting that S_o is related to the batch mass, M, by $S_o = 6 \, M/(d_p \, \rho_s)$.

The true physical significance of the two kinetic parameters was not resolved, although they are known to carry both external mass transfer, pore diffusion and chemical significance.

2.3.6 Sulphation Models - Extension to Fluidised Combustion Part 2.

The incorporation of the above simplified sulphation models into a generalised fluidised combustor model is relatively straightforward, the overall sulphation rate being simply the integral of the individual rate over the range of particle residence times. Such an approach assumes that

1. combustion and sulphation are decoupled
2. the attendant assumptions of two phase flow with regard to gas mixing in particlulate and bubble phases apply
3. bed solids are well mixed
4. the size of sorbent particles does not change with time
5. freeboard sulphation is ignored.

Both Fieldes (1979) and Zheng et al (1982) followed this approach, effectively assuming a monosized sorbent population. Zheng et al used a mean residence time, given, for a well mixed system, simply by W/F_o, where F_o is the sorbent feed rate and W is the mass of bed solids. Fieldes defined particle residence time in terms of the time for pore closure, t_s.

Zheng et al defined an average reaction rate, Q_{avg}, over the whole fluidised combustor, in terms of a mean sorbent particle reactivity (again borrowing from catalytic deactivation theory).

$$Q_{avg} = \int k_s . C_a . S_o \; a \qquad 2.25$$

where $a = \exp(-k_d t) . 1/\tau \exp(-t/\tau) \, dt$, and τ is the mean residence time of sorbent particles in the bed.

The expression for average reaction rate reduces to

$$Q_{avg} = \frac{6 \; k_s \; C_a \; \tau \; F_o}{\rho_s d_p (1 + k_d \tau)} \left[1 - \exp -\left(\frac{t_s}{\tau} + k_d \; t_s\right)\right] \qquad 2.26$$

The bulk SO_2 concentration, C_a, is found from an SO_2 mass balance over the bed, for unit coal feed, i.e.

$$w_s/32 = A\ U_{mf}\ C_p + A(U-U_{mf})\ C_b + Q_{avg} \qquad 2.27$$

Furthermore, from continuity,

$$AUC_a = AU_{mf}C_p + A(U-U_{mf})C_b \qquad 2.28$$

Using the relationship between particulate and bubble phase SO_2 concentrations i.e. $C_b = C_p(1 - \exp-\underline{X})$, where $\underline{X}$ is the interphase exchange coefficient, given by eq. 2.9, and noting that, under normal operating conditions in a fluidised combustor, $\underline{X}$ is large, eqs. 2.27 and 2.28 reduce to

$$C_a = \frac{w_s/32}{AU\left[1 + \frac{6\ k_s\ \tau\ F_o}{\rho_s d_p(1 + k_d\tau)UA}\ \left[1 - \exp\left(\frac{-t_s}{\tau} + k_d\ t_s\right)\right]\right]} \qquad 2.29$$

The efficiency of sulphur retention is defined as

$$\eta = 1 - C_a/C_{ao} \qquad 2.30$$

If the release of SO_2 from coal is total, $C_{ao} = w_s/(32UA)$

The sulphation efficiency reduces to

$$\eta = 1 - \left[\frac{1}{1 + \frac{6\ k_s\ \tau\ F_o}{\rho_s d_p(1 + k_d\tau)\ UA}\ \left[1 - \exp\left(\frac{-t_s}{\tau} + k_d t_s\right)\right]}\right] \qquad 2.31$$

Zheng et al discounted the negative exponential term. The term F_o/UA (the ratio of sorbent to air flow rates) was recast in terms of R_{cs}, the calcium to sulphur molar ratio, which is the common design parameter against which sorbent performance is measured. Relating the air flow rate to coal flow via the excess air factor, x, gives

$$F_o/UA = 3.47\ \frac{0.21\ w_s\ \rho_A\ f_s\ R_{cs}}{32\ (w_c/12 + w_H/4 + w_s/32 + w_N/28 - w_o/32)\ (1+x)} \qquad 2.32$$

where the $w_{i\cdot s}$ are the mass fractions of coal constituents, f_s is the sorbent purity, and x is the fraction excess air.

It should be noted that the comparable expression proposed by Zheng at al is in error. Their original weighting factor was given as 2.5. This

should equal the ratio of sorbent to air molar masses, which is 3.47.

Substituting 2.32 into 2.31 , and dropping the negative exponential term, gives

$$\eta = 1 - 1/(1 + K R_{cs}) \qquad 2.33$$

where K, an overall sulphation constant, is given by

$$K = \frac{0.137\ k_s\ \tau \rho_A\ f_s}{\rho_s d_p (w_C/12 + w_H/4 + w_N/28 + w_S/32 - w_O/32)(1 + x)(1 + k_d\ \tau)} \qquad 2.34$$

The Zheng formalism is attractive because it gives directly the amount of sorbent required to effect a specified reduction in flue gas SO_2 levels. The parameters, k_s and k_d, are constant for a specific sorbent under a given set of combustor operating conditions. As such, this model lends itself to use in the assessment of a wide range of sorbents. The authors restricted their evaluation of the model to the action of one U.K. limestone sample which appeared to display moderate sulphation capability. This model's description of sulphation kinetics is presented in Chapter 3 for several South African sorbents. Results of the overall model (given by eq. 2.33), applied to three South African sorbents in a 10 MW FBC, are presented in Chapter 7.

The principal limitation of this model is its restriction to a monosized, time invariant, sorbent population. This is examined further in Chapter 6.

A more comprehensive fluidised combustor model which considers sorbent feed size distribution and freeboard sulphation has been proposed by Dennis (1985). The specific reaction rate expression corresponded to that proposed by Dennis and Hayhurst (1986b) and given by eq. 2.12. Sorbent attrition was not considered. Elutriation was modelled by the empirical correlation proposed by Wen and Chen (1982).

The complexity of the model which accounts for freeboard sulphation does not appear to be warranted. When sulphation data generated by Wright (1979) were fitted to this complex model, and to a simplified version in which a monosized feed distribution, with no fines, was considered, differences between the two models could be discerned only at R_{cs} values

in excess of 1.5. At $R_{Ca} = 2$, the difference in the two model predictions was comparable to their overshoot of the experimental value. This is consistent with other models which consider freeboard sulphation. Fee et al (1984) found that the contribution of freeboard sulphation to overall sulphur retention was in the region of 8% only. Dennis concluded that fines do not contribute significantly to sulphur removal because of their very short residence time in the bed. The entrainment of coarse particles lowers overall sorbent utility because of the slower reaction rate in the freeboard (lower SO_2 concentration).

As stated above, this model does not consider sorbent attrition. It is anticipated that, if attrition is significant, the interplay between fines generation / elutriation and the renewal of "fresh" sorbent surface by paring away of the sulphate layer, will be complex, and, depending on the relative magnitudes of sulphation time and particle residence time, may lead to either an enhancement of, or a decrease in, sorbent utility. Dennis claims that the lack of substantive attrition rate data precludes its inclusion in an overall sulphation model. This question is approached in Chapter 6.

2.4 Conclusions

The complexity of diffusion models for sulphation of porous sorbent particles effectively precludes their use in an overall model of sulphation in a fluidised combustor.

The simplicity of several reviewed kinetic models is attractive. There is little loss of physical significance. The specific rate constant(s), measured by simple batch experiment, possess both chemical and mass transfer components, and allow for pore and product layer diffusional resistance.

A simple experimental technique from which to derive sulphation rate data in a fluidised bed environment was reviewed. The ability of this technique to incorporate coal combustion, and the ease with which rate data are collected are seen as major advantages over TGA or differential reactor studies.

Sorbent performance is very much a function of its physical properties.

There exists a requirement to evaluate the performance of a selected sorbent by simple batch addition tests.

Experimental observations of sulphation showed that, for sorbent particles in the size range typical of fluidised combustion, sorbent utility was low due to the formation of a dense layer of sulphate product in close proximity to the external particle surface. This was confirmed by a wide range of models.

A largely unexplored aspect of sorbent performance is the impact of attrition on utility. Attrition rate data are required to establish the particle size distribution and hence residence time distribution of sorbents within a fluidised combustor.

CHAPTER 3 - SULPHATION KINETICS OF SOUTH AFRICAN SORBENTS

3.1 INTRODUCTION

It was established in Chapter 2 that the sulphation kinetics of a specific calcareous sorbent could be determined with confidence by simple batch additions to a fluidised combustor fired on coal. It was also stressed that the physical properties of both the natural sorbent, and its calcine, played major roles in dictating sorbent performance under a specified set of combustor operating conditions. In this chapter, the extent to which sorbent specificity dictates fluidised bed sulphation kinetics is addressed for a wide range of South African sorbents whose use is anticipated in new coal fired power plant.

Thereafter, a comparison is made between the simplified kinetic models of Fieldes (1979) and Zheng et al (1982) discussed in Chapter 2, using data derived as above. The performance of South African sorbents is compared with data generated by both TGA and fluidised bed studies for UK and USA sorbents.

3.2 EQUIPMENT CONFIGURATION

The fluidised combustor in which batch sulphation experiments were conducted was built "in-house", and its detailed mechanical design, and that of ancillary feed systems and dust control equipment have been reported elsewhere [Motherwell (1986)]. An abridged description is given below.

The combustor vessel is a 316L stainless steel pipe, 104 mm in diameter and 1.5 m in length, encased in a castable refractory to an external diameter of 300 mm. Between the wall of the combustor and the interior of the refractory lining is a 50 mm annular section through which cooling air is blown by a small centrifugal fan to control bed temperature.

Fluidising air is supplied by a Roots blower. The air distributor plate consists of a series of 6 mm I.D nozzles (closed at the top) screwed

into the base plate of the combustor tube, on a triangular pitch of 15 mm. Four 1.5 mm diameter holes were drilled near the top of each nozzle to achieve the distrubutor pressure drop required for adequate fluidisation.

The combustor vessel is heated by a 3 kW nichrome element wound to the outside of the combustor tube. The power supply to this resistive element is controlled by a 25 amp variable voltage transformer. Both coal and limestone, previously crushed and prescreened to the desired size range, were fed pneumatically to the combustor at the height of the distributor plate. The coal feeder was calibrated by diverting the pneumatic flow line to a measuring cylinder sitting atop a Mettler pan balance. During normal operation, this technique was supplemented by observing the volumetric flow of coal through a glass tube immediately below the feed container. Bulk density measurements were taken at regular intervals. Solids removal from the combustor vessel (to maintain bed height) was effected via an ash discharge port centrally located in the distributor plate. Medium and high efficiency cyclones removed particulate from flue gases before these were discharged to atmosphere. No provision was made for fines recycle to the combustor.

The combustor was extensively instrumented with type K thermocouples and pressure tapping points to which 0-25 kPa pressure transducers were fitted. All temperature and pressure signals were logged by a multipoint recorder.

All gas analyses were conducted on flue gas samples extracted from the primary cyclone inlet line. It was assumed that the ducting geometry was sufficient to ensure a well mixed sample volume at the draw-off point. Sample lines were 6 mm stainless steel tubing. The length of sample probe exposed to high temperatures was restricted to 150 mm in order to minimise SO_2 conversion to SO_3 on the hot stainless steel surfaces. Gas sample conditioning included two stage drying (via a polymer drier, supplied by PermaPure, Farmingdale, N.J. U.S.A. and condensate removal via a custom-built refridgeration chamber) as well as particulate removal - a coarse glass wool filter in series with a 5 μm Balston cartridge filter. The sample lines were trace heated with electrical heating tape to a point immediately upstream of the refridgeration unit. All analytical instruments were supplied by Smith-Kline-Beckman, U.S.A.

Flue gas oxygen was measured with the aid of a polarographic analyser (Model No. 7003); carbon monoxide, carbon dioxide and total hydrocarbons from a combined non-dispersive infra red analyser (Model No. 591, operating ranges 0-1%, 0-15%, 0-2000 ppm respectively); NO/NO_x with a chemiluminescence analyser (model No. 955, operating ranges 0-10000 ppm); SO_2 with a non dispersive infra red analyser (model No.865, operating range 0-2500 ppm) . Output signals from all analysers were, after suitable amplification, fed to another multipoint recorder. With the exception of the O_2 analyser, which was calibrated on dry air, all other analytical instruments were calibrated with bottled gases metered through rotameters. A constant flowrate of 1.5 litres/minute sample gas to the analyser bank was achieved with a small positive displacement metering pump.

A schematic layout of equipment is given in Figure 3.1

3.3 MATERIALS

The coal used for all the batch sulphation tests was a poor quality discard coal from Ballengeigh Colliery, South Africa. Its composition is given in TABLE 3.1. Such a coal is typical of the vast quantities of discard material currently being stockpiled in South Africa. Its generation is a consequence of coal beneficiation practice. The sulphur composition is not abnormally high (some other discard coals tested in the preliminary stages of this project, but not reported here, had sulphur content in the region 8-10%), but, under normal combustion conditions, it gave rise to reasonable SO_2 levels, which were in the range of the Beckman SO_2 monitor, thus avoiding unnecessary flue gas dilution. This coal sample was crushed and screened from a top size greater than 50 mm to produce a workable fraction of -2 mm + 0,5 mm.

The sixteen sorbents used in this investigation are listed in TABLE 3.2, with compositional details. The "as-received" samples varied considerably in size distribution. In no case was it possible to obtain an ideal narrow size fraction directly from the suppliers. The products most suited to this investigation in terms of size classification, were agricultural limestones (typically - 2 mm) and metallurgical fluxing agents (typically - 5 mm). On receipt of samples, all sorbents were screened to -0,6 mm +0,3 mm by a mechanical sieve-shaker prior to their

addition to the combustor.

The inert fluidising medium was a high purity filter sand, grade 16/30, whose size distribution is given in TABLE 3.3

3.4 EXPERIMENTAL PROCEDURE

The bed was filled with sand to a static height of 200 mm and the electrical element switched on. The total air flow to the combustor was the sum of the coal conveying air and that supplied through the distributor by the Roots blower. Air flow through the distributor plate was regulated by a globe control valve upstream of the measurement orifice, to give the total required flow of 0.7 ms^{-1} at 1123 K. This corresponded to a fluidising velocity approximately equal to four times the minimum fluidising value for this size sand at this temperature, as predicted by the modified Ergun equation cited by Yates (1983), and by the experimental correlation of Kunii and Levenspiel (1969). These correlations were validated by a graphical plot of bed pressure drop versus velocity at ambient temperature. Although an operating velocity of 0.7 ms^{-1} failed the slugging flow criterion of Stewart and Davidson (1967), a prediction of bubble diameter at a bed height of 200 mm (according to Mori and Wen (1975)) inferred that the maximum bubble size which would develop was in the region of 40 mm, which is considerably less than the combustor vessel diameter (104 mm). It was therefore assumed that slugging tendency was minimal. This was reinforced by the lack of mechanical vibration, which became severe only when the fluidising velocity was increased beyond 1 ms^{-1}.

When the average of the two thermocouples in the bed registered 820 K, coal flow was initiated. Once the temperature reached 970 K, the process was deemed to be self sustaining, and power to the electrical element was switched off. The desired temperature (of 1123 K) and excess air level (of 20%) were achieved by adjusting coal flow and trimming the cooling air supply to the annular section of the combustor unit. Coal flow, bed temperature, flue gas oxygen and sulphur dioxide were monitored continuously. Deviation from smooth operation could be detected further by periodic monitoring of flue gas CO and CO_2 levels. Once stable operating conditions were achieved, a 15 gram sample of uncalcined sorbent was blown into the combustion chamber at the height

of the distributor nozzles, and the change in SO_2 level noted. The reaction was assumed to be complete when the SO_2 level steadied for 20 minutes at a value approximately equal to the base measurement prior to limestone addition. The next sample could be added once the calibration of the SO_2 analyser was checked.

3.5 RESULTS

The following general points pertain to these batch sulphation trials.

1. The total system reponse (analyser plus lag time due to volume of flue gas in sample tubing) is in the region of 15 seconds. The sampling system is treated as a plug flow section in series with the fluidised combustor (itself modelled as a pseudo-homogenous stirred tank reactor, with SO_2 liberated uniformly throughout the bed). This flow behaviour stems from the fact that the interphase exchange coefficient for this combustor unit is large (see APPENDIX B.1, based on eq. 2.9). Time response data for all sorbents are offset by this 15 second lag time.

2. The temperature was treated as being uniform throughout the bed region of the combustion chamber - the two thermocouples within the bed differed by typically 10 -15 degrees - which supports the claim that solids are well mixed. The temperature of the flue gases at the sampling point was in the region of 870 K, which implies that freeboard combustion was negligible. This is consistent with operation at the low fluidising velocity where elutriation losses are low. The subject of elutriation from fluidised beds is discussed in greater detail in Chapter 5, which looks at particle size effects.

3. Combustion efficiencies, measured from carbon-in-ash figures, according to BS 1016. part 3, 1973, were in the region of 90%. This figure is realistic for this scale of apparatus and the low reactivity of the coal burned. This gave base flue gas SO_2 levels in the range 1000-1500 ppm. No attempt was made, during these experiments, to measure the effect of SO_2 adsorption by calcium present in the coal ash (CaO present in coal ash fraction is 3.62 %). There is good reason, with high ash coals, to suspect that such a sulphur capture mechanism is not unimportant, and this is the subject of further investigation in the analysis of pilot plant data in Chapter 7.

A typical flue gas SO_2 response curve to sorbent addition, allowing for measurement lag time, is given in FIGURE 3.2. Data are plotted as SO_2 concentration (ppm) against time. This curve was similar in form to those generated by both Fieldes (1979) and Zheng et al (1982). There is one marked difference, however, over the results of Fieldes. Sorbent particles are firstly calcined over a short, but finite, time period. Because of the distribution in particle size in the sorbent charge, some particles will calcine before others, and, during this initial period, the sulphation reaction rate will rise from zero to its maximum value immediately the entire batch of particles is fully calcined. After this time, the initially high reaction rate decreases monotonically. Fieldes (1979) presented results from a gas mixture experiment in which the measured concentration of SO_2 fell instantly to a minimum, which effectively implied instantaneous calcination. In a coal combustion atmosphere, however, the presence of CO_2 in the flue gas will retard calcination to some extent (see APPENDIX A), which accounts for the more gradual decrease in SO_2 level found in these experiments, and in those reported by Zheng et al (1982). From the composition of the coal used in the current set of tests, and for a typical coal flow of 0.7 kg/hr, the CO_2 level in the flue gas is around 10%. In the local region of the coal injection point, this value is expected to be higher. It is into this region that the sorbent batches were added.

Fieldes (1979) required that each sample charge to the reactor be of constant surface area. Given the obvious topography (non sphericity) of sorbent particles as evidenced by the electron micrograph images in APPENDIX D, and the difficulty in accurately determining mean sorbent particle size without resorting to elaborate techniques such as image analysis, the interpretation of sulphation kinetics based on the addition of a constant mass of sorbent particles appeared to offer a much simpler approach. Assuming spherical particles, which can be described by an arithmetic mean diameter, the approximate external surface area of each sorbent charge was 730 cm^2. This is a factor of 3.5 times that used by Fieldes, but approximately 0.75 that employed by Zheng et al. The size of the sorbent charge in this work was necessary to ensure good mixing within the bed bulk (bed height to diameter in this work was 2:1 compared with 1:1 in the case of Zheng et al and 0.7:1 in the work of Fieldes).

to the same classification would behave similarly. This is discussed further in Chapter 4, under the influence of sorbent geology.

The ultimate conversion, X_∞, given by eq. 2.6., with $t = t_s$, is proportional to the shaded area in Figure 3.2. This integration was performed numerically for the Lyttelton, Marble Hall and Bredasdorp sorbent samples. The dry flue gas molar flow was calculated for a flue gas O_2 level of 4%. A sample calculation is given in APPENDIX B.2. Type A (Lyttelton) sorbents have the lowest capacity for SO_2, whilst Type C (Bredasdorp) sorbents have the greatest absorptive capacity. The difference in utility of these three sorbents is considerable. The ultimate conversion of the Lyttelton sample was measured at 15.5%, of the Marble Hall sample at 23.7%, and of the Bredasdorp sample at 32.5%. Of interest was the fact that the maximum conversion attained for the Bredasdorp sample, which was the most reactive, was considerably lower than the theoretically attainable maximum of 57%. The utility of the Lyttelton sample ran contrary to the expected trend in dolomites, where pore volume created by calcination of $MgCO_3$ should be available to accommodate $CaSO_4$ product. This confirms the importance of particle pore size distribution in defining sorbent performance.

If sorbent utility was governed largely by chemical purity, then the Marble Hall sample should prove to be a more reactive material than the sample from Bredasdorp. This is clearly not so. Furthermore, a qualitative examination showed that the difference in surface texture across all three samples was pronounced, with the more reactive sorbents tending also to be the more friable. This is consisitent with one of the proposed mechanisms of attrition, where, in those cases where particle residence time exceeds sulphation time, the wearing away of the sulphate product layer in the region of the external particle surface will lead to enhanced utility.

It would thus appear that the physical properties of the natural sorbents exert considerable influence on sorbent performance. This theme is developed further in Chapters 4 and 5.

0.11-0.15 ms^{-1}, which is, for practical purposes, effectively constant. However, with no apriori knowledge of sorbent performance, it is unwise to assume that k_s, or K_{so}, is constant for a given set of combustor operation parameters. A point worthy of note is that Fieldes' conclusion was based on sulphation experiments with a simulated flue gas. It could be argued that calcination conditions will differ when coal combustion is taking place, and that this may, for selected sorbents, drastically influence the evolving porosity of the calcine. A discussion on porosity of natural sorbents and their calcines is held over to Chapter 4.

A comparison of Fieldes and Zheng models is given in Figures 3.5 - 3.7 for Lyttelton, Marble Hall and Bredasdorp sorbents respectively. The reaction rate constant, K_s is plotted against conversion. Note that, in the model of Zheng et al, $K_s = K_{so} \exp(- k_d.t)$. Experimental values of K_s are derived from the bubbling bed model. The value of K_{so} used in the Zheng model is that measured, assuming the combustor to be a well mixed vessel, whereas K_{so} in the Fieldes model is predicted from the Penrith limestone data set.

For both the Lyttelton and Marble Hall samples, there is good agreement between both models in the value of K_{so}. This is not so of the Bredasdorp sample, where the Fieldes model underestimates K_{so} by a factor of 3. In all cases the Fieldes model overpredicts the maximum sorbent conversion, X_m. This is a consequence of the exceedingly long pore closure time, t_s, predicted by the model. In all batch experiments with South African sorbents, flue gas SO_2 readings returned to their value prior to sorbent addition in less than one hour, which would imply that typical pore closure times were in the region of 3600 seconds. An example of a calculation for t_s given in Appendix B predicts t_s values typically a factor of 10 times greater than those measured. It is surmised that the pore geometry / pore plugging criteria employed by this model do not correspond to calcine structures developed in a coal combustion atmosphere. The relationship between porosity, pore volume and sorbent performance is discussed in Chapter 4.

The choice of gas flow model for predicting K_s values from flue gas SO_2 levels is critical for the Bredasdorp sample. Figure 3.8 shows this effect clearly. At low conversions, a well-mixed gas flow model, in which $K_s = (AU/S)(y_o^*/y_o - 1)$ predicts similar K_s values to those derived

from a bubbling bed model. K_s values predicted by assuming gas to be in plug flow, with an absence of bubbles,
i.e. where $K_s = (AU/S)(-\ln y_o/y_o^*)$, are significantly lower than either of the other gas flow models. Fieldes correctly stated that, in a gas injection experiment, there is little difference between K_s values derived from any of the three gas flow models considered here. However, in a coal combustion experiment, where SO_2 is released uniformly throughout the bed, a plug flow gas model would produce erroneous results. In the case of the Lyttelton and Marble Hall samples, where the relative magnitudes of y_o/y_o^* and $1/\underline{X}$ in eq. 2.8, particularly at low conversions, differ more than they do for the Bredasdorp sample, errors incurred in assuming plug flow of gas are less severe.

Figure 3.9 is an overlay of Figures 3.7 and 3.8 and summarises the discussion above. At the combustion conditions employed here, the bubbling bed model is more closely approximated by a well mixed single phase gas model than by a plug flow model. Overall, the well mixed flow model of Zheng et al, in which the reaction rate is modelled by an exponentially decreasing time-dependence, more closely resembles the sulphation kinetics of South African sorbents than does the model of Fieldes.

The effect of fluidising velocity on sulphation kinetics was demonstrated by Zheng et al, where, for an increase in fluidising velocity from $U/U_{mf} = 2$, to $U/U_{mf} = 3.5$, the value of K_{so} increased by a factor of 3. The effect on k_d was less pronounced - k_d increased by a factor of 1.5. The true physical significance of k_d is unclear, other than that it incorporates chemical and diffusional influences. It is, however, a simple matter to resolve K_{so} into an external mass transfer component, k_g, and a kinetic/diffusion component, K_{wo}, according to eq. 2.17. Dennis and Fieldes(1986) determined that external mass transfer was significant at early reaction times, and we would thus expect to see a marked change in K_{so} with fluidising velocity. Since the sulphation kinetics of South African sorbents was established for one fluidising velocity only ($U/U_{mf} = 4$), a discussion of its exact effect on sulphation propensity is held over until Chapter 7, where continuous sulphation trials for three sorbents over a range of fluidising velocities are described.

3.7 COMPARISON OF SOUTH AFRICAN SORBENTS WITH INTERNATIONAL STANDARDS

The sulphation performance of the three representative South African sorbents is shown in TABLE 3.5 along with the fluid bed results of Fieldes (1979) and two USA studies. The first USA study concerns the Argonne Laboratory TGA data of Vogel et al (1977) for 10 sorbents. The second USA study relates to the performance of five limestones in a fluidised combustor at Westinghouse Research Laboratories [Ulerich et al (1980)].

The Westinghouse samples (mean d_p = 1 mm) were precalcined at 1088 K in a 15% CO_2 atmosphere, before sulphation at the same temperature. Maximum sorbent conversions were found by graphical extrapolation of sulphation data. Values of X_∞ thus derived ranged from 0.14 - 0.25, which are in the range found for most of the South African sorbents, and for the two limestones tested by Fieldes. The low values of K_{so} stem from the fact that particle sizes are larger, and also that calcines were preserved at 1088 K for four hours prior to sulphation. This prolonged exposure to high temperatures is known to result in a loss of pore volume due to sintering of the calcines.

The Argonne data reflects a wide range in sulphation capacities, from the almost total conversion of the reactive Tymochtee dolomite (X_∞ = 0.97), to a low of X_∞ = 0.15 for Limestone 1359 and Dolowhite. Initial rate constants were predicted from the Lee and Georgakis (1981) manipulation of this TGA data set (see APPENDIX B.3). K_{so} values derived from TGA data were considerably lower than those reported for any of the fluid bed studies. This is consistent with results reported by Ulerich et al (1980) for parallel TGA studies on the same group of five limestones whose fluid bed sulphation capabilities are reported in TABLE 3.5. Ulerich et al (1980) reported also that a well mixed gas flow model was a better predictor of sorbent sulphation in a combustion atmosphere than a plug flow model, which reinforces the points made earlier from a comparison of the models of Fieldes and Zheng et al.

Of interest is that Fieldes reported a considerably lower value for X_∞ of Tymochtee dolomite (0.802) than was derived from the TGA figure (0.97) although the latter was for slightly larger particles. This is

inconsistent with the model findings of Chapter 2 in which X_m varies as d_p^{-1}, and cannot be explained entirely by the fact that the TGA data was collected at the slightly elevated temperature of 1173 K.

From TABLE 3.5 it can be seen that South African sorbents generally display intermediate reactivity when compared to international "standards". None of these "standards" display K_{so} values as high as the South African Bredasdorp sample. This sample, however, is not unique. From TABLE 3.4, three other samples were identified as displaying Type C activity. Both Saldanha and Slurry limestones and Umzimkulu dolomite have K_{so} values in excess of 0.25 ms^{-1} and k_d values less than 0.0026 s^{-1}.

It was stated in Chapter 2 that the physical properties of a sorbent exert considerable influence on its sulphation propensity. Surface area, pore volume and pore size distribution were highlighted. It was noted in the current batch sulphation tests that other physical properties such as topography, granularity, and "friability" appear to also affect sulphation rate and capacity. These latter properties relate to the geology of the parent sorbent body. Their significance has come to light mainly through the selection of sorbents of widely varying geologic typing, and could well have gone unnoticed in a smaller data sample (as evidenced by the fact that half of the 16 sorbents examined produced similar sulphation kinetics, as in the work of Fieldes). Chapter 4 is thus devoted to an analysis of sorbent physical properties in the hope of drawing a correspondence between sorbent geology and sulphation propensity.

3.8 EFFECT OF CATALYTIC AGENTS ON SULPHATION

The simplicity of batch addition sulphation tests described above prompted a similar investigation of sorbents chemically modified by catalytic action. The chemical modification of sorbents is not a new idea. Marier and Ingraham (1972) highlighted a 30-40% increase in the sulphation capacity of a specific precalcined lime when 5% Fe_2O_3 was mixed integrally with the lime powder. Desai and Yang (1983) pinpointed the optimum amount of Fe2O3 for maximum sulphation. For a particular dolomitic sorbent, which had previously been shown by Borgwardt and Harvey (1972) to achieve high sulphation yields, an addition of iron

oxide, at 1% by weight of CaO, produced a 40% reduction in sorbent requirement over the uncatalysed case, whilst effecting a sulphur removal efficiency of 90%. Increasing the amount of iron oxide beyond this level served to increase the initial rate of reaction, although the overall capacity of the sorbent was reduced, in some cases even to a level below the uncatalysed case. Of interest is that these findings were not duplicated with a test limestone, and both the rate and capacity were decreased by the addition of iron oxide. This discrepancy is attributed to the pore size distribution of the test sorbents: it is surmised that, for sorbents with a high percentage of pores less than 0.5 μm in diameter, impregnation with iron oxide serves to block the pores directly. The initial sulphation rate constant increased linearly with iron oxide addition, up to an Fe_2O_3 concentration of about 1%, whereafter the dependence was much less acute.

Addition of an aqeous solution of a sodium salt (as promotor) served to increase both the sulphation rate and capacity of the same dolomite. This is consistent with findings of Burdett (1983) who stated that the addition of small amounts of sodium salts to a calcining limestone enhance its subsequent sulphation capacity by forming transient eutectic melts, increasing ionic diffusion rates, and accelerating the rearrangement of CaO molecules as CO2 is evolved. Small grains with relatively large pores are produced in this manner.

A more recent and comprehensive study of the effect of additives on sorbent performance was conducted by Dennis (1985). Addition of 2.8 mol% Na_2CO_3 to Penrith limestone increased sorbent capacity from 24% to 29%. Increasing Na_2CO_3 content to 4.7 mol% improves sorbent utility further to 36%. In no case was the initial rate constant K_{s_o} affected. Similar treatment with oxidised $Fe(NO_3)_3$ produced a decrease in X_{∞} from 24% to 18%. Again, K_{s_o} was unchanged.

The mechanism whereby iron and sodium salts act on calcareous sorbents is fundamentally different. Whereas the action of the former is inherently chemical in nature (often cited as an enhancement in rate of SO_2 oxidation to SO_3), the latter modifies pore structure, shifting the pore size distribution to wider mean pore size. However, the variation in reaction patterns exibited by selected sorbents on Fe_2O_3 addition points to a complicated reaction mechanism in which pore structure plays

a major role.

It is not the intention of this work to unravel this reaction mechanism, but rather simply to investigate the addition of iron and sodium salts to one of the least reactive South African sorbents and to reassess its sulphation propensity. The logic behind such an exercise is straightforward. Much of South Africa's coal reserves are in a region traversed by dolomitic rocks (eg. Lyttelton) which belong to the least reactive class of sorbents, i.e. Type A, whereas the more reactive sorbents such as Bredasdorp are physically remote (> 1000 km) from most coal fired combustion plant. The costs of transport are high and there is a need to identify ways of improving the utility of the Type A sorbents.

3.8.1. Experimental

Batch addition of treated Lyttelton sorbent followed the same basic procedure as outlined in Section 3.4. Sorbent batches were first soaked in a 1 M solution of iron(III) nitrate for a predetermined length of time (ranging from 10 to 60 minutes). Samples were then filtered and dried before oxidation at 770 K for a period of one hour. At this temperature, the retained nitrate is readily oxidised, but little calcination of the sorbent takes place. Another series of experiments, in which 1% sodium carbonate was added to the iron(III) nitrate solution before oxidation, were conducted in parallel. From the change in mass of the sample before and after oxidation, the amount of iron oxide retained by the sorbent was established. This quantity is given in TABLE 3.6, showing the correspondence with initial soaking time.

3.8.2 Results

The initial reaction rate constant, K_{so}, and ultimate sorbent conversion, X_{∞}, are displayed in TABLE 3.6 for each of the different sorbent treatments. In all cases, the addition of Fe_2O_3 led to a reduction in the ultimate sulphation capacity of the Lyttelton sample over the base case. The initial rate constant K_{so} also decreased, although the addition of 1% Na_2CO_3 seemed to improve K_{so} over the values found for Fe_2O_3, though not to the level of the base sulphation case with no additives. The effect of increasing the dosage of iron salt on

both X_∞ or $K_{s\infty}$ was minimal.

These results are consistent with the effect of iron oxide addition to to Penrith limestone, as noted by Dennis (1985). The mean pore diameter of the Lyttelton calcine, prepared in a parallel fluidisation at 1123 K for 2 hours, is 0.26 μm, which is below that value cited by Desai and Yang (35) as being necessary for iron catalysis to be effective. The potentially beneficial effect of sodium salt addition is obscured by the negative effect of iron oxide. The decrease in initial reaction rate constant is attributed to the deposition of iron oxide in pore mouths, leading to an effective decrease in the base porosity of the calcine.

It would appear that, for chemical addition to be effective in increasing the performance of a particular sorbent, careful attention must be paid to the porosity of the natural sorbent, and to that developed through calcination. Because the effect of additives on the sulphation of the Lyttelton sample was disappointing, it was not pursued further. However, in Chapter 4, the pore volume, porosity, and pore size distribution of all the South African sorbents are identified, and suggestions made regarding possible sorbents which would benefit from chemical doping.

3.9 CONCLUSIONS

The sulphation kinetics of a wide range of sorbents were determined by batch addition of the material to a fluidised bed combustor. In this way, the influence of the combustion atmosphere could be measured directly, and sorbent precalcination was not a necessary pre-requisite.

Two simple sulphation models were fitted to the kinetic data. A better degree of correspondence was obtained with one which assumed the contents of the reactor to be well mixed, and in which the time dependence of reaction rate was stated explicitly as a decreasing exponential.

Sorbent type greatly affects sulphation performance. The total group of South African sorbents could be divided into three classes according to their sulphation propensity, which was quantified by the magnitude of the specific sulphation reaction rate. Contrary to present

understanding, the initial sulphation rate was not independent of sorbent type. Properties such as topography, granularity, and friability were observed to play a role.

South African sorbents generally display intermediate reactivity compared to their UK and USA counterparts.

The performance of a representative sorbent from the "low reactivity" class was not enhanced by addition of sodium or iron salts.

CHAPTER 4 - CHARACTERISATION OF SOUTH AFRICAN SORBENTS

It is evident from the previous discussion that there is tremendous variability in the performance of different sorbents. As outlined in Chapter 1, one focus of this research is to quantify the behaviour of South African sorbents. Before embarking on an analysis of sorbent properties and their effect on sulphation, it is expedient to summarise the local resource base, and to characterise both the quality and quantity of this resource according to standard geologic classifications. This is undertaken in APPENDIX C. The sorbent samples whose sulphation kinetics were measured in Chapter 3 were drawn from 16 operational quarries dispersed throughout the country. Although experimental observation is limited to this group of 16 sorbents, a comparison is made, where possible, with the properties of other sorbents for which significant performance data are available.

4.1 CHEMICAL PROPERTIES OF SORBENT BASE

The chemical composition of these sorbent samples is reflected in TABLE 3.2. Eight of the samples can be labelled calcitic, whilst the remaining eight are dolomitic. The average calcium carbonate content of the limestones is 90.7 % whereas that of the dolomites is 51.9 %. On an overall mass basis, these figures imply maximum attainable sorbent conversions of 51.7% for the limestone samples and 51.9% for dolomitic samples, though the theoretical utility of calcium in a dolomitic sample is 100%. Of interest is the wide range in impurities reflected in this table. Attempts to identify absolutely the relationship between chemical composition and sorbent efficacy have generally been unsuccessful [Ulerich et al (1979)]. Iron, sodium and potassium often have positive effects on the sulphation capacity of calcareous rocks, although this was not borne out by the addition of iron and sodium salts to the Lyttelton sample, as reported in Chapter 3. All the samples from the northern part of the country contain iron (as Fe_2O_3) in the region of 1 %. This contrasts markedly with the coastal deposits, and those of the South Western Cape, where iron content as low as 0.06 % is reported. Silica is generally perceived as being deleterious to sulphation. Within the South African data set, the silica content varies from a low of

0.05 % for the very pure Holrivier calcite sample, to a high of 13.4 % for the Leo dolomite sample. Howéver, at temperatures typical of fluidized combustion operation, chemical bonding of silica with calcium oxide would appear not to pose a problem. As with those sorbents with high clay content (reflected by alumina values in TABLE 3.2), it is surmised that the action of silica is simply one of pore blockage. Other interesting anomalies are the abnormaly high phosphate concentration in the Saldanha sample, and the high alumina concentration in the Leo, Slurry, and Lichtenburg deposits. It has been mooted [Rudman (1987)] that P_2O_5, deposited at grain boundaries, can cause severe decrepitation under thermal stress. The presence of even minute quantities of sulphur, too, is reported to lead to decrepitation by evolution of hydrogen sulphide during calcination [Schie (1987)]. The sample from Holrivier has been reported to calcine explosively due to this mechanism.

Chemical impurities in geologically recent carbonates are often present in the form of calcareous "muds" and other plastic components which deposit at grain boundaries and in large pores, and, although effective in reducing the inherent porosity of the natural stone, generally contribute favourably to the quality of the calcine produced on thermal treating. This is in contrast to the effect of silica and other impurities present in well-formed crystals. There is evidence, too, that some of the samples, such as that from Umzimkulu, contain small gas pockets (presumably trapped at formation stage as the result of organic decomposition) which affect the overall structure of prepared calcines, due to gaseous evolution at a rate not explicitly dependent on the CO_2 atmosphere [Schie (1987)].

There is no correspondence between sorbent purity and geologic age, only that the type of impurities tend to change with age. Young sediments of marine origin, although relatively impure, may contain local regions of shelly deposits which are effectively pure calcite. Older sorbents generally carry dolomitic inclusions.

4.2 SORBENT PHYSICAL PROPERTIES

The findings of Chapters 2 and 3 infer that, within the general classification of limestones and dolomites, it is the physical, rather than chemical properties of sorbents which affect their sulphation capacity, and that any chemical influences result principally in changes to the physical structure of the sorbent. Those physical properties which are expected to play a role in the sulphation reaction are those which directly (or indirectly) influence the porosity and surface area of the calcined product, the character of which has been shown in the previous chapters to be highly significant in determining both the rate of reaction and the capacity of a particular sorbent for SO_2 absorption.

Physical properties of interest are therefore -

a). sorbent particle size

b). surface area and pore size distribution

c). sorbent granularity and degree of crystallinity

d). sorbent particle topography

e). sorbent structural strength.

4.2.1. Particle Size

The choice of sorbent particle size in fluidized combustion is dictated largely by factors other than sulphation efficacy. Bed hydrodynamics affect the quality of fluidization, and the degree of entrainment and elutriation. Particle size is selected to optimise retention times in the combustor. Mechanical considerations too, such as feeder arrangement, lead to the use of preselected of size ranges. Furthermore, the costs of screening quarried material to a narrow size fraction are considerable - most limestone quarries are dedicated to a specific end use, such as cement manufacture, and are not capable, without sufficient financial incentive, of modifying their process to produce the ideal sorbent feed.

As a result, most sorbent feed to fluidized combustors is loosely sized from a few hundred microns to about 2 millimeters. In this current investigation, most of the experimental results were obtained for a much narrower size fraction, 300 - 600 μm. When particle size effects were measured directly, other closely sized ranges were examined. None of the "as received" sorbent samples conformed to these size specifications, and both wet and dry sieving was required to produce the desired fraction.

4.2.2 Pore Structure / Surface Area / Porosity

Borgwardt and Harvey (1972) demonstrated experimentally that the pore size distribution, porosity and surface area of calcined sorbents interact in a complex manner to determine overall sulphation capacity. The importance of natural sorbent porosity was also highlighted. It is well established, however, that natural sorbents are generally non porous compared to their calcines prepared under conditions typical of fluidised combustion. Both Ulerich et al (1979) and Borgwardt and Harvey (1972) cite pore volumes of natural sorbents in the range 0.01 - 0.04 cm^3/g and calcine pore volumes in the region of 0.25 - 0.4 cm^3/g. The one exception to these figures was a friable marl examined by Borgwardt and Harvey. As this is an unlikely candidate for use in fluidised combustion, the above pore volume ranges can be thought of as generalised values.

An attempt was made to see how well these measurements were matched by the South African sorbent stock. Given the anticipated low pore volumes of the natural sorbent samples, the initial focus on sorbent specificity was restricted to an analysis of calcine properties. Pore volumes / pore size distributions of sorbent calcines were measured by mercury intrusion porosimetry. Calcines were firstly prepared at 1170 K for 4 hours in a laboratory muffle furnace. Surface areas were calculated by the method outlined by Lowell (1979), assuming that all pores are cylindrical. Mean pore radii were calculated from pore volume distribution curves, a typical example of which is given in FIGURE 4.1, for the Bredasdorp sample. TABLE 4.1 presents values for unit pore volume, unit surface area and mean pore radii for the calcines of all 16 samples. The range of calcine pore volumes measured is wider than that cited above, spanning 0.06 cm^3/g - 0.6 cm^3/g. Two points are worth

noting about these values.

1. The Leo dolomite sample had a mean particle size of 100 μm, as opposed to 450 μm for all the other samples. A severe limitation of the mercury intrusion technique for determining pore volume is that, in small particles which are relatively non-porous, low pressure intrusion cannot resolve inter particle void spaces and large pores, leading to erroneously large pore volume measurement. This is consistent with the relatively large mean pore size reported for Leo dolomite. Like all the other dolomitic samples, it had relatively little surface topography or macroporosity, and the large mean pore size reported is obviously an artefact of the instrumentation, and corresponds, more correctly, to interparticle void detection. This complication is less serious with the larger particles of other sorbents. The large pore volume figure of 0.6 cm^3/g for this sample should thus be treated with caution. Harris (1988) suggested that pore volume associated with pores greater than 500nm in diameter be discounted in samples of low porosity in order to give a true measure of intraparticle pore volume.

2. Calcination conditions played an important role in pore volume measurement. Calcination times for sorbent preparation were guided largely by literature values. The very low pore volumes of some samples prompted a more rigorous analysis of calcination, which is given in APPENDIX A. A series of calcination experiments was performed on one representative sorbent taken from each of the sulphation reactivity classes identified in Chapter 3. The chosen sorbents were Lyttelton (Type A), Marble Hall (Type B), and Bredasdorp (Type C). Calcination times were shown to differ significantly with sorbent type, with the dolomitic sample being fully calcined in roughly half the time it took for the limestone samples. At 1170 K, calcination was completed for all samples in one hour. Holding calcined samples at elevated temperatures beyond the time required for complete calcination leads to pore collapse, and a shift in mean pore size to larger values, with a corresponding decrease in total pore volume. It is surmised that this condition was responsible for some of the low pore volumes reported in TABLE 4.1. Further calcines were thus prepared from these three sorbents. Calcination times were reduced to match those identified in APPENDIX A as ensuring complete calcination. It should be noted that these calcination times are much longer than would be anticipated in a

fluid bed environment. TABLE 4.2 shows the comparison between pore volumes for the two sets of calcines prepared from these three samples. The second set of pore volume measurements have a much narrower spread 0.31 - 0.34 cm^3/g, and correspond more closely to the ranges cited by Borgwardt and Harvey (1972).

In the light of the above two findings, it is anticipated that pore volume measurements for correctly prepared calcines of all, identically sized, 16 samples, would fall in the range listed by Borgwardt and Harvey. Such a narrow spread belies the real variation in sorbent performance found in Chapter 3, and confirms that calcine pore volume measurement, in isolation, is a poor predictor of sorbent capability. The value of the data contained in TABLE 4.1 is therefore purely in assessing the pore structure of one sorbent relative to another. The analysis of pore structure is hereafter restricted to the data contained in TABLE 4.2, which also contains pore structure information on the three natural sorbents prior to calcination. The pore volumes of the three raw sorbents range from 0.013 - 0.049 cm^3/g, which closely resembles the range cited by Borgwardt and Harvey (1972).

In an effort to avoid errors in pore volume analysis due to the presence of interparticle voids, calcine mean pore radii figures were derived by firstly discounting that pore volume associated with pores of diameter greater than 500 nm [Harris (1988)]. When natural sorbent particles were analysed by mercury intrusion porosimetry, significant instrument noise was encountered at low pore radii, due to the fact that natural sorbents have low inherent porosity. This places great uncertainty on the value of mean pore radius derived for these natural sorbent particles. It is nonetheless still possible to make some general observations about sorbent pore size distributions. Comparing the mean pore sizes of both raw and calcined samples from TABLE 4.2 shows that there is an obvious shift to smaller diameter pores on calcination. Furthermore, it is interesting to note that, though there is a significant difference in the mean pore size of uncalcined particles of different sorbents, this does not carry through to the calcined state. The Bredasdorp calcine, unlike the other two samples, displays a bimodal pore size distribution, as shown in FIGURE 4.2. This is attributed, in part, to its geology - it being a fairly unconsolidated marine sediment. The presence of larger pores too would explain its improved sulphur retention capacity over the

other two sorbents. The Lyttelton calcine has the smallest pores, which is consistent with its poor sulphation capability.

Surface area figures derived from pore volume distribution curves were checked against direct measurements by nitrogen adsorption (the B.E.T. method), according to BS 4359 (1969). These check figures are shown in column 5 of TABLE 4.2. The degree of correspondence is fair. Both measurement techniques are prone to inaccuracies. The porosimetry technique assumes that all pores are cylindrical in shape. An examination of FIGURE D.1 which is an example of a calcined Bredasdorp particle, shows that this is clearly not so. On the other hand, the detection limit of the nitrogen adsorption technique is about 50 nm [Kuelerman (1987)], and surface area due to pores of greater diameter goes undetected by this method. The natural Bredasdorp sample has a unit surface area approximately ten times that of the other two samples, although its mean pore size is only slightly smaller than the Lyttelton sample. It is believed that this large surface area is the result of significant surface irregularity. This topography is clearly evident in the SEM images in APPENDIX D (FIGURES D2-D4). The point is made in Chapter 5 that this surface topography plays a role in defining the attrition propensity of this particular sorbent.

It can be concluded from the above observations that there is no obvious correspondence between any of the parameters in TABLE 4.1 and sulphation propensity. This is reinforced by the data in TABLE 4.2. In general, the calcines of dolomitic particles possess larger surface areas than those of limestones, which is coincident with their lower mean pore size. As shown in Chapter 3, the dolomitic sorbents were generally less reactive than limestones - the smaller diameter pores of their calcines become more easily blocked by sulphate product, and overall conversion is lower. The Umzimkulu dolomite is a notable exception. It displayed Type C (high) reactivity, yet its unit pore volume and mean pore size are low. Such anomalies echo the conclusions of Borgwardt and Harvey (1972) and point to a more complex interdependence of sorbent physical properties. These authors confirmed that pore diffusion limited sulphation capacity in sorbents whose mean pore radius was less than 350 nm. Ulerich et al (1979) concluded from an analysis of a further 5 limestones that sorbent calcines with pore diameters in the range 50-300 nm were totally blocked during sulphation, and capacity was

limited by product layer diffusion. This would imply, for the South African sorbent base, where mean pore diameters of calcines are all less than 300 nm, that sulphate deposition is restricted to a layer near pore mouths, and overall utilities are low.

Potter (1969) suggested that sorbent activity was a function of the pore volume fraction arising from pores with a mean radius greater than 300 nm. If this criterion is applied to the three sorbents in question, Marble Hall (Type B - intermediate activity), rather than Bredasdorp (Type C), would display the highest sulphation capacity. Snyder, as reported by Jonke (1977), proposed that only pores greater than a stipulated minimum size contributed active surface area for sulphation. This critical size is an empirical function of the calcium and magnesium content of the sorbent. This correlation, however, failed to predict the sulphation capacity of 11 sorbents [Ulerich et al (1979)]. When applied to Lyttelton, Marble Hall, and Bredasdorp samples, it produced minimum effective pore radii of 25 nm, 65 nm and 74 nm respectively. As can be seen from FIGURE 4.2, the total pore volume of the Lyttelton sample would thus be available for sulphation. As there was little difference in measured pore volumes of the three calcines, this would imply that the Lyttelton sample had the greatest sulphation capacity. Clearly then, this criterion has little value as a comparative tool.

To summarise thus far, there is little difference in the pore volumes of the three representative South African sorbent calcines, and the use of this parameter as a predictor of sorbent performance is minimal. Pore blockage by sulphate product restricts the reaction to a region near the external surface of individual particles. Mean pore radius does provide some indication of sorbent worth. The fraction of total pore volume found in larger pore sizes is, in itself, of no more value than total pore volume as a measure of sorbent utility, at least using the criteria of Potter and Snyder. However, further examination of pore size distribution curves for the three samples shows that the Bredasdorp sample alone has significant pore volume found in pores of diameter larger than 400 nm (see FIGURE 4.2). Although pore diffusion remains the rate controlling step for these larger pores, they are less likely to be filled by sulphate at pore mouths. This criterion appears to offer the best indication of sorbent performance.

Effective porosities were determined for the three samples from measured pore volumes. These figures are given in TABLE 4.2. True solid densities of the limestone samples were taken to be those of pure calcium carbonate (2710 kg/m^3) whilst magnesium rich sorbents were assumed to have the true solid density of dolomite (2872 kg/m^3). All three sorbents had measured porosities of 51 - 53%, yet the inherent porosities of the natural sorbents varied from 3.4% to 11.7 %. These measured calcine porosities were compared with the geometrical model predictions of Hartman and Coughlin (1974) from eq. 2.1 with X=0, which are also listed in TABLE 4.2. Correspondence with measured values is good, with the model overpredicting porosity by a maximum of 13%. This discrepancy can be attributed, in part, to assuming that sorbent densities could be described by the pure carbonate values. It has been reported [Borgwardt and Harvey (1972)] that the inherent porosity of natural sorbents "carries through" to the calcined state. This is not entirely obvious for the three samples here - the effect appears to be masked by the radical increase in pore volume from natural to calcined state. This is supported by Ulerich et al (1979), who found no correlation between the pore volume or surface areas of five limestones, and the corresponding properties of their calcines. Calcine porosity, on its own, is therefore a poor indicator of sorbent utility. The natural porosity of these sorbents, however, does reflect the same trend as sorbent performance. The abnormally high base porosity of the Bredasdorp sample is a consequence of its extensive topography, and the presence of "super" macropores - see FIGURE D.5. These pores are not destroyed on calcination. It is therefore surmised that sorbents which display extensive macroporosity would be effective in sulphur capture. This assertion is supported by the grain theory model of Hartman [1976] where a strong relation was predicted between the inital sorbent porosity and concentration gradients set up within the particle during sulphation, and the time to pore closure. At this point solid diffusional limitations become so severe that the reaction rate effectively falls off to zero. Another example of a sorbent with visible macroporosity is that from the Saldanha region - FIGURES D.7-9. The massive voids in this sample are related to its geology, for, like the Bredasdorp sample, it is of Recent marine origin.

The effect of calcination temperature on surface area is demonstrated in TABLE 4.3 for Bredasdorp limestone. The B.E.T. surface area decreases

with increased temperature, as expected, due to sintering of product.

In conclusion, calcination shifts the mean pore size of sorbent particles to lower values, with little variation seen across a variety of samples. High sorbent utility can be linked to the existence of large pores in calcined particles. It is reasoned that macroporosity is some intrinsic function of the natural porosity of the sorbents. Hartman and Coughlin [1974] concluded that uncalcined stones of high porosity achieved greater utility in conversion to sulphate product. Hartman et al [1978] stressed further the significance of uncalcined stone porosity in determining the rate as well as the extent of sulphation. The relationship to sorbent geology, alluded to above, prompts an examination of sorbent granularity and crystallinity and their effect on porosity. These properties are discussed in Section 4.2.3. The external topography of natural sorbent particles is also thought to impact on sorbent performance, and its influence is described in Section 4.2.4.

4.2.3 Granularity / Crystallinity

All limestones and dolomites are crystalline materials, although the size of individual crystallites, grain size and texture, and degree of consolidation are extemely variable, and are complicated functions of their formative geology.

Grain size and crystal texture tend to affect sorbent utility by the following mechanisms:

* providing a base porosity which influences the final porosity of the calcine, and thus the conversion to sulphate product

* creating points of defect within sorbent particles, which, under the action of applied stress, result in particle deformation and fracture. The new surface created improves the overall sorbent utility

The first mechanism has been referred to extensively in the previous section. Its importance has also been established by other researchers. Harvey (1970) found that porous grain textures displayed greater reactivity than tightly interlocking grain structures. The presence of

surface irregularites in the presence of voids resulted in improved sorbent utilisation. Borgwardt and Harvey (1972) demonstrated that more closely grained and highly crystalline sorbent particles tended to develop the finest pore structures on calcination leading to sulphate blocking of pore mouths. Finely grained, highly microporous and incoherent carbonates developed calcines in which the total pore volume was accessible to sulphate product. It was also established that the presence of physical imperfections and grain boundaries in crystalline samples tended to enhance their sulphation propensity. The degree of crystal consolidation in natural sorbents affects the rate of CO_2 release during calcination, which, in turn, affects final calcine porosity. The most rapid CO_2 evolution occurs in naturally porous sorbents with inherent structural defects, whereas the slowest occurs in highly crystalline sorbents with minimal porosity. Boynton (1980) concluded that soft, fine grained limestones are more reactive than hard but finely crystalline samples, and that finely grained dense sorbents were more reactive than coarse grained highly crystalline samples.

As stated above, sorbent crystallinity and granularity also affect sorbent structural integrity. The intrinsic particle strength defines the extent to which sorbent particles break up in a fluidised bed. This, in turn, affects the sorbent particle size distribution in a combustor, with fines generated by attrition being elutriated. On the positive side, controlled attrition may help to improve overall sorbent utility by removing sulphate deposit from external particle surfaces.

It has been noted by Lowrison [1974] that the ultimate strength of granular materials is inversely proportional to the square root of grain size. Furthermore, within a crystal matrix, the packing density of individual crystallites induces defects into the particle body which serve as failure points when the material is subjected to compressive or shear stresses. Large grains possess more extensive (i.e. continuous) surfaces over which shearing forces may act. Smaller grains tend to obstruct directional forces and are therefore usually stronger than large grains. Stated another way, the more isotropic a polycrystal matrix is, the stronger it will tend to be. The interfaces between individual crystals in a polycrystal network are additional points of weakness. This is aggravated by the presence of chemical impurities which tend to collect at grain boundaries, and serve to weaken

intergranular adhesion. This effect was discussed in Section 4.1 which looked specifically at the chemical composition of the sorbents utilised in this investigation. Murray (1956) found that higher porosity was obtained with pure carbonates, as the presence of SiO_2 and Al_2O_3 gave rise to a fluxing action resulting in pore blockage. Murray was however concerned with effects at higher temperature than typical of FBCs, where chemical bonding of silicates is unlikely to occur.

In general, crystal defects or intergranular stresses are indistinguishable from other stress components such as inherent porosity or surface cracks (the latter being caused, for example, through metamorphic action) in their effect on sorbent particle integrity. When sorbent particles are composed of interlocking granular subunits, and yet contain no cracks or inherent porosity, then the principal points of failure are at the interatomic level, corresponding to changes in either crystal growth rate or form (crystallographic structure).

Measurements of crystal structure and granularity of the South African sorbents were complicated by the availability of only preselected size ranges of sorbent particles. The generation of narrow size ranges by sieving action tends to destroy the natural distribution in grain sizes displayed by the raw sorbent. Sieving tends to normalise grain size, producing a unimodal distribution. In order to truly assess the variation in both crystallite and grain sizes present in the natural sorbent, it is necessary to investigate differences in character from a large number of narrow size ranges, and to map grain and crystallite size variance. This is something which is often overlooked when trying to assess the significance of these variables in the sulphation reaction. For example, Hartman (1976), from an analysis of 10 Czechoslovakian sorbents, observed marked topography in all samples within select size ranges, but made no reference to granularity. Some high crystallinity was observed.

In general, large rock samples provide the most valuable information on crystal and grain size variation. Older carbonates, such as marble, have small, very uniform crystals, whereas young carbonates display very wide variations in grain sizes, often to several orders of magnitude.

The samples of South African carbonates that were supplied were already

pre-seleceted on the basis of size, rendering a comprehensive anlysis of grain character impossible. Information on grain size available from sorbent suppliers, was, with the exception of Umzimkulu (where grains are coarse and as large as 15 mm), unobtainable, and scanning electron microscopy was used to provide this information.

The uniform crack distribution in FIGURE D.10 was assumed to coincide with grain boundaries of the Lyttelton sample. The mean grain size of this sorbent was estimated at between 50 and 100 microns. The Bredasdorp and Saldanha samples do not show corresponding patterns. The unconsolidated nature of the Saldanha sample is clearly evident from FIGURE D.11, in which very small shelly fragments can be seen. FIGURE D.5 shows the isotropy of the Bredasdorp sample, with "superpores" of 50 microns and above clearly in evidence. Grain size for both these Recent carbonates is expected to be of the order of several microns. The planar structure of the metamorphic Marble Hall sample (FIGURE D.12) hints at an average grain size in the same range as the marine carbonates even though this a metamorphosed sample.

The relationship between granularity, crystallinity, and porosity developed on calcination has been described above. Coarse grained, highly crystalline rocks, develop calcines whose sulphation capacity is low compared to that of calcines of poorly consolidated, incoherent carbonates. The high microporosity of these latter sorbent types is transferred to their calcines to enhance their utility as sulphur sorbents. Employing granularity as a performance index, then, the sandy/shelly carbonates would be expected to be more reactive than the older calcitic and dolomitic rocks. Little information can be gained beyond this generalised picture.

4.2.4 Topography

The granularity of a sorbent also influences the general shape or topography of its individual particles. Surface protrusions are areas of stress concentration which aggravate the tendency of individual particles to fracture or abrade. Furthermore, where sorbents have a preponderence of large surface voids (resembling indentations rather than "super" pores) sulphation capacities tend to be improved, diffusional constraints are minimised, and pore closure does not result.

The literature on fineparticles is extensive (see excellent review by Kaye (1982)), and much attention has been given to shape characterisation and surface irregularity. Common to most of these techniques is their inability to characterise particle topography simply. One exception is the concept of fractal geometry propounded by Mandelbrot (1977). Simply stated, certain solid shapes, because of their topology (space filling capacity), can be characterised by a unique number which is a fractional dimension between 2 and 3. Smooth particles have a fractal dimension close to 2, whilst particles of convoluted shape, with extensive porosity, have a fractal dimension closer to 3. This principle was adopted by Avnir and Farin (1983), who related nitrogen adsorption B.E.T surface areas of narrow sized ranges of sorbent particles to fractal dimension thus:

$$\ln S_a = (n-3).\ \ln d + \text{constant} \qquad 4.1$$

where S_a is B.E.T. area, d is mean particle size, and n is the unique fractal dimension associated with the degree of particle surface irregularity. The technique assumes that all particles of a given sorbent have the same shape. The main advantage of this technique is that it does not require extensive sampling of sorbent particles to obtain statisticallly significant results.

Where samples have measurable inherent porosity, however, the technique fails because gas adsorption provides a measure of this porosity as well as of surface ruggedness. It is difficult, with this technique, to distinguish between samples which display marked topography and others which are reasonably smooth but have significant porosity. In addition, sieving particles into preselected size ranges may induce a certain skewness into the results. Because grain boundaries and voids are points of stress concentration, sieving action promotes fracture at these regions, thereby destroying any inherent porosity in sorbents of low compressive strength, or (a worse scenario) preferrentially concentrating this porosity into specific size ranges.

B.E.T surface areas for narrow size fractions of two natural sorbents, which differed markedly in reactivity (Bredasdorp and Lyttelton), were obtained by nitrogen adsorption. It is clear from the data presented in

TABLE 4.4 that no correlation between particle size and surface area exists for either of the samples. Indeed, in the Bredasdorp sample which has major surface indentations, measured surface areas first decrease, and then increase, as particle size is increased. This is attributed to the interplay between internal surfaces accompanying pore development and external surfaces due to marked topography. It also implies that particle shape is not consistent across the particle size range. In the case of the Lyttelton sample, measured values of BET surface area were essentially constant across the size range investigated. At first glance, this could imply a fractal dimension of 3, coincident with a highly topographic sample. From a look at optical images of individual Lyttelton particles, FIGURES D.13-14, this appeared unreasonable. Given the uncertainty over exactly which fractal dimension (external shape or internal pore surface) was being characterised by this technique, it was not pursued further.

An alternative measure of general topography was derived from electron microscopy images of 5 sorbents which spanned the full lithostratigraphic range (see APPENDIX C).

There are marked differences in particle shape of each sorbent. The Bredasdorp particles (FIGURES D.2-D.4) show distinct protuberances of considerable size. Cleavage lines of 35 - 50 microns are evident in FIGURE D.6, and major indentations extend to the very centre of the particle (FIGURE D.5). If the intrinsic sorbent strength is such as to prevent particle breakup, these lineal indentations act as very large pores for sulphur capture, and their total volume is accessible to sulphate product. The Saldanha particles (FIGURES D.7-D.9) show evidence of marine origin, with some very large indentations present in each particle. Unlike the Bredasdorp samples, the external surface of the Saldanha particles is relatively smooth. Little obvious difference exists between the images of Lyttelton particles (FIGURES D.13-D.14) those of the Marble Hall particles (FIGURES D.15-D.16). The external surfaces of both are reasonably smooth, with neither displaying the topographical features ("superporosity") of the previous two Recent sediments. This confirms that the external surface fractal dimension for Lyttelton is much closer to 2 than to 3. The Marble Hall particles would appear to be the more friable of the two, judging by the fine fragments in view. Only the Umzimkulu particles (FIGURES D.17-D.19) display any

obvious crystallinity, where cleavage has taken place along intergranular lines. If fracture / abrasion of this sorbent is favoured under FBC conditions, it is anticipated that it would continue down to single crystal level, and occur independently of the apparently smooth external surface. This is discussed further in the analysis of attrition results (Chapter 5).

The previous discussion attests to the significance of surface topography in the promotion of attrition, and the resultant creation of "fresh" sorbent surface which participates in the sulphation reaction. Attrition propensity cannot, however, be determined absolutely without an a priori knowledge of sorbent structural strength and the magnitude of intraparticle stresses. Suffice it to say that topographical features are points of stress concentration which affect structural strength directly. There is no merit in trying to quantify the effect of topography beyond the above general description. Only where there are extensive surface indentations (as in Bredasdorp particles) or "superporosity" (in the case of the Saldanha particles) is there a direct correspondence between sorbent utility and topography, and this does not depend on attrition propensity. If surface topography alone defines attrition tendency, and high sulphation utility is commensurate with a high attrition propensity, then the sandy / marine sorbents would rank ahead of the older dolomitic and metamorphosed samples, with the highly crystalline sample displaying intermediate behaviour.

4.2.5.Sorbent Structural Strength

The importance of particulate strength in defining the attrition potential of free granular solids in fluidized beds has been identified by many authors [Blinichev et al (1968) and (1973), Kutyavina and Baskakov (1972), Merrick and Highley (1974), Vaux (1978), Kono (1981)] to name but a few. Vaux and coworkers [(1979), (1980), (1982) and (1983)] were concerned specifically with attrition of calcareous sorbents and its effect on their subsequent sulphation. It was inferred that the attrition propensity of a particular sorbent type could be characterised by the structural strength of its individual particles. It is equally apparent from these studies that there is little consensus over the exact role of sorbent structural strength, and, indeed, over what measure of this property is appropriate to the description of

attrition in fluidised beds.

According to Boynton (1980), the crushing (compressive) strength of limestones and dolomites spans the range 8.27 - 195.8 MPa, whilst tensile strengths range from 2.41 - 6.21 MPa, and shear strengths from 4.1 - 20.3 MPa. Kono (1981) lists compressive strengths of coarse mullite particles (expected to display values greater than limestones) in the range 4-20 MPa. Blinichev et al (1973) reported compressive strengths of limestones in the range 18.6 - 24.3 MPa, and shear strengths of 3.7 MPa. Vaux and Schruben (1983) defined an alternative measure of particle strength which was related to a force per unit length, analogously to the effect of surface tension in the stabilisation of liquid droplets. Typical values cited were $2x10^5$ dyne/cm for raw sorbents and $4x10^4$ dyne/cm for calcined particles.

A precise definition of limiting structural strength is of fundamental importance to the characterisation of sulphur sorbents. It affects not only the choice of experimental hardware used in its measurement, but also the perceived variability between species - note the range of compressive strengths reported by Blinichev et al(1973), yet the constancy in shear stress for the same sorbents. For the purpose of this investigation, the inherent strength of sorbent particles is defined by that applied load which causes permanent structural damage. Two deformation processes are possible. The first results in change to the external shape of particles by cleavage at points of stress concentration such as apical protrusions or areas of macroporosity i.e as some function of sample topography. The second mechanism relates to cleavage at grain boundaries, resulting in extensive particle fracture. Within a fluidised bed it is reasonable to assume that individual particles would "fail" firstly by the loss of external protrusions due to interparticle contact - a classic abrasion mechanism. Sorbents which do not display this marked topography would "fail" by fracture at grain boundaries, or other, internal, points of stress concentration. The extent to which either process occurs is a function of particle contact forces within the fluidised bed. This conceptual model of particle "failure" is advanced in FIGURE 4.3. From this picture, it can be postulated that individual particles will "fail" over a distance proportional to particle diameter. This exact distance is related to the size of surface protrusions or indentations, and is a function of

particle topography. Where no such features exist, the "failure" distance is taken to be the particle diameter. The topography of sorbent particles can be quantified by an asperity number, f, equal to the ratio of the largest surface irregularity to particle diameter. Only the marine sorbents (of which Bredasdorp and Saldanha are examples) display significant topography, and, for these two, a value of f=0.3 (measured from SEM images of a large number of sorbent particles) was used. Having defined particle failure thus, the "force per unit length" definition of structural strength proposed by Vaux et al (1968) is appropriate.

The literature abounds with information on the experimental determination of solids' strength, including a number of "standard" test procedures for natural building stone (ASTM C-170, 1950), cohesive soils (ASTM D-2166, 1979), catalysts and catalyst carriers (ASTM D-4179, 1982). In these cases a pre-formed sample is subjected to a unidirectional load, and the point of failure noted. The compressive strength is then determined simply by the ratio of applied load to the calculated area of the bearing surface. Other determinations of mechanical strength include crushability in free-fall, attrition tests in a rotating drum, and disintegration by high velocity impingement on a flat surface. None of these methods are ideal representations of the fluidised bed environment. The loading tests require a compacted sample of reasonable size, which is inappropriate for sorbents. The latter set of test procedures lacks the capacity to express failure stress absolutely, with results generally being reported as a "crushing strength index" or fraction of the initial charge which failed under the specific test conditions [Pomeroy (1957), Zenz (1982)]. An ideal test procedure must be able to duplicate the particle-to-particle interactions evident in a fluidised bed, take into account the statistical variation in structural strength of a number of discrete particles, and provide an absolute measure of the failure stress.

A reasonable experimental compromise is found in a modification of a technique employed by Franceschi et al (1981). These authors subjected a fixed mass of presized sorbent particles, constrained in a piston cylinder, to a constant load, and defined a crushing index in terms of the change in mean particle size on application of the load. The sample charge is of sufficient size that

* interparticle contact area far exceeds that between particles and

chamber surfaces

* the variability in structural strength between individual particles is accommodated.

In this current work, an INSTRON materials testing machine was used to measure the structural strength (in compression) of five South African sorbents for which granularity and topographical information is available. A 10 gram mass of each sample, in the size range 300-600 μm, was inserted into a 13 mm diameter cylinder fitted with a frictionless piston. This arrangement was placed between the loading arms of the INSTRON and subjected to a continually increasing load. The failure load was established from the output trace of load versus piston displacement. A zero load was registered during the initial rearrangement of particles to maximum packing density. Once this point was reached, the registered load increased rapidly with piston movement. Representative curves for the five sorbents are given in FIGURE 4.4 . The initial slope of the deformation curve gives a measure of the variability in structural strength as a function of sorbent type. The limiting structural strength, σ, is defined as

$$\sigma = \frac{dF/d\underline{x}\ (@\underline{x}=0).d_p(1-f)}{d_p} \qquad 3.2$$

where F is the applied force, f is the asperity number, and $\underline{x}$ is the piston displacement. TABLE 4.5 gives average σ values for the five sorbents. Compressive strength values span the range 63700 Nm^{-1} to 256000 Nm^{-1}. It is interesting to note that the highly crystalline Umzimkulu sample has the lowest value, followed by the two marine samples, then the metamorphic Marble Hall sample, with the Lyttelton dolomite showing the greatest structural integrity. This trend is consistent with the previous discussion. The Umzimkulu sample, with its large granular structure is expected to have a low structural strength. The topographical features of the two marine samples impose surface stresses which cause these samples to "fail" sooner than would have been envisaged on the basis of their grain size alone.

These experiments were repeated with sorbent calcines (prepared at 1170 K in an air atmosphere) to ascertain the effect of calcination on structural strength. TABLE 4.5 shows typical values for these tests. The variation with sorbent type is less pronounced than was observed with

the natural sorbents. It is significant that the Bredasdorp calcine now "fails" ahead of the other samples. Bredasdorp particles displayed greater inherent porosity than any of the other samples, and it is felt that, on calcination, there is a significant stress redistribution to accomodate this base porosity, precipitating early "failure" of the resultant calcine. This serves to emphasise further the importance of the structural properties of natural limestones and dolomites in defining their potential as sulphur sorbents.

The structural stength figures reported above cannot be compared directly to the crushing stress figures reported by Boynton (1980) and Blinichev et al (1973) but provide a good indication of the effects of sorbent structure on attrition potential. The relationship between sorbent strength and attrition is more fully described in Chapter 5, which examines classic attrition models and defines the attrition propensity of selective South African sorbents. At this point it is sufficient to note that those sorbents with low structural strength will display the greatest attrition.

4.3 SULPHATION PATTERNS

Section 4.2 attempts to relate the sulphation performance of South African sorbents to their distinctive physical properties. Reference is made to the sulphation capacity of typical sorbents identified by the simple batch sulphation experiments of Chapter 3. It is possible to summarise these findings in a few electron micrographs which show the extent of sulphur penetration into sorbent particles. FIGURES D.20-D.22 reflect sulphur line scans for typical Lyttelton, Marble Hall and Bredasdorp particles respectively, prepared in the laboratory FBC described in Chapter 3. Only with the Bredasdorp particle is there an extensive presence of sulphur throughout the particle volume. This is consistent with its high measured reactivity (it is an example of a Type C sorbent, as described in Chapter 3) and is commensurate with the presence of large pores in the natural sorbent. The Lyttelton and Marble Hall particles, in contrast, show a concentration of sulphur near the external surface of the particles which is indicative of pore blockage. Once again, this pattern is consistent with their low natural porosities and the small pores developed on calcination. It is therefore possible to characterise sorbent performance in terms of the above physical

properties. The Umzimkulu sample does not, on preliminary examination, seem to comply with this analysis. It has negligible inherent porosity, yet is an example of a Type C sorbent. FIGURE D.23 helps resolve this contradiction. The line scan shows that sulphur does indeed penetrate the total particle volume. It is also apparent from this micrograph that extensive fracture of this particle has occurred - there are noticeable fissures traversing the entire particle. This is consistent with its low structural strength but also reflects its chemical composition - it was noted in Section 4.1 that this sorbent was an example of one which contained gaseous deposits, which, on calcination, would lead to fracture.

4.4. RELATIONSHIP BETWEEN SULPHATION CAPACITY AND SORBENT GEOLOGY

The experimental hardware needed to fully characterise a sorbent both chemically and physically is extensive. Although it is possible to relate the sulphation propensity of a particular sorbent to its fundamental properties, it would be a cumbersome and costly process to do so for all sorbents of interest. However, as shown in APPENDIX C, limestones and dolomites are used extensively in other process industries, and their geologic properties are well defined, and more importantly, generally well documented. It has already been shown that many physical properties such as granularity and crystallinity are direct functions of parent stone geology. If a formative link could be made between sorbent geology and performance, it would prove invaluable for rating potential sorbents.

TABLE 4.6 groups the 16 South African sorbents according to their geologic age. Their sulphation rating is also shown. It is immediately apparent that sorbent sulphation performance decreases with increased geologic age. The Recent marine /sandy limestones are highly reactive (type C), whilst the older primary limestones and dolomites are less so (types A and B). With the exception of the Umzimkulu sample, which has already been shown to be somewhat atypical, all dolomites are less reactive than limestones within the same lithostratigraphic group. Where other exceptions are noted (e.g Slurry limestone, which should, by this identity, display type B behaviour) these are attributed to the degree of sample consolidation (Slurry limestone is a friable calcrete).

It may be concluded from TABLE 4.6 that highly reactive sorbents are generally poorly consolidated, which confirms the importance of natural porosity and topography (already identified). Particles of older sorbents tend to be relatively smooth because of the presence of large single crystals, and because of attrition they have suffered through prolonged geologic movement which accompanied their deposition. Crystal size tends to be uniform, with low inherent porosity, and these sorbents display a large degree of anisotropy. Their structures are stable, often following metamorphosis. Geologically recent sediments, on the other hand, tend to be loosely consolidated agglomerations of small crystals, displaying marked attrition potential. Young sediments can display much higher porosity because of this poor consolidation. In addition, if these sediments are marine in origin, then, incorporated into their final structure are the remnants of food and gas passages from the decomposition of organic remains, both of which boost local porosity.

The geologic assessment of a potential sorbent should therefore give a good indication of its sulphation capability. Such a predictive tool is of value to persons invloved in sorbent selection, and reduces the requirement for extensive bench and pilot scale experimentation to determine sorbent performance.

4.5. CONCLUSIONS

The importance of sorbent physical properties in determining sulphation capacity has been established for a wide range of geologically dissimilar South African sorbents. The process of calcination significantly alters pore structure. The mean pore size decreases on calcination to a value which generally ensures pore blockage and a sulphate deposit buildup near the external surface of particles. The pore size distribution and topography of natural sorbent particles exert considerable influence over sorbent performance.

A relationship exists between sorbent utility and parent stone geology, with "younger", more unconsolidated samples displaying the highest capacity.

The attractive features of sorbent particles for sulphation tend also to impart a high attrition propensity to these particles. Sorbent attrition

may prove beneficial by removing the sulphate product layer thereby improving unit conversion. It may also result in an increased loss of active sorbent surface due to increased elutriation. The extent to which these two competing mechanisms interact is the suject of the remainder of this thesis.

CHAPTER 5 - ATTRITION AND ELUTRIATION OF SORBENT PARTICLES.

5.1 INTRODUCTION

The development of this thesis thus far has been concerned principally with the sulphation behaviour of sorbent particles in isolation from the macroscopic effects of a fluidised combustor. It was shown in Chapter 2 that the few tractable models of fluidised bed sulphation which are available [Zheng et al (1982), Dennis (1985)] rely on several critical assumptions regarding the time variance of sorbent particle size. Neither makes allowance for sorbent attrition, though Dennis recognised its importance. Severe sorbent attrition may result in excessive loss of sorbent material through elutriation, placing an additional burden on downstream dust handling equipment. Controlled attrition, on the other hand, could enhance sorbent utility by the generation of additional surface area for reaction, and the removal of the sulphate layer from the external surfaces of sorbent particles. In Chapter 3, a direct link between sorbent performance and "friability" was established - the most reactive sorbents appeared, at least qualitatively, to be the most friable. The relationship between these two properties and the fundamental physical characteristics of sorbent particles was explored in Chapter 4. There is now an obvious need to quantify the attrition propensity of South African sorbents in terms of these properties and the operational parameters of a fluidised bed combustor. Thereafter it should be possible to include this description of attrition in a robust overall sulphation model. This Chapter is devoted to an analysis of the kinetics of attrition, and of classic elutriation models.

Attrition is a collective name given to all those processes occurring within a fluidised bed combustor which result in particle size reduction with time. The principal mechanisms of attrition are related to:

1. mechanical forces (acting in feed and recycle streams e.g. screw conveyor and cyclone separators)
2. hydrodynamic forces (resulting from jet and bubble formation as well as splashing into the freeboard region of the bed)
3. thermal stresses (solid shattering on entry to hot bed)
4. chemical stresses (due to calcination and sulphation)

5. phase change stresses.

Some of these stresses, caused by collisions with feedlines and cyclones, and by thermal decrepitation on entry to the combustor, are instantaneous "once-off" effects, whereas others, caused by interparticle collisions due to air jetting and bubbling action, collisions with bed internals, and chemical reaction, act continuously over time. A comprehensive attrition model must take cognisance of these different time dependencies and give due weighting to individual mechanisms.

The literature on attrition is ambiguous over the significance of each of these contributory factors. The most detailed research summary comes from the Westinghouse Corporation, where sorbent attrition was measured from an analysis of elutriated solids in pilot scale investigations [O'Neill et al (1977), Sun et al (1980), Newby et al (1982) and (1983)], as well as "standardised" laboratory tests [Vaux and Fellers (1981), Vaux and Schruben (1983)]. Whereas laboratory tests highlighted thermal shock, calcination reaction, distributor jetting action and bed bubbling as principal attrition sources, pilot plant data confirmed coarse particle residence time, gas velocity and bed internal configuration as the most important components. Others attach different weightings to attrition mechanisms. Blinichev et al (1968) found that attrition occurred mainly in a region close to the distributor grid and was the result of high velocity jet impacts. This was confirmed by Chen et al (1980) in a laboratory scale study. However, Lin et al (1980) attributed the bulk of attrition in a bed of char to bubble wake activity.

One of the main problems in analysing attrition data from different sources is the lack of consistency in the definition of attrition. Much of the data is equipment specific, with little exptrapolative merit.

5.2 DEFINITION OF ATTRITION

It is useful to think of attrition in terms of its potential effect on sorbent sulphation, and to define attrition rate accordingly.

The sulphation reaction is limited by accessible sorbent surface area. Pore diffusion and product layer diffusion, for most sorbent types,

limit sulphate deposition to a region in close proximity to the external surface of particles. Sorbent attrition should therefore be related to the creation of new particle surface area, either by breaking (or cleavage) of particles along grain boundaries or at other points of stress concentration, or by gradual abrasion i.e. the continuous wearing of external surfaces. The first mechanism would tend to generate a wide size range of particles including fines, whereas the second would leave the total number of coarse particles essentially unchanged but cause significant fines generation. There is ample evidence in the literature [Kutyavina and Baskakov (1972), Ulerich et al (1980)] to suggest that attrition proceeds mainly by abrasion, even for structurally weak sorbents. Sulphation kinetics have been described in Chapters 2 and 3 in terms of particle size, and it is simpler to equate this generation of new particle surface through attrition to a generation of fine particle mass, or equivalently, to a loss of particles larger than a specified size.

Following the Westinghouse approach [Ulerich et al (1980)], the attrition rate, R, which is proportional to the energy input to the system, is defined formally as the loss of coarse particle mass per unit mass of coarse particles per unit time.

$$R = -\frac{1}{M}\frac{dM}{dt} \qquad 5.1$$

The extent of attrition is then defined simply as

$$\underline{A} = \int R\, dt \qquad 5.2$$

The definition of "coarse" and "fine" particles is essentially arbitrary. Ulerich et al (1980) considered "fines" as those fragments, generated by attrition, which would be elutriated under the normal operating conditions of the combustor. In this current work, it is assumed, additionally, that "fines", either generated by attrition, or present in the feed stream to the combustor, are themselves not subject to attrition. This constraint is important to the development of the sorbent particle balance in the combustor which is discussed in Chapter 6. These statements together implicitly assume that attrition is dominated by an abrasion mechanism. It is assumed furthermore that attrition is restricted to bed and splash regions. Only where solid recycle rates are excessive will freeboard behaviour exert any influence

on attrition rate.

Literature on attrition testing is extensive, and the hardware used of varied form [Bemrose and Bridgwater (1987), Zenz (1982)]. Fluid bed studies make up a large portion of this literature, with much of this subset devoted to sorbent attrition. Most of these tests measured the extent of attrition from the mass of elutriated solids generated in unit time. This again presupposes that only fine fragments are generated i.e. abrasion is the dominant mechanism

It is simplest to view attrition rate as made up of two components - an instantaneous one, which is influenced by such things as sorbent feed size distribution, bed temperature and feed mechanism; and a continuous one which is affected by gas velocity, bed depth, solids residence time, bed particle size distribution, feed rates, and the configuration of internal heat transfer surfaces.

5.3 ATTRITION EXPERIMENTS

The 100 mm diameter combustor vessel used for batch sulphation experiments was used here in an attempt to resolve the fundamental dependence of sorbent properties and combustor operating conditions on attrition. The effects of

fluidising velocity,
bed depth,
combustor temperature and atmosphere,
sorbent type and particle size

were investigated in a modified factorial experiment. Five South African sorbents were examined - the three which represented the different sulphation classes i.e. Lyttelton, Marble Hall and Bredasdorp, and two others (Saldanha and Umzimkulu) which, as shown in Chapter 4, displayed interesting topography. The test approach was straightforward and follows closely the method outlined by Ulerich et al (1980). The combustor vessel was filled to a predetermined height with a closely sized sorbent charge. Unless stated otherwise, the combustor operated at ambient temperature. Fluidisation was initiated at a pre-set velocity for a set time period (starting at 15 minutes). The bed contents were then drained and dry-sieved (in a mechanical sieve-shaker) to determine the amount of "fines" present. "Fines" are defined as fragments smaller

than the particles charged to the bed initially. In most experiments, sorbent particles were in the size range 300-600 μm, and "fines" generated are therefore less than 300 μm. The mass of fines collected by the bank of cyclones downstream of the combustor was added to this sieve fraction to give a measure of attrited "fines". Allowance was made for the effect of sieve action on attrition - see APPENDIX E. It was assumed that sieving would produce fines by abrasion, and could thus be considered analogously to fluid bed attrition.

The coarse particles were thereafter returned to the bed, sufficient "fresh" material added as make-up to ensure constant bed height, and the experiment continued for increasing time increments until the attrition rate became constant. For most of the individual tests, the total attrition time period was in the region of 25 - 40 hours. This time dependence of attrition is often ignored in the literature and leads to great difficulty in comparing data from different sources. The introduction of "fresh" sorbent material after each time increment caused problems in defining the true measure of attrition for the total bed contents. This complexity was resolved by assuming that the new material would, during the first time increment following its addition, wear at a rate corresponding to that measured for the bulk sample during the first time increment. Since the required makeup amount decreased with time, the error in this technique is minimal. This makeup quantity was omitted from the Westinghouse analysis, casting some doubt on the veracity of the final model for attrition rate [Ulerich et al (1980)].

5.4 EXPERIMENTAL RESULTS

Except where the effect of sorbent type, explicitly, was investigated, all attrition tests were conducted with Bredasdorp limestone. This sample was chosen because it exhibited the highest sulphation capacity of the 16 sorbents tested and because it appeared to display a marked attrition propensity. In all tests, the choice of fluidisation parameters (air velocity and bed depth) was guided by slugging criteria (see Chapter 3). Bed depth was limited to 200mm i.e. an aspect ratio, $H/D_c = 2$, and fluidising velocities to $U/U_{mf} = 3$.

5.4.1 Effect of Fluidising Velocity

The effect of the fluidising air stream on sorbent attrition is the sum of activity in the high velocity jetting region near the air distributor grid plus that caused by vigorous bubbling higher up in the bed. Attrition in the lower bed region is the result of high velocity impact between particles or against internal metal surfaces. Within the bubbling zone of a combustor, particles are expected to abrade directly by grinding of particle surfaces. Blinichev et al (1968) confirmed that attrition of limestone proceeded by the latter mechanism except at "high fluidisation numbers" i.e. at multiples of U/U_{mf} >5.

The energy potential for attrition is related to the reduced velocity, $(U - U_{mf})$, analogously to Rittinger's law of abrasion [Merrick and Highley (1974), Vaux and Schruben (1983)]. This is a reasonable assertion, in that, up to the point of minimum fluidization, solids within the bed simply move in bulk flow as bed voidage increases. It assumes that the average particle velocity is proportional to bubble rise velocity [Vaux (1978)]

In other words,

$$R = k_1 (U - U_{mf})^{c1} \qquad 5.3$$

where c1 is a constant and k_1 is a time dependent parameter, incorporating the effect of all other system variables.

The effect of fluidising velocity was investigated by holding this reduced velocity constant. The combustor bed depth in these tests was 200 mm. Attrition rate data are given in TABLE 5.1, for gas velocities equal to $(U_{mf} + 0.2\ ms_{-1})$ and $(U_{mf} + 0.3\ ms_{-1})$. The difference in the extent of attrition between these two tests is extreme. After 20 hours, the extent of attrition at the higher fluidisation velocity approached 11% whilst at the lower velocity, this figure was closer to 3%. In both cases, the attrition rate decreased continuously from its maximum value at time zero. FIGURE 5.1 shows the increase in attrition with time for the two velocities. The form of these curves suggests that the extent of attrition can be modelled by a general equation of the form

$$\underline{A} = a_0 + a_1 t + a_2 \exp (a_3 t) \qquad 5.4$$

where the a_i's are constant for the specific set of operating conditions. Equation 5.4 is of the same form identified by Vaux and Schruben (1983). The data in TABLE 5.1 were fitted to an equation of this form using a numerical least squares regression technique. The calculated values of the a_i regression constants are given in TABLE 5.6. The attrition rate, R, equal to $d\underline{A}/dt$, is given simply by

$$R = a_1 + a_2.a_3 \exp (a_3 t) \qquad 5.5$$

FIGURE 5.2 shows the variation in attrition rate with time. Average attrition rates were calculated over the time period required for steady state attrition to develop (in this case 8 hours). The exact dependence of attrition rate on fluidising velocity was then established from the definition of R given by eq. 5.3, and the ratio of the two averaged attrition rates, giving a value of c_1 equal to 2.2

i.e. $R = k_1 (U - U_{mf})^{2.2}$.

This differs from the result of Vaux and Schruben (1983) and Merrick and Highley (1974), who both reported that attrition rate varied linearly with this reduced velocity. Both groups of authors were concerned with low velocity impacts in the bubbling zone of the combustor, where the rate of energy influx to the bed is given by the pressure - flow rate energy per unit bed mass i.e. $g(U - U_{mf})$. The air distributor in the test chamber employed by Vaux was a porous plate which would inhibit jet formation and attrition would therefore result solely from the effect of bubbling action in the bed bulk. This, however, was not the case in the British Coal unit employed by Merrick and Highley, where a bubble cap distributor was installed.

Vaux and Keairns (1980), in a study of attrition arising from impingement of limestone particles against a steel plate, confirm a dependence of attrition on U^2, which is in accord with a high velocity impact mechanism, where the energy potential for attrition is related to particle kinetic energy. Blinichev et al (1968) reported a complicated empirical expression for attrited mass, in which the velocity dependence was given by $U^{0.6}$, which is at odds with all other reported data.

Although this last expression has been used for design purposes, its applicability, in the light of the present investigation, is questionable.

In this current work, no distinction is made between high velocity and low velocity impacts causing attrition. Both are assumed to result in particle abrasion. The present findings do indicate, however, that high velocity impacts near the bed base govern the attrition rate. It is in this region that jetting action is dominant. In a generalised fluidized system, one would expect attrition effects to be additive, and that, if bubbling action did contribute to attrition, its influence could be simply added to that of the jetting component. Newby et al (1983) hinted at such a combination of influences in their analysis of Babcock and Wilcox pilot plant data. They erroneously concluded that a cubic dependence on velocity is to be expected, whereas, in reality, a dependence on the order of U^2 will prevail. It is interesting to note that the non-linear regression of the B&W data originally provided a velocity dependence of $U^{12.54}$ [Newby et al (1982)] which was later changed to U^3 on theoretical grounds. Kono (1981), too, developed an empirical correlation in which attrition rate is proportional to U^3.

Noting that both Newby et al and Kono consider a dependence on fluidising velocity, U, rather than one related to $(U-U_{mf})$, it is worthwhile to recast the current experimental results in terms of absolute velocity for comparison. When this is done, the average attrition rate becomes proportional to $U^{3.18}$, which, allowing for experimental inaccuracies, corroborates the results of Newby and Kono. However, as stated above, the contribution to attrition comes only from that component of air velocity in excess of minimum fluidising velocity, and therefore this latter approach is in error.

The exponent of velocity equal to the measured value of 2.2 is consistent with a contribution from bubbling action, although this is small.

5.4.2 Effect of Bed Height

Following the same experimental approach as above, Bredasdorp limestone was fluidised at $U = U_{mf} + 0.3\ ms^{-1}$, for bed depths of 100, 150, and 200 mm. The study of deeper beds was precluded because of the tendency of the bed to degenerate to a slugging mode of operation at aspect ratios (H / D_c) greater than 2. Experimental data are presented in TABLE 5.2 whilst FIGURE 5.3 shows extent of attrition / time-response curves for these test conditions. The three curves are similar, each displaying the same negative exponential time dependence, which decreases to a linear relationship at large times. The variation in attrition extent with bed height is not as pronounced as that noted for increased fluidising velocity. Steady state attrition rates are almost identical. These curves are of the same form identified for the effect of fluidising velocity on attrition, and are fitted to eq. 5.4, with the instantaneous attrition rate then given by eq. 5.5. Values of the a_1 regression constants are given in TABLE 5.6.

From a definition of $R = k_2 \cdot H^{c_2}$, and using average attrition rates calculated over a large time period, c_2 is calculated as 0.81. Allowing for errors incurred in analysing the attrition of bed "make-up", this is close enough to a value of 1 to infer a linear dependence of bed height on attrition rate, which is supported by the model of Vaux (1978).

5.4.3 Effect of Sorbent Particle Diameter

Two particle size ranges of Bredasdorp limestone were tested for attrition: a 300 - 600 μm fraction, and an 850 - 1180 μm fraction, at a fluidising velocity of $U=U_{mf} + 0.3\ ms^{-1}$, and bed depths of 100 and 200 mm. Both size fractions were prepared from the same raw stock of Bredasdorp stone. Note that U_{mf} increased from $0.11\ ms^{-1}$ for the smaller size fraction, to a value of $0.57\ ms^{-1}$ for the larger fraction (predicted by the modified Ergun equation for pressure drop across the bed [Yates (1983)]). Extent of attrition data are displayed in TABLE 5.3. FIGURES 5.4 and 5.5 show the effect of particle diameter on extent of attrition for both bed heights. It can be seen that attrition is more pronounced for the smaller particles in deeper beds.

The form of the curves in FIGURES 5.4 and 5.5 is identical to that defined by eq. 5.4. The regression constants derived from a least squares fit of eq.5.4 to the data are given in TABLE 5.6. In a similar manner to above, the dependence of particle diameter on attrition rate can be found from the ratio of average attrition rates for each size fraction, at each of the bed depths examined, noting that $R = k_3 . d_p^{c3}$. These average ratios are

$R_{300-600} / R_{850-1180}$ @ 100 mm depth = 1.358

$R_{300-600} / R_{850-1180}$ @ 200 mm depth = 1.655

If a mean ratio of 1,5 is used, this gives a value of c3 = -0.5 i.e. the particle size dependence on atttrition rate is represented by $d_p^{-0.5}$.

At first glance, this dependence appears to be spurious. It was shown in Section 5.4.1 that high velocity collisions were responsible for the bulk of attrition in this fluidised bed. According to Wei (1977) high velocity impacts resulting in attrition would entail a linear dependence on particle size, since the kinetic energy of a particle is proportional to d_p^3 yet the energy required to create new solid surface is proportional to d_p^2. The general literature, however, does not present a consistent picture for particle size effects on attrition. The Westinghouse model for attrition in the bubbling zone of the combustor [Ulerich et al (1980)] carries no dependence on particle diameter, yet experimentation showed "a strong effect of particle size on the rate of creation of new surface". The exact nature of this dependence was not specified. Gwyn (1969) developed an expression for the attrition rate of an alumina catalyst in which particle size dependence is given by $d_p^{-2/3}$. Vaux and Keairns (1980) modelled high velocity impact of particles in a fluid bed against an immersed steel plate, yet found a zero dependence on particle size. Tarman and Punwami (1975) found that attrition rate varied as d_p^{-1}. Blinichev (1968) reported a complicated negative dependence on particle diameter. The empirical correlation of Newby et al (1983) describing attrition in the Babcock and Wilcox pilot plant carries a dependence on particle size given by $d_p^{0.374}$. The lack of consistency in these reported figures is alarming and calls for further investigation.

Franceschi et al (1981) argued that the explicit dependence of particle size on attrition was complicated by the effect of d_p on U_{mf}. Since attrition results in a decrease in particle size with time, this should

be included in an overall expression for U_{mf}. In the region of interest for these tests i.e. $N_{Re} < 20$, $U_{mf} \propto d_p^2$, and therefore the excess velocity $(U-U_{mf})$ will vary accordingly. Although such an enhancement could not be considered in this work without an <u>apriori</u> knowledge of the change in particle size with time, this assertion does cast some doubt on the appropriateness of the Westinghouse results, where a zero dependence on particle diameter was noted. Plausible explanations for the observed dependence on d_p are given below.

At the point of minimum fluidisation, bed voidage is effectively independent of particle size [Yates (1983)]. However, in a given bed volume, there will be a greater number of point contacts between smaller particles than between larger ones, and, as the attrition rate is a function of the number of interparticle collisions in unit time as well as of particle kinetic energy, it is not unreasonable to expect a higher attrition rate with smaller particles. This effect is expected to be more pronounced in the distributor region where particle kinetic energies are higher. Another key uncertainty in this analysis is the assumption that all particles of the same sorbent type have the same shape, regardless of size. If, momentarily, it is assumed that the attrition rate per particle is independent of size (being more a function of particle topography and inherent structural strength), then, per unit bed volume, and in unit time, it is surmised that the mass of fines generated will be greater for a bed containing smaller particles. This implies a greater overall attrition rate from a bed of smaller particles. It is is this overall rate which is measured experimentally.

Moreover, for a fixed value of $(U - U_{mf})$, a bed of smaller particles will show greater expansion than one of larger particles. This relationship between particle size and expanded bed height was inadvertently overlooked in these attrition tests. It was shown in Section 5.4.2 that deeper beds result in higher attrition rates, this effect being linear with bed height. One could therefore expect an implicit dependence of attrition on particle diameter. Coincidentally, both Lewis et al (1949) and Shen and Johnstone (1955), by application of the two phase theory of fluidisation, described a relationship between bed height and particle size of the following form:

$$H/H_{mf} = 1 + p(U-U_{mf}) \,/\, d_p^{0.5} \qquad 5.6$$

where H is the expanded bed height, H_{mf} is its value at minimum fluidisation, and p is a system constant. Therefore, noting the effect of bed height on attrition, the measured dependence of attrition on $d_p^{-0.5}$ appears reasonable. The dependence on bed height should more correctly refer to the slumped bed value, which then allows for the explicit dependence on particle diameter as measured experimentally.

Furthermore, it will be shown below that, given the dependence on air velocity and bed height from this set of experiments, dimensional constraints, too, are consistent with a dependence on partice size given by $d_p^{-0.5}$.

5.4.4 Effect of Sorbent Type

Attrition data for the five selected sorbents are listed in TABLE 5.4, for a series of tests conducted at $U=U_{mf} + 0.3$ ms^{-1}, in a 200 mm deep bed. FIGURE 5.6 is the graphical representation of the same data. As expected, the Bredasdorp sample displays a greater attrition propensity than the Lyttelton dolomite sample, with the Marble Hall sample again showing intermediate behaviour. This is consistent with the results of the batch sulphation tests, and the porosity and topographical features described in Chapter 4. All samples approached a steady state attrition rate after about 6 hours of fluidisation (see FIGURE 5.7). The attrition character of the other two samples merits consideration. The very high attrition rates experienced by the Saldanha sample can be attributed directly to its geology - it, like the Bredasdorp sample, is of recent marine origin. It is distinct, however, in that individual particles are penetrated by exceedingly large voids which significantly reduce its structural strength (see Chapter 4). The Saldanha sample suffered extreme attrition, losing 10% of its mass in the first hour. The Umzimkulu dolomite was also characterised by a low structural strength, which should ensure a high attrition propensity, to a level not justified by particle shape or porosity alone. Attrition of the Umzimkulu sample was found to match that of the Bredasdorp sample.

It is apparent from FIGURE 5.6 that sorbent physical strength exerts an influence on attrition propensity, with "harder" particles being more resilient to attrition than "softer" ones. It therefore seems

appropriate to characterise the attrition tendency of different sorbent types by their intrinsic structural strength. The curves in FIGURE 5.6 could be characterised in terms of eq. 5.4. The individual regression constants are tabulated in TABLE 5.6. Average attrition rates were found for each sorbent type from the corresponding curve in FIGURE 5.6 and used to assess the influence of structural strength according to $R = k_3 . \sigma^{c3}$. A comparison of structural strength data for all sorbents, relative to Bredasdorp, produces a value of c3 equal to -0.91. Allowing for errors in the analysis of the load / displacement curves for sorbent structural strength (the coefficient of correlation for the regression fit to raw data was typically 0.95), this value is close enough to -1 to infer that attrition rate is inversely proportional to the measure of structural strength as defined in Chapter 4.

5.4.5 Effect of Temperature

The effects of combustor temperature on attrition rate are twofold. Firstly, on entry to the bed, during their initial heat-up, particles develop temperature gradients which lead to thermal stresses and decrepitation. Secondly, intraparticle forces are weakened resulting in an expected decrease in structural strength.

This first effect was studied by the rapid injection of a known mass of closely sized particles to the fluid bed combustor which had been preheated to 1100 K. Bed depth was kept constant at 100 mm. The sample was then fluidised at $U=U_{mf}+0.3$ ms^{-1} for 15 minutes and the extent of attrition noted. This experiment was repeated for all sample types.

The results are interesting. Excluding the sample from Umzimkulu, the average increase in attrition, over samples fluidised at ambient temperature for the same time period, was 27%. For example, the extent of attrition of the Bredasdorp sample increased from 2.0% to 2.7% over this 15 minute time period, a relative increase of 35%. The Umzimkulu sample, however, showed an absolute increase in the extent of attrition from 1.6% to 8.3%, a relative gain of over 400%. This was attributed to the rapid expansion of gas pockets trapped in the sample [Schie (1987)] and serves to emphasise the need to fully characterise potential sorbents. This "explosive" attrition is evident too in the SEM micrograph, FIGURE D.23.

The effect of prolonged exposure to elevated temperatures was examined for Bredasdorp limestone at 1100 K, at a depth of 100 mm, and a fluidising velocity of $U=U_{mf}+0.3$ ms^{-1}. Samples were held at this elevated temperature for increasingly longer time periods until the attrition rate reached its steady state value. The coarse fraction was not returned to the bed bed following sieve analysis. Rather, a fresh sample was prepared and the experiment repeated from the beginning, but for a longer time period. A small (10 gram) mass was isolated after each test and calcined to constant mass in a muffle furnace at 1100 K to determine the extent to which calcination had occurred during the fluidised bed attrition test. The coarse particle fraction was then normalised for this CO_2 loss. Attrition data are contained in TABLE 5.5. FIGURE 5.8 shows a comparison with attrition at T=298 K, under otherwise identical conditions. Attrition rates are significantly enhanced at elevated temperatures. Over a period of 20 hours, the Bredasdorp sample lost roughly 18% of its mass by attrition at 1100K, compared to approximately 7% at ambient temperature. The form of the attrition curve at high temperature follows eq.5.4. The individual regression constants are given in TABLE 5.6.

It was anticipated that exposure of the sample to elevated temperature would result principally in a change to the structural properties of the sorbent, and that this would be manifest in a change to the measured structural strength of sorbent particles. It was reasoned that attrition rates at two different temperatures could be related to the ratio of sorbent particle strength at these two temperatures. During calcination, the structural properties of the sample will change continuously as CO_2 is evolved. Once calcination is complete, the structural strength will remain constant. For this reason, a comparison of attrition rates achieved at the two temperatures was restricted to an analysis of the steady state values. At 1100 K, R_{ss} = 0.31 %/hour, whilst at 298 K, R_{ss} = 0.07 %/hour. The structural strength of a Bredasdorp sample, calcined at 1100 K, was measured (by the INSTRON apparatus) at 35020 Nm^{-1}, compared to a value of 95400 Nm^{-1} at 298 K (see TABLE 4.5).

Assuming that attrition rate can be described by a relationship of the form $R = k_4 \rho_s \sigma^{c3}$, and allowing for changes in particle density from raw material to calcine, the decrease in structural strength corresponds

to a value of c3 = -1.2. Making allowances for the determination of structural strength of the calcined sample, the computed value of c3 is sufficiently close to -1 to infer that attrition rate is inversely proportional to the structural strength of the sorbent in question.

Discounting the anomalous behaviour of the Umzimkulu sample, it is reasonable to conclude that thermal shock effects play a minor role in attrition compared to calcination and prolonged exposure to elevated temperature. The effect of temperature on attrition rate is accommodated by its effect on sorbent structural strength and solid density (due to calcination).

5.4.6 Effect of Calcination Atmosphere

Under normal operation, the flue gases in a fluidized combustor burning coal will contain 10-15 %v/v CO_2. Since sorbent calcination rate is directly affected by CO_2, and this, in turn, affects the structure of the final calcine product, there is merit in investigating the attrition of samples calcined under a range of CO_2 concentrations.

Calcines of Bredasdorp limestone (300 - 600 μm) were prepared at 1100 K in atmospheres of 100 % N_2, 15 % CO_2 and 60 % CO_2. Calcination times were guided by the tests described in APPENDIX A. The calcine samples were added to the fluidised combustor to a depth of 100 mm and fluidised for a period of 1 hour at $U=U_{mf}+0.3$ ms^{-1}. The following averaged attrition rates were obtained.

CALCINE CONDITIONS	ATTRITION RATE
100 % N_2	13,1 %
15 % CO_2	10,1 %
60 % CO_2	10,0 %

These figures can be compared to an attrition rate of 5,7% for the uncalcined sample after one hour. The data is not comprehensive but it does suggest that CO_2 concentration has a relatively small effect on attrition. It would also appear that attrition is enhanced by a rapid release of CO_2, which is consistent with an increase in intraparticle stresses caused by such release.

5.5 MODEL FOR ATTRITION IN FLUIDISED BEDS

The experimental findings on sorbent attrition indicate an attrition rate response of the form

$$R \propto k(t).\ (U-U_{mf})^2.H.d_p^{-0.5}\ \rho_s\ /\ \sigma(f) \qquad 5.7$$

where k(t) is a function of time, and, for large t, k(t) = p', a constant. Dimensional constraints provide the final form of the relationship:

$$R = k(t)\ \frac{(U-U_{mf})^2\ H\ \rho_s}{\sigma(f)}\ \left[\frac{g}{d_p}\right]^{1/2} \qquad 5.8$$

The right hand side of eq. 5.8 can be expressed as $k(t).N_{We}$ where N_{We} is a modified Weber number and describes the ratio of inertial forces to surface forces. This is consistent with the proposed mechanism of attrition whereby particle inertia promotes abrasion but is resisted by surface forces.

The transient function, k(t), at large times, reduces to a value, p', which multiplied by the remaining components on the RHS of eq.5.8 gives the steady state attrition rate for the specific set of test conditions. Rewriting eq.5.5 as

$$R = a_1\ (1 + a_2.a_3/a_1.\ \exp\ (a_3.t) \qquad 5.9$$

shows that this steady state attrition rate is given simply by the a_1 regression constants in TABLE 5.6. It is thus a straightforward exercise to calculate this proportionality constant for any given set of operating conditions i.e.

$$p' = \frac{a_1\ \sigma(f)}{(U-U_{mf})^2\ H\ \rho_s}\ \left[\frac{d_p}{g}\right]^{1/2} \qquad 5.10$$

The transient form of the attrition rate expression is unwieldy, and a revised form is needed for the sorbent particle population balance which serves as input to an overall sulphation model. It is opportune to recast eq. 5.8 in terms of the total amount of fines generated with time.

When this is done, eq.5.8 becomes

$$R = F(\underline{A})\ \frac{(U-U_{mf})^2\ H\ \rho_s}{\sigma(f)}\ \left[\frac{g}{d_p}\right]^{1/2}$$

$$= 1/p'.\ a_1.\ F(\underline{A}) \qquad 5.11$$

where a_1 is the steady state attrition rate, given by eq. 5.10 and $F(\underline{A})$ is a monotonically decreasing function of $\underline{A}$, the extent of attrition. $F(\underline{A})$ expresses the time dependence of attrition and is described by an equation of the form

$$F(\underline{A}) = 1 + b_1 \exp b_2.\underline{A}$$

Equation 5.11 is the final form for the attrition rate expression.

The extent of attrition, $\underline{A}$, from 5.2 can be written as $\underline{A} = \ln (M_o/M_1)$ where M_o and M_1 are the masses of coarse particles in the bed before, and after, an interval of attrition. If attrition is predominantly by loss of surface protrusions, analogously to a shrinking core reaction model, then

$$\underline{A} = \ln \left[\frac{d_{pn}}{d_p}\right]^3 \qquad 5.12$$

where the mean size of sorbent particles changes from d_{pn} to d_p over the time interval of attrition. The attrition rate transient term $F(\underline{A})$ can now be recast as a function of d_p using 5.11 and 5.12.

The attrition rate for a batch process is thus

$$R = 1/p'.\ a_1.\ F(d_p) \qquad 5.13$$

Extension of this model to continuous sorbent feed is discussed in Chapter 6.

5.6 ELUTRIATION IN FLUIDISED BEDS

The potentially beneficial effect of new surface generation on sorbent sulphation is tempered by increased loss of fine particles from the bed by elutriation. A knowledge of this elutriation is required to predict both the size and residence time distributions of sorbent particles in

the fluidised bed.

It is possible to model elutriation by a first order rate expression, where the flux of particles of a given size is proportional to their weight fraction in the bed, and the elutriation rate constant is described in terms of such variables as particle size, fluidising velocity and bed dimension. Many such correlations for elutriation velocity constant exist, and this historical development of elutriation theory is ably covered by Wen and Chen (1982). Most of these simple correlations are based on experimental data collected in small laboratory combustors, and have little value for predicting elutriation rates from large scale industrial units.

Wen and Chen (1982) derived an empirical correlation for the elutriation rate constant based on a range of experimental data from 14 different investigator groups. A summary of this model is given in APPENDIX F. The accuracy of the model was only ± 50% on a log scale. The great variation in available elutriation rate data, and the lack of standardisation in experimental conditions, are points often re-iterated. George and Grace (1981) concluded that, when all available elutriation data are correlated, the prediction of elutriation rate constant may differ by as much as two orders of magnitude. Although the Wen and Chen model has been used in an overall fluid bed sorbent sulphation model by Dennis (1985), its accuracy was not clearly established.

Having described above the generation of fines by sorbent attrition, it is appropriate to consider explicitly the effect of these fines on the elutriation of coarse particles. The model of Geldart et al (1979) allows for such an analysis. According to this model, the elutriation of coarse particles is enhanced in the presence of significant fines. Holdup of fines in the freeboard leads to an effective increase in gas density, with a resultant decrease in the terminal settling velocity of coarse particles, and hence their increased elutriation. The pertinent equations of this model are outlined in APPENDIX F.

5.6.1. Elutriation Experiments

The above two models were investigated by measurement of elutriation rates during coal combustion in a 300 mm diameter fluidised bed with a freeboard height of 4.5 m. The unit had a thermal capacity rating of about 200 kW and was used for exhaustive tests on the combustion of low grade South African coals (not reported here). Its design is similar to that of the 100 mm diameter vessel used for batch sulphation and attrition tests. The main differences are that propane gas was used to increase bed temperature to the point where coal combustion could be supported, all solids were screw-fed to bed base, and fines recycle was possible via a return leg from the primary cyclone to the coal feed line. Dust samples could be removed from various positions along the freeboard length by an isokinetic sampler connected to a cyclone and cloth filter. The unit has been described in detail elsewhere [Petrie (1985)]. A schematic layout is given in FIGURE 5.9. This unit was used in this study in preference to the smaller combustor, primarily for two reasons. At the air velocities of interest, the bed clearly operated in the bubbling regime. Secondly, the tall freeboard ensured that dust samples extracted from the top of the unit were representative of the elutriate mass.

Elutriation rates were measured during the combustion of a coal whose composition is given in TABLE 5.7, for a fluidising velocity range of 1.0 - 1.75 ms^{-1} from a bed depth of 400 mm. No sorbents were added to the bed during these tests. A sieve analysis was performed on the elutriate mass with the aid of an ATM ultrasonic sieve shaker.

5.6.2 Elutriation Results

Measured elutriation rates are given in TABLE 5.8 with sieve analyses of the elutriate quantities. Derived values of elutriation rate constants are given in TABLE 5.9 for these data.

FIGURE 5.10 gives an indication of the Wen and Chen model fit to elutriation data. The degree of correspondence with measured data is poor, with a large portion of the data lying outside the ± 50% accuracy limit cited by the authors. On this basis, use of this model is not recommended. The model of Geldart provided more encouraging results.

FIGURE 5.11 shows a least squares regression fit of this form against measured data.

The numerical values of the regression coefficients differ, however, from those listed by Geldart, and the final form of the correlation is

$$E / \rho_e U = 1.78 \exp(-1.84\ U_{ts}/U) \qquad 5.14$$

This form of the elutriation rate coefficient is used in Chapter 6 to derive an expression for the residence time distribution of the variously sized sorbent particles in the fluidised bed.

5.7. CONCLUSIONS

A sorbent attrition model has been derived, based on extensive experimentation in a laboratory fluidised combustor. The model applies to batch fluidisation, where all particles have the same age in the bed. The final form of this model (eq.5.11) describes only those attrition components which derive from continuous particle motion within an FBC. It is envisaged that any "once-off" attrition effects, such as thermal shock, can be accommodated in an overall solids population by their effect on the feed size distribution. This is the approach adopted in Chapter 6. Though the development of this model has borrowed much from the Westinghouse model for attrition in the bubbling zone of a fluidized bed [Vaux and Scruben (1983)], it has been generalised to include the effect of high velocity impacts, whilst the exact dependence on particle diameter, structural strength, and topography has been substantiated by experiment.

Two experimentally derived elutriation rate expressions were assessed using elutriation data gathered from a pilot scale combustor burning coal. The best fit of measured data was obtained with the model of Geldart (1979) which considered the effect of fines generation on the elutriation of coarse material.

Both the attrition and elutriation models are of a form which can be linked to sorbent sulphation kinetics, and incorporated, via particle size and residence time distributions, directly in an overall model for

sorbent sulphation in a fluidised bed combustor. This is developed further in Chapter 6.

CHAPTER 6 - FLUIDISED BED SULPHATION MODEL

6.1. INTRODUCTION

The complexity of the fluidised combustion process in which SO2 removal is effected by sorbent addition was discussed briefly in Chapter 1. The mathematical description of the sulphation rate process was defined in Chapter 2, and supported by experimental evidence gained for a wide range of South African sorbents in Chapter 3. Sorbent properties were shown in Chapter 4 to dictate overall utility. The interaction of sorbent physical properties and bed fluid dynamics was addressed under the headings of sorbent attrition and elutriation in Chapter 5. It is now possible to relate these findings in an overall process model for sorbent sulphation in a fluidised combustor with continuous sorbent feed.

The primary requirement of such a process model is that it be capable of predicting the behaviour of any sorbent in a fluidised combustor, independently of equipment scale. Overall sulphation models fall into two classes. In the first case, sulphation propensity is described by simple expressions which ignore sorbent specificity completely, and make no attempt to describe sulphation kinetics. Sulphur retention is generally given as an empirical function of Ca/S molar ratio. This approach has been followed where sorbent performance is deemed to be secondary to the understanding of coal devolatilisation and char combustion [Bukur and Amundson (1981), Rajan and Wen (1981)]. The second class of process models derives from sulphation kinetic data coupled to equations which describe the fluid dynamics of a combustor. Included in this set are those models which describe sulphation kinetics by empirical correlations based on large sets of experimental data [Koppel (1970), Keairns (1975)]. Although such a description may have wide applicability in terms of sorbent selection, its extrapolative merit with regard to equipment scale is in question.

To an extent this limitation is overcome in the modelling approach of Fieldes (1979), where sulphation kinetics are described in terms of true physical processes occurring in the combustor. This model can be scaled

directly to industrial sized units. This approach was simplified by Zheng et al (1982) without loss of physical accuracy (see Chapter 3). These two models assume that all particles are of the same size and age within the system, and therefore possess the same reactivity. No allowance is made for feed size variation nor particle shrinkage kinetics due to attrition. One of the most sophisticated sulphation models (due to Dennis (1985)) makes allowance for the distribution of particle sizes and ages within the system, and goes as far as to consider the significance of freeboard sulphation due to the hold up of fineparticles. However, this model, too, fails to consider sorbent attrition.

The information at hand on the attrition propensity of South African sorbents allows this deficiency to be rectified.

6.2 MODEL OF SULPHUR CAPTURE FOR SORBENT FEED OF WIDE SIZE DISTRIBUTION

The starting point for this development is the simple model of Zheng et al (1982). This model is attractive because the sulphation propensity of a selected sorbent is described directly in terms of sorbent feed rate, for a given set of combustor operating conditions. This makes its use by design engineers straightforward. The current approach is to link sulphation kinetics (described by the kinetic parameters proposed by Zheng et al) to combustor fluid dynamics, utilising the attrition and elutriation rate expressions developed in Chapter 5.

A schematic layout of the combustor is shown in FIGURE 6.1. Sorbent feed is continuous, and bed level is maintained by a solids draw-off stream. Sorbent fines leave the bed by elutriation. The following assumptions pertain:

1. The combustor operates at steady state
2. The two phase fluidisation theory applies. Gas and solids are well mixed within the particulate phase, whilst bubbles are in plug flow. The sulphation reaction occurs only in the particulate phase.
3. Sorbent calcination is rapid.
4. Combustion and sulphation are decoupled. Coal devolatilisation is instantaneous, and SO_2 is released uniformly throughout the bed during this process.

5. Freeboard sulphation is unimportant
6. Attrition occurs predominantly by an abrasion mechanism. Fragments thus generated are themselves not subject to further attrition
7. The total number of coarse particles in the combustor is unchanged with time.
8. Fines generated by attrition, or present in the feed stream, do not take part in the sulphation reaction, because of their short residence time.
9. Attrition is a continuous process; any instantaneous effects are accommodated by changes to the feed size distribution
10. Sulphation of coal ash particles is treated separately. The measured "base" SO_2 levels refer to those subsequent to ash adsorption

6.2.1 Validity of Model Assumptions

Some of the assumptions made in the previous section are uncomplicated and are given only a brief treatment in the discussion which follows. Where their validity is less clear, a more detailed discussion is offered.

* Assumptions 1 and 2 are common to fluidised combustion processes. Sorbent particles are sulphated over a time period of about 1 hour.
* Assumption 3 is supported by experimental evidence [Dennis (1985)]. The sorbent population balance described below therefore refers to solid flows on a calcined basis. Likewise, sorbent attrition is described by the compressive strength of sorbent calcines.
* Assumption 4 is a reasonable assertion, and is the basis of most coal combustion modelling studies where devolatilisation is considered [Gibbs (1975), Horio and Wen (1978), Park et al (1979)]. The uniform release of SO_2 stems from bed solids being well mixed.
* Assumption 5 follows from Dennis (1985). The significance of fines generation is treated at length in Sections 6.4.2.3 and 6.4.2.4.
* Assumption 6 is supported by much evidence - see discussion in Chapter 5. Assumption 7 follows directly from this definition.
* Assumption 8 is readily supported [Dennis (1985)]. Furthermore, it is a necessary condition of this model - the sorbent population balance outlined below applies to coarse particles only
* Assumption 9 is made in the interest of simplicity. Little work has been undertaken on "once-off" attrition effects, though the

investigative team at Westinghouse attribute only about 25% of total attrition to continuous bubbling bed activity [Vaux (1978)]. A rigorous treatment of this attrition component would require a statistical mechanical approach in terms of "birth" and "death" entities, which is incompatible with the methodology followed here. Incorporation of this effect into feed stream changes is consistent with the steady state hypothesis.

The interplay of sorbent and coal ash particles requires closer scrutiny. At steady state, the mass of carbon particles in the fluidised bed is typically in the region of 1-2% [Bukur and Amundson (1981)]. It can therefore be assumed that the bed contains only calcined sorbent and coal ash particles. This is a reasonable assertion, particularly when high ash coals are combusted. Noting, furthermore, that solids in the bed are well mixed, the steady state mass of sorbent particles in the bed, W, is found from

$$W = \frac{F_o\, M}{F_o + w_a F_c} \qquad 6.1$$

where F_o is the mass flow rate of sorbent on a calcined basis, F_c is the coal feed rate, with an ash content, w_a, and M is the total mass of solids in the bed. In the derivation of the sorbent population balance which follows, sorbent particle residence times are based on sorbent mass in the bed, whilst the feed stream is assumed to comprise sorbent particles only. It can be seen that this is equivalent, in terms of mean solids residence time, to considering the total flow (sorbent plus coal ash) in a bed of mass M. This simplifies the population balance equations, as no knowledge of the coal ash feed stream size distribution, or of ash attrition propensity, are required. The extent to which coal ash is effective as a sulphur sorbent is examined for a specific coal sample in Chapter 7.

6.2.2 Sorbent Population Balance

The derivation of the sorbent population balance follows the approach of Kunii and Levenspiel (1969) for continuous sorbent feed. The mass distribution functions for particles of size d_{pi} in the feed, bed, bed overflow and elutriation streams are given by $p_o(d_{pi})$, $p_B(d_{pi})$, $p_1(d_{pi})$ and $p_2(d_{pi})$ respectively. These mass distribution functions refer to the

normalised mass of calcium oxide in each stream of size d_{pi}. Each distribution function is normalised over the particle size range. Furthermore, because bed solids are well mixed, $p_B(d_{pi}) = p_1(d_{pi})$. The steady state mass balance for particles in the size range d_{pi} to $d_{pi} + \delta d_{pi}$, in unit time, is as follows:

$$\left[\begin{matrix}\text{solids in}\\ \text{feed}\end{matrix}\right] - \left[\begin{matrix}\text{solids in}\\ \text{overflow}\end{matrix}\right] - \left[\begin{matrix}\text{solids in}\\ \text{carryover}\end{matrix}\right] + \left[\begin{matrix}\text{solids shrinking}\\ \text{from larger size}\end{matrix}\right]$$

$$- \left[\begin{matrix}\text{solids shrinking}\\ \text{to smaller size}\end{matrix}\right] + \left[\begin{matrix}\text{solid generation}\\ \text{in this interval}\end{matrix}\right] = 0 \qquad 6.2$$

Using the above distribution functions, and noting that the number of particles in the size interval d_p to $(d_p + dd_p)$ is given by

$$N(d_p) = \frac{W\, p_1(d_p)\, dd_p}{\rho_s\, \pi\, d_p^3} \qquad 6.3$$

where W is the total weight of sorbent particles in the bed, eq. 6.2 becomes

$$F_o\, p_o(d_p)\, dd_p - F_1\, p_1(d_p)\, dd_p - W\, K^*(d_p)\, p_1(d_p)\, dd_p - W \frac{d}{dd_p}\left[r(d_p)\, p_1(d_p)\right] dd_p + \frac{3\, W}{d_p}\, r(d_p)\, p_1(d_p)\, dd_p = 0 \qquad 6.4$$

where $r(d_p) = dd_p/dt$, defines the kinetics of particle shrinkage due to attrition, using assumptions 6 and 9 above, and K^* is the elutriation velocity constant. The overall balance for all sorbent solids in the system is

$$F_2 + F_1 - F_o = \int \frac{3\, W\, p_1(d_p)\, r(d_p)\, dd_p}{d_p} \qquad 6.5$$

At this point there is no need to preclude the possibility of elutriation of coarse particles. The elutriation rate constant, $K^*(d_{pi})$, for particles of mean size d_{pi}, is found from the expression for E (eq. 5.14), according to $K^*(d_{pi}) = E\, A/W$, and is defined as

$$K^*(d_{pi}) = \frac{F_2\, p_2(d_{pi})}{W\, p_1(d_{pi})} \qquad 6.6$$

The above three equations form the basis of the sorbent population balance. After manipulation, their final form is

$$p_1(d_p) = \frac{F_o d_p^3}{W r(d_p)} \; I \int \frac{p_o(d_p) dd_p}{d_p^3 \; I} \; dd_p, \quad \text{where } I = \exp\left[-\int \frac{F_1/W + K^*(d_p)}{r(d_p)} dd_p\right] \qquad 6.7$$

$$\frac{W}{F_o} = \int \frac{d_p^3}{r(d_p)} \; I \int \frac{p_o(d_p) dd_p}{d_p^3 \; I} \; dd_p \qquad 6.8$$

where all integrations are performed over the interval
$d_p \; @t=\infty < d_p < d_{p\,max}$

The expressions for $r(d_p)$ and $K^*(d_p)$ derived in Chapter 5 are non linear functions of particle diameter, d_p. Their incorporation into the sorbent population balance equations 6.7 and 6.8 necessitates the discretisation of these equations, and iteration about the unknown solid flow streams until a solution is found. Such an exercise is prone to inaccuracy unless a very large number of size intervals is used. Overturf and Kayihan (1979) favoured a solution obtained by discretisation of eq. 6.4 - 6.6 using the discrete distribution analogs of $p_1(d_p)$. Using this method, an accurate solution can be obtained with a much smaller number of size intervals. Following this approach, then, the working form of the sorbent population balance equations is given by

$$F_2 + F_1 - F_o = 3W \; \Sigma \left[\frac{F_1(d_{pi}) \; r(d_{pi})}{F_1 \; d_{pi}}\right] \qquad 6.9$$

$$\frac{F_1(d_{pi})}{F_1} = \frac{F_o(d_{pi})\delta d_{pi} - W/F_1 . r(d_{pi+1}) . F_1(d_{pi+1}) . (\delta d_{pi}/\delta d_{pi+1})}{-Wr(d_{pi}) + F_1 \delta d_{pi} + WK^*(d_{pi})\delta d_{pi} - (3W/d_{pi}) r(d_{pi}) \delta d_{pi}} \qquad 6.10$$

$$\Sigma \frac{F_1(d_{pi})}{F_1} = 1 \qquad 6.11$$

$$F_2(d_{pi}) = W \frac{F_1(d_{pi})}{F_1} K^*(d_{pi}) \qquad 6.12$$

The residence time for sorbent particles of size d_{pi} is then given by

$$\tau(d_{pi}) = \frac{1}{F_1/W + K^*(d_{pi})} \qquad 6.13$$

6.2.3 Overall Process Model

Using the assumption that sulphation is restricted to the bed region of the combustor, the overall sulphur mass balance is given by eq. 2.27. From the sample calculation in APPENDIX B, the interphase exchange coefficient, $\underline{X}$, is large, and this equation reduces to

$$F_c \, w_s/32 = AUC_a + Q \qquad 6.14$$

where Q is the overall rate of reaction for sorbent particles of all sizes, and F_c is the coal feed rate.

Following the methodology of Zheng at al (1982), the overall rate of reaction of sorbent particles of size d_{pi} is given, similarly to eq. 2.25 by

$$Q(d_{pi}) = \int_0^{t_s(C_a)} C_a \, S_c \, k_s . \exp(-k_d . t) \frac{1}{\tau(d_{pi})} \exp\left[-\frac{t}{\tau(d_{pi})}\right] dt \qquad 6.15$$

where, $\tau(d_{pi})$ is the residence time of particles of size d_{pi} in the bed, given by eq. 6.13, and t_s, the sulphation time of individual sorbent particles, is dependent on the bulk SO_2 concentration in the fluidised bed.

The overall rate of reaction for all sorbent particles is then simply

$$Q = \int_0^{d_{p\,max}} Q(d_{pi}) \, dd_p \qquad 6.16$$

Noting that, for spherical particles, $S_c = \frac{6W}{\rho_s \, d_p}$ where W = bed weight

eq. 6.16 becomes

$$Q = \int_0^{d_{p\,max}} \int_0^{t_s} \frac{6 \, k_s \, W}{\rho_s \, d_{pi}} C_a \exp(-k_d . t) \frac{1}{\tau(d_{pi})} \exp\left[-\frac{t}{\tau(d_{pi})}\right] dt \, dd_p \qquad 6.17$$

Zheng at al (1982) showed that both k_s and k_d were essentially independent of d_p, or, at least, that the dependency was weak, and masked by the accuracy of the batch sulphation experiments used to determine the kinetic constants. This was confirmed by Motherwell (1986) who measured sulphation kinetics for four size fractions of the South African Marble Hall limestone. For these experiments, k_s values ranged

from 9 - 11 cm/s for particles of mean size from 250 μm - 750 μm. These values are slightly less than the mean value reported in this work for the same sample, and is thought to be a consequence of the "freehand" graphical procedure used by Motherwell to determine k_s. Fieldes (1979) did detect some dependence of sulphation kinetics on external mass transfer, which would imply that k_s is proportional to $1/d_p$. However, from his TABLE 8, values of k_s ranged from 12,1 to 13,7 cm/s for sorbent particles in the size range $0,78 < d_p < 2,0$ mm which is typical of sorbent particles fed to fluidised combustors. This confirms that the dependence on particle size is weak. Fieldes also confirmed that, for a given flue gas SO_2 concentration, t_s does not depend on particle size, which supports the stated claim that k_d is also independent of d_p.

Using the definition of sulphation efficiency given by eq. 2.30, and, with eqs. 6.14 and 6.17, this becomes

$$\eta = 1 - \left[\frac{1}{1 + \int_0^{d_{p\,max}} \int_0^{t_s} \frac{6\ k_s\ W}{\rho_s\ d_{pi}} C_a \exp(-k_d.t)\ \frac{1}{\tau(d_{pi})}\ \exp\left[-\frac{t}{\tau(d_{pi})}\right] dt\ dd_p} \right] \qquad 6.18$$

This is the final form of the overall process model for sorbent sulphation in a fluidised bed combustor. Sulphation kinetics are included through the parameters, k_s and k_d, whilst attrition and elutriation rate constants are coupled to the residence time distribution through the sorbent population balance expressions 6.9 - 6.12.

Unlike the simple epxression of Zheng et al (1982) for single sized particles, the calcium to sulphur molar ratio does not appear as an explicit parameter in 6.18. However, the mass of sorbent particles, W, in the bed at steady state is related to the sorbent feed rate, F_o, by

$$W = \int F_o\ p_o(d_p)\ \tau(d_p)\ dd_p \qquad 6.19$$

whilst the calcium to sulphur molar ratio, R_{cs}, is defined simply as

$$R_{cs} = \frac{F_o\ f_s/56}{F_o\ w_s/32} \qquad 6.20$$

It is thus a straightforward exercise to find the degree of sulphur retention in eq. 6.18 for any given R_{os} value.

6.3. STEP BY STEP SOLUTION PROCEDURE

To ascertain the degree of SO_2 abatement which can be achieved for addition of a known quantity of a specified sorbent, the following information is required:-

* k_s and k_d for the sorbent in question
* sorbent purity, f_s
* coal feedrate, F_c, and its sulphur and ash content, w_s and w_a
* $p_o(d_p)$, the size distribution of sorbent feed
* fluidising velocity, U
* total mass of bed contents
* sorbent compressive strength and topographic data, $\sigma(f)$

The sulphation kinetic parameters are obtainable by a simple batch experiment in a fluidised combustor (Chapter 3), whilst measurement of compressive strength is established by the piston press experiments described in Chapter 4. Calculation of Ω, the fractional reduction in SO_2 emissions, from eq. 6.18, proceeds as follows:

(i) For a given Ca/S molar ratio, sorbent feed rate (on a calcined basis) is calculated from eq. 6.20, and the steady state mass of sorbent particles in the bed, W, from eq. 6.1.

(ii) An expression for $r(d_p) = dd_p/dt$, required by eq. 6.10, is found from eqs. 5.1, 5.11 and 5.13 i.e.

$$R = - d_p/3 \; dd_p/dt \qquad 6.21$$

$$R = 1/p' \; a_1 . \; F'(d_p) \qquad 6.22$$

where p', a_1, and $F'(d_p)$ are fixed for a specific sorbent and a given set of combustor operating conditions. Therefore,

$$r(d_p) = dd_p/dt = -3/d_p . \; 1/p' \; a_1 \; F'(d_p) \qquad 6.23$$

which can be used directly in the population balance expressions 6.9-6.12. The use of this equation is straightforward only for a feed stream of uniform size, where particle shrinkage can be equated directly to the length of time a particle has spent in the bed. The assumptions necessary to achieve a solution for the case of a general feed distribution are discussed in Section 6.4. In the interim, the development outlined below assumes that a workable form of eq. 6.23 is available.

(iii) The solution strategy for the discretised population balance expressions follows that of Levenspiel (1979). The size range of sorbent particles is divided into a small number (say 10) of size intervals based on available sieve apertures. The arithmetic mean particle size for each interval is then established.

(iv) The elutriation rate constant, $K^*(d_{pi})$, is calculated for the mean particle size in each interval using the modified Geldart (1979) correlation, eq. 5.14

(v) An estimate is made of F_1, and eq. 6.10 solved for each size increment. This process is repeated until the summation constraint of eq. 6.11 is met.

(vi) The carryover flowrate, F_2, is then found from eq. 6.9, and the composition of this stream from eq. 6.12

(vii) At this stage all three sorbent flow streams and their size distributions are known. The residence time of the mean particle size in each increment is now easily calculated from eq. 6.13.

(viii) The time integral of eq. 6.18 can be evaluated analytically.

Thereafter, from eq. 6.18

$$\eta = 1 - \left[\frac{1}{1 + \int_0^{d_{p\,max}} \frac{6\, k_s\, F_0(d_p)\, \tau(d_p)}{\rho_s d_p\, UA(1 + k_d\, \tau(d_p))} \left[1 - \exp\left[- \frac{t_s}{\tau(d_p)} (1 + k_d \tau(d_p))\right]\right] dd_p} \right] \qquad 6.24$$

The integral term in eq. 6.24 is evaluated numerically by discrete summation over the sorbent particle size range, using $\tau(d_{pi})$ from (vii). The reduction in SO_2 emission level is now available directly from eq. 6.24.

6.4 SIMPLIFIED MODEL

6.4.1. Attrition Rate Dependence

Use of eq. 6.24 is complicated by inclusion of the size specific particle residence time, whose derivation is dependent on the non linear term for particle shrinkage in eq. 6.23, which, as shown above, is strictly valid only for a monosized sorbent feed. Where the feed stream has a wide size distribution, the solution approach requires the use of joint size / age distribution functions [Hulbert and Katz (1964), Randolph and Larson (1971), Schruben and Vaux (1983)], and the procedure described above is in error.

However, the relative magnitudes of particle residence time and transient attrition rate time constant, permit eq 6.23 to be simplified, and a solution to the population balance equations can still be obtained by the approach of Kunii and Levenspiel (1969). This simplification is described below.

It was shown in FIGURE 5.7 that, for all five sorbents tested, the attrition rate R(t) approached its steady state value after an age in the bed of approximately 4 - 6 hours. However, under normal operating conditions, and for the sorbent particle size range typical of fluidised combustors (APPENDIX G), residence times are in the region of 10 - 35 hours. It is therefore surmised that little loss of accuracy would be incurred if the attrition rate was described in the population balance equations by the steady state term. This is particularly so at low Ca/S ratio, where residence times are greatest. Eq.6.23 is then replaced by

$$r(d_p) = dd_p/dt = -3/d_p .\ 1/p'\ a_1 \qquad 6.25$$

where p' and a_1 are available from experimental attrition data. This approximation allows the numerical integrations of eq. 6.10 and 6.24 to be performed with ease, for any generalised feed distribution, with the

qualification that fines do not contribute to the sorbent population balance.

6.4.2. Effect of System Parameters

This revised model is used to ascertain the effect of fluidised combustor system variables on sorbent performance. APPENDIX G provides an example of the calculation procedure. The choice of size intervals used was based on available sieve apertures. In all parameter studies, the pore plugging time was held constant at 1 hour. This is consistent with sulphation times measured in Chapter 3 for South African sorbents, where the bulk SO_2 concentration was between 1000 - 2000 ppm. Furthermore, the fluid bed operating temperature was fixed at 1123 K (which was the temperature at which the sulphation kinetics of the South African sorbents were measured). All simulations were carried out for a fluid bed height of 1 metre.

6.4.2.1 Sorbent Type

The predictive value of the sulphation model was investigated for three sorbents which, on the basis of their measured sulphation kinetics (Chapter 3), displayed widely varying sulphation patterns. FIGURE 6.2 shows the fractional reduction in flue gas SO_2 levels for Bredasdorp, Lyttelton and Marble Hall sorbents, plotted as a function of Ca/S molar ratio, for a uniformly sized feed, d_p = 750 μm, U = 1 ms^{-1}, R(t) = 5% hr^{-1}. As expected from the magnitude of their respective kinetic constants, the Bredasdorp sample displayed the highest reactivity, followed by the Marble Hall sample, with the Lyttelton dolomite being the least reactive. An 80% reduction in base emission level is attainable with Bredasdorp lime at a Ca/S ratio of about 1.25, whereas a value in excess of 4 would be required of the other two sorbents for the same degree of SO_2 reduction. This difference is exaggerated when the comparison is made on a mass basis, particularly for the dolomitic Lyttelton sample.

6.4.2.2. Fluidising Velocity

FIGURE 6.3 shows the model prediction of the effect of fluidising velocity on the sulphation propensity of Bredasdorp limestone. Fluidising velocities spanned the range 1 - 2 ms^{-1}, which is typical of conventional bubbling fluidised combustors. Feed size distribution, attrition rate and bed temperature are all as above. As expected, increasing U results in a decrease in SO_2 retention because of the reduced sorbent particle residence time in the bed. This effect more than offsets the marginal improvement in reaction rate due to increased particulate phase SO_2 [Dennis (1985)]. At the fluid bed operating conditions chosen for the batch sulphation studies in Chapter 3, the interphase exchange coefficient is large enough such that $C_a = C_{ap}$. Doubling the fluidising velocity from U=1 ms^{-1} to U=2 ms^{-1} increases the sorbent flow required to effect an 80% reduction in base SO_2 emissions by a factor of 3.2 i.e. the required Ca/S ratio increases from 1.25 to 4. For these velocities, and for the particle size range of interest, where fines are discounted, $\tau(d_p)$ exceeds t_s, and, in the absence of attrition, particles leave the bed only once pore blockage has occurred. Moderate attrition at this velocity therefore enhances sorbent sulphation capacity by removal of the external sulphate layer and exposure of "fresh" sorbent surface for reaction.

The numerical values of the sulphation kinetic parameters, k_s and k_d, used in this comparison, are those derived via the batch sulphation experiments described in Chapter 3, for U = 0.7 ms^{-1}. It was shown by Zheng et al (1982) that both k_s and k_d increased with fluidising velocity. The exact nature of this dependence was unspecified but was thought to contain both external mass transfer and pore diffusion components. In this current work, no attempt is made to unravel the nature of this dependence, and both k_s and k_d are used simply as empirical parameters to describe the sulphation kinetics of a given sorbent. It is assumed, for the purpose of investigating the effect of fluidising velocity on sulphation efficiency, that both k_s and k_d display the same dependence on U. The implications of this assertion are detailed below.

For the following set of typical conditions

$\tau(d_{p\ mean})$ = 15 hours (see APPENDIX G)

t_s = 1 hour (from sulphation kinetics study)

k_d = 0.003 s^{-1} (from TABLE 3.4)

the exponential term in eq. 6.24 can be neglected, and eq. 6.24 effectively reduces to

$$\eta = 1 - \left[\frac{1}{1 + \int \frac{6\ k_s\ F_o(d_p)}{\rho_s\ d_p\ k_d\ U\ A}\ dd_p}\right] \qquad 6.26$$

from which it can be seen that, if both k_s and k_d are governed by the same dependence on fluidising velocity, this dependence disappears from the sulphation rate term in eq. 6.26, leaving a rate contingent on 1/U. This condition is examined further in Chapter 7 with sulphation data generated by a large scale fluidised combustor.

Another attendant simplification of the above analysis is that, over the range of velocities considered, the total bed inventory does not change. The population balance expressions were solved for a constant mass of solids in the bed, independently of fluidising velocity. This is not strictly correct. Bed expansion will be greater at higher velocities, which will affect the mass of solids in the bed and the magnitude of the overflow stream through the desire to maintain constant bed height. However, for a large scale fluidised bed, in which the ratio H/D_c is small, this effect can be neglected.

6.4.2.3 Feed Size Distribution

The attrition model developed in Chapter 5 does not make allowance for those forces which result in "once-off" attrition of sorbent. For ease of numerical handling, the effect of mechanical stresses in sorbent feed lines, and thermal stresses acting on sorbent particles on their entry to the fluidised bed, are lumped together in this work, and considered as changes to the sorbent feed distribution. There are two consequences of instantaneous attrition. The sorbent flow rate to the bed must be modified to reflect only the mass flow of coarse particles - i.e. any fines generated in feed lines etc., do not form part of the solids population balance and should be discounted. In addition, the size distribution of coarse particles must be adjusted to account for this

wear effect. The extreme case would be one where a feed of single sized sorbent particles is subjected to "once-off" abrasion. This example is presented in FIGURE 6.4 for Bredasdorp lime, fluidised at U=1 ms^{-1}, at T_{bed} = 1123 K. The reduction in SO_2 emissions for a single sized feed of d_p = 750 µm is compared with that obtained from two modified distributions - the first being a log normal distribution ($d_{p\ mean}$ = 750 µm, σ^2 = 1,25), and the second a linear distribution where the total feed stream is split evenly over the three largest size intervals

i.e. $F_o(d_{p1})$ = 1/3 F_o		500µm <d_p< 1000µm
$F_o(d_{p2})$ = 1/3 F_o		300µm <d_p< 500µm
$F_o(d_{p3})$ = 1/3 F_o		212µm <d_p< 300µm

From FIGURE 6.4 it can be seen that, whereas a Ca/S molar ratio of approximately 1.5 is required to effect an 80% reduction in flue gas SO_2 level for the single size feed, the log normally distributed feed achieved the same reduction with a Ca/S of 1.2, and the "1/3 linear" distributed feed with a Ca/S of 0.8. This is equivalent to a spread in required sorbent feed rates of 100%, which has obvious economic implications.

The calculations detailed in FIGURE 6.4 focussed only on the effect of changes to the feed distribution, and did not consider the loss of viable sorbent mass due to instantaneous fines generation, and its subsequent elutriation. This loss will offset, by an unknown extent, the advantages gained by opting for a feed with a wider size distribution. This point notwithstanding, the arbitrary feed distributions examined above provide an indication of the extent to which the size distribution of sorbent particles in the feed stream affects sulphur retention.

6.4.2.4 Attrition Rate

Following the discussion in Section 6.4.1, the influence of attrition rate on sulphur capture efficiency can be examined through the effect of the steady state attrition term, R_{ss}. Since calcination is assumed to be rapid, attrition rates incorporated in the sulphation model refer to those experienced by sorbent calcines. The effect of attrition rate was considered for a monosized feed ($d_{p\ mean}$ = 750 µm) of Bredasdorp

limestone fluidised at a velocity U = 1 ms^{-1}, in a bed 1 metre in height. The compressive strength of this calcined material was taken as 35020 Nm^{-1} (TABLE 4.5). Under these conditions, R_{ss}, calculated from the attrition model (eq. 5.11) is equal to 8.5 %/hr (APPENDIX G). Since the Bredasdorp sample was one of the more friable materials, it seemed reasonable to investigate the effect of attrition over the range 0%/hr < R_{ss} < 10 %/hr. This upper bound is greater than attrition rates commonly cited in the literature [Ulerich et al (1979) quoted a value of R_{ss} = 4%/hr for a lightly sulphated Tymochtee dolomite] but compensates, to an extent, for the higher rates measured during the transient period.

On examination, it was found that R_{ss} values in excess of about 9% per hour could not be accommodated by the overall sulphation model - because of the excessive fines generation accompanying such high attrition rates, the coarse particle population balance (eq. 6.10 and 6.11) could not be satisfied. This places an obvious applicability limit on the sulphation model as postulated. However, because attrition rates measured in practice are typically less than this figure, this does not pose too great a problem.

From FIGURE 6.5 it can be seen that an 80% reduction in flue gas SO_2 level can be achieved with a Ca/S ratio of 1.6 for R_{ss} = 1% / hour. This sorbent feed requirement is decreased as attrition rate is increased, until, at R_{ss} = 9% / hour, a Ca/S ratio of 1.2 only is required. This equates to a 33% reduction in sorbent requirement, which is not insignificant. The potential benefit of controlled attrition increases slightly with the requirement for greater reduction in SO_2 levels - at 90% reduction, R_{ss} = 9%/hr ensures a 40% reduction in sorbent feed rate over the base case of R_{ss} = 1%/hr.

The effect of varying attrition rate, from FIGURE 6.5 is not as pronounced as might first be expected. This is a consequence of the assumptions made in the derivation of the sulphation model, in which the reaction is constrained to the bed region, and the influence of fines generated by attrition is discounted. In addition, it was assumed that the sulphation time t_s is a function only of SO_2 concentration. In reality, t_s will increase as attrition proceeds. This effect was not examined.

The influence of fines generation and freeboard sulphation on overall sorbent performance is not uncomplicated. It is commonly accepted that the residence time of sorbent fines is too short to lead to any substantial improvement in sorbent utility. The model, as postulated, does not make allowance for larger fragments (say ± 150 μm) which may result from abrasive wear of sorbent particles with significant topography - these fragments are expected to be elutriated and do not form part of the solids population balance. However, U_{ts} for these particles is, according to Geldart (1979), in the region of 1 ms^{-1}, and their residence time in the bed is, in reality, of sufficient magnitude for them to be fully sulphated.

The significance of freeboard sulphation is not clear. Fee et al (1984) estimated that this mechanism contributed about 10% to overall sulphation, whilst Dennis (1985) argued that the dilution of SO_2 by bubble phase gas in the freeboard led to an overall decrease in utility compared to the case where all sulphation occurred in the bed.

In this current work, any attempt to consider the potential benefit of fines generation would necessitate the reformulation of the sulphation model in terms of joint size / RTD. This approach was followed by Vaux and Schruben (1983) but only for an attrition rate model which was independent of particle size. Extension to more general attrition kinetics was not attempted.

However, it is felt that the model, as proposed, does represent the effect of attrition on sulphation with reasonable accuracy. Because of the way in which the model is formulated, predicted sorbent flow rates for a desired reduction in SO_2 are conservative and should thus serve as useful guidelines for design purposes.

6.5 CONCLUSIONS

A model has been proposed for sulphation of sorbent particles in a fluidised bed during coal combustion. Sulphation was assumed to occur within the bed bulk only, and the action of fines was discounted. The model is straightforward to use, and requires a minimum of experimental support data. The predictive capability of the model was examined for different sulphation kinetics, fluidising velocity, feed size

distribution and attrition kinetics.

Fluidising velocity exerts considerable influence on SO_2 retention as predicted by this model. This is a consequence of reduced particle residence time. However, it is sorbent selection, and hence the choice of sulphation kinetics, which exert the greatest influence on SO_2 retention. The effect of sorbent attrition, although significant, proved to be less important than was originally anticipated. The correspondence between attrition propensity and sulphation capacity described in Chapters 3,4, and 5 is therefore partially misleading. Although sorbent physical characteristics, such as porosity, topography, granularity and crystallinity are important in defining attrition tendency, it is their effect on the generation of calcine pore volume, and on the distribution of pores within the calcine matrix, which largely dictates the sulphation capacity of a particular sorbent.

The effect of instantaneous sorbent attrition on sulphation was inferred through the feed size distribution. If the mechanism of attrition in feed lines etc is one of abrasion, resulting predominantly in fines generation, and if fluidising velocities are high enough to ensure elutriation of this fine material, such attrition would be deleterious to sulphation. However, should instantaneous attrition result, rather, in particle fracture (and there is little evidence to suggest otherwise), the sulphation model predicted an enhancement in sulphur uptake with attrition. The implications of this statement for fluidised combustor design and operation are clearly evident. Where possible, sorbent selection must ensure a low fines content, and a mean particle size such that elutriation is minimised. Attrition sites in sorbent feed lines which result in fines generation should be redesigned to minimise such action.

Although the process model proposed here is based on sulphation and attrition kinetic data collected from small scale equipment, the rate expressions derived from these data are founded, where possible, on sound physical principles, or are, at least, supported by data sets from other research groups. As such, the sulphation model is thought to have general applicability, and should prove to be of value in assessing sorbent performance in industrial-scale fluidised combustors. This assertion is examined in more detail in the next chapter.

CHAPTER 7 - PREDICTION OF SORBENT PERFORMANCE IN AN INDUSTRIAL FLUIDISED COMBUSTOR

7.1 INTRODUCTION

Fluidised bed combustion is a relatively new technology to South Africa and, to date, little quantitative information on the performance of South African coals in industrial scale FBC units has been collected. The number of industrial units currently in operation is small (less than 10) but duties include gasification, steam raising and hot gas generation duties [Eleftheriades (1987)]. None of these units employs desulphurisation technology, primarily because local air pollution regulations do not require a reduction in SO_2 levels below base emissions. However, this picture is expected to change with a move towards increased utilisation of low grade, high sulphur coals, as outlined in Chapter 1. For this reason, there is a need to generate a data base of sorbent performance in fluidised combustors operating under conditions of continuous sorbent feed.

Prior to the batch sulphation studies conducted in Chapter 3, there did not exist any data on the performance of local sorbents in FBCs. Attempts to use this same 100 mm diameter combustor for continuous sorbent feed proved unsuccessful- severe problems were encountered with pneumatic feed of sorbent particles through the same line as coal feed. Some preliminary tests were conducted using the 300 mm diameter combustor described in Chapter 5, using Lyttelton dolomite. This specific sorbent was chosen simply because of its low cost and availability. A high ash coal sample from Ballengeich Colliery in Natal, whose composition is given in TABLE 3.1, was combusted under the following operating conditions:

operating temperature	1100 K
superficial air velocity	1,0 ms^{-1}
bed depth	400 mm
excess air	20 %

Under these conditions, a combustion efficiency of 95.2 % was attained. A calcium to sulphur molar ratio of 4.2 was required to effect a 50 % reduction in base SO_2 emission levels. Operation of this unit, too, was

problematical, and further tests were discontinued. This trial seemed to indicate that sorbent usage was excessive, even for this low reactivity sorbent. It could not be confirmed whether this result was a consequence of this low reactivity, or an artefact of combustion equipment scale, and thus the need for prolonged testing under conditions of continuous sorbent feed remained.

Attempts to "prove" FBC locally, at a reasonable scale, have gained momentum recently with the establishment of a national demonstration facility (NFBC) which is accessible to both research and industrial communities. The central component of the NFBC is an atmospheric pressure, bubbling bed combustor coupled to a membrane wall boiler rated at 10 MW_{th}. The combustor vessel (3.05 x 3.05 m^2), operated at bed depths in the region of 1 m, and its contents were fluidised at a velocity range of 0.7 - 1.75 ms^{-1}. Key features of this plant have been described elsewhere [Eleftheriades and North (1987)], and their duplication here is unnecessary. Two points are worthy of note. The unit typically achieved overall thermal efficiencies in the range 74 - 79% when burning low grade coals. Boiler turndown is effected by zonal separation, accompanied by partial slumping of the bed. Under normal operating conditions, roughly 70% of total bed area was actively fluidised.

The availability of the NFBC provided an ideal opportunity to investigate sorbent performance at an industrial scale and to test the validity of the overall sulphation model developed in Chapter 6.

7.2. CONTINUOUS SULPHATION TRIALS

In line with the results of the batch sulphation tests reported in Chapter 3, one sorbent from each reactivity class was selected for extensive tests. Lyttelton dolomite was selected as an example of Type A reactivity, and Bredasdorp limestone as an example of Type C reactivity. Significant quantities of Marble Hall limestone were unavailable, and an alternative Type B sorbent was selected. The limestone sample from Lime Acres is a higher purity calcite like that from Marble Hall, but it displayed comparable reactivity (see Ch. 3) and was therefore chosen as the Type B sorbent. It was assumed, furthermore, that the Lime Acres sample would display similar calcination and attrition properties to the

Marble Hall sample. The specific sample used in these tests originated at the Union Lime quarry in the Lime Acres region.

7.2.1 Experimental Details

All trials were conducted with a discard coal sample obtained from Greenside colliery in Transvaal. The ultimate analysis of this product is given in TABLE 7.1. Because of the nature of this product, and its method of generation (it is a by product of beneficiation), these composition figures should be seen as average quantities only. The "as received" sample had a top size of +100 mm. All coal used was crushed to - 6 mm prior to gravity feed (overbed) to the combustor. None of the sorbent quarries marketed a product ideally sized for FBC operation. All sorbent suppliers were therefore asked to prescreen samples to a size specification of - 2mm + 0,5 mm. This was deemed necessary to minimise elutriation of sorbent from the combustor, whilst ensuring reasonable sorbent utilisation. Unfortunately, the sorbent samples supplied contained some fines. A more realistic size distribution was $150\ \mu m < d_p < 2000\ \mu m$. All samples could be characterised by a log normal distribution over this size interval, with $d_{p\ mean} = 750\ \mu m$, and $\sigma^2 = 1,25$. Sorbents, too, were fed in an overbed manner to the combustor. This was principally a matter of expedience (the sorbent and coal feeders would have otherwise required significant modification). The combustor was heated up from ambient conditions using sand ($d_{p\ mean} = 750\ \mu m$) as the fluidising medium.

Sorbent utilisation was investigated as a function of two variables only - combustor temperature and fluidisation velocity. Sorbent tests spanned the range 1093 K - 1183 K and $0.8\ ms^{-1}$ - $1.6\ ms^{-1}$. In all tests the combustor bed height was kept constant at one metre by continuous ash removal.

Boiler control was reasonably straightforward. It was reasoned that, as the sulphation reaction involved the combustion chamber principally, the boiler could effectively be uncoupled from the combustor during these experimental trials, and steam demand / coal flow used solely as a means of controlling combustor temperature at the target value, and excess air level in the range 4-6%. Steam delivery pressure was only loosely controlled. Because the combustion chamber is designed as a number of

interconnecting zones which can be fluidised separately, gas velocity through the bed was controlled (for an essentially constant air flow rate) by varying the active distributor area. The required Ca/S ratio was achieved by linking sorbent feed rates to the coal flow set point. Both coal and sorbent flows were metered through calibrated screw feeders, with averaged flows checked against load cells attached to the respective feed hoppers. Sorbent tests were conducted without ash return from the primary cyclone, as this would have unduly complicated the sorbent mass balance. Solid flow rates were measured at primary cyclone, bag filter housing and bed overflow points to complete the solids mass balance. It was appreciated that, under such a set of test conditions, boiler operation might conceivably be far from optimum, although high combustion efficiencies could be ensured by close control of temperature, velocity and excess air.

Sulphur dioxide, carbon monoxide and dioxide were measured by non dispersive infra-red moitors, whilst flue gas oxygen was measured by a paramagmetic analyser.

The test structure was simple. The combustor was allowed to reach steady state operation, whilst burning coal at the specified conditions of velocity and temperature. Sorbent feed was initiated at a predetermined level, and steady state SO_2 level in the flue gas allowed to re-establish. The process was repeated several times with increasing sorbent feed rate until the original base SO_2 level had been reduced by between 70 and 90 %. In some cases, particularly at lower combustor temperatures, the initial steady state condition was established with sorbent flow, and SO_2 levels corresponding to zero sorbent flow were inferred by the method described below.

7.2.2 Process Model Parameters

Before the model developed in Chapter 6 can be applied to sulphation data generated by this fluid bed boiler, the steady state attrition rate, R_{ss}, must be established for the three samples at boiler operating conditions. With calcine compressive strength data available from TABLE 4.5, R_{ss} values can be calculated from eq. 5.8. The constant p', which relates measured R_{ss} values (given by the regression constant, a_1, in eq. 5.5) to the steady state form of the attrition model, is expected to

show some scatter about a mean value. This is a consequence of the variability in the original attrition data. The largest set of attrition experiments was conducted with Bredasdorp limestone, and, for this sample, calculated values of p' spanned the range 1,92 ± 0.5 (see APPENDIX G). Since the simulation studies of Chapter 6 showed that the model was not overly sensitive to sorbent attrition rate, it is reasonable to use this mean value of p' to predict R_{ss} values where no measured values are available. This is the case for all test conditions of the NFBC. For a mean sorbent particle size of 750 μm, at a temperature of 1123 K, U_{mf} = 0.17 ms^{-1} [Yates (1983)]. Hence, for U =1 ms^{-1}, and H = 1 m,

R_{ss} - Bredasdorp = 8.5 % / hr
R_{ss} - Lyttelton = 5.3 % / hr
R_{ss} - Union Lime = 5.3 % / hr

These figures were applied to NFBC data through eq. 6.9 - 6.12.

The method of ash removal did not permit close control of bed inventory - at best ± 10%. Nonetheless, in all model predictions the mass of bed contents was taken as a constant, given by $M = ß\ A_b\ \rho_b$, where A_b is total bed area (3.05 x 3.05 m^2), ß is the active portion of bed flow area (typically 70%), and ρ_b is the bulk density of bed solids (1600 kg m^{-3}). This gives a value of M = 10000 kg.

7.2.3 Test Results

A summary of test conditions is given in TABLE 7.2. The quantity of Lyttelton dolomite supplied was sufficient for only one test at a fluidising velocity of 1.1 ms^{-1}. Both limestones, however, were supplied in sufficient quantity to map sorbent performance over a wide range of fluidising velocities and combustor temperatures.

Two points of interest stem from this table. Firstly, the values of combustion efficiency derived from carbon-in-ash figures span the narrow range 87.4 % to 91.5 % which corresponds well with earlier reported figures for this unit [Eleftheriades and North (1987)] and supports the earlier stated claim that decoupling boiler operation from the combustor would not adversely affect the latter's performance. This narrow

performance range belies the wide variation in combustor temperature and fluidising velocity over which the unit operated. Secondly, the stated method of combustor operation allowed reasonable control of excess air, as evident in flue gas oxygen levels, which ranged from 4.5 % - 7.5 %.

TABLE 7.3 gives the effect of increased sorbent feed on sulphur retention for all three sorbents.

7.2.4 Calcium in Coal Ash as SO_2 Sorbent

When coals with a high ash content, such as Greenside discard, are combusted in a fluidised bed, there is significant accumulation of calcium oxide in the bed over time. Greenside discard contains typically between 3.4 % and 5.4 % calcium in ash. Average coal flow to the 10 MW_{th} unit was in the region of 1500 kg/hr. These figures translate to an injection of between 25 and 40 kg/hr of calcium, which is on a par with the amount of sulphur entering the bed. There is thus merit in investigating the absorptive capacity of this calcium for SO_2.

The "true" base level SO_2 emissions shown in TABLE 7.2 have been computed from flue gas flows determined from coal and air flows, and the measured combustion efficiency. These figures correspond to SO_2 levels which would be measured if the calcium in coal ash was completely ineffective as a sorbent. The difference between these figures and the measured "zero sorbent" SO_2 base levels (also shown in TABLE 7.2) gives an indication of the absorptive capacity of the calcium originally present in the coal supplied. FIGURE 7.1 reflects the SO_2 reduction capacity of the calcium present in coal ash, as a function of Ca/S molar ratio. Without an understanding of the form in which calcium is arranged within ash particles, or the nature of their porosity, it is unwise to assume that their sulphation would proceed by the same mechanism as that of sorbent particles. For this reason, the data in FIGURE 7.1 is fitted simply to a linear relationship, which applies only over the range of data presented. A least squares regression of these data points gives

$$\eta = 0.6\ R_{Ca} \qquad 7.1$$

with a coefficient of correlation of 0.86. As mentioned above, several

tests were initiated with sorbent feed because of temperature control problems - it was found that, if steady state conditions were established without sorbent feed, subsequent addition of sorbent perturbed bed temperature dramatically and it was difficult to re-establish smooth operation. In these cases, SO_2 levels corresponding to zero sorbent feed were inferred from calculated values of "true" base SO_2 and the calcium content of the coal sample, using eq.7.1.

It can be seen from FIGURE 7.1 that a reduction in base SO_2 levels of between 15 % and 30 % was attainable simply through the absorptive capacity of calcium in coal ash. This is a point often overlooked, and its significance cannot be overstated, particularly when environmental legislation is promulgated. If a desired reduction in SO_2 is based on coal sulphur content rather than on the observed "zero sorbent" emission level, the required sorbent dosage would be considerably lessened due to the beneficial effect of calcium in the coal ash.

7.2.5. Effect of Fluidising Velocity

The effect of fluidising velocity on sulphur retention is shown for the Bredasdorp sample in FIGURE 7.2 and for the Union Lime sample in FIGURE 7.3. In both cases, an increase in fluidising velocity resulted in an increased sorbent requirement for a given reduction in SO_2 levels. The predictive value of the model derived in Chapter 6 is shown by the solid lines in these same figures. The model fit is good, particularly at low velocities. However, the model tends to overpredict the degree of sulphur retention at low sorbent flows (corresponding to Ca/S values less than 1). This behaviour is more clearly evident in FIGURE 7.3, for the Union Lime sample. The overall process model postulated by Dennis (1985) produced a similar trend, where it was mistakingly attributed to the sulphation capacity of fine particles, which in reality are lost to the system by elutriation. The current model excluded the action of fines, and the overprediction was thought rather to be a consequence of poor mixing of sorbent particles, particularly at such low flow rates. Overbed feed of sorbent material caused a degree of shortcircuiting to occur, resulting in a decrease in mean residence time. This finding reinforces the need to fully investigate possible alternatives to sorbent feed mechanisms, particularly where the feed stream contains a

high percentage of particles whose terminal velocity is close to the fluidising value.

The significance of particle residence time at low sorbent flow rates is at variance with the conclusions of Fieldes (1979) and Dennis (1985). Both maintained that, at low Ca/S ratios (less than, say, 1.5), where mean residence times are large relative to particle sulphation time, the degree of sulphur retention is expected to be governed by X_∞, according to $\eta = R_{cs} X_\infty$ (note the similarity to eq. 7.1). When this relationship is applied to both Bredasdorp and Union Lime data, ($U = 0.8\ ms^{-1}$, $R_{cs} = 1$) it predicts values of X_∞ equal to 0.75 and 0.5 respectively. These values are much larger than those measured from batch sulphation experiments at the same conditions (Chapter 3). Furthermore, the Bredasdorp value is in excess of the theoretical maximum of 0.57. This model, in effect, gives a value of X_∞ for coal ash particles equal to 0.6, which seems high.

The only data presented by Dennis from a large scale coal combustor [Wright (1979)] produced a similar inconsistency. The measured value of X_∞ for the sorbent in question was 0.22, whereas the value predicted by the above limiting relationship, at $R_{cs} = 1$, was 0.4. It is difficult to comment further on the validity of the above limiting relationship because of a lack of continuous sulphation data from other sources. However, it may be postulated that significant sulphur retention is possible by sorbent fragments ("near-fines") whose size is such that their residence time may be comparable to their sulphation time. This would negate the validity of the above limiting relationship, even at low sorbent flow rates. This is consistent with the discussion of the effect of sorbent feed distribution on sulphation capacity as presented in Chapter 6. The method of predicting X_∞ values from continuous sulphation data should therefore be held in question, except in those cases where a thorough knowledge of sorbent size distributions (both in the feed stream and in the bed) is available.

It was proposed in Chapter 6 that the sulphation kinetic constants, k_s and k_d varied in proportion to each other with respect to fluidising velocity. The sulphation data presented above makes possible an examination of this postulate. British Coal researchers [NCB (1971)] concluded from experimental data that, with all other parameters

constant, the reduction in SO_2 levels could be described by an inverse dependence on velocity i.e.

$$C_{ao}/C_a - 1 = c2/U + c3 \qquad 7.2$$

where C_{ao} is the base SO_2 emission level, C_a is its steady state value for a given sorbent flow, and c2 and c3 are constants. FIGURE 7.4 presents the data for Bredasdorp limestone cast in this form. Sulphation data were collected for only three values of fluidising velocity. The evaluation of eq. 7.2 was restricted to two values of R_{cs} for which sulphur retention data were available at all three velocities. Despite these limitations, it can be seen from FIGURE 7.4 that eq. 7.2 is valid, with c2 increasing with increased R_{cs}. The model prediction for $R_{cs} = 2$ is shown for completeness. Sulphur retention is thus proportional to 1/U, which, confirms, from eq. 6.26, that both k_s and k_d must carry the same dependence on fluidising velocity. This relationship can be generalised to all sorbents. It is therefore possible to describe the sulphation performance of a selected sorbent at any fluidising velocity condition, provided the sulphation kinetic parameters, k_s and k_d, are known at any one value of U.

7.2.6 Effect of Combustor Temperature

Not much has been said thus far on the influence of combustor temperature on sorbent performance. FIGURES 7.5 and 7.6 show this effect for Bredasdorp and Union Lime samples respectively, over the temperature range 1100 - 1180 K. Both figures show that sulphation performance falls off as the temperature is increased much beyond 1100 K. This reduction in SO_2 retention at elevated temperatures is attributed to a decreased porosity in the calcined stone [Dennis and Hayhurst (1986b)]. Although sulphation rate increases with temperature over this range, the mean pore diameter has decreased and pore blockage occurs more rapidly. Overall sorbent utility is decreased.

When considering the extension of the sulphation model to the performance of sorbents in industrial scale combustor units, it is not wise to use values of k_s and k_d derived at a temperature much removed from the operating temperature of the large scale combustor.

7.2.7 Effect of Sorbent Type

The parametric study of Chapter 6 predicted that Bredasdorp limestone would out-perform the other two sorbents. This is indeed confirmed in FIGURE 7.7, for a series of experiments conducted at U = 1 ms^{-1} and T = 1100 K. Model predictions are shown as solid lines in the same figure. Model accuracy is better for the more reactive Bredasdorp sample than for the other two sorbents. The poor fit to Lyttelton data, relative to the other two sorbents, is thought to be a consequence of the excessive amounts of this dolomitic material that were needed, on a mass basis, to achieve a desired reduction in SO_2 level. This large sorbent flow posed severe problems for control of bed temperature and inventory. Bed temperatures were lower, on average, for the Lyttelton experiments than for the other two sets. The more frequent drainage of solids, to maintain constant bed level, led to significant fluctuation in bed depth due to poor operation of the ash removal screw conveyor.

Overall, however, the model fit is reasonable, and provides reassurance of its extrapolative benefit to large fluid bed combustors, independently of sorbent type.

7.3 IMPROVEMENT OVER SIMPLE MODEL OF ZHENG

The prime motivation for the development of the model in this work was that the simplified version due to Zheng et al (1982) did not consider particle size or age distributions and ignored sorbent attrition. The sulphation data collected from the NFBC can be used to substantiate the need for the more elaborate treatment of sulphation offered by the model in Chapter 6.

The simple model reduces to eq. 2.33 i.e.

$$\eta = 1 - 1/(1 + K R_{cs})$$

where K, given by eq. 2.34, is a function of k_s and k_d. TABLE 7.4 gives K values for the series of tests defined in TABLE 7.2.

These K values are used to predict sulphur retention efficiency as a

function of fluidising velocity for both Bredasdorp and Union limestones. The results are shown in FIGURES 7.8 - 7.10 for Bredasdorp, and FIGURES 7.11- 7.12 for Union Lime. It is clearly evident that, in all cases, the model of this work provides a much closer representation of the measured sulphation data than does the simple model given by eq. 2.33. It is apparent that, at the low end of the velocity range, the simple model consistently underestimates the sulphur retention capability of both limestones, whereas, at the high velocities, the trend is reversed, again with consistency.

Both these observations can be explained by the relative interplay between particle size distribution and residence time, with specific reference to "near fines" material either present in the feed stream or generated by attrition of coarse sorbent particles. At low velocities, this material will remain in the bed for sufficient time to be fully sulphated, and the simple model (which ignores this material) will underestimate sulphur retention. At higher velocities, this material will be elutriated from the bed, and the simple model (which ignores elutriation), will produce optimistic results of sulphur retention.

These findings confirm the need for a model which adequately represents the size distribution of sorbent material in the feed stream and in the bed, and includes the effects of attrition and elutriation.

7.4 SOLIDS LOADING ON GAS CLEANING EQUIPMENT

The prior discussion of sorbent attrition and elutriation pertains only to an analysis of their role in SO_2 capture. From a design standpoint, it is important to ascertain what effect, if any, the choice of sorbent will have on the general operation of the combustor and its ancillary equipment.

It has been demonstrated above how the size distribution of sorbent material in the bed is affected by attrition and elutriation rates. It could be expected that the extent, and size distribution, of the carryover stream will be similarly affected, with more friable sorbents producing a larger elutriate stream. This has a direct bearing on the sizing of downstream gas cleaning equipment. Once again, the data generated by the NFBC provided an opportunity to assess the significance

of this aspect of sorbent use.

A comparison was made between the reactive (highly friable) Bredasdorp limestone and the less reactive (less friable) Lyttelton dolomite. Average solid flows through primary cyclone and bag filter housing were measured under combustor operating conditions of U = 1.1 ms^{-1} and T = 1100 K. All solid flows are reported in TABLE 7.2, from which it can be seen that, as the coal flow (and composition) are similar in both cases, any difference in the solids loading to this equipment could be attributed directly to sorbent selection. The sorbent flows recorded in this table refer to steady state values required to effect a 60% reduction in base SO_2 levels. Although the Lyttelton dolomite flow to the combustor was in the region of four times that of the Bredasdorp flow, the total solid loading of both primary cyclone and bag filter was greater in the latter instance. This is a consequence of the increased attrition tendency of Bredasdorp lime. The size distributions of product in both cyclone and bag filter are shown in FIGURES 7.13 and 7.14 respectively. Size analyses were performed by a MALVERN 2600 laser diffraction particle sizer. The mass flow ordinates in both these bar charts have been normalised against the total average solid flow (coal plus sorbent) to the combustor. It can be seen from both these figures that the Bredasdorp sample produced a greater quantity of fines than the Lyttelton dolomite. Because this latter sample does not abrade to the same extent, most of the sulphated product is removed via the bed overflow stream. This too is supported by the figures in TABLE 7.2. A point of general interest is that all solid flows are of considerable magnitude relative to coal flow. This is a direct consequence of the high ash content of the Greenside discard coal sample used in these combustor tests.

From a design standpoint, the implication of the above comparison is simply that reactive sorbents will generate a disproportionately large amount of fines, and gas cleaning equipment must be sized accordingly. The choice of sorbent will affect other aspects of combustor design (such as feeders etc.,) but these were not examined here.

7.5. SORBENT ECONOMICS

Sorbent selection is also guided by overall cost effectiveness. This is obviously dependent on a large number of factors, many of which may be site specific. For this reason, a general assessment of economic viability is impossible. It is nevertheless possible to make some general observations for South African sorbents, based on the experimental data produced by this industrial fluid bed boiler.

South Africa has extensive deposits of both limestone and dolomite. Much of the limestone is located in the coastal belt whereas dolomite reserves are to be found in close proximity to major coal reserves. Because transportation costs play a major role in defining the final cost of any solid product, the economics of FBC desulphurisation would appear, at first glance, to favour the use of dolomite over limestone. However, from the experimental work above, roughly five times the mass of dolomite over limestone would be required to achieve an 80 % reduction in SO_2 levels. Serious thought should therefore be given to limestone usage in preference to dolomite. The costs associated with limestone procurement could be reduced further by precalcination, assuming that no loss in sorbent reactivity would be incurred by shipping the calcined product over long distances.

All sorbent suppliers stressed the high cost of producing narrow size fractions of their products. The size range investigated in this work was a trade-off between available material, and sorbent elutriation considerations. Reducing the mean sorbent size will improve utility, and the costs of such a prescreening exercise could well be off-set by the reduction in sorbent usage. Once more, this pretreatment option would be particularly attractive where transportation costs are excessive.

7.6 CONCLUSIONS

The validity of the sulphation model derived in Chapter 6 has been substantiated by extensive data on sorbent performance in a large industrial FBC. The analysis was constrained to three South African sorbents for which sulphation kinetic data are available. The fact that the model adequately represents the performance of sorbents whose sulphation kinetics were derived at laboratory scale confirms the

ability of the model to scale to large FBC units.

This analysis confirmed that simplified models, such as those of Zheng et al (1982) which assume a mono sized sorbent population, and which take no account of attrition or elutriation, are poor predictors of sorbent performance at this large scale.

It was shown that sorbent attrition markedly affects the solids loading on downstream gas cleaning equipment.

CHAPTER 8 CONCLUSIONS AND RECOMMENDATIONS

8.1. CONCLUSIONS

This dissertation is concerned with an investigation of the reaction between sorbent particles and sulphur dioxide in a fluidised combustor. The thesis development has been guided throughout by the motivation that its outcome be of immediate use to design engineers and operating personnel of FBC plant concerned with the control of SO_2 emissions. The overriding objective of this work has been to develop the necessary tools whereby the performance of an arbitrary sorbent in an FBC of any scale can be predicted from minimum experimental data. The degree to which this objective has been met is discussed below.

8.1.1 Sulphation Kinetics

The sulphation kinetics of sorbent particles are described by a simple kinetic model, where model parameters are measured during a batch sulphation experiment in a fluidised combustor. The simplicity of the experimental technique, and the fact that the influence of coal combustion can be assessed directly, make it more attractive than the classic experimental techniques of TGA or differential reactor studies, where a simulated flue gas environment is invariably standard. There is little loss of physical significance in the use of such a model over more complex models which consider fully the diffusion of reactants through a complicated pore structure. Pertinent features of the sulphation reaction, including the decrease in reaction rate with conversion, and subsequent pore plugging, are reflected in the simple model. The time dependence of the sulphation reaction rate is described by a first order rate expression. The complexity of other kinetic models, where this decrease in reaction rate with time is framed in terms of the effect of sulphate deposition on pore geometry, does not appear to be warranted. When coal combustion takes place, a model which describes the reactor contents as well mixed gives a better representation of the variation in sorbent rate constant with conversion than does one in which gases are assumed to be in plug flow.

When this, most simple, sulphation kinetic model is incorporated in an overall fluidised combustor model, an analytical solution is possible for a monosized, time invariant sorbent population. However, such an idealised case bears little resemblence to the true situation with sorbent feed to large FBCs. This deficiency received considerable attention in this work.

8.1.2 Sorbent Specificity / South African Resource

The model for sulphation kinetics has been substantiated by sulphation data for 16 South African sorbents. Both sulphation rate and maximum attainable conversion are shown to be functions of sorbent type. The variation in initial sulphation rate with sorbent type has not been reported elsewhere. Its identification here has come about only through extensive sorbent sampling. The total sorbent resource base can be classified into three groups according to the magnitude of the two model parameters. Sorbents of highest reactivity tend to be highly friable sandy or marine limestones whilst those of lowest reactivity are "older" in the geologic sense, often dolomitic, and have undergone recrystallisation. The intermediate class of sorbents are generally of a geologic age somewhere between the two extremes. This information provides a rapid, first order, indication of sorbent performance. Geologic descriptions of potential sorbents are readily available (their use in other process applications being well established). A simple check of this description will ascertain whether a material offers any promise as a sulphur sorbent. At this stage, there is no requirement for any experimental validation of sorbent performance. Although this assessment was restricted to an analysis of South African sorbents, the group of 16 samples is extensive enough, and spans a sufficiently wide range of geologic types, that this relationship is expected to have general applicability.

A more detailed experimental investigation of the relationship between sorbent type and sulphation propensity highlighted the role played by the physical properties of both natural sorbent and calcine. The pore structure developed on calcination is a function of pore size distribution, crystallinity and topography of natural sorbent particles. This serves to reinforce the relationship between sulphation propensity and sorbent geology described above. It is significant that those

properties which ensure a high sulphation rate and capacity in certain sorbents also promote particle attrition. The measured structural strength of sorbent particles proved to be a good indicator of the severity of this attrition.

South African sorbents displayed intermediate reactivity compared to U.K. and U.S.A. materials for which sulphation rate data are available. It is interesting to note that none of the eight dolomites achieved an ultimate conversion anywhere near the theoretical maximum of 100%, although the initial reaction rate of these materials is comparable to that attained by other highly reactive dolomites (compare the South African Lyttelton dolomite with U.S.A. Tymochtee dolomite - Table 3.5).

8.1.3 Attrition and Elutriation

A model of sorbent attrition in a fluidised bed has been developed from experimental measurements in a laboratory scale combustor. Attrition proceeds by an abrasion mechanism, where surface irregularities are removed with time, producing more spherical - like particles. Most of the abrasion takes place in a region near the air distributor where high velocity jetting action is important. Attrition due to bubbling action higher up in the bed is small by comparison, though its effect is additive. The nozzle - type distributor plate in the experimental unit is expected to produce a similar pattern of gas movement to that found in large FBCs fitted with bubble cap distributor plates. It is therefore anticipated that the attrition model developed in this work would also be applicable to these large scale units. The model dependence on fluidising velocity, bed depth, particle diameter, structural strength and surface topography has been substantiated by experiment. Deep beds of soft, friable material produce the greatest amount of attrition. However, contrary to popular understanding, smaller particles exhibit a greater attrition propensity than larger ones, though this has been shown (for a fixed fluidising velocity) to be a function of the greater bed expansion which results from use of smaller particles.

The attrition rate falls off rapidly with time to a steady state value which is much lower than the original rate. Though this variation in attrition rate has important implications for the operation of an FBC, it is a point often overlooked in the literature.

The model developed in this work considers only those elements of attrition which result from the continuous motion of bed solids. It is recognised that significant attrition can occur due to various "once - off" influences, such as thermal shattering on entry to the bed, as well as through movement in feed lines and cyclones. It is proposed that these "instantaneous" attrition components can be viewed as causing changes to the size distribution of the sorbent feed stream. This assertion allows for their direct inclusion in an overall sorbent sulphation model.

The generation of sorbent fines by attrition has been shown to influence the elutriation of coarse particles from the bed. An elutriation model, which considers the effect of fines holdup in the freeboard on the terminal velocity of coarse particles, is used to map elutriation data generated under coal combustion conditions in a large laboratory FBC. The predictive capability of this model appears to be significantly better than other empirical models commonly used.

8.1.4 Extension to Large Scale FBCs

Together, the three models (of sulphation kinetics, sorbent attrition and elutriation) defined above, coupled to a sorbent population balance, can be used to predict the sulphur retention capability of any sorbent in an FBC with a generalised feed distribution. This overall process model requires little supportive experimental data - sulphation kinetic parameters and sorbent structural strength only - and both sets of experiments can be conducted easily in any laboratory.

The model predicts that choice of sulphation kinetics exerts the greatest influence on sulphur capture, though fluidising velocity, attrition rate and feed size distribution play a role. Natural sorbent physical properties are important in defining sulphation propensity, moreso for their effect on the generation of calcine pore volume and pore size distribution, than for any direct influence on attrition tendency.

The predictive capability of the model has been substantiated for three dissimilar South African sorbents in a 10 MW_{th} FBC. These sorbents were

from the original group of 16 whose sulphation kinetics were measured. The data set from the large unit confirmed that the sulphation propensity of a selected sorbent, at any velocity condition, can be predicted from sulphation kinetics measured at one arbitrary fluidising velocity. This analysis also confirms the deficiency of simpler process models which take no account of the distribution of sorbent particle ages in the fluidised bed.

8.1.5 Summary

Two main points arise from this work.

1. The performance of selected sorbents has been mapped from laboratory to industrial scale FBC units. These sorbents are representative of a much wider sample whose reactivity with sulphur dioxide has been described in detail and related to their formative geology.

2. Although the overall process model is based on sulphation and attrition kinetics measured at laboratory scale, it is reasonably successful in predicting the sulphation propensity of these same sorbents in a typical industrial FBC.

Taken together, these findings attest to the degree to which the primary objective of this thesis has been met. Design engineers can apply the process model to finding the required sorbent flow rate for a given reduction in SO_2 emissions. Experimental requirements are minimal. The information on attrition is invaluable to the design of downstream gas cleaning equipment. Operators of FBC plant can assess the implications of changes in sorbent supply by observing the relationship between sorbent geology and sulphation performance.

8.2. RECOMMENDATIONS

8.2.1 Model Extensions

There are two principal limitations of the current model.

a). The contribution of "once-off" attrition effects to the sorbent population model was included through changes to the feed size

distribution. Investigating the influence of several idealised feed distributions on sorbent performance gives little indication of the severity of this instantaneous attrition component, though it is expected to be at least as severe as that caused by continuous solid motion wothin the combustor. A more fundamental assessment of this inherently transient phenomenon would require that the model be recast in terms of joint size / age distribution functions. Such an approach would remove the constraint that attrition be viewed exclusively as an abrasion process, where the number of particles in the bed does not change with time.

b). The model does not consider the sulphation potential of fine particles, either in the feed stream or generated by attrition, though their residence time in the bed may be of the order of particle sulphation time. As above, such a refinement would require that the model be reformulated.

8.2.2 General

a). It was shown that the calcium content of high ash coals is sufficient to effect a considerable reduction in SO_2 emission levels. Little is understood of the way in which calcium is dispersed in ash particles, and whether sulphation of these particles follows the same pattern as that of limestone and dolomite. It would be interesting to pursue this further, to investigate whether this mode of sulphur capture can be improved, for instance, by controlled attrition.

b). The data base of South African sorbent performance in a large scale FBC should be extended to other sorbents whose sulphation kinetics are known. In particular, the effect of alternative sorbent feed arrangements (such as in-bed sorbent feed), and fines recycle from the primary cyclone should be investigated .

c). The economic viability of FBC is dependent, to a large extent, on sorbent requirements. Sorbent transportation costs are often important. For this reason, it would be worthwhile to investigate the possibility of sorbent precalcination, prior to its transport. For a high purity limestone this would result in almost a 100% reduction in sorbent bulk, with a proportional reduction in transportation costs. Precalcination

also offers the possibility of optimising calcine structure for sulphur capture. Such an exercise would require close collaboration with lime manufacturers, whose expertise in this area could prove invaluable.

REFERENCES

AVEDESIAN, M.M and J.F Davidson (1973) Trans. Inst. Chem. Engrs 51, p.121

AVNIR, D and D.Farin (1983) J. Chem Phys., 79(7), p. 3566

BEMROSE, C.R., and J. Bridgwater (1987) Powder Tech., 49, p. 97

BHATIA, S.K and D.D Perlmutter (1981), AIChE J. 27 (2), p.226

BLINICHEV, V.N et al (1968) Intl J. Chem. Eng 8(4), p. 615

BLINICHEV, V.N. et al (1973) Int'l. Chem. Eng., 13(2), p.221

BORGWARDT, R.H (1970) Env. Sci. & Tech. 4(1), p. 59-63

BORGWARDT, R.H (1985) AIChE J. 31 (1), p 103

BORGWARDT, R.H, and R.D. Harvey (1972) Env. Sci. & Tech. 6(4), p.350

BOSMAN, H.H. (1987) "Summarizing World Atmospheric Sulphate Deposition Load with Special Reference to South African Conditions". Dept. Water Affairs. Pretoria, South Africa

BOYNTON, R.S (1980) "Chemistry and Technology of Lime and Limestone" 2nd ed. John Wiley and Son. New York

BUKUR, D and N.R. Amundson (1980) Chem. Eng. Sci 36(7), p.1239

BURDETT, N (1983) Inst. Energy J. Dec, p. 98

BURNS and Roe Inc., (1978) "Conceptual Design of an Atmospheric Fluidized Combustion Electric Power generating Plant" Interim report V, HCP/T2455-15/5

CHANG, E.Y and G.Thodos (1984) AIChE J. 30(3), p.450

CHEN, T.P., C.I. Sishtla, D.V. Punwani, H. Arastoopour, (1980) Fluidisation III, Engineering Foundation Conf. Henniker, N.H.

CHESTER, P.F (1987) in "CEGB Research - Acid Rain", Central Electricity Generating Board, U.K. Aug., p 62

CHESTER, P.F. (1986) Energy World, No. 133, Feb., p.2

CONGALIDIS, J.P and C. Georgakis (1980) Chem. Eng. Sci, 36(9), p.1529

CRANE, A.J and A.T. Cocks (1987) in "CEGB Research - Acid Rain", Central Electricity Generating Board, U.K. Aug., p. 3

DARTON, R.C et al (1977) Trans. Inst. Chem. Engrs 55, p.274

De Grys, A. (1980) "Stratigraphy of South Africa" Handbook No. 8 Geologic Survey, Dept. of Mineral and Energy Affairs. S. Africa

De JAGER (1982) "An Evaluation of Coal Reserves of the Republic of South Africa", Dept. of Mineral and Energy Affairs, S.A

DENNIS J.S and R.B Fieldes (1986) Chem. Eng. Res. & Dev. 64, p. 279

DENNIS, J.S (1985) "The Desulphurisation of Flue Gases using Calcareous Materials" PhD Thesis, University of Cambridge, UK

DENNIS, J.S and A.N. Hayhurst (1985) in proc. of Twentieth International Symposium on Combustion. Combustion Inst. Pittsburgh.

DENNIS, J.S and A.N. Hayhurst (1986a) in "Fluidization V", Eng. Foundation Conf. Elsinore. Denmark

DENNIS, J.S and A.N. Hayhurst (1986b) Chem. Eng. Sci 41(1), p.25-36

DESAI, N.J., and R.T. Yang (1983) I&EC Proc. Des. Dev., 22, p.119

DOGU, T (1981) Chem. Eng. Jour. 21, p. 213

ELEFTHERIADES, C. (1987) in proc. of "Steam Generating Plant - Current and Future", Energy Research Institute, University of Cape Town

ELEFTHERIADES, C., and B. North (1987) 9th Intl. Conf. on FBC. Boston.

ENVIRONMENTAL PROTECTION AGENCY (1979) "New Source Performance Standards". U.S.A

ERLICH, S (1984) Inst. of Energy, 3rd Intl conf.on FBC, London. UK

EVANS, I and C.D Pomeroy (1966) "The Strength, Fracture and Workability of Coal", Pergamon Press

FEDERAL REPUBLIC OF GERMANY (1984) "Resolution of the Ministers for Environmental Protection with regard to Sulphur Dioxide Emissions".

FEE, D.C, K.M. Myles et al (1984) Chem. Eng. Sci 39(4), p.731

FIELDES, R B; and J.F Davidson (1978) Paper presented at AIChE National Meeting, Miami. USA.

FIELDES, R.B (1979) "Reaction of Sulphur Dioxide with Limestone Particles" PhD Thesis. University of Cambridge, U.K

FRANCESCHI, J et al (1981) in Sixth Int'l Conf. on FBC, Engineering Foundation Conferences.

GELDART, D et al (1979) Trans. Inst. Chem. E, 57, p.269

GEORGE, S.E. and J.R. Grace (1981) Can. J. Chem. Eng. 59, p.279

GIBBS, B.M (1975) Inst. Fuel Symp. Ser. No.1, p A5.

GROBBELAAR, C, J (1986) "South African Discard and Duff Coal: National Inventory". Dept. of Mineral and Energy Affairs. S.A.

GUPTA, V.S, D.W. Fuerstenau and T.S. Mika (1975) Powder Tech. 11 p. 257

GWYN, J.E. (1969) AIChE J., 15, p. 35

HAIGH, N (1985) in "Control of Acid Emissions in the U.K." Inst. Chem. Eng., U.K

HARRIS, P, (1988) Council for Mineral Technology, South Africa. Personal Communication

HARTMAN, M and R.W Coughlin (1974) I&EC Proc. Des. Develop. 13 (3), p.248

HARTMAN, M and R.W. Coughlin (1976) AIChE J. 22 (3), p.490

HARTMAN, M, J. Pata, and R.W. Coughlin (1978) I&EC Proc. Des. Develop 17 (4), p. 411

HARVEY, R.D (1970) Environ. Geol. Notes 38, Illinois State Geo.Survey

HILLS, A.W.D (1968) Chem. Eng. Sci., 23 p 297

HORIO, M, and C.Y. Wen (1978) AIChE Symp. Ser. 74(176), p.101

HULBERT, H.M., and S.Katz (1964) Chem. Eng. Sci. 19, p.555

HYATT, E.P., I.B. Cutler, and M.E. Wadsworth (1958) Amer. Ceramic Soc. J. 41 (2), p. 70

INGRAHAM, T.R and P. Marier (1963) Can. J. Chem. Eng, 41, Aug., p 70

IRELAND, F (1987) The Chemical Engineer, May, p.64

JONKE, A.A. (1977) "Supportive Studies in Fluidized Bed Combustion" Argonne National Laboratory, Monthly Progress Report for EPA and ERDA, January.

KAYE, B.H. (1981) "Direct Characterisation of Fineparticles" Wiley. New York

KEAIRNS, D.L et al (1975) "Fluidized Combustion Process Evaluation. Phase ii - Pressurised Fluidized Bed Coal Combustion Development", Westinghouse Research Laboratories. EPA Report No. EPA-650/2-75-027-C

KONO, H (1981) AIChE Symp. Ser. 77(205), p.96

KOPPEL, L.B (1970) "Supportive Studies in Fluidized Bed Combustion" Argonne National Laboratory. ERDA Report.

KRUEGER , D.L.W. (1986) "S.A. Coal R&D Strategy", M.Sc. Thesis, University of Cape Town

KUELERMAN, L. (1977) African Explosives and Chemical Industries Ltd. Research Dept. Personal Communication

KUNII, D and O. Levenspiel (1969) "Fluidization Engineering" John Wiley and Sons. New York

KUTYAVINA, T.A, and A.P. Baskakov (1972) Chem & Tech Fuel Oils 8(3), p.210

LA NAUZE, R.D (1985) Chem. Eng. Res.& Dev. 63, p.4

LEE, D.C and C.Georgakis (1981) AIChE J. 27(3), p. 472

LEVENSPIEL, O. (1979) "Chemical Reactor Ominbook" OSU Press, Corvallis, Oregon

LEWIS, W.K. et al (1949) Ind.& Eng. Chem. 41, p.1104

LIN, L., J.T. Sears, and C.Y. Wen, (1980), Powder Tech. 27, p105.

LOWELL, S. (1979) "Introduction to Powder Surface Area" Wiley Interscience, New York

LOWRISON, G.C. (1974) "Crushing and Grinding - The Size Reduction of Solid Materials" Butterworths. London.

MANDELBROT, B.P (1977) "Fractals: Form, Chance and Dimension" Freeman, San Francisco.

MARIER, P and T.R. Ingraham (1972) Canadian Metallurgical Quarterly 11(4), p.617

MARTINI, J.E.J (1987) "Limestone and Dolomite Resources of South Africa" Handook No. 9 Geologic Survey, Dept. of Mineral and Energy Affairs, S. Africa

MEETHAM, A.R et al (1981) "Atmospheric Pollution - Its History, Origins and Prevention" 4th ed. Pergamon Press, Oxford

MERRICK, D., and J. Highley (1974) AIChE Symp. Ser. 70(137), p.366

MORI, S and C.Y. Wen (1975) AIChE. J., 21 (1), p. 109

MOTHERWELL, k (1986) National Diploma Tech. Thesis. Cape Technikon, Cape Town

MULLINS, R.C and J.D Hatfield (1970) "Effects of Calcination Conditions on the Properties of Lime" in The Reaction Parameters of Lime ASTM Special Tech. Publ.No. 472

MURRAY, J.A (1956) "Summary of Fundamental Research on Lime". National Lime Association, U.S.A.

MURRAY, J.A., H.C. Fischer, and D.W. Sabean (1950) ASTM Proc. 50, p 1263

MURRAY, J.A., H.C. Fischer, and L.S. Rolnick (1953) Amer. Ceramic Soc. J. 37 (7), p 323

NATIONAL Coal Board (1971) "Reduction of Atmospheric Pollution" Final Report prepared for U.S.A. E.P.A. Office of Air Programs, Durham, North Carolina DHB 060971

NEWBY, R.A., W.G. Vaux, and D.L. Keairns (1983) in "Fluidization 4" Engineering Foundation Conf. Kashikojima. Japan.

NEWBY, R.A., W.G. Vaux, N.H. Ulerich, A. Y. Randive, and D.L. Keairns, (1982) 7th Intl Conf. on FBC, Eng. Found. Conf. Pittsburgh, PA.

O'NEILL, E.P., and D.L. Keairns, (1977), AICHE Symp. Ser. 73(161), p100.

O'NEILL, E.P., D.L. Keairns, and M. A. Malvin, (1977) "Sorbent Selection for the CAFB Residual Oil Gasification Demonstration Plant", EPA -600/7-77-029.

O'NEILL, E.P., N.H. Ulerich, R.A. Newby, and D.L. Keairns, (1979) "Criteria for the Selection of SO2 for AFBCs. Vol. 1", EPRI FP -1307, Project 721-1.

OVERTURF and Kayihan (1979) Powder Tech. 23, 143

PARK, D etal (1979) 72nd AIChE National Meeting, San Francisco.

PERRY and Chilton (1973) "Chemical Engineer's Handbook" 5th ed. Mc Graw Hill, New York.

PETRIE, J.G and R.K. Dutkiewicz (1983) in "Fluidization 4" Eng. Foundation Conf. Kashikojima. Japan

PETRIE, J.G (1985) "Fluidized Combustion of South African Coals", Energy Research Institute, Report No. 83, University of Cape Town

PETRIE, J. G (1988) SA Inst. Chem E. National Meeting. August.

POMEROY, C.D. (1957) J.Inst. Fuel 30, p.50

POTTER, A.E (1969) Ceramic Bulletin 48 (9), p.855

RAJAN, R.R and C.Y Wen (1980) AIChE J 26(4), p.642

RAMACHANDRAN, P.A and J.M Smith (1977) AIChE J 23 p.353

RANDOLPH, A.D., and M.A. Larson (1971) "Theory of Particulate Processes", Academic Press, New York.

ROBERTS, A.G. et al (1975) Inst. Fuel Symp. Ser. 1(1), p. D4

RUDMAN, R (1987) Chief Metallurgist, Pretoria Portland Cement, Ltd. Johannesburg. Personal Communication

SCHIE, F. (1987) Union Lime Company. South Africa. Personal Communication.

SCHRUBEN, J.S., and W.G. Vaux (1983) Chem. Eng. Comm. 33, p.337

SHEN, C.Y., and H.F.Johnstone (1955) AIChE J. 11, p.550

SIMONS, G.A and A.R. Garman (1986) AIChE J. 32 (9), p.1491

SIMONS, G.A and W.T Rawlins (1980) I&EC Proc. Des. & Dev. 19 (4), p.565

SIMONS, G.A. (1988) AIChE. J. 34(1), p.167

SIMONS, G.A. A.R. Garman, and A.A.Boni (1987) AIChE. J. 33(2), p.211

SPITSBERGEN, U et al (1983) in proc. of "Fifth Intl. FBC and Applied Tech. Symp.", Beijing, Peoples Republic of China

SPITSBERGEN, U., et al (1981) J. Inst. Energy, June, P. 94

STEWART, P.S.B, and J.F. Davidson (1967) Powder Tech., 1, p.61

SUN, C.C., C.H. Peterson, and D.L. Keairns, (1980) "Experimental /Engineering Support for EPA's FBC Program: final report 111, Solid Residue Study", EPA-600/7-80-015c.

SZEKELY, J, J.W. Evans, and H.Y. Sohn (1976) "Gas Solid Reactions" Academic Press. New York

TARMAN, P.B., and D.V. Punwami (1975) Interim report No. 2. to ERDA. IGT. Chicago

ULERICH, N.H et al (1980) "Experimental/Engineering Support for EPA's FBC Program: Vol.1 Sulphur Oxide Control" report no. EPA-600/7-80-015a.

ULERICH, N.H. et al (1977) "The influence of Limestone Calcination on the Utilization of the Sulfur-Sorbent in Atmospheric Pressure Fluid-Bed Combustors" EPRI Report FP-426.

ULERICH, N.H. et al (1978) Thermochimica Acta 26 p. 269

ULERICH, N.H. et al (1979) "Criteria for the Selection of SO2 Sorbents for Atmospheric Pressure Fluidized Bed Combustors - Vol. 2" EPRI Report FP-1307

UMAN, M.F. (1983) in "Acid Rain - Planning for the '80s", Zimmer, M.J., and J.A. Thompson eds., Government Inst. Inc., Rockville, MD.

VAUX, W.G (1978) in Proc. American Power Conf. 40, p.793

VAUX, W.G and D.L. Keairns (1980) in "Fluidization 3" Engineering Foundation Conf. Henniker, New Hampshire.

VAUX, W.G., and A. W. Fellers, (1981), AICHE Symp. Ser. 77(205), p.107

VAUX, W.G., and J.S. Schruben, (1983), AICHE Symp. Ser. 79(222), p.97

VOGEL, G.J et al (1977) "Supportive Studies in Fluidized Bed Combustion" Argonne National Laboratory. ERDA Report ANL/ES-CEN-1019.

WAKAO, N and J.M Smith (1962) Chem. Eng. Sci. 17, p. 825

WEAST, R.C and Astle, M.J. (1982) "CRC Handbook of Chemistry and Physics", 63rd ed. CRC Press. Florida

WEI, J et al (1977) Chem. Eng. Sci. 32(10), p.1211

WEN, C.Y., and L.H. Chen (1982) AIChE J. 28(1), p.117

WEN, C.Y. and S. Dutta, (1977), AICHE Symp. Ser. 73 (161), p.1

WHITAKER, R (1983) in "Acid Rain Research - A Special Report", EPRI

WRIGHT, M.A (1979) Report PC17 British Coal, Stoke Orchard,UK.

YATES, J.G (1983) "Fundamentals of Fluidised -Bed Chemical Processes" Butterworths Monographs in Chemical Engineering. London

YU, H-C, and S.V Sotirchos (1987) AIChE J, 33(3), p.382

ZAWADZKI, J, and S. Bretsznajder (1938) Trans. Faraday Soc. 34 p 951

ZENZ, F.A. (1982) "Studies of Attrition in Fluid Particle Systems" Particulte Solid Research Inc. New York

ZHENG, J, J.G. Yates and P.N. Rowe (1982) Chem. Eng. Sci 37(2), p.167

APPENDIX A - CALCINATION OF SOUTH AFRICAN SORBENTS

A.1 Overview

Calcination directly affects the pore structure, and hence sulphation propensity, of sorbent particles. The mechanism of sorbent calcination has been well researched [Zawadzki and Bretsznajder (1938), Murray et al (1950, 1953), Hyatt et al (1958), Ingraham and Marier (1963), Hills (1968), Ulerich et al (1977), Spitsbergen et al (1983), Borgwardt (1985), Dennis and Hayhurst (1986)]. This last paper offers the most comprehensive study of the reaction in fluidised beds, and confirms that, under conditions typical of atmospheric pressure FBC operation, calcination of 0.75 - 2 mm sorbent particles proceeds to completion in about two minutes. This compares with typical sulphation times of 1 - 2 hours (see Chapter 3). In the discussion of sorbent sulphation presented in this thesis, the calcination reaction can therefore be described by an infinitely fast reaction rate without loss of overall accuracy.

A.2 Experimental

Some work was undertaken on the fixed bed calcination of selected South African sorbents. Sorbent calcines, prepared in a muffle furnace, were examined for variation in their physical properties (Chapters 4 and 5). The very rapid calcination times representative of fluidised bed reaction were not achieved under these conditions, and it was therefore necessary to investigate this mode of calcination in greater depth.

Calcination times were monitored as a function of sorbent type, temperature (1073 - 1223 K), and furnace atmosphere (CO_2 concentrations in the range 0 - 60%). Bredasdorp, Saldanha and Marble Hall limestones, and Lyttelton dolomite were examined. Five gram masses of each sample (in the size range 300 - 600 μm) were placed in crucibles and heated under the required conditions of T and CO_2 atmosphere, until sample mass was constant, at which point calcination was assumed to be complete. Samples were removed from the furnace prior to weighing. To overcome problems associated with loss of sensible heat during this weighing period, tests were carried out with a number of identical samples held

at elevated temperatures for different, and increasingly long, time periods. Samples were not returned to the furnace after mass measurement. In this way, a picture of continuous calcination could be developed from this data set.

A.3 Results

FIGURES A.1 - A.3 show the effect, on calcination time, of sorbent type, furnace temperature and CO_2 atmosphere respectively. Calcination times were considerable longer than those reported above in fluidised beds. At T = 1170 K, $[CO_2]$ = 15%, calcination of the three limestone samples was completed in about 1 hour, and in about half this time for the Lyttelton dolomite sample. Calcination times decreased with an increase in furnace temperature and a decrease in $[CO_2]$ partial pressure. Such findings are consistent with the general body of literature referred to above.

These calcination times were used as a guide in the preparation of calcined samples for the analyses of Chapters 4 and 5.

A.4. Discussion

The experimental data at hand permitted a rudimentary investigation of the calcination mechanism. Defining a dimensionless radius r_c^* such that

$$r_c^* = \left[\frac{m_t - m_\infty}{m_o - m_\infty} \right]^{1/3} \qquad \text{A.1}$$

where m_t, m_o, and m_∞ is the mass of the sorbent charge at time t, time zero, and when calcination is completed, and assuming, furthermore, that calcination rate is controlled by chemical reaction according to shrinking core kinetics, gives a relationship in which r_c^* should vary linearly with time, t. This is indeed borne out by FIGURE A.4 for calcination of Bredasdorp limestone under different $[CO_2]$ partial pressures.

Folowing the development of Dennis (1985), calcination time, t_c, should vary with the inverse of the excess $[CO_2]$ partial pressure over its equilibrium value at a given temperature. This is borne out by FIGURE A.5.

Both these figures confirm that calcination rate is controlled by chemical reaction, with the influence of heat transfer being minimal. This claim is supported by FIGURES A.1 -A.3 from which it can be seen that sorbent particles lose mass immediately on entry to the furnace - there is no perceptible heat-up time. The fact that calcination times are longer in the muffle furnace than in a fluidised bed is attributed to the localised high concentration of CO_2 in the region of the sorbent charge.

APPENDIX B - SAMPLE CALCULATIONS FOR SULPHATION KINETICS

B.1 Interphase Exchange Coefficient

The interphase exchange coefficient, $\underline{X}$, which pertained to batch sulphation experiments described in Chapter 3, is found from eq.2.9.

Summary of combustor operating conditions:

$U = 0.7\ ms^{-1}$

$H = 200\ mm$

d_p (sorbent) = 300 - 600 μm

d_p (sand) = 750 μm

$T_{bed} = 1123\ K$

Minimum fluidisation velocity, U_{mf}, from Yates (1983)
Effective bubble diameter, $\underline{D}_e$, from Darton (1977)
Under these conditions,

$$U_{mf} = 0.17\ ms^{-1}$$

$$\underline{D}_e = 0.54\ (U - U_{mf})^{0.4}\ (h + 4\sqrt{A_o})^{0.8} / g^{0.2} \qquad B.1$$

$$= 4.2\ cm$$

$$D_g = 1.39\ cm^2/s \text{ (from Fieldes, Table 6)}$$

$$\epsilon_{mf} = 0.43 \text{ [from Babu et al(1974)]}$$

From eq.2.9,

$$\underline{X} = \frac{6.34\ H_{mf}}{D_e\ (gD_e)^{1/2}} \left[U_{mf} + \frac{1.3\ \epsilon_{mf}\ D_g^{1/2}\ g^{1/4}}{(1 + \epsilon_{mf})\ D_e^{1/4}}\right] \qquad B.2$$

Taking $H_{mf} = H = 0.2$ m and using values for other parameters as above, gives

$$\underline{X} = 8.87$$

This value of $\underline{X}$ is sufficiently large that errors in assuming the fluidised bed to be well mixed are small.

B.2 Maximum Sorbent Conversion for Selected South African Sorbents

The maximum conversion of the three South African sorbents (Lyttelton, Marble Hall and Bredasdorp) is found from numerical integration of eq.2.6 i.e

$$X_\infty = Gy_o^*/M \int_0^{t_\infty} (1-y_o/y_o^*)\, dt \qquad B.3$$

The dry flue gas flow, G, is found from an O_2 mass balance over the laboratory combustor as follows:

Coal flow, F_o = 0.65 kg/hr
Excess O_2 in flue gas, on average = 4%
Average combustion efficiency = 90%
Coal composition from TABLE 3.1

Air flow to combustor, F_A = 6.48×10^{-5} kmol/s

From coal composition figures, molar flow of combustion products
= 6.99×10^{-6} kmol/s

Dry flue gas flow, G = (0.79 F_A + 6.99×10^{-6} + x_A) kmol/s
where x_A is excess air flow.

But, flue gas $[O_2]$ = 4%. The excess air flow, x_A, can now be calculated.

Therefore, $0.21\, x_A/G = 0.04$ and $x_A = 1.4.\ 10^{-5}$ kmol/s

Thus, G = 7.19×10^{-5} kmol/s.

This value is used in eq. B.3 to predict X_∞ for the three South African sorbents. For the sulphation of Bredasdorp limestone, y_o^* = 800 ppm, whereas for Lyttelton and Marble Hall tests, y_o^* = 985 ppm. This difference was attributed to variations in coal composition between

tests. The molar CaO charge, M, was calculated from sorbent purity, for a sample mass of 15 grams.

M - Lyttelton = 8.089×10^{-5} kmol
M - Marble hall = 1.377×10^{-4} kmol
M - Bredasdorp = 1.331×10^{-4} kmol

The integral term in eq. B.3 was evaluated from the SO_2 / time response data (as in FIGURE 3.2). Integration was performed using a Simpson's rule algorithm with 10 subdivisions.

The calculated value of X_∞ for the three sorbents is thus

X_∞ - Lyttelton = 0.155
X_∞ - Marble hall = 0.237
X_∞ - Bredasdorp = 0.325

B.3 Sulphation Time from Model of Fieldes

Following the methodology of Fieldes (1979), the sulphation time, t_s, is found as follows:

$$X_\infty = \left[(K_{so} + 1/B) \ln(1 + BK_{so}) - K_{so} \right] \frac{\pi d_p^2 C P_c}{Z K_{so} B} \qquad B.4$$

where P_c is a model parameter, related to pore plugging time. C is the bulk $[SO_2] = 1.085 \times 10^{-5}$ gmol/cm^3.

B is found from eq. 3.1, and $Z = \pi d_p^3 f_s / 6.56$

Using X_∞ for Bredasdorp, along with the measured value of $K_{so} = 0.466$ ms^{-1}, gives a value for $P_c = 23.2$ s.

The sulphation time is related to the model parameter, P_c, by $t_s = P_c / y_p^*$, where y_p^* = particulate phase $[SO_2]$, equal to $y_o^*(1/2 + 1/\underline{X})$.

Using the calculated value for $\underline{X}$ from eq B.2 gives a calculated value of $t_s = 37862$ s.

Measured sulphation times were, from Chapter 3, equal roughly to 3600 s. The model of Fieldes predicts a sulphation time roughly 10 times this value.

B.4 Initial Sulphation Rate Constants from Argonne TGA Data

The initial sulphation rate constant, K_{so}, can be found from TGA data as follows:

$$K_{so} = \left.\frac{dX}{dt}\right|_{t=0} \frac{\rho\, d_p}{6\, C} \qquad \text{B.5}$$

where C is ambient $[SO_2]$. Lee and Georgakis (1981) provided an expression for $dX/dt|_{t=0}$.

$$\left.\frac{dX}{dt}\right|_{t=0} = \frac{Q_o}{Z} \qquad \text{B.6}$$

where Q_o is initial reaction rate, and Z is moles of CaO per particle. Q_o was defined in terms of a sulphation time constant, τ_{sf}. Values of τ_{sf} were reported for the ten sorbents for which TGA data were available from Argonne national Laboratory. Using eq B.5 and B.6, a final expression for K_{so} is:

$$K_{so} = \frac{d_p}{6\, f_s\, \tau_{sf}} \qquad \text{B.7}$$

where f_s is fractional purity of sorbent particle. K_{so} values calculated from eq. B.7 are shown in TABLE 3.5 for the Argonne sorbents.

APPENDIX C.

SOUTH AFRICAN CARBONATE RESOURCE

South Africa, with its well established mining, industrial and agricultural base, generates a significant demand for lime and limestone / dolomite. Principal users of this raw material are

1. the cement industry

2. the agricultural sector, for the stabilisation of clay soils, and the neutralisation of acidic soils (aggravated by acidic deposition from thermal power stations)

3. the metallurgical industry, as a flux in iron and steel processing, for acid neutralisation during gold and uranium processing, and as a flux in platinum refining

4. the carbide industry, for acetylene production

5. the pulp/paper and sugar industries, where lime is used in the regeneration of caustic soda, and the optimisation of pH respectively

6. in water treatment

Product specifications for each of these applications are rigid, both in chemical purity, and required size distribution. This has major implications for the quarrying of this valuable resource. Of interest is that, beyond the sometime requirement for select size ranges, little emphasis is placed on the physical properties of the material.

It should be stressed that the quality and extent of limestone deposits, in South Africa, is poor by world standards (using Western Europe and the USA as examples). An additional feature of the industry is that the largest deposits are significantly remote from the site of large coal fired power plant. Discounting areas where the known deposit is defined as less than 5 M te, the total extent of local calcium based carbonate

resources (recoverable by open cast mining)is estimated to be in excess of 23 100 million tonnes, of which more than 80 % is calcitic in nature, and includes significant resources of calcrete and travertine. The known reserves at existing quarries exceed 9000 million tonnes, of which again, more than 80% is calcitic [Martini (1987)]. Existing quarry operations exploit the medium to high grade deposits, although these terms are relative - their chemical purity is low by world standards.

The 16 sorbents examined in this thesis have been obtained from operational quarries, whose geographical locations are identified in FIGURE C.1. What follows is a summarised geologic description of each of these deposits, giving their local stratigraphic typing, as well as international descriptors (South Africa has only recently embarked on a program to standardise on terminology used to describe the complex, and variable geology of the region [de Grys, 1980]). Current mine tonnages are quoted where known, and the existing markets for the various products identified. This information is required for the planning of any scenario in which the use of these carbonates for flue gas desulphurisation is envisaged.

Limestones and dolomites belong to the sedimentary classification which displays the widest distribution in South Africa. Older rocks are often indurated and metamorphosed, with little natural porosity, whilst younger ones may be soft and poorly consolidated [Martini (1987)]. Other significant classes of calcareous materials are calcretes and dolocretes which form under mildly arid climatic conditions by accumulation of $CaCO_3$ in soil. The texture, porosity and robustness of a limestone depend largely on the nature of the sediment from which it consolidated.

A brief description of the geology of each sorbent is given below.

Robertson: This dolomite is part of the Malmsbury Group, stratigraphically belonging to the Namibian Erathem. Its USA classification would be Precambrian Z.
The Malmsbury Group is regarded as a geosynclinal succession of sedimentary and low grade metemorphic rocks, and is predominantly marine in character. The carbonate at Robertson is a light grey material, easily broken, with silica (originally present as chert) being the main impurity. Used principally as a source of agricultural lime, it is

quarried at the rate of 180000 Te/yr. Recoverable reserves have been defined as 8 million tonnes (in 1980).

Lichtenburg: This sorbent in its raw form is a calcrete (limestone precipitate in soil, from evaporation of groundwater; usually dolomite base). This material belongs to the Malmani Subgroup of the Vaalian Erathem, and can be classified as Precambrian X. This specific deposit contains inclusions of magnesium carbonate and detrital material, and as such, is of variable quality. It is used in cement production, and known reserves are in excess of 500 million tonnes.

Immerpan: This resource can be described as a dolocrete (as per calcrete, but with significant $MgCO_3$) which overlays Karoo sediments. The deposit lacks uniformity, with the top layer being richer in magnesium carbonate. This secondary limestone is part of the Transvaal Supergroup of rocks, and belongs to the Vaalian Erathem (Precambrian X). Reserves of this soft dolocrete are estimated at 150 million tonnes (1980), and this resource is quarried at the rate of 1 million tonnes annually, exclusively as an agricultural lime.

Bredasdorp: This Tertiary-to-Recent marine deposit, belonging to the Cenozoic Erathem (the youngest division of the Phanerozoic subdvision), contains a calcreteous overburden, and variable silica content (sometimes as high as 20%.) Quarried for agricultural lime and metallurgical applications, this material is highly friable, with reserves of good quality limestone known to exceed 1000 million tonnes.

Saldanha: The chronostratigraphy of this poorly consolidated, sandy, Recent limestone, is identical to the Bredasdorp sample. Depending on the exact location from which samples are taken, this deposit contains significant shelly fragments. If the full extent of the deposit is considered, reserves exceed 2000 million tonnes.

Marble Hall: This metamosphosed white marble, belonging to the Transvaal Sequence (and thus of Vaalian age - Precambrian X), contains the minerals diopside, fosterite and tremolite, and its principal impurity is chert. Overall purity is variable, and reserves of good grade product are put at not much beyond 20 million tonnes.

Hol River: This very pure calcite is part of the Nama Group of rocks and its age is somewhere between late Phanerozoic and Namibian Erathem. Quarrying is very select, and the deposit is not considered extensive.

Slurry: This material is also calcreteous, and is quite friable. Its chronostratigraphy corresponds to the Lichtenburg deposit, and its principal use is in cement production. Known reserves are thought to be comparable to the Lichtenburg deposit.

Moorreesburg: This is a very small limestone deposit, with reserves totalling only 200000 Te. Part of the Malmsbury Group (Namibian Erathem - Precambrian Z), it is used exclusively for building lime.

Lyttelton: This valuable deposit of primary dolomite is almost chert free, although in places it does contain traces of quartzite and shale. Belonging to the Malmani Subgroup - Vaalian Erathem (Precambrian X), this deposit is quarried extensively as a metallurgical flux. Reserves are essentially unlimited.

Olifantsfontein: This deposit is located in close proximity to the Lyttelton deposit, and is not geologically dissimilar.

Leo: This dolocrete is similar to that at Immerpan, although it tends to be powdery. Total reserves of the Immerpan region could approach several hundred million tonnes.

Lime Acres: This primary limestone comprises the largest single reserve of high purity limestone in the country. Part of the Ghaap Plateau group of rocks, it is of Vaalian age - Precambrian X. Reserves are unlimited.

Glen Douglas: This dolomite is part of the same formation as the Lyttelton and Olifantsfontein deposits, and it too, is quarried for its value as a metallurgical flux.

Vredendal: This quaternary dolomitic deposit is part of the Nama Group (Namibian erathem - Precambrain Z). It is quarried at the rate of 150000 tonnes per year, for use as a refractory base. Resources are estimated at several hundred million tonnes.

Umzimkulu: This is a very coarse grained deposit with calcite and dolomite interspersed. Its chronostratigraphy spans both Precambrian X and Y, and its South African typing is the Mokalian Erathem. The deposit is not uniform, and in places contains metamorphic silicates, and in places has undergone several recrystallisations. Toal reserves of calcitic marble are in the region of 1500 million tonnes, whilst dolomite reserves approach 600 million tonnes.

APPENDIX D - ELECTRON MICROGRAPH IMAGES

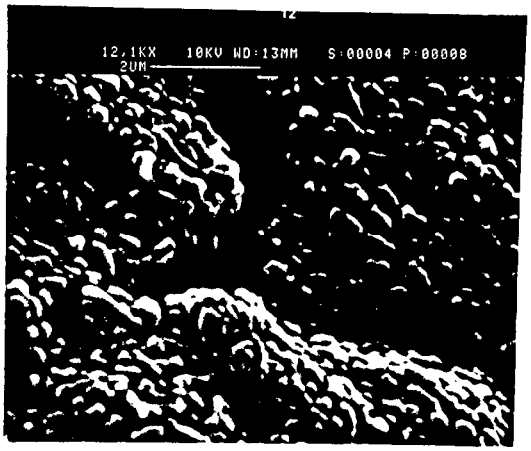

FIG D.1 BREDASDORP CALCINE
NON CYLINDRICAL PORES

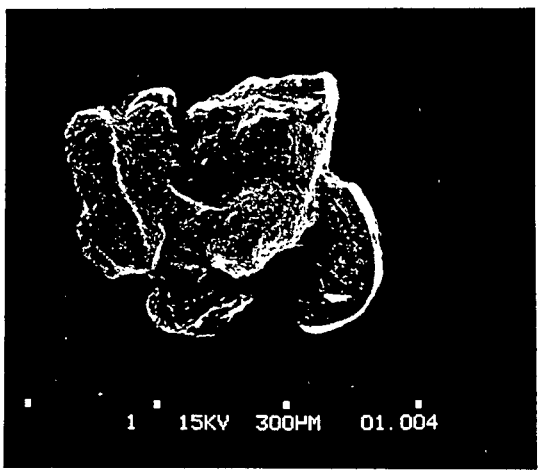

FIG D.2 BREDASDORP
NATURAL TOPOGRAPHY

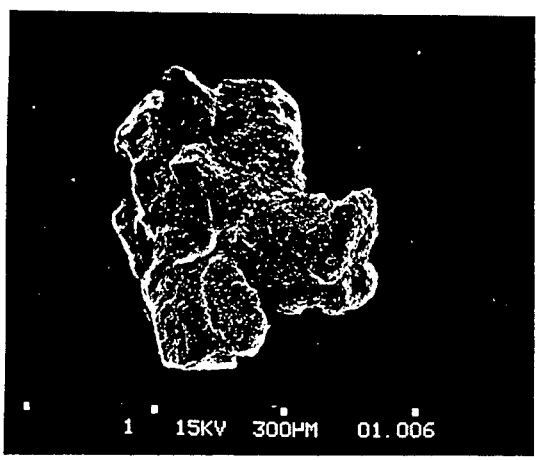

FIG D.3 BREDASDORP
NATURAL TOPOGRAPHY

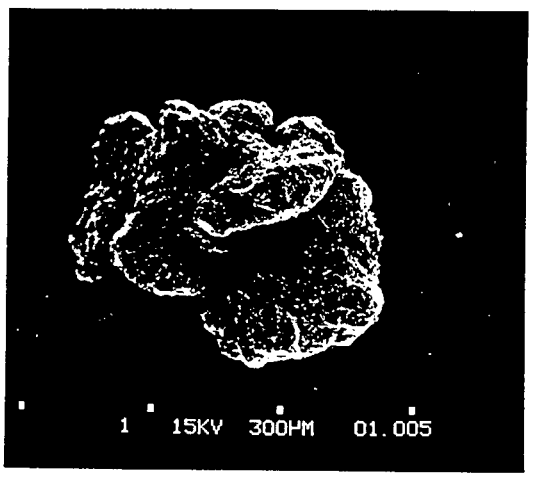

FIG D.4 BREDASDORP
NATURAL TOPOGRAPHY

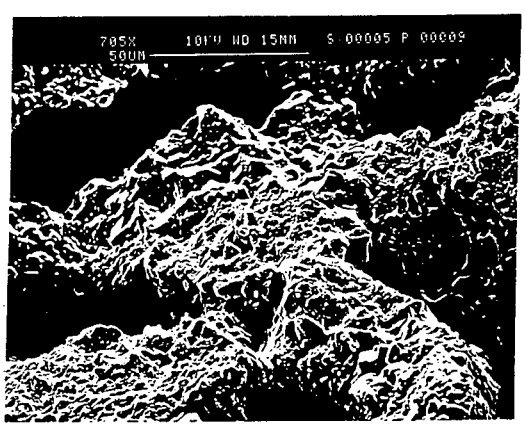

FIG D.5 BREDASDORP
SUPERPOROSITY

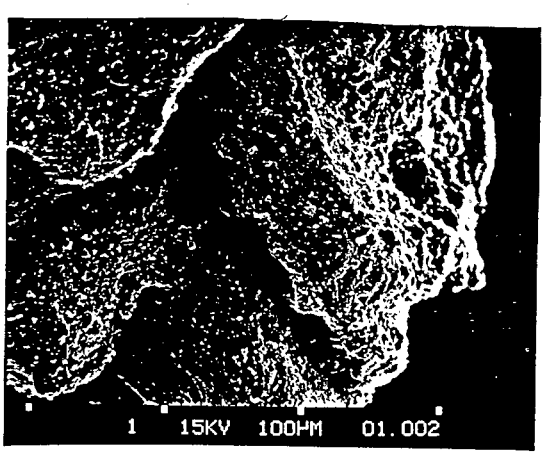

FIG D.6 BREDASDORP
CLEAVAGE LINES

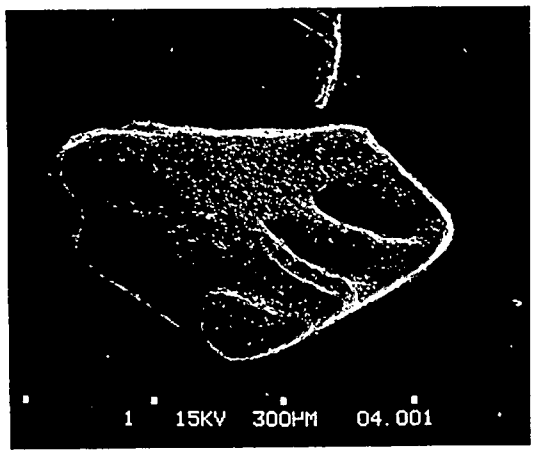

FIG D.7 SALDANHA
NATURAL TOPOGRAPHY

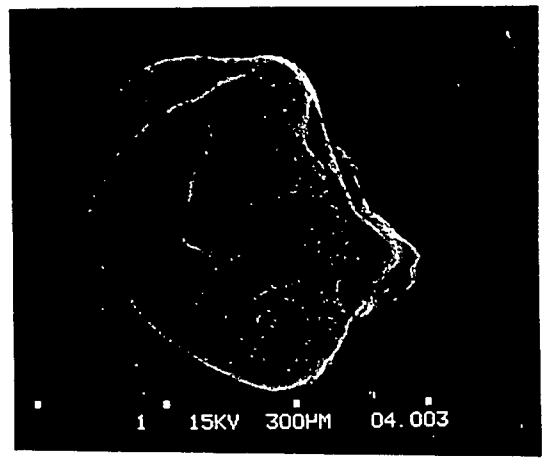

FIG D.8 SALDANHA
NATURAL TOPOGRAPHY

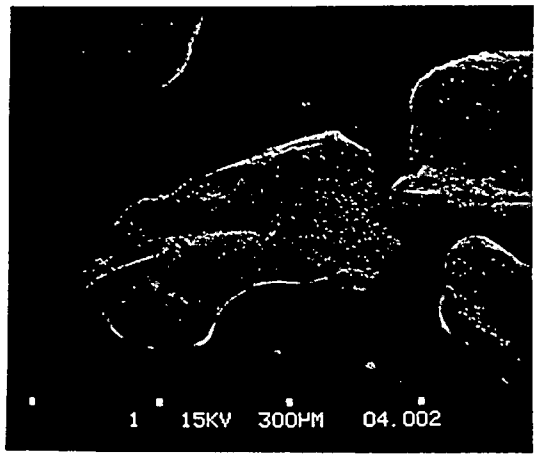

FIG D.9 SALDANHA
NATURAL TOPOGRAPHY

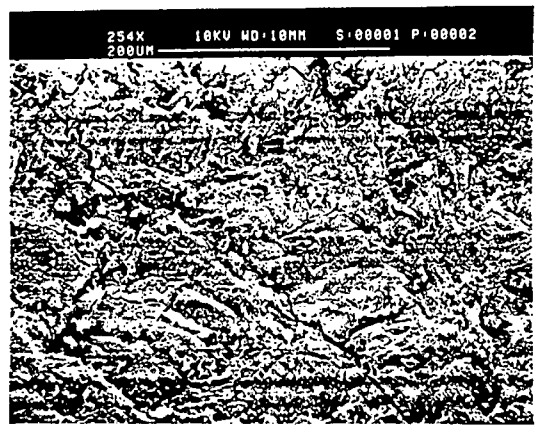

FIG D.10 LYTTELTON
GRAIN BOUNDARIES

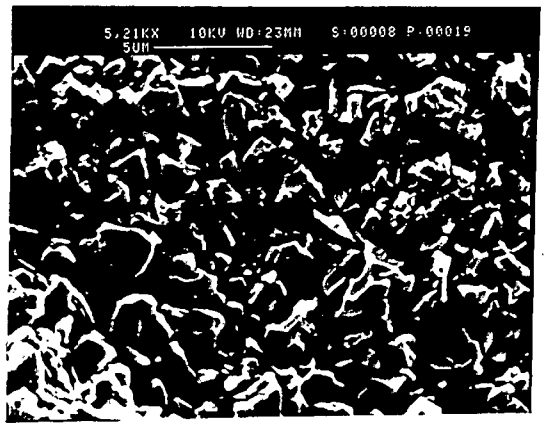

FIG D.11 SALDANHA
SHELL FRAGMENTS

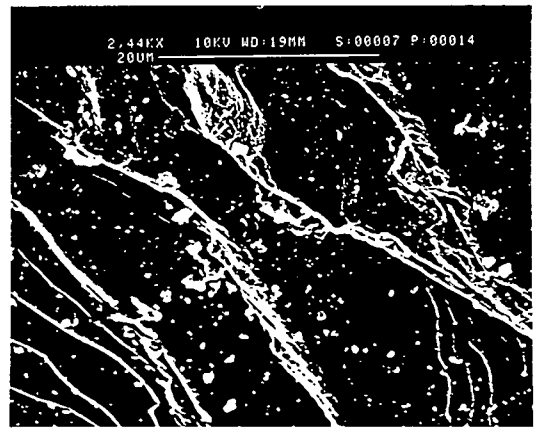

FIG D.12 MARBLE HALL
PLANAR STRUCTURE

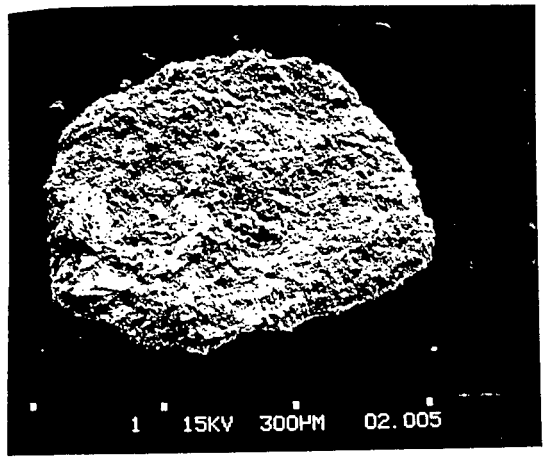

FIG D.13 LYTTELTON TOPOGRAPHY

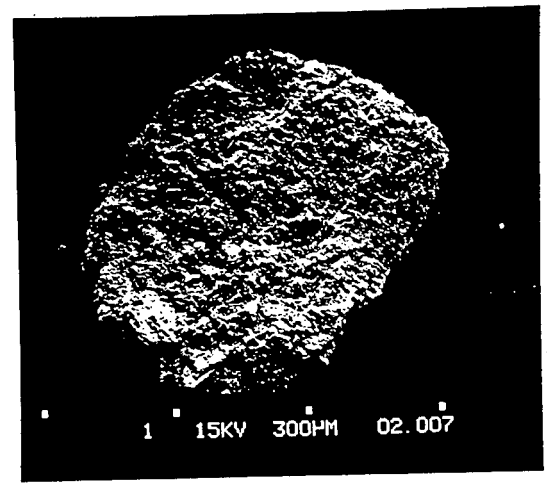

FIG D.14 LYTTELTON TOPOGRAPHY

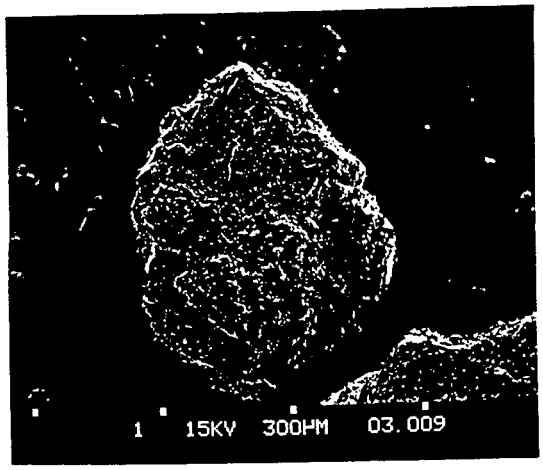

FIG D.15 MARBLE HALL TOPOGRAPHY

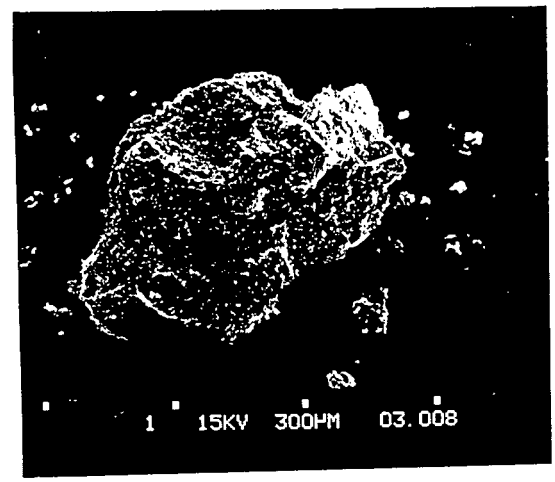

FIG D.16 MARBLE HALL TOPOGRAPHY

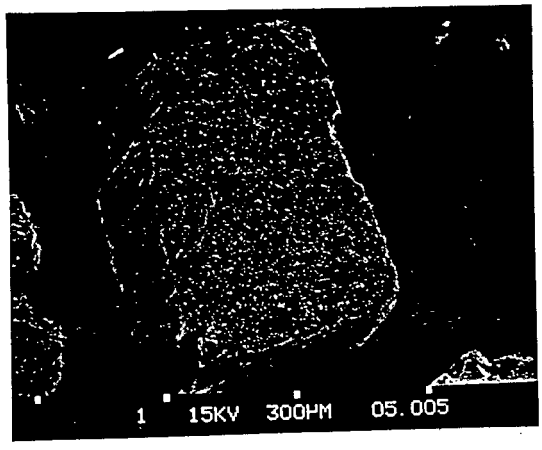

FIG D.17 UMZIMKULU TOPOGRAPHY

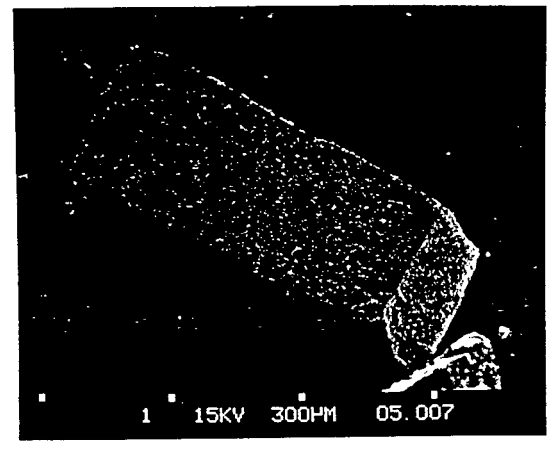

FIG D.18 UMZIMKULU TOPOGRAPHY

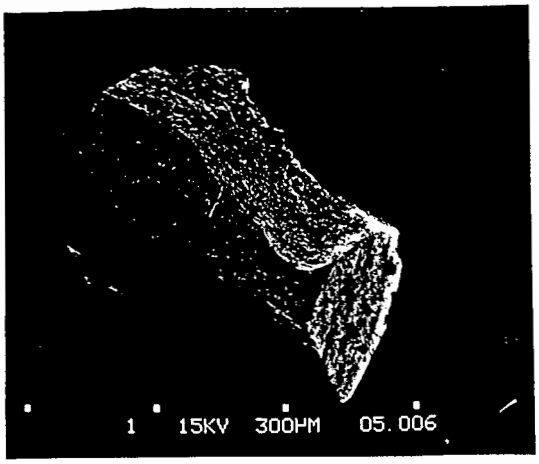

FIG D.19 UMZIMKULU
TOPOGRAPHY

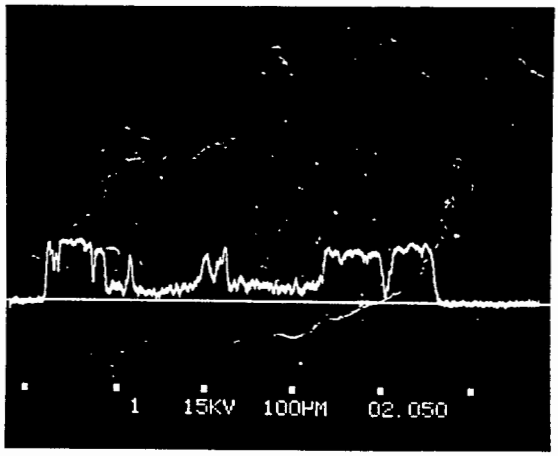

FIG D.20 LYTTELTON
SULPHUR LINE SCAN

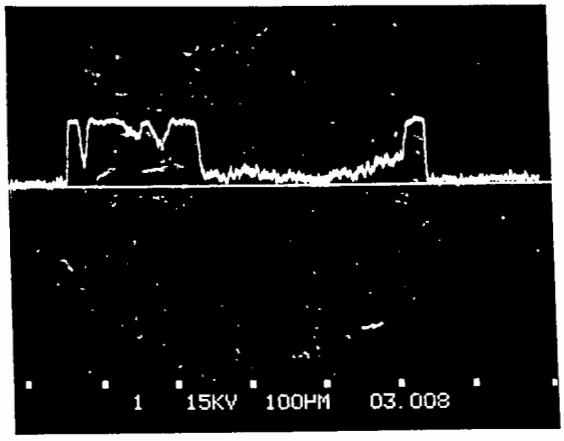

FIG D.21 MARBLE HALL
SULPHUR LINE SCAN

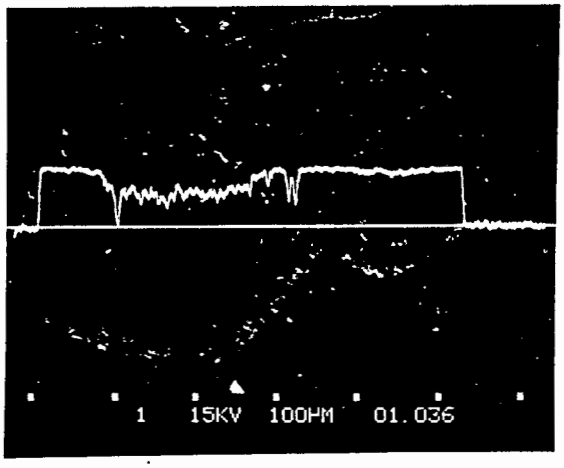

FIG D.22 BREDASDORP
SULPHUR LINE SCAN

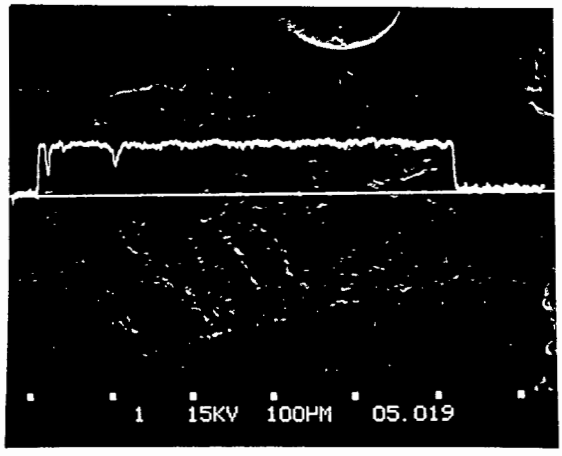

FIG D.23 UMZIMKULU
SULPHUR LINE SCAN

APPENDIX E - EFFECT OF SIEVE ACTION ON SORBENT ATTRITION

The extent of attrition during fluidisation was quantified by sieving out any fines generated. However, it has been recognised that sieving action is, of itself, a major attrition mechanism [Gupta et al (1975)]. Therefore, in measuring the amount of sorbent attrition caused by fluid bed action, allowance must be made for the contribution of "sieve - attrition".

In this current work, the amount of fines generated by sieving was shown to be both a function of sieving time and the mass of sorbent placed on the sieve pan. Although the first dependence was to be expected, and is consistent with experimental results reported by Gupta et al (1975), the second requires some clarification. It is intuitively felt that, as the mass of sorbent particles placed in the sieve pan is decreased from the maximum that the pan can physically hold, interparticle motion becomes more evident, and the effective kinetic energy of individual particles is increased. If, under these conditions, attrition is a function of the kinetic energy of these particles, then the amount of fines generated also increases. As the sample mass is decreased further, interparticle contact decreases, and the extent of sieving attrition should level off to some constant value.

The fluid bed attrition tests were conducted with sample masses typically of 1 - 2 kg. After each incremental fluid bed attrition run, the total charge was split into three fractions for sieve analysis. Sieving time was kept constant at 15 minutes. The sieve pan mass thus varied between 330 and 660 grams. Over this range it was possible to fit the mass of fines generated by sieve action to a plot of the form

$$\underline{A} = c_1 - c_2 \times m \qquad \text{E.1}$$

where $\underline{A}$ is the extent of attrition, defined by eq. 5.2, m is the sieve pan mass, and c_1 and c_2 are functions of sample type. For the Bredasdorp sample, in the size range 300 - 600 μm, $c_1 = 0.135$ and $c_2 = 1.5 \times 10^{-4}$.

It was assumed that sieving action would generate fines by the same

mechanism as fluidisation i.e. abrasion would dominate. It could therefore be expected that "sieve - attrition" would display the same time dependence as "fluidisation - attrition". Assuming this to be true, it is necessary to measure the amount of fines generated by sieve action only at the start of each fluidised attrition study. In each successive time increment, the amount of "sieve fines" could be then inferred from the incremental change in fines generated by fluidisation, assuming the two attrition curves to be parallel.

The true measure of fluidised bed attrition could then be calculated by subtracting the "sieve fines" from the total mass of fines measured i.e

$$\underline{A} = \ln [M_o / (M_{coarse} + M_{sieve\ fines})]$$

where M_o is the mass of sorbent charged to the fluidised combustor, M_{coarse} is the mass of particles remaining in the 300 -600 μm fraction after the attrition trial, and $M_{sieve\ fines}$ is the mass of fines generated by sieving action.

For other size ranges of the Bredasdorp sample, the effect of sieve attrition was assessed by scaling upwards, to the total fluidised bed sample mass, the amount of fines generated in a sieve charge of 500 grams. Fines generated by this method corresponded to initial values, prior to any fluidised bed attrition. These figures are shown below

d_p = 600 - 850 μm: 500 g sieve charge gives 22.95 g fines
d_p = 850 - 1180 μm: 500 g sieve charge gives 19.7 g fines

For the other sorbents examined in Chapter 5, attrition tests were conducted only at one bed depth, and for one particle size. The contribution which "sieve - attrition" makes to fines generation was inferred, as above, by scaling from a sieve charge of 500 grams. These figures are reported below.

	500 gram sieve mass
Lyttelton	20,3 g fines generated
Saldanha	80,5 "
Marble Hall	33,6 "
Umzimkulu	14,9 "

APPENDIX F - SUMMARY OF ELUTRIATION MODELS

Two popular elutriation models were assessed in Chapter 5. Their development is repeated below.

F.1. Wen and Chen Model

This model is based on the classic first order elutriation rate expression, whereby the flux of particles of size i is proportional to their mass fraction in the bed. Thus

$dx_i/dt = K^* x_i$, where K^* is the elutriation velocity constant.

Wen and Chen proposed that the elutriate flow rate per unit bed surface, of particles of size i, F_i, is given by

$$F_{i\infty} = E_i x_i$$

and

$$F_\infty = \Sigma F_{i\infty}$$

where the elutriation rate constant $E = K^* W/A$, where W is the bed mass and A is the bed area.

The elutriation rate constant is given by

$$E_{i\infty} = \rho_s (1 - \epsilon_i) U_{si}$$

where U_{si}, the solid velocity of a given particle size, is approximated by the difference between the the superficial gas velocity and the terminal velocity of particles of size i. Thus

$$U_{si} = U - U_{ts}$$

The freeboard voidage, ϵ_i, is derived from a force balance on the combustor walls, and can be expressed as

$$\epsilon_i = \left[1 + \frac{\Gamma\ (U - U_{ts})^2}{2\ g\ D_c} \right]^{-1/4.7}$$

where Γ is the coefficient of friction due to interparticle contact, and their contact with the combustor walls.

Γ was correlated against system parameters thus:

$$\frac{\Gamma \rho_s}{d_p^2} \left[\frac{\mu}{\rho_g}\right]^{2.5} = \begin{cases} 5.17\ Re_p^{-1.5}\ D_c^2 & \text{for } Re_p <= Re_{pc} \\ 12.3\ Re_p^{-2.5}\ D_c & \text{for } Re_p >= Re_{pc} \end{cases}$$

where $Re_{pc} = 2{,}38/D_c$ and $Re_p = \rho_g\ (U-U_{ts})\ d_p\ /\ \mu$

F.2 Geldart Model

This model differs fundamentally to that of Wen and Chen in that the holdup of fines in the freeboard increases the effective gas density, thereby lowering the terminal velocity of coarse particles and increasing their elutriation rate.

This model, too, assumes a first order relationship between elutriation flux and the mass of particles of a given size in the bed. The final form of the model is

$$\frac{E}{\rho_e\ U} = C_1 \exp\left[- C_2 \frac{U_t}{U}\right] \qquad \text{F.1}$$

where $\rho_e = \rho_g + \Sigma \rho_i$, and C_1 and C_2 are system constants. The solids loading of particles of size i, in the freeboard, is given by

$$\rho_i = F_i\ /\ UA$$

The terminal velocity of particles of size i is calculated from the expression proposed by Heywood (as reported by Coulson and Richardson,1968) with a particle drag force $F_D = 3\pi\mu d_p\ U\ (1 + 0{,}15\ Re_p^{0.687})$.

The model is implemented for discrete particle sizes. The solids loading of the smallest size fraction is calculated from the mass of elutriated solids and its sieve analysis. The effective gas density,

"seen" by the next largest size, is then simply $\rho_s + \rho_l$. U_{ts} for this size fraction is then calculated, and, with the measured value of E, used to substantiate eq. F.1. The process is repeated with increasing particle size, until all sizes have been accommodated.

APPENDIX G - MODEL PARAMETERS

G.1 Steady State Attrition Rate

From eq. 5.10,

$$p' = \frac{a_1\ \sigma(f)}{(U-U_{mf})^2\ H\ \rho_s} \left[\frac{d_p}{g}\right]^{1/2} \qquad G.1$$

where a_1 is the measured steady state attrition rate. Values of a_1 can be found in TABLE 5.6 for laboratory attrition studies. Substituting the a_1 values for the Bredasdorp sample attrition tests into eq G.1, gives a mean value of $p' = 1.91 \pm 0.5$.

This mean value of p' is used to ascertain stady state attrition rates under conditions where no measured values are available e.g. in the 10 MW_{th} FBC studied in Chapter 7. Under typical operating conditions for this unit ($H = 1$ m, $U = 1$ ms^{-1}, $d_p = 750$ μm),

R_{ss} Bredasdorp = 8.5 %/hr
R_{ss} Lyttelton = 5.3 %/hr
R_{ss} Lime Acres = 5.3 %/hr

G.2 Sample Model Calculations

The accompanying tables, G.1 - G.4 show the discretisation of the solids population model for $U = 1$ ms^{-1}, $R_{ss} = 5$%/hr, a feed stream of constant size $d_p = 750$ μm, and R_{cs} values of 0.5, 1, 2, 4. The columns referred to as Terms 1-6 are in fact the individual components of the discretised population balance, each one being equal to a term on the RHS of eq 6.10.

Under these conditions, the mean particle diameter increases from 600 μm to 637 μm as sorbent feed rate is increased over this range of R_{cs} values.

Coarse particles are defined as those whose terminal velocity exceeds the fluidising value ($U = 1$ ms^{-1} in this case). The residence time of these particles (from TABLES G.1 - G.4) ranges from about 10 - 35 hours.

Using the argument, developed in APPENDIX F, that the holdup of fines in the freeboard increases coarse particle carryover, it can be shown that particles of 150 μm and larger have U_{ts} values greater than 1 ms^{-1}, and they should not be elutriated from the bed. It is interesting to note that the model predicts finite residence times for much smaller particles, e.g. at $R_{cs} = 2$, $\tau(d_p = 53\ \mu m) = 0.93$ hours, which is comparable to the sulphation time t_s. However, these small particles are present in negligible amounts in the bed (for a feed of constant size), and their contribution to sulphation is small. When a sorbent feed stream with a wide size distribution is used, fine particles make up a greater proportion of bed bulk, and their effective contribution to sulphation should not be discounted. The action of fines on sulphation is not included in the present model because of the requirement that, at steady state, the total number of particles in the bed be constant.

The population balance gives $\tau(d_{pi})$ for discrete particle sizes. This information is used in conjunction with the discrete analog of eq. 6.24 to give the overall sulphation efficiency for the full range of particle sizes in the fluidised bed. The summation term in eq. 6.24 is evaluated over the same discrete size intervals used in solving the population balance expression (eq. 6.10).

TABLE 2.1 SUMMARY OF SULPHATION EXPERIMENTS BY OTHER RESEARCH GROUPS

Research Group	Reactor Type	d_p (mm)	T (K)	Calc. Condition	Gas Atmosphere
Potter (1969)	Fixed bed	0.92	1253	precalcined	No.2 fuel oil + CS_2
Spitsbergen (1981)	1.TGA	0.2	1123	precalcined	SO_2 = 0.2% CO_2 = 15% O_2 = 2 % N_2 = 82.8%
	2.FBC	0.2	1123	precalcined	
	3.Pilot FBC	0.2 0.4 0.65	1123	uncalcined	coal comb. %S = 1.03
Borgwardt and Harvey (1972)	Fixed bed	1.3 0.25 0.096	1253	precalcined	flue gas SO_2 = 3000 ppm
Hartman and Coughlin (1974)	Fixed bed	0.565 1.2	1123	precalcined	SO_2 = 0.29% CO_2 = 10.1% O_2 = 3.5% N_2 = balance
Ulerich et al (1978)	TGA	1-1.2	1033 to 1223	precalcined	SO_2 = 0.5% O_2 = 4% N_2 = balance
Dogu (1981)	TGA	15	1033 to 1373	precalcined	SO_2 = 0.5% O_2 = balance
Vogel (1977)	TGA	0.92	1173	precalcined	SO_2 = 0.3% O_2 = 5% CO_2 = 20% N_2 = balance
Fieldes (1979)	Fluid bed	0.256 0.465 0.78 1.09 1.55	1050 to 1200	uncalcined	SO_2 = 0.258% balance air or coal comb. SO_2 = 0.24%
Zheng et al (1982)	Fluid bed	0.15 0.62	1073 1123	uncalcined	coal comb. %S = 2.55

TABLE 3.1 BALLENGEIGH COAL COMPOSITION

Carbon	50.06 % m/m
Hydrogen	3.54
Ash	33.9
Moisture	3.08
Sulphur	1.53
Nitrogen	1.25
Oxygen	6.64
GCV (MJ/kg)	20.25

TABLE 3.3 SIEVE ANALYSIS OF FLUIDISING MEDIUM

Aperture (mm)	% Retained
3.36	0
2.83	0.1
2.38	0.2
2.00	0.4
1.68	0.4
1.41	0.9
1.19	5.0
1.00	16.0
0.84	27.8
0.71	24.9
0.59	16.5
0.50	7.1
0.42	0.6
0.35	0.1
0.3	0

TABLE 3.2 COMPOSITION OF SOUTH AFRICAN SORBENTS

Sorbent Source	CaO	MgO	SiO_2	Fe_2O_3	Na_2O	P_2O_5	MnO	Al_{2O3}	K_2O
Robertson	27.9	21.7	4.4						
Lichtenburg	47.5	1.7	10.4	1	0.1		0.25	1.14	0.15
Immerpan	27.9	19.3	6.3	0.7	0.1	0.06	0.05	1.01	0.11
Bredasdorp	49.7	0.25	10.4	0.29					
Saldanha	50.4	0.82	6	0.91	0.5	0.89	0.1	0.91	
Marble Hall	51.4	3.41							
Holrivier	54.3	0.36	0.05	0.06			0.01	0.15	
Slurry	45.8	1.84	11.1	0.92	0.05		0.3	1.27	0.06
Mooreesburg	52.4	0.5	4.1	0.6					
Olifantsfontein	29.5	20	4	1.3				0.2	
Lyttelton	30.2	21	2.5	0.9	0.17	0.05	0.07	0.31	
Leo Dolomite	25.3	19.1	13.4	0.87	0.19	0.02	0.03	1.66	0.13
Lime Acres	54	0.7	1	1	0.03		0.62	0.18	
Glen Douglas	29.9	20.6	1.7	0.9			0.7	0.25	
Vredendaal	29.1	20.7	4.3	0.17				0.15	
Umzimkulu	32.5	19.2	2.4						

TABLE 3.4 SULPHATION KINETIC PARAMETERS

Sorbent Source	k_s (ms^{-1})	k_d (s^{-1})	Coeff. of Correlation
Robertson	0.132	0.00458	0.963
Lichtenburg	0.181	0.00099	0.991
Immerpan	0.105	0.00161	0.98
Bredasdorp	0.466	0.00233	0.994
Saldanha	0.365	0.00265	0.965
Marble Hall	0.155	0.00220	0.997
Holrivier	0.118	0.00109	0.995
Slurry	0.257	0.00193	0.98
Mooreesburg	0.110	0.00244	0.984
Olifantsfontein	0.143	0.00357	0.993
Lyttelton	0.138	0.00514	0.992
Leo Dolomite	0.285	0.00545	0.981
Lime Acres	0.154	0.00229	0.994
Glen Douglas	0.240	0.00418	0.987
Vredendaal	0.176	0.00422	0.995
Umzimkulu	0.249	0.00192	0.994

TABLE 3.6 EFFECT OF Fe AND Na ADDITION ON SORBENT UTILITY

Sorbent Batch	Soaking Time (min)	$\%Fe_2O_3$ in sample after soaking	K_{so} (ms^{-1})	X_∞
Batch 1	10	1.47	0.06	0.119
Batch 2	30	3.3	0.05	0.116
Batch 3	60	3.9	0.05	0.120
Batch 4*	5	1.42	0.08	0.121
Batch 5*	10	1.47	0.07	0.112
Base Test	-	-	0.138	0.155

* indicates batches with 1% Na_2CO_3 added

TABLE 3.5 COMPARISON OF SORBENT REACTIVITY

Sorbent Source	Max Conversion X_∞	Initial Rate Const. k_s (ms-1)
SOUTH AFRICAN:		
Bredasdorp	0.325	0.466
Marble Hall	0.237	0.155
Lyttelton	0.155	0.138
U.S.A.(1)		
Tymochtee	0.97	0.034
D. 1337	0.88	0.043
L. 1351	0.76	0.037
L. 1360	0.58	0.028
Greer L.	0.48	0.019
L. 2203	0.37	0.02
L. 1343	0.32	0.02
L. 1336	0.29	0.018
Grove (L. 1359)	0.15	0.016
Dolowhite	0.15	0.016
U.S.A.(2)		
Lowellville	0.17	0.06
Brownwood	0.14	0.035
Ames	0.15	0.06
Bellefonte	0.15	0.06
Mississippi	0.25	0.06
U.K.(3)		
Penrith	0.23	0.128
L6(4)	0.15	0.126
D1(5)	0.80	0.130

Notes:

(1) These data were obtained at Argonne National Laboratory by TGA. Mean d_p = 1 mm.
(2) This data set is from Westinghouse Corp. Sorbent utilities were obtained by graphical extrapolation of FBC data. Mean d_p = 1 mm.
(3) The Penrith sample had a mean d_p = 0.46 mm. THe mean size of the L6 and D1 samples was 0.78 mm
(4) L6 is Grove limestone.
(5) D1 is Tymochtee dolomite. The value for sorbent utility reported by Fieldes (1979) from a coal combustion experiment in FBC is lower than the value reported by Lee and Georgakis (1981) from Argonne TGA data.

TABLE 4.1 POROSITY AND SURFACE AREA DATA FOR SORBENT CALCINES

Sorbent Source	Pore Vol. (cc/g)	Surface Area (m^2/g)	Mean Pore Radius (nm)	B.E.T Area (m^2/g)
Robertson	0.178	5.42	186	
Lichtenburg	0.159	3.52	304	
Immerpan	0.399	5.94	350	4.93
Bredasdorp	0.247	2.13	494	2.15
Saldanha	0.206	0.59	941	0.55
Marble Hall	0.102	0.92	489	
Holrivier	0.06	0.18	945	0.26
Slurry	0.317	3.81	418	
Mooreesburg	0.271	1.02	676	
Olifantsfontein	0.297	4.38	200	4.38
Lyttelton	0.322	4.67	180	4.53
Leo Dolomite	0.605	3.83	640	
Lime Acres	0.393	4.12	398	
Glen Douglas	0.395	5.26	553	
Vredendaal	0.207	6.65	135	5.85
Umzimkulu	0.088	5.10	151	

TABLE 4.2 EFFECT OF CALCINATION CONDITIONS ON PORE STRUCTURE

Sorbent Source Calc.	Pore[1] Vol. 1 (cm^3/g)	Pore[2] Vol. 2 (cm^3/g)	Mean pore Radius (nm)	Surf. Area (m^2/g)	B.E.T Area (m^2/g)	ϵ[3] Meas.	ϵ[4]
Bredasdorp(C)	0.247	0.34	153	6.0	5.2	0.53	0.572
MarbleHall(C)	0.101	0.323	157	4.9	5.7	0.517	0.524
Lyttelton(C)	0.323	0.313	78	8.8	8.3	0.51	0.578
Bredasdorp(N)	-	0.049	506	0.75	0.86	0.117	-
MarbleHall(N)	-	0.022	1971	0.06	0.09	0.056	-
Lyttelton(N)	-	0.013	780	0.06	0.13	0.034	-

(C) refers to calcines, prepared at 1170 K: max time = 1 hr

(N) refers to natural sorbent

1. Pore volumes based on calcines prepared under conditions of TABLE 4.1
2. Pore volumes based on optimal calcination time at 1170 K
3. Based on measured pore volumes
4. From eq 2.1 with X=0 (from Hartman and Coughlin (1974))

TABLE 4.3 EFFECT OF CALCINATION TEMPERATURE ON PARTICLE SURFACE AREA

Temperature (K)	B.E.T. Surface (m^2/g)
1073	14.4
1123	9.5
1173	8.1
1223	4.8

Note: All calcines prepared in an air atmosphere; held at T for two hours

TABLE 4.4 EFFECT OF PARTICLE SIZE ON UNIT SURFACE AREA OF CALCINED SAMPLES

Particle Size (μm)	Bredasdorp B.E.T.(m^2/g)	Lyttelton B.E.T.(m^2/g)
53	8.3	14.0
75	10.0	13.5
106	7.3	14.6
150	7.7	13.2
212	7.8	14.5
500	9.2	14.1

Note: All calcines were prepared at 1170 K for 2 hours in air.

TABLE 4.5 STRUCTURAL STRENGTH DATA FOR SELECTED SOUTH AFRICAN SORBENTS

Sorbent Source	Natural Sorbent σ ($N\ m^{-1}$)	Calcined Sorbent σ ($N\ m^{-1}$)
Bredasdorp	95400	35020
Saldanha	71000	39230
Marble Hall	156500	56040
Lyttelton	256000	56040
Umzimkulu	63700	56040

TABLE 4.6 RELATIONSHIP BETWEEN SORBENT GEOLOGIC AGE AND SULPHATION PERFORMANCE

Lithostratigraphic Typing	Sorbent Utility Classification
1. TERTIARY / QUATERNARY	
1.1 Recent Marine/Sandy Limestones	
Bredasdorp calcite	C
Saldanha calcite	C
1.2 Secondary Limestones	
Slurry calcrete	C
Lichtenburg calcite	B
Immerpan dolocrete	B
Leo dolomite	A
2. PRIMARY CRYSTALLINE LIMESTONE/DOLOMITE	
2.1 Malmesbury Group	
Mooreesburg calcite	B
Holrivier calcite	B
Vredendaal dolomite	A
Robertson dolomite	A
2.2 Mzimkulu Formation	
Umzimkulu dolomite.	C
3. TRANSVAAL SUPERGROUP PRIMARY LIMSTONE/DOLOMITE	
Lime Acres calcite	B
Marble Hall calcite	B
Lyttelton dolomite	A
Olifantsfontein dol.	A
Glen Douglas dolomite	A

Note: Sorbent classifications based on sulphation kinetics - Chapter 3.

TABLE 5.1 EFFECT OF FLUIDISING VELOCITY ON ATTRITION

Total Attrition Time (hr)	Coarse Mass (g)	Sieve Att. Mass (g)	Extent of Attrition (%)
Bredasdorp; $(U-U_{mf})=0.3\ ms^{-1}$; H = 0.2 m; Mass = 1987 g; d_p=300-600 μm			
0	1987	0	0
0.25	1856.2	69.9	3.115
0.5	1746.1	128.7	5.816
1	1680.9	163.4	7.449
2	1634	188.5	8.642
4.04	1594.6	209.5	9.654
10.37	1560.8	227.6	10.53
20.26	1533.4	242.2	11.247
Bredasdorp; $(U-U_{mf})=0.2\ ms^{-1}$; H = 0.2 m; Mass = 1987 g; d_p=300-600 μm			
0	1987	0	0
0.25	1904.4	69.9	0.641
0.5	1813.6	146.7	1.352
1	1770.4	183.2	1.692
3	1690.7	250.7	2.322
4	1658.4	278.0	2.577
8	1621.1	309.6	2.875
16	1597.3	329.7	3.065
58.7	1562.6	359.1	3.334

TABLE 5.2 EFFECT OF BED HEIGHT ON ATTRITION

Total Attrition Time (hr)	Coarse Mass (g)	Sieve Att. Mass (g)	Extent of Attrition (%)
Bredasdorp; $(U-U_{mf})=0.3$ ms^{-1}; H = 0.1 m; Mass = 994 g; d_p=300-600 µm			
0	994	0	0
0.25	915.8	58.5	2.0
0.5	836.5	117.8	4.071
1	776.1	163.0	5.676
4.25	746.8	184.9	6.465
14.72	715.8	208.1	7.306
23.45	694.3	223.1	8.018
Bredasdorp; $(U-U_{mf})=0.3$ ms^{-1}; H=0.15 m; Mass = 1490.3 g; d_p=300-600 µm			
0	1490.3	0	0
0.5	919.5	175.5	5
1	856.5	194.9	6.97
2.02	774.7	220.0	7.88
4.02	760.3	224.5	7.73
9.19	678.3	249.7	8.25
16.19	691.2	245.7	9.11
Bredasdorp; $(U-U_{mf})=0.3$ ms^{-1}; H = 0.2 m; Mass = 1987 g; d_p=300-600 µm			
0	1987	0	0
0.25	1856.2	69.9	3.115
0.5	1746.1	128.7	5.816
1	1680.9	163.4	7.449
2	1634	188.5	8.642
4.04	1594.6	209.5	9.654
10.37	1560.8	227.6	10.53
20.26	1533.4	242.2	11.247

TABLE 5.3 EFFECT OF PARTICLE SIZE ON ATTRITION

Total Attrition Time (hr)	Coarse Mass (g)	Sieve Att. Mass (g)	Extent of Attrition (%)
Bredasdorp; $(U-U_{mf})=0.3$ ms^{-1}; H = 0.1 m; Mass = 994 g; d_p=300-600 µm			
0	994	0	0
0.25	915.8	58.5	2.0
0.5	836.5	117.8	4.071
1	776.1	163.0	5.676
4.25	746.8	184.9	6.465
14.72	715.8	208.1	7.306
23.45	694.3	223.1	8.018
Bredasdorp; $(U-U_{mf})=0.3$ ms^{-1}; H = 0.2 m; Mass = 1987 g; d_p=300-600 µm			
0	1987	0	0
0.25	1856.2	69.9	3.115
0.5	1746.1	128.7	5.816
1	1680.9	163.4	7.449
2	1634	188.5	8.642
4.04	1594.6	209.5	9.654
10.37	1560.8	227.6	10.53
20.26	1533.4	242.2	11.247
Bredasdorp; $(U-U_{mf})=0.3$ ms^{-1}; H = 0.1 m; Mass = 798 g; d_p=850-1180 µm			
0	798	0	0
0.25	741.4	43	1.724
0.75	702.7	72.4	2.918
1.75	675.9	92.6	3.75
3.75	653.1	110.0	4.47
8.5	632.9	125.3	5.11
24.05	613.3	140.2	5.74
Bredasdorp; $(U-U_{mf})=0.3$ ms^{-1}; H = 0.2 m; Mass =1596 g; d_p=850-1180 µm			
0	1596	0	0
0.25	1497	62.9	2.288
0.75	1436	101.6	3.725
1.75	1390.9	130.3	4.80
3.67	1348.2	157.4	5.829
18.82	1313.1	179.7	6.68

TABLE 5.4 EFFECT OF SORBENT TYPE ON ATTRITION

Total Attrition Time (hr)	Coarse Mass (g)	Sieve Att. Mass (g)	Extent of Attrition (%)
Bredasdorp; $(U-U_{mf})=0.3$ ms^{-1}; H = 0.2 m; Mass = 1987 g; d_p=300-600 µm			
0	1987	0	0
0.25	1856.2	69.9	3.115
0.5	1746.1	128.7	5.816
1	1680.9	163.4	7.449
2	1634	188.5	8.642
4.04	1594.6	209.5	9.654
10.37	1560.8	227.6	10.53
20.26	1533.4	242.2	11.247
Lyttelton; $(U-U_{mf})=0.3$ ms^{-1}; H = 0.2 m; Mass = 2349 g; d_p=300-600 µm			
0	2349	0	0
0.58	2220	95.13	1.449
1.05	2149.7	147.1	2.25
2.05	2098.5	184.9	2.836
4.63	2047.3	222.6	3.425
15.7	2017.8	244.4	3.77
38.6	1992.2	263.2	4.063
Marble Hall; $(U-U_{mf})=0.3$ ms^{-1}; H = 0.2 m; Mass = 2347 g; d_p=300-600 µm			
0	2347	0	0
0.5	2127.3	157.8	2.674
1.13	2035.7	223.5	3.811
2.23	1987.6	258.0	4.413
4.58	1943.3	289.9	4.972
10.04	1913.2	311.5	5.351
18.34	1883.2	333	5.732
42	1862	348.3	6.003
Saldanha; $(U-U_{mf})=0.3$ ms^{-1}; H = 0.2 m; Mass = 2327 g; d_p=300-600 µm			
0	2327	0	0
0.5	1707.3	374.5	11.136
1.06	1543.1	473.7	14.3
2.08	1457.5	525.5	16
4.17	1387.4	567.8	17.4
9	1331.4	601.7	18.54
19	1307.1	616.4	19.05
Umzimkulu; $(U-U_{mf})$ = 0.3 ms^{-1}; H = 0.2 m; Mass = 2443 g; d_p=300-600 µm			
0	2443	0	0
0.51	2263.5	72.65	4.473
1.03	2171.8	109.7	6.836
2.03	2089.4	143.1	9.01
4.03	2047.9	159.8	10.12
8.13	2025.4	169	10.73
23.5	1994	181.7	11.58

TABLE 5.5 EFFECT OF TEMPERATURE ON ATTRITION

Total Attrition Time (hr)	Coarse Mass (g)	Sieve Att. Mass (g)	Extent of Attrition (%)
Bredasdorp; $(U-U_{mf})=0.3$ ms^{-1}; H = 0.1 m; Mass=994 g; d_p=300-600 μm; T=298 K			
0	994	0	0
0.25	915.8	58.5	2.0
0.5	836.5	117.8	4.071
1	776.1	163.0	5.676
4.25	746.8	184.9	6.465
14.72	715.8	208.1	7.306
23.45	694.3	223.1	8.018
Bredasdorp; $(U-U_{mf})=0.3$ ms^{-1}; H = 0.1 m; Mass=994 g; d_p=300-600 μm; T=1100 K			
0	incremental sieve		0
0.25	analysis did not		2.44
0.5	apply to this		9.31
1	high temperature		11.05
2	test run		11.87
4			13.0
20.6			18.22

TABLE 5.6 REGRESSION CONSTANTS FOR ATTRITION RATE DATA

Test Conditions	a_0	a_1	a_2	a_3
$(U-U_{mf})=0.2$ms^{-1};H=200;d_p=300-600	2.34	0.049	-2.33	-1.36
$(U-U_{mf})=0.3$ms^{-1};H=100;d_p=300-600	6.29	0.072	-6.43	-1.97
$(U-U_{mf})=0.3$ms^{-1};H=150;d_p=300-600	7.50	0.102	-7.45	-2.25
$(U-U_{mf})=0.3$ms^{-1};H=200;d_p=300-600	8.99	0.119	-8.99	-1.81
$(U-U_{mf})=0.3$ms^{-1};H=100;d_p=850-1180	4.24	0.066	-4.08	-1.49
$(U-U_{mf})=0.3$ms^{-1};H=200;d_p=850-1180	5.24	0.079	-5.07	-1.69
Bredasdorp at T = 1100 K	11.89	0.306	-12.23	-2.06
Lyttelton at T = 298 K	3.40	0.018	-3.39	-0.94
Saldanha at T = 298 K	16.43	0.155	-16.39	-2.08
Marble Hall at T = 298 K	4.89	0.030	-4.82	-1.36
Umzimkulu at T = 298 K	10.04	0.067	-9.99	-1.09

Unless stated otherwise, all tests refer to Bredasdorp limestone at T=298 K

TABLE 5.7 COMPOSITION OF COAL USED IN ELUTRIATION MEASUREMENT

Carbon	70.6 % m/m
Hydrogen	4.2
Ash	13.7
Moisture	1.0
Sulphur	0.7
Nitrogen	1.6
Oxygen	8.2
GCV (MJ/kg)	28.95

TABLE 5.8 MEASURED ELUTRIATION DATA FROM 300 MM COMBUSTOR

Velocity (m/s)	1.0	1.0	1.25	1.25	1.5	1.5	1.75
Total Elutriate ($kg/m^2/s$)	0.0388	0.0387	0.0423	0.0444	0.0421	0.0412	0.0657
Sieve Analysis of Elutriate (%)							
Sieve Aperture (μm)							
10	9.012	6.686	9.09	9.421	7.903	6.223	6.943
20	18.785	20.64	15.403	17.468	13.866	13.21	16.25
38	13.167	14.47	11.282	11.111	10.017	10.4	11.236
53	16.302	16.477	14.64	13.644	13.07	13.377	13.262
75	16.104	16.696	15.343	14.289	14.405	14.571	12.766
106	15.24	14.938	16.477	15.331	15.723	16.425	13.398
150	7.753	7.326	11.738	11.193	12.566	13.372	11.664
212	2.03	1.918	5.477	5.246	9.28	9.243	11.056
300	0.481	0.253	1.344	1.930	2.804	2.487	4.634
500	0.123	0.246	0.168	0.119	0.365	0.348	0.368

TABLE 5.9 ELUTRIATION RATE CONSTANTS

Velocity (m/s)	1.0	1.0	1.25	1.25	1.5	1.5	1.75
Elutriation Constant $kg/m^2/s$							
Sieve Aperture (μm)							
10	1.75	1.29	1.92	2.09	1.67	1.28	2.28
20	2.08	2.28	1.86	2.21	1.67	1.56	3.05
38	2.04	2.24	1.91	1.97	1.69	1.72	2.95
53	2.53	2.55	2.48	2.42	2.20	2.21	3.48
75	1.25	1.29	1.30	1.27	1.21	1.20	1.68
106	1.12	1.16	1.39	1.36	1.33	1.35	1.76
150	0.10	0.09	0.17	0.17	0.18	0.18	0.26
212	0.006	0.005	0.017	0.017	0.028	0.027	0.052
300	0.001	0	0.002	0.002	0.003	0.003	0.008
500	0	0	0	0	0	0	0

TABLE 7.1 COMPOSITION OF GREENSIDE DISCARD COAL

Carbon	34 - 36 % m/m
Hydrogen	2 - 2.5
Ash	45 - 52
Moisture	1.9 - 2.1
Sulphur	2.6 - 3.3
Nitrogen	0.7 - 0.8
Oxygen	6 - 9
GCV (MJ/kg)	13 - 16

TABLE 7.4 CALCULATION OF K VALUES FROM ZHENG'S MODEL

Test	C	H	N	O	S	xs O_2	xs AIR	K
SCBL1	0.407	0.026	0.01	0.05	0.0324	0.057	0.342	2.293
SCBL2	0.399	0.023	0.01	0.06	0.0272	0.061	0.372	1.967
SCBL4	0.385	0.024	0.01	0.07	0.0274	0.067	0.438	1.821
SCBL5	0.39	0.024	0.01	0.06	0.0232	0.045	0.254	1.898
SCBL6	0.397	0.027	0.01	0.04	0.0268	0.054	0.327	1.909
SCLD1	0.414	0.026	0.01	0.05	0.0319	0.061	0.386	0.168
SCUL1	0.388	0.024	0.01	0.05	0.0285	0.062	0.392	0.723
SCUL2	0.386	0.024	0.01	0.05	0.0293	0.075	0.524	0.689
SCUL3	0.387	0.024	0.01	0.06	0.0295	0.069	0.458	0.721
SCUL4	0.372	0.023	0.01	0.06	0.03	0.045	0.253	0.897
SCUL5	0.369	0.023	0.01	0.06	0.0263	0.056	0.334	0.777
SCUL6	0.391	0.025	0.01	0.05	0.0263	0.06	0.381	0.656

TABLE 7.2 TEST CONDITIONS FOR 10 MW_{TH} FBC UNIT

Test	Coal (kg/hr)	Air (kg/hr)	Sorbent (kg/hr)	T (K)	U (m/s)	O_2 (%)	Carbon in ash	Comb. eff.	%S coal	Base SO_2 (ppm)	SO_2[1] (ppm)	Cyclone (kg/hr)	Filter (kg/hr)	Overflow (kg/hr)
SCBL1	1556	8773	200	1103	1.08	5.7	0.115	87.9	3.24	4206	3558	593	280	246
SCBL2	1610	10484		1108	1.43	6.1	0.114	87.4	2.72	3626	2823	865	224	258
SCBL4	1380	7220		1183	0.94	6.7	0.097	88.6	2.74	3540		365	165	167
SCBL5	1540	6500		1093	0.79	4.5	0.102	88.8	2.32	3423		395	160	303
SCBL6	1556	7256		1128	0.91	5.4	0.084	90.8	2.68	3495		454	166	394
SCLD1	1633	8239	748	1093	0.99	6.1	0.085	91.5	3.19	3843		484	173	519
SCUL1	1386	7201		1143	1.01	6.2	0.086	90.4	2.85	3681	2486	315	171	210
SCUL2	1397	9698		1137	1.33	7.5	0.08	91	2.93	3468	2472	416	227	164
SCUL3	2000	10893		1142	1.51	6.9	0.093	89.5	2.95	3685	2742	657	292	150
SCUL4	1500	6296		1134	0.79	4.5	0.089	89.2	3	4602	3600	380	147	266
SCUL5	1870	8854		1093	0.98	5.6	0.099	87.9	2.63	3867		561	223	297
SCUL6	1552	7503		1163	1.1	6	0.08	91	2.63	3386		426	164	124

TABLE 7.3 STEADY STATE SO2 EMISSIONS AS A FUNCTION OF SORBENT FEED RATE

Test	F_o (kg/hr)	$[SO_2]$ (ppm)	R_{Ca}	%red
SCBL1	0	3558	0	0
	56.7	2615	0.242	26.5
	152	1575	0.647	55.7
	231.8	1249	0.986	64.9
	309.8	1108	1.318	68.9
SCBL2	0	2823	0	0
	56.6	2361	0.229	16.4
	160.2	1825	0.649	35.4
	246.5	1301	1.0	53.9
	327.6	921	1.33	67.4
SCBL4	0	3136	0	0
	74.4	2848	0.421	9.2
	224.5	1977	1.273	37.0
	467.9	841	2.654	73.2
	546.7	616	3.1	80.4
	595.6	423	3.378	86.5
SCBL5	0	2503	0	0
	92.3	1300	0.488	48.1
	160.2	898	0.918	64.1
	246.6	580	1.408	76.8
	328.1	245	1.925	90.2
	459.9	106	2.699	95.7
SCBL6	0	3092	0	0
	64.3	1690	0.331	45.3
	75.4	1663	0.388	46.2
	152.2	1378	0.783	55.4
	233.3	928	1.2	70.0
	310.2	768	1.595	75.2
	386.3	645	1.987	79.1
	562.2	258	2.891	91.7
SCLD1	0	2050	0	0
	506.7	1050	1.703	48.8
	510.3	1038	1.715	49.4
	763.9	808	2.402	60.6
	1021.2	526	3.268	74.3

TABLE 7.3 CONTINUED

SCUL1	0	2486	0	0
	60.6	2255	0.358	9.3
	126.2	2015	0.714	18.9
	192.7	1673	1.156	32.7
SCUL2	0	2472	0	0
	133.4	1740	0.724	29.6
	203.7	1474	1.102	40.4
	260.9	1143	1.411	53.8
	395.2	901	2.137	63.6
SCUL3	0	2742	0	0
	111.4	2436	0.414	11.2
	223	2100	0.828	23.4
	341.2	1855	1.267	32.3
	455.1	1585	1.691	42.2
	564.3	1216	2.096	55.7
SCUL4	0	3600	0	0
	72.8	2991	0.378	16.9
	145.7	2560	0.756	28.9
	330	1520	1.712	57.8
	396	1150	2.054	68.1
	473	998	2.454	72.3
	573.1	921	2.973	74.4
SCUL5	0	3048	0	0
	105.3	2310	0.481	24.2
	207.9	1714	0.923	43.8
	305.5	1252	1.412	58.9
	504.7	753	2.333	75.3
	730.8	483	3.328	84.2
	784.9	434	3.575	85.8
SCUL6	0	2720	0	0
	81.2	2243	0.444	17.5
	163.9	1918	0.955	29.5
	258.5	1600	1.485	41.2
	338.7	1384	1.88	49.1
	430	1200	2.33	55.9
	714.4	693	3.783	74.5

TABLE G.3

$U = 1\ ms^{-1}$; $R_{ss} = 5\%/hr$; $T = 1123\ K$; $R_{os} = 2$

Sieve Size	Avg r(μm)	K*	dr/dt	Term 1	Term 2	Term 3	Term 4	Term 5	Term 6	$p_i(r)dr_i$	$\tau(r_i)$ (hr)
1000											
500	375	6.6e-14	-6.25	58550	0	-14872	27875	0	-29745	0.8077	21.34
300	200	6.6e-5	-3.33	0	-4804	-7932	11150	15.77	-11898	0.1550	21.31
212	128	0.0178	-2.13	0	-541	-5076	4906	1863	-5235	0.0316	15.47
150	90.5	0.1452	-1.51	0	-113.3	-3589	3456	10710	-3688	0.0052	5.21
106	64	0.4387	-1.07	0	-13.5	-2538	2453	22967	-2617	0.0004	2.06
75	45.3	0.7766	-0.75	0	-0.78	-1794	1728	28643	-1844	0.	1.21
53	32	1.0311	-0.53	0	-0.03	-1269	1226	26990	-1308	0.	0.93

$F_o = 234.2$ kg/hr $\Sigma\ p_i(r_i)\ dr_i = 1$
$F_1 = 111.5$ kg/hr $d_{p\ mean} = 616\ \mu m$
$F_2 = 3.8$ kg/hr

TABLE G.4

$U = 1\ ms^{-1}$; $R_{ss} = 5\%/hr$; $T = 1123\ K$; $R_{os} = 4$

Sieve Size	Avg r(μm)	K*	dr/dt	Term 1	Term 2	Term 3	Term 4	Term 5	Term 6	$p_i(r)dr_i$	$\tau(r_i)$ (hr)
1000											
500	375	6.6e-14	-6.25	117100	0	-24027	68025	0	-48054	0.8358	14.12
300	200	6.6e-5	-3.33	0	-8032	-12814	27210	25.48	-19221	0.1355	14.11
212	128	0.0178	-2.13	0	-764	-8201	11972	3009	-8457	0.0242	11.29
150	90.5	0.1452	-1.51	0	-139.5	-5798	8435	17304	-5958	0.0037	4.63
106	64	0.4387	-1.07	0	-15.3	-4100	5986	37104	-4228	0.0003	1.96
75	45.3	0.7766	-0.75	0	-0.86	-2899	4217	46276	-2979	0.	1.18
53	32	1.0311	-0.53	0	-0.03	-2050	2993	43604	-2114	0.	0.91

$F_o = 468.4$ kg/hr $\Sigma\ p_i(r_i)\ dr_i = 1$
$F_1 = 272.1$ kg/hr $d_{p\ mean} = 637\ \mu m$
$F_2 = 4.2$ kg/hr

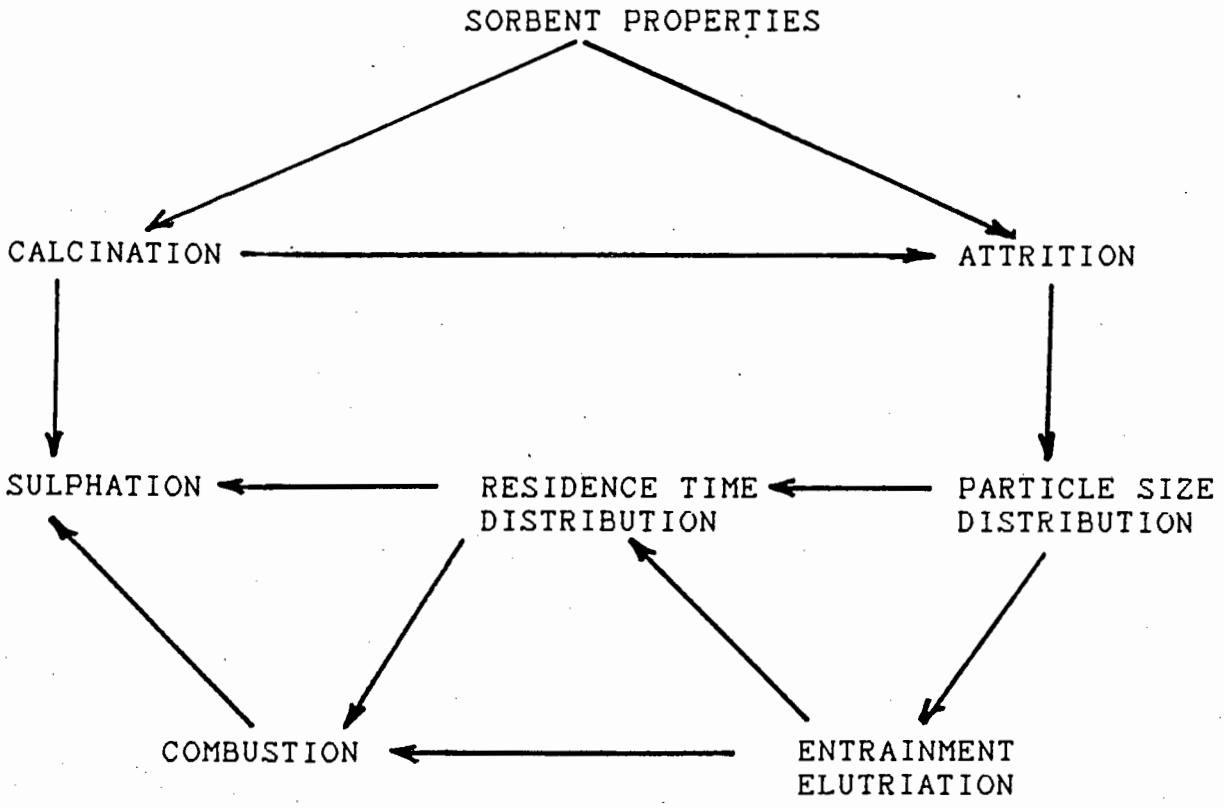

FIGURE 1.1 CONCEPTUAL MODEL FOR FBC SULPHUR CAPTURE

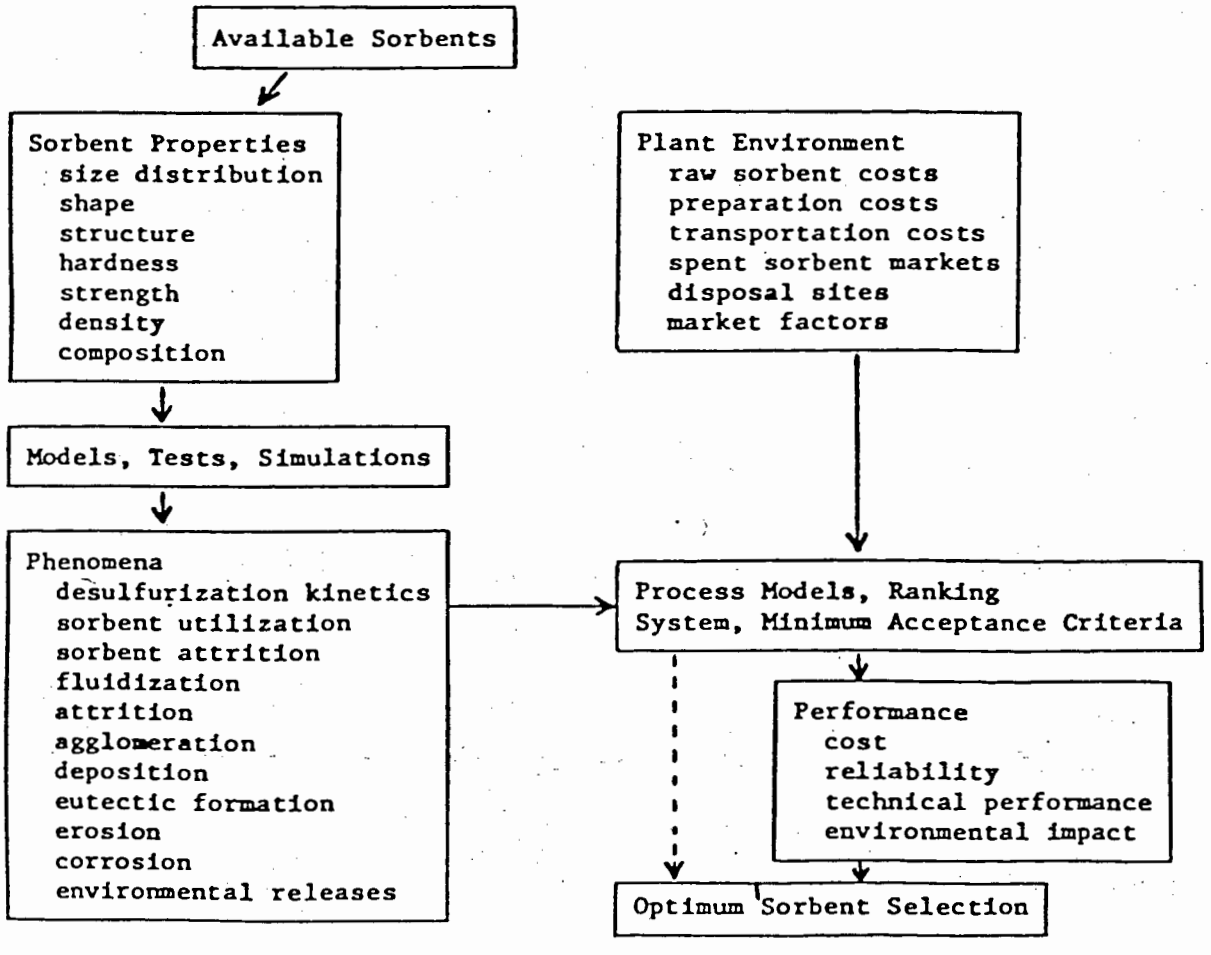

FIGURE 1.2 SORBENT SELECTION PROCESS LINE DIAGRAM

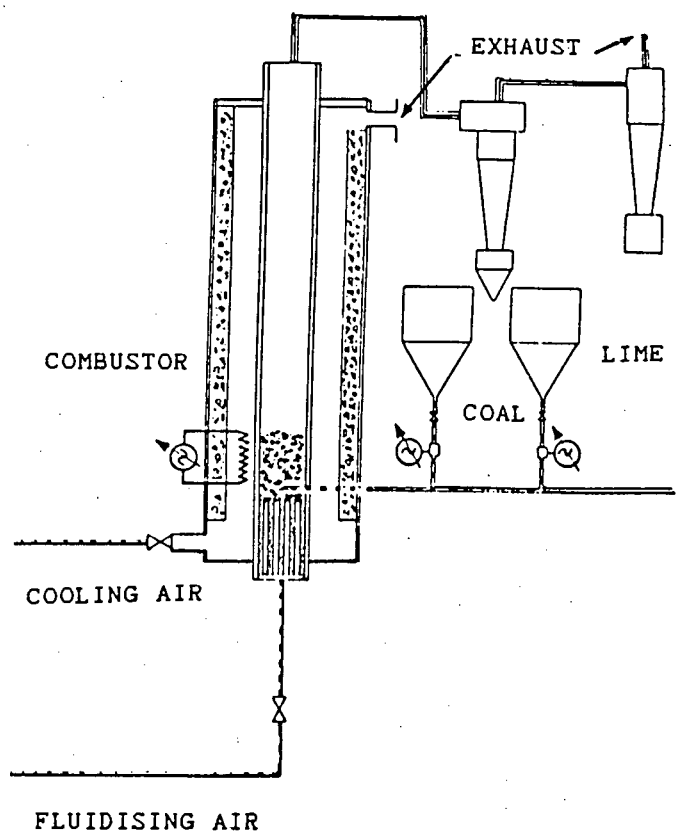

FIGURE 3.1 SCHEMATIC LAYOUT OF 100 mm COMBUSTOR

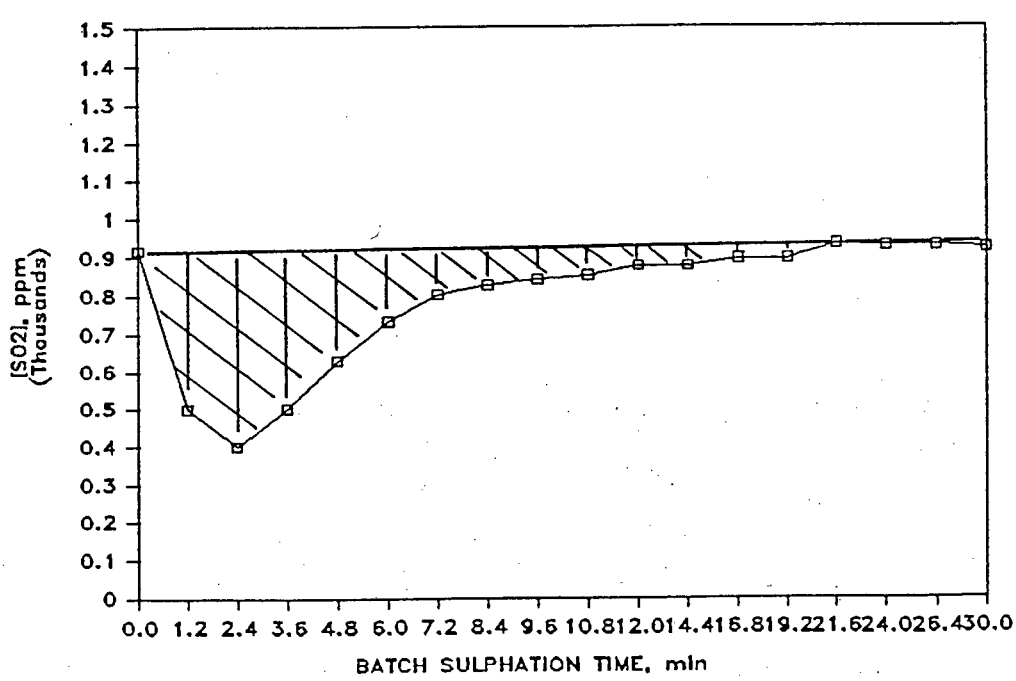

FIGURE 3.2 FLUE GAS SO2 RESPONSE TO SORBENT ADDITION

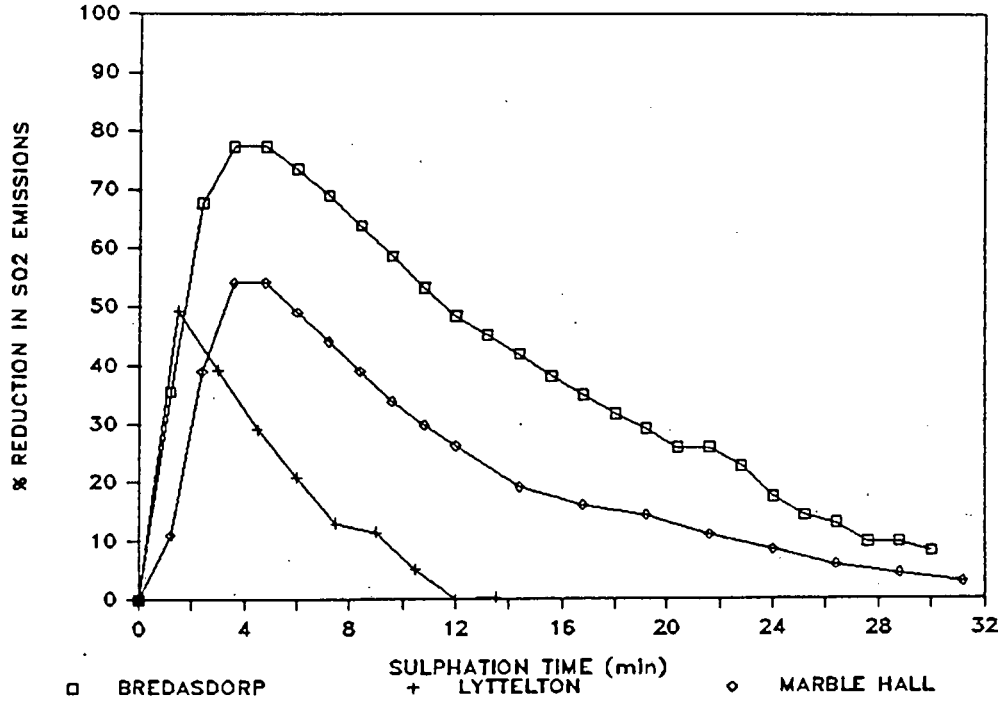

FIGURE 3.3 COMPARISON OF SORBENT EFFECTS ON REDUCTION IN SO2 EMISSIONS

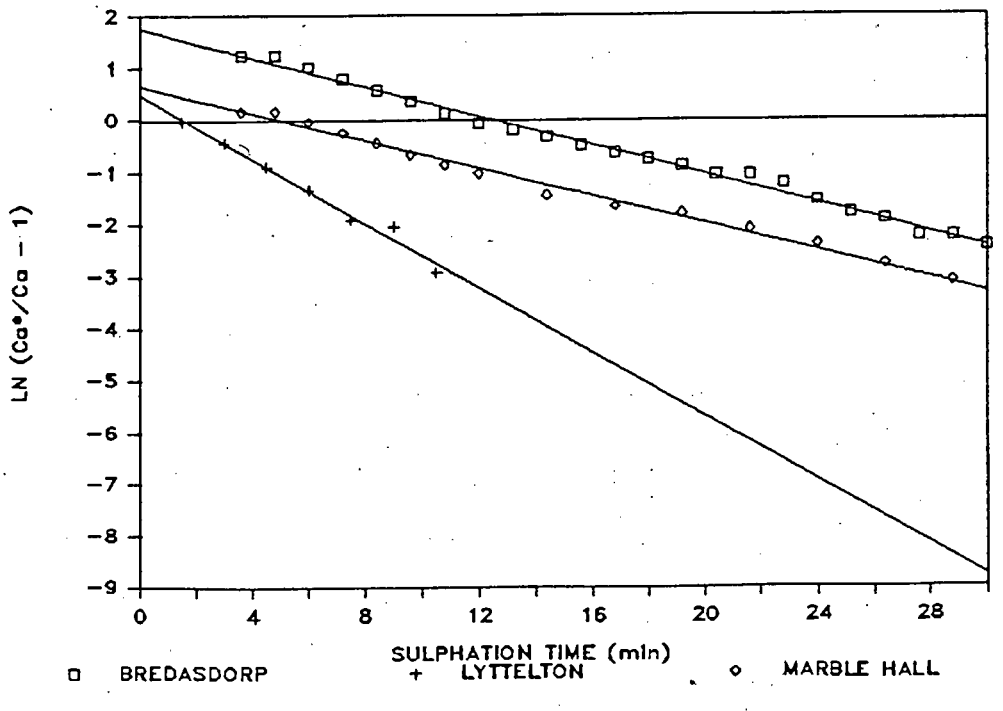

FIGURE 3.4 LINEARISED SULPHATION RATES FOR THREE SORBENTS

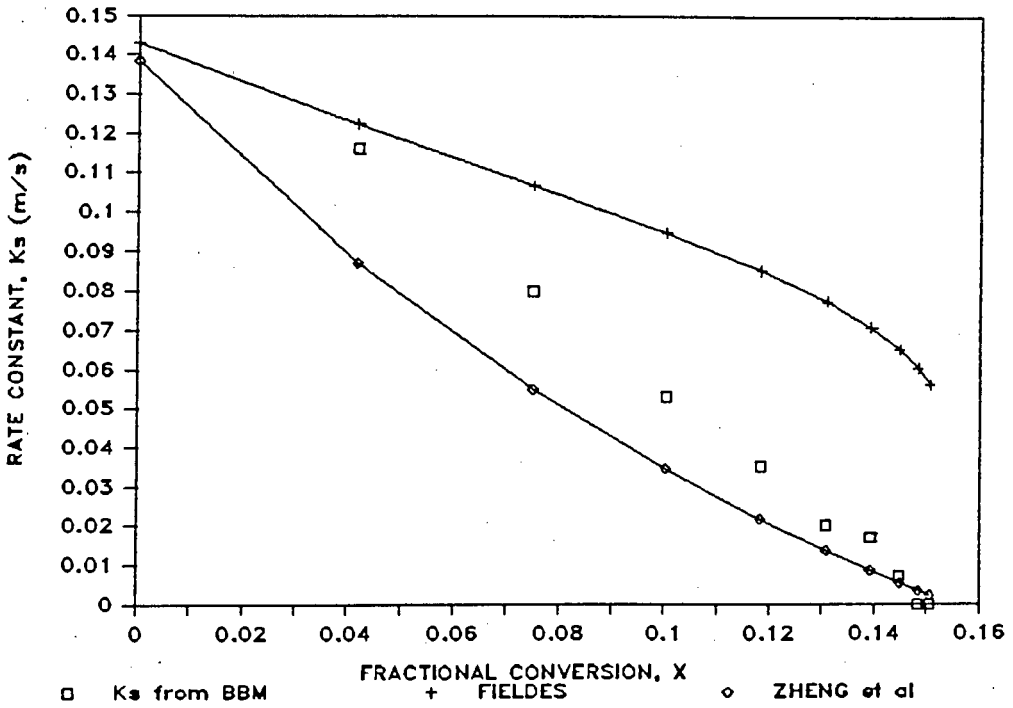

FIGURE 3.5 COMPARISON OF MODELS OF FIELDES AND ZHENG FOR SULPHATION OF LYTTELTON DOLOMITE

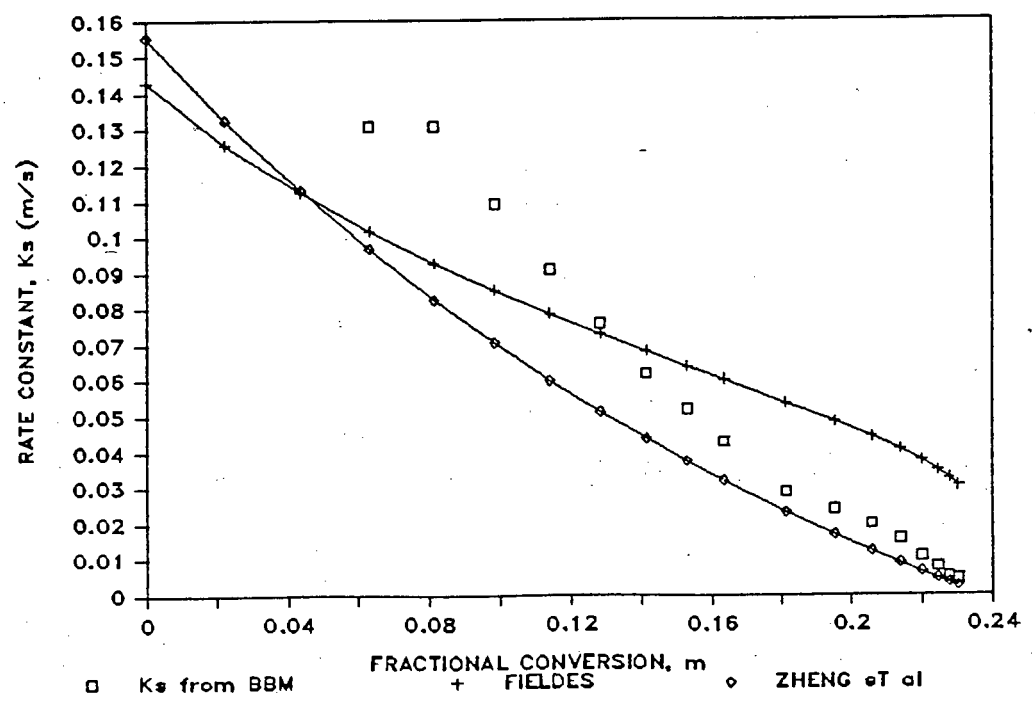

FIGURE 3.6 COMPARISON OF MODELS OF FIELDES AND ZHENG FOR SULPHATION OF MARBLE HALL LIMESTONE

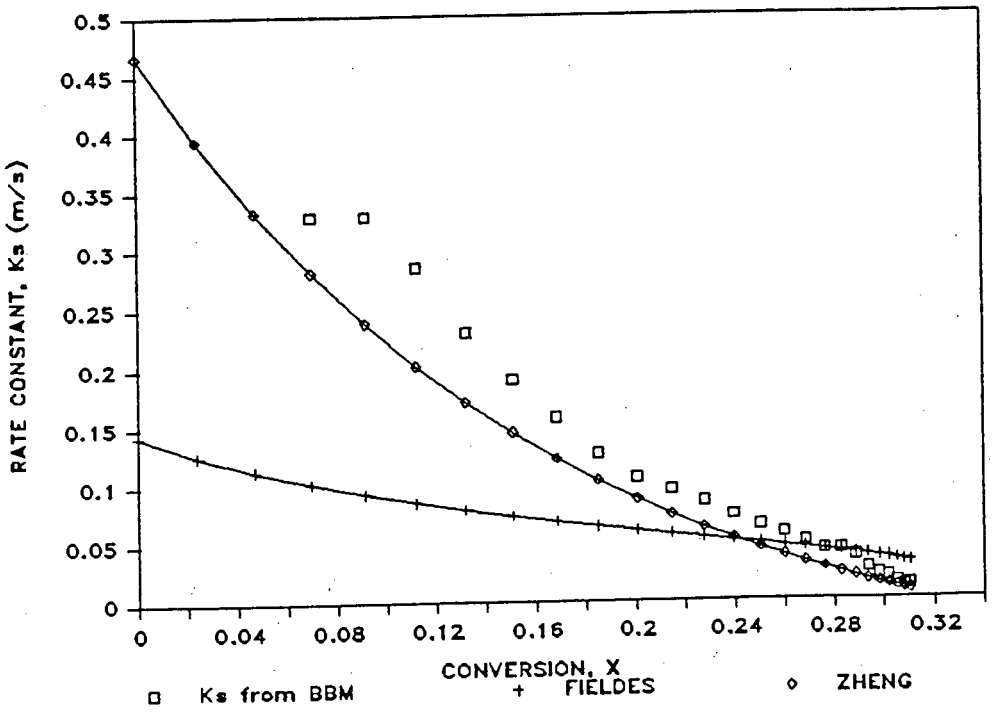

FIGURE 3.7 COMPARISON OF MODELS OF FIELDES AND ZHENG FOR SULPHATION OF BREDASDORP LIMESTONE

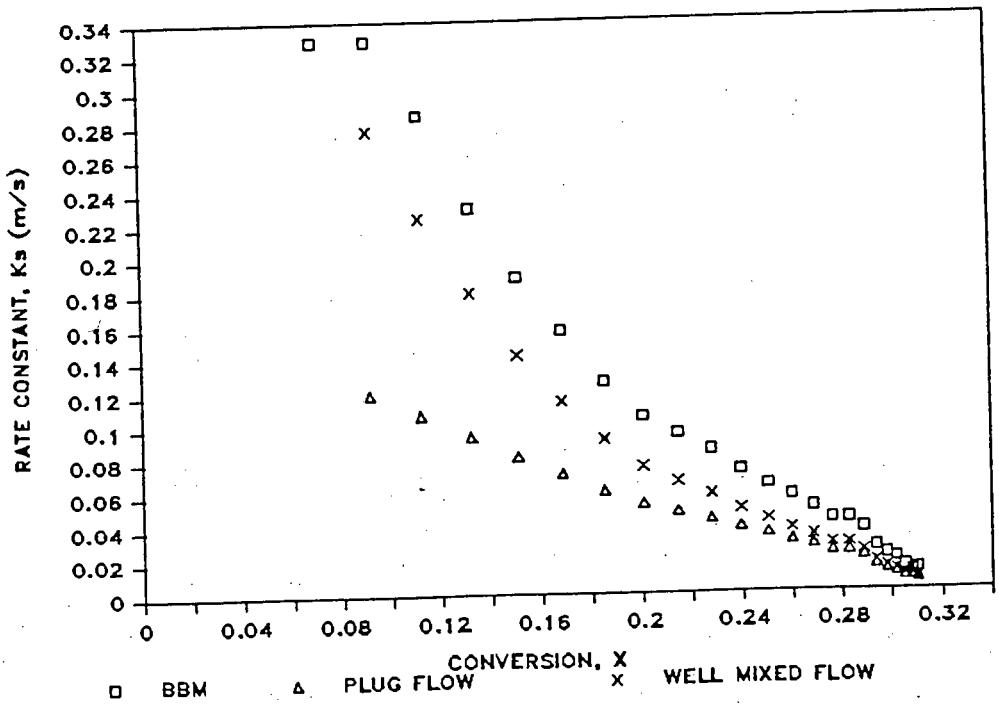

FIGURE 3.8 COMPARISON OF GAS FLOW MODELS FOR SULPHATION OF BREDASDORP LIMESTONE

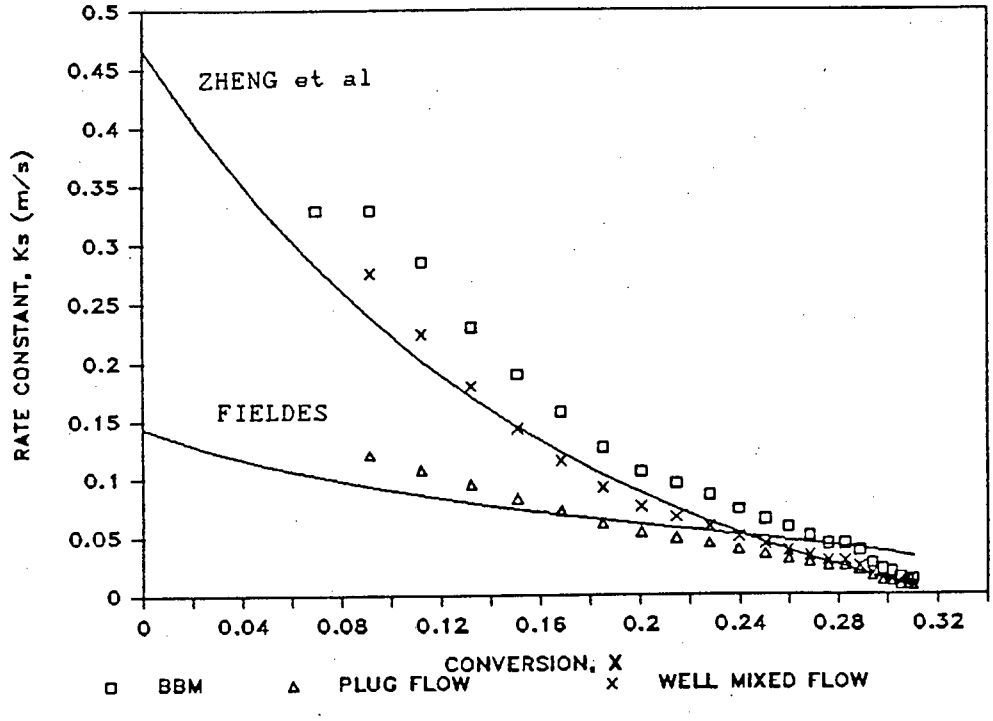

FIGURE 3.9 COMPARISON OF FIELDES AND ZHENG MODELS WITH SINGLE PHASE GAS MODELS FOR SULPHATION OF BREDASDORP LIMESTONE

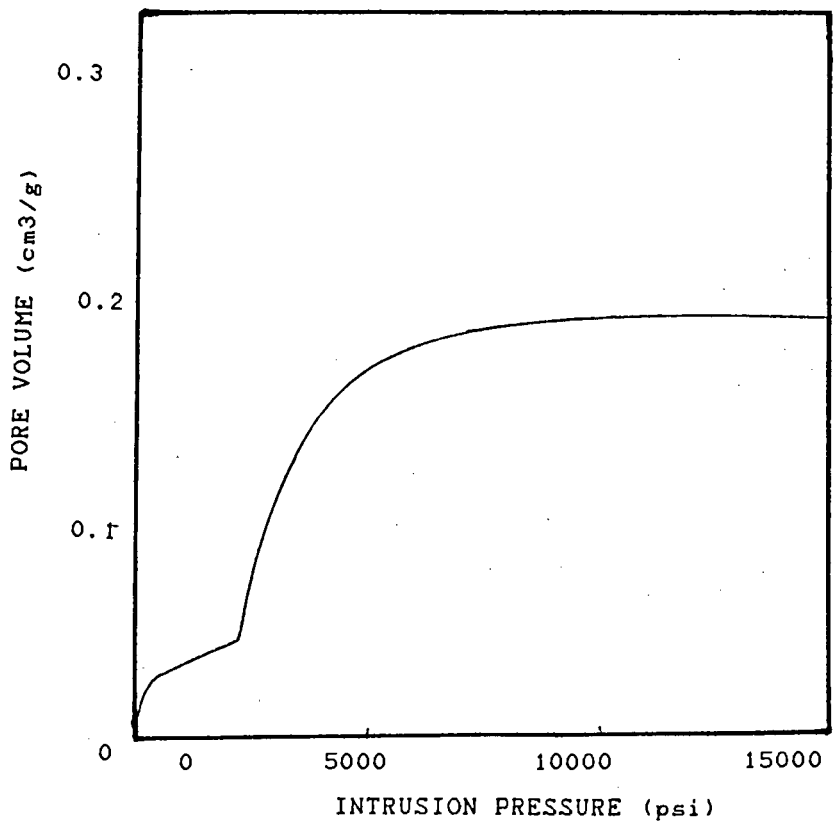

FIGURE 4.1 Hg INTRUSION CURVE FOR BREDASDORP

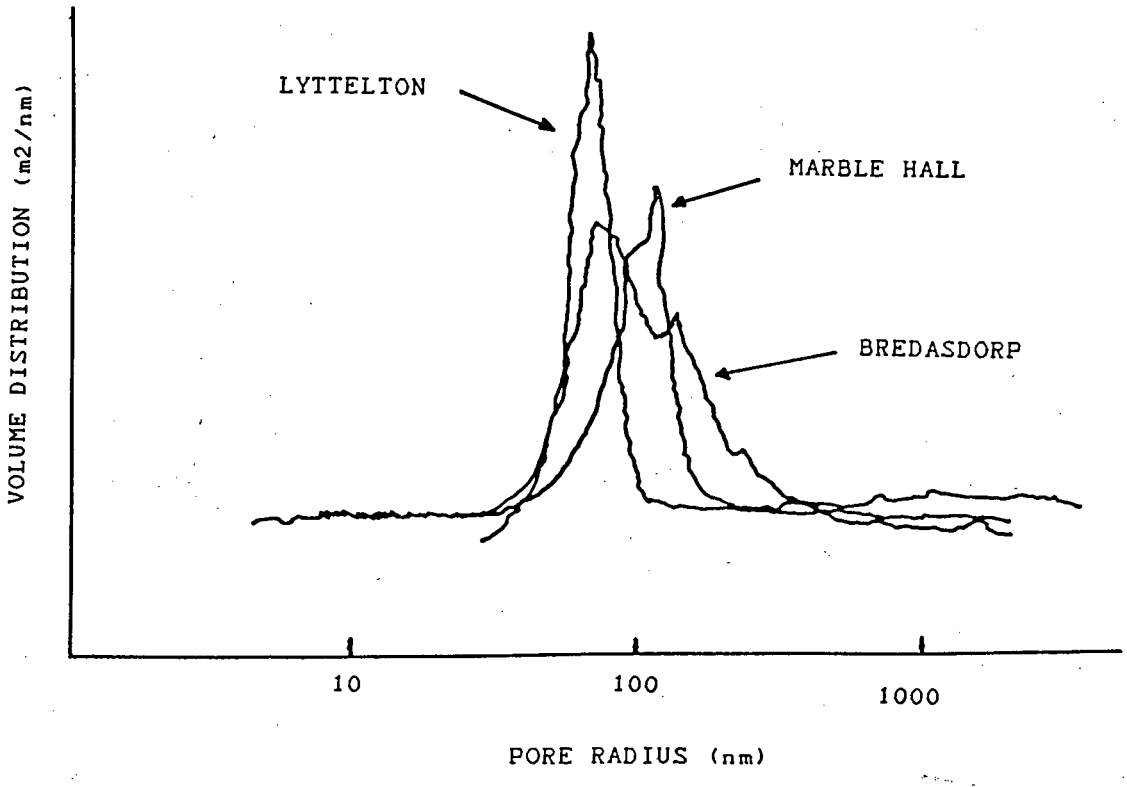

FIGURE 4.2 PORE SIZE DISTRIBUTIONS OF THREE SOUTH AFRICAN SORBENTS

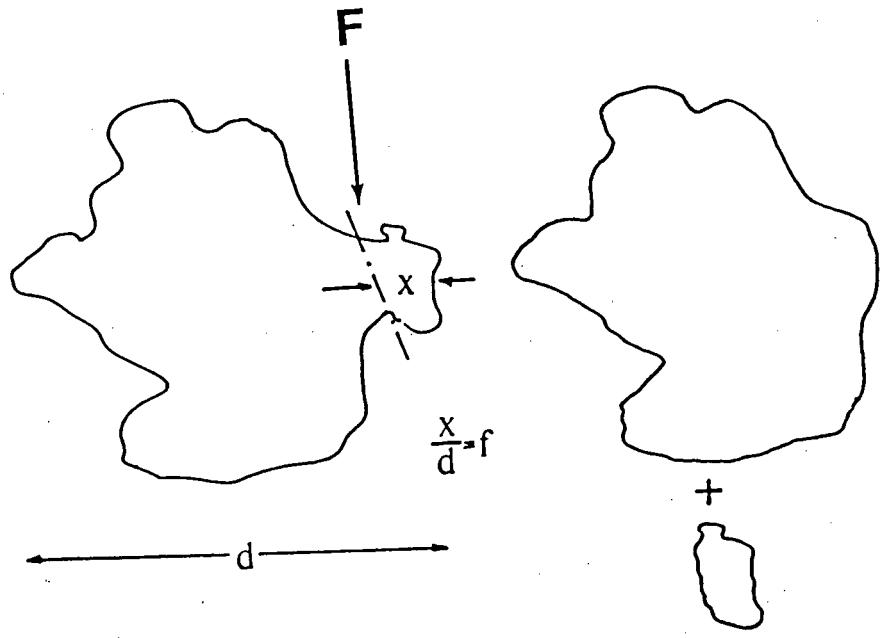

FIGURE 4.3 CONCEPTUAL MODEL OF SORBENT PARTICLE FAILURE

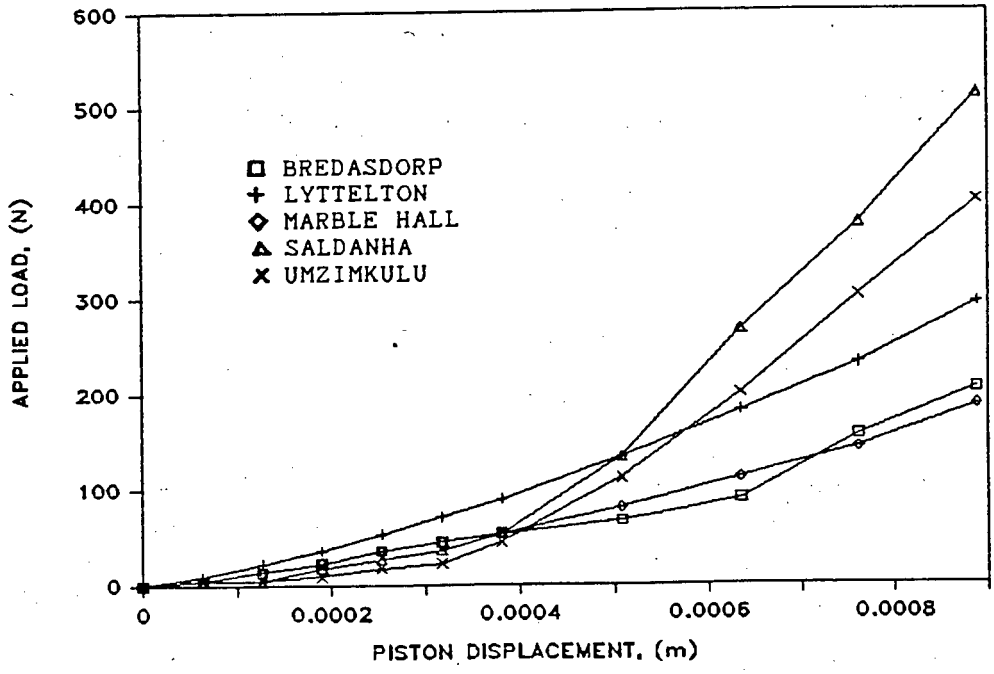

FIGURE 4.4 LOAD DEFORMATION OF SORBENT PARTICLES IN CLOSED PACKING

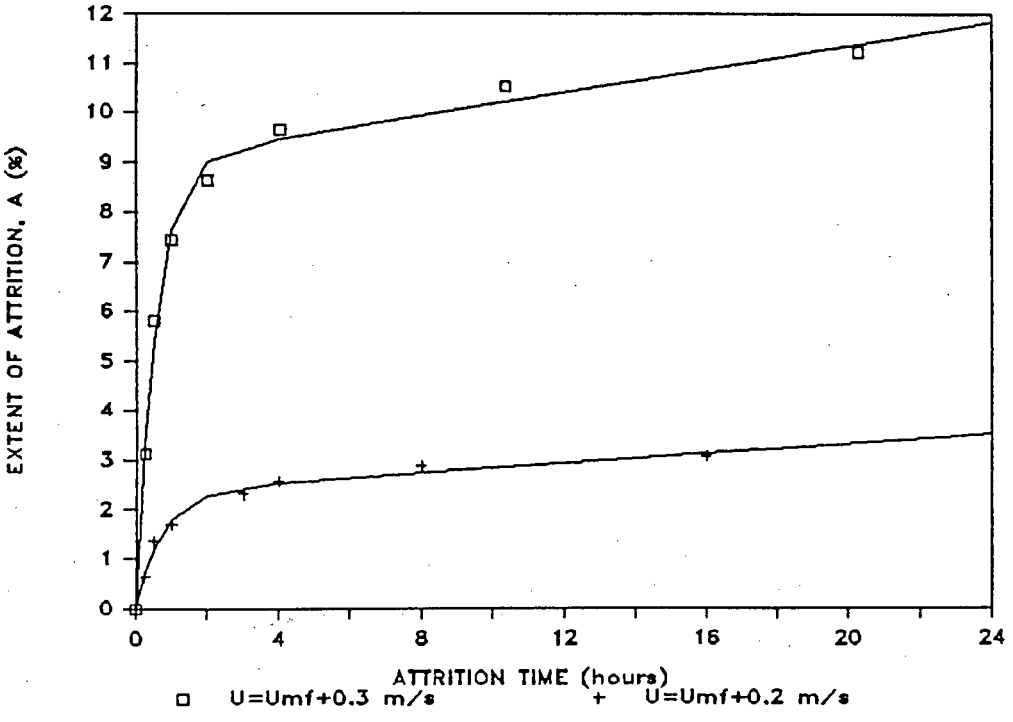

FIGURE 5.1 EFFECT OF FLUIDISING VELOCITY ON ATTRITION EXTENT

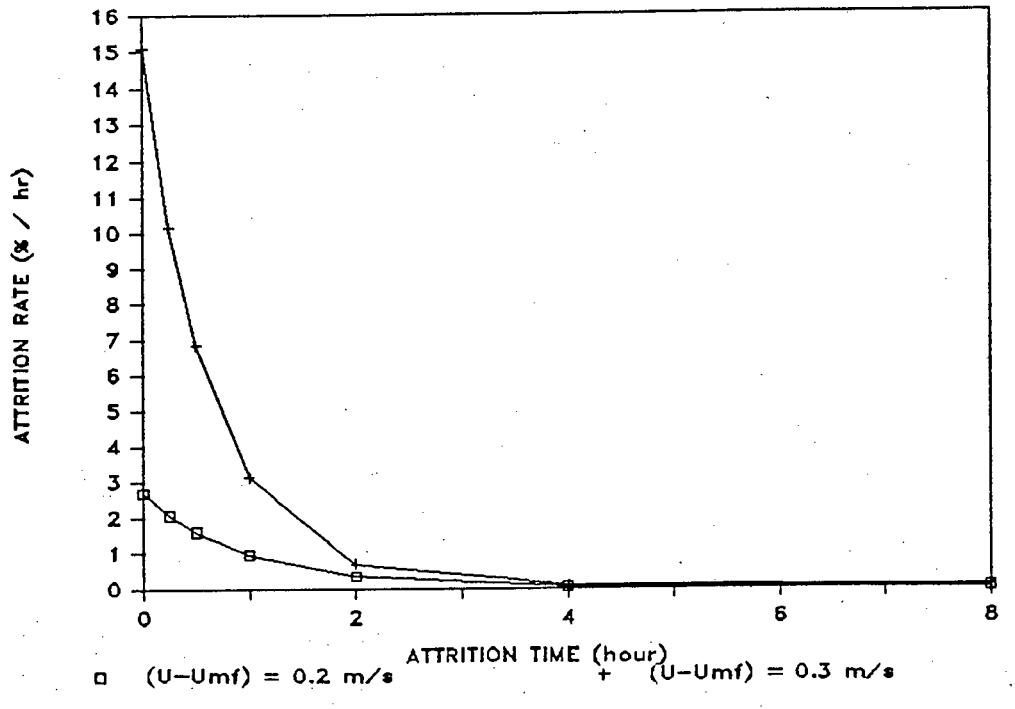

FIGURE 5.2 EFFECT OF FLUIDISING VELOCITY ON ATTRITION RATE

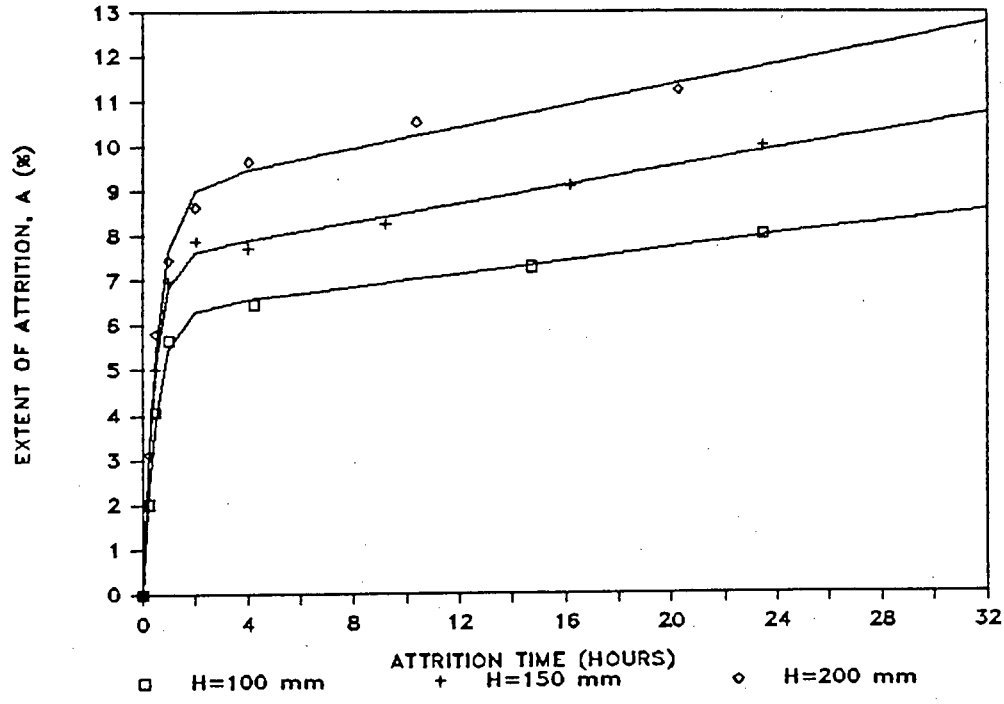

FIGURE 5.3 EFFECT OF BED HEIGHT ON ATTRITION EXTENT

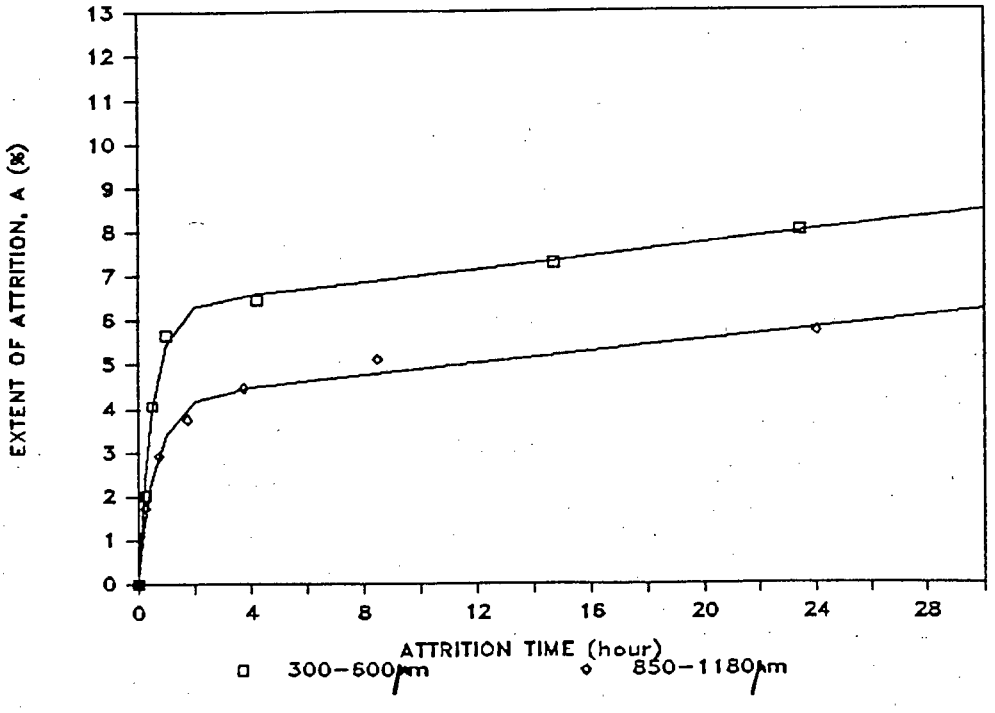

FIGURE 5.4 EFFECT OF PARTICLE SIZE ON ATTRITION EXTENT
FOR BED HEIGHT = 100 mm

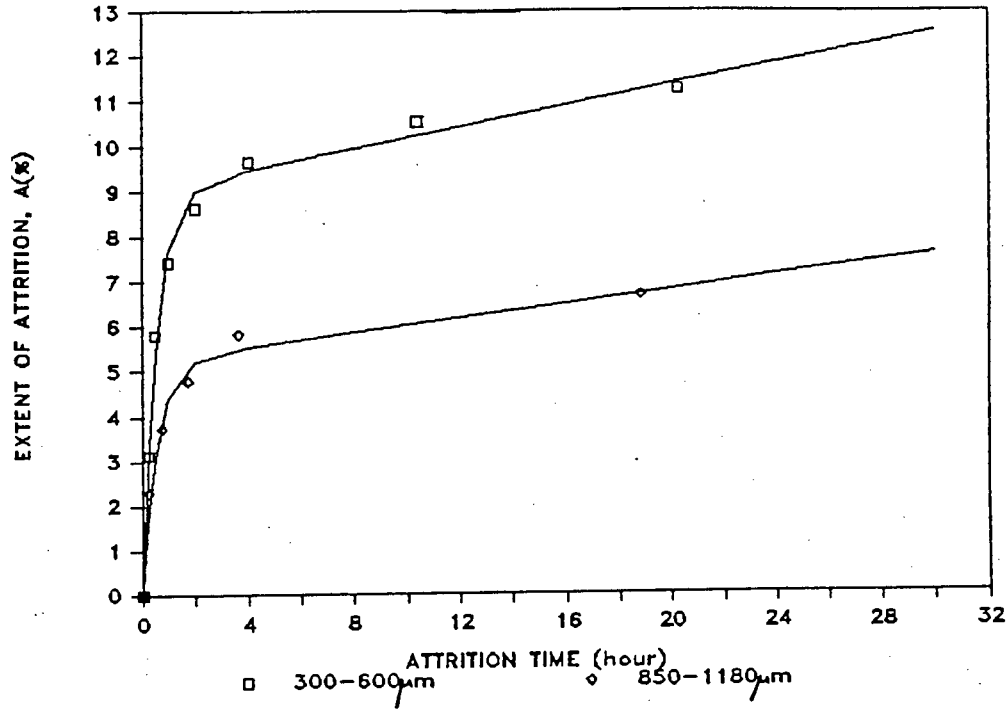

FIGURE 5.5 EFFECT OF PARTICLE SIZE ON ATTRITION EXTENT FOR BED HEIGHT = 200 mm

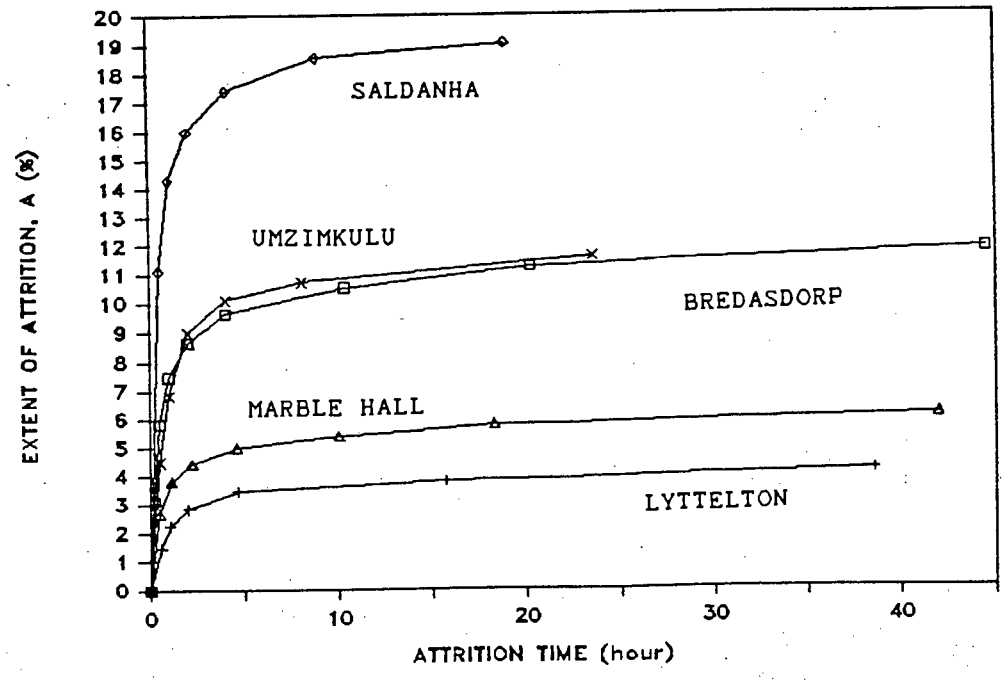

FIGURE 5.6 EFFECT OF SORBENT TYPE ON ATTRITION EXTENT

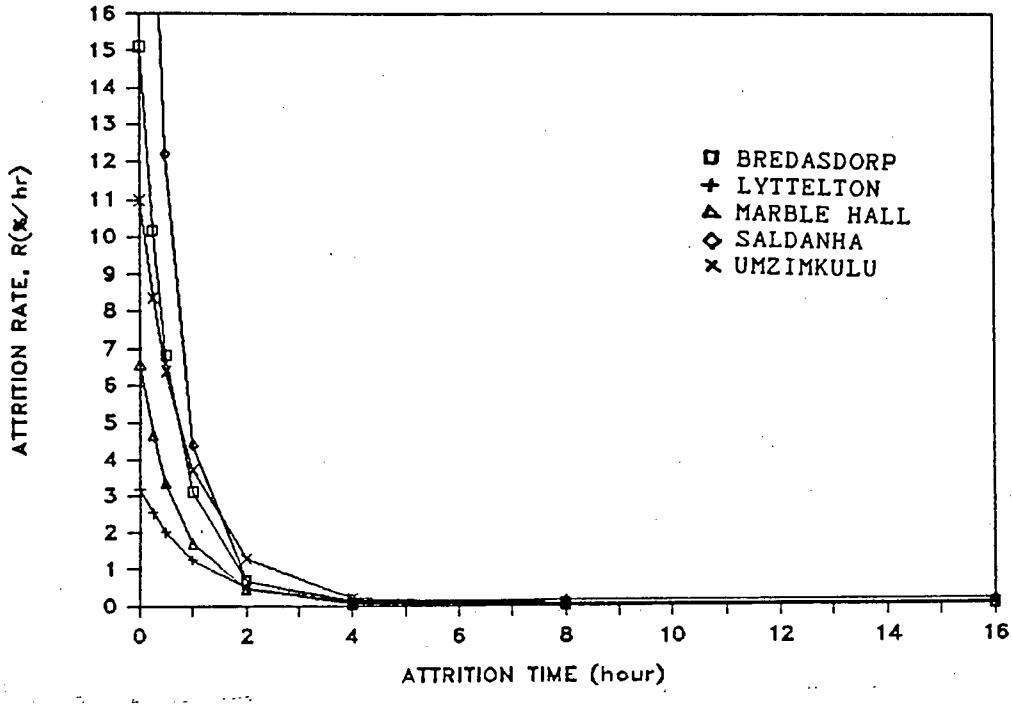

FIGURE 5.7 EFFECT OF SORBENT TYPE ON ATTRITION RATE

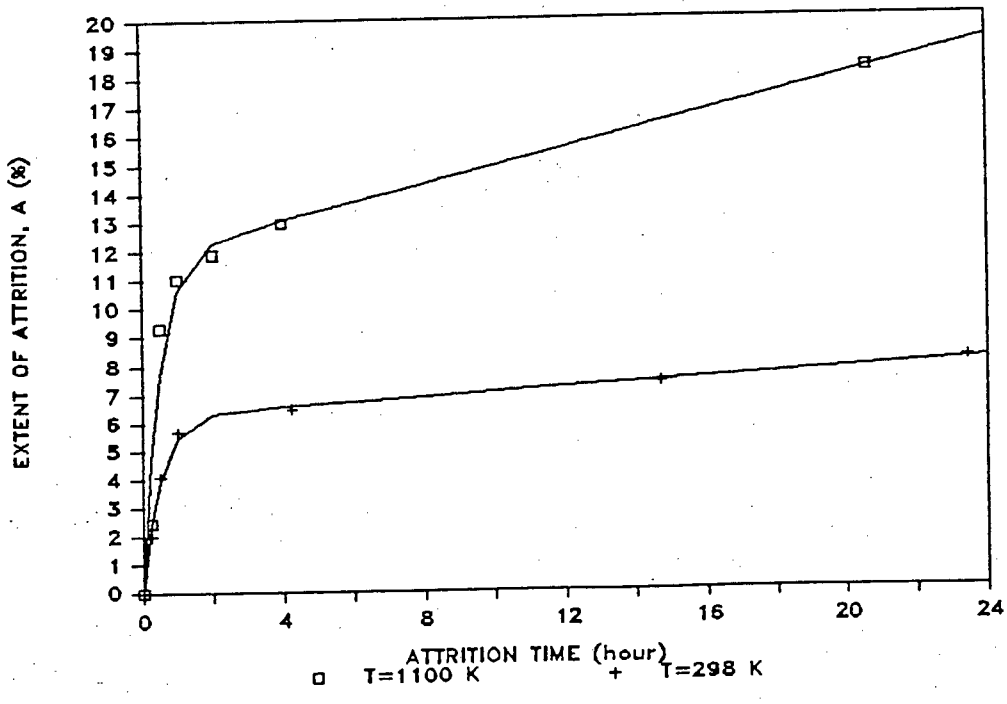

FIGURE 5.8 EFFECT OF TEMPERATURE ON ATTRITION EXTENT

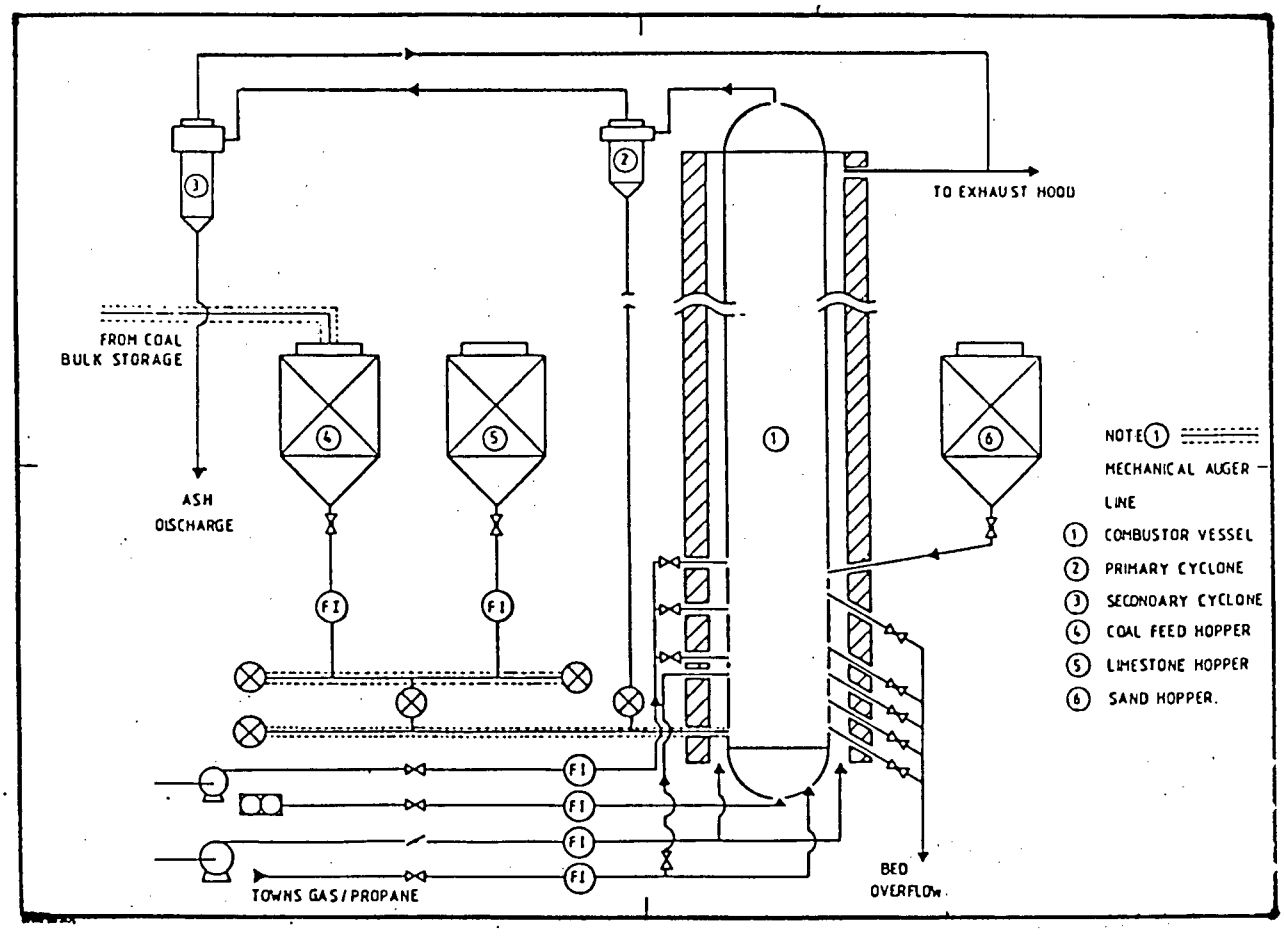

FIGURE 5.9 SCHEMATIC OF 300 mm FBC UNIT

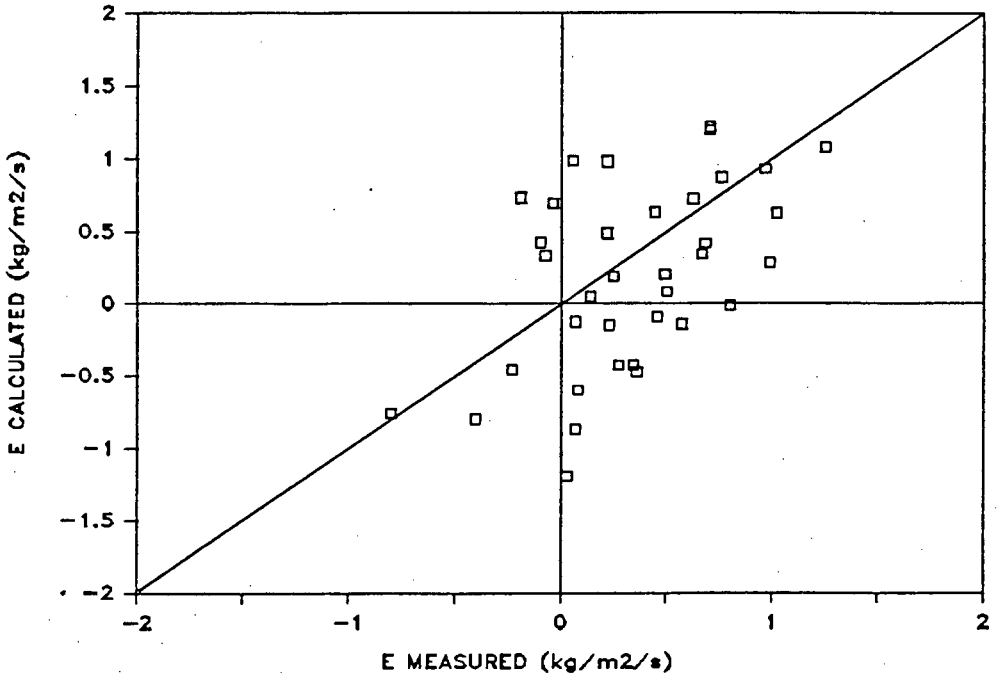

FIGURE 5.10 VALIDITY OF WEN AND CHEN ELUTRIATION MODEL

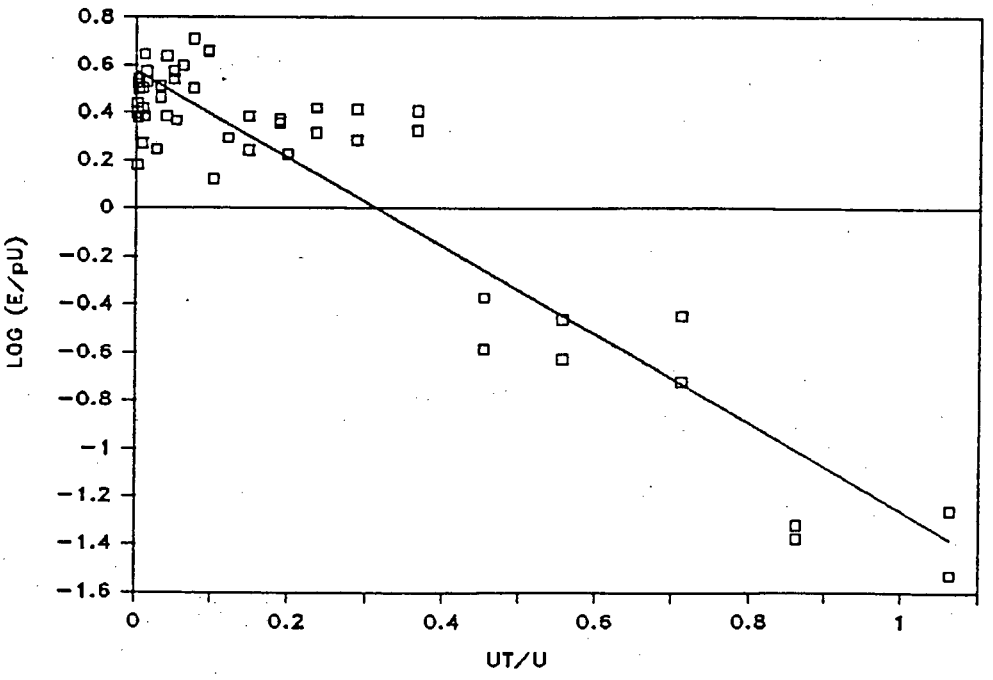

FIGURE 5.11 VALIDITY OF GELDART ELUTRIATION MODEL

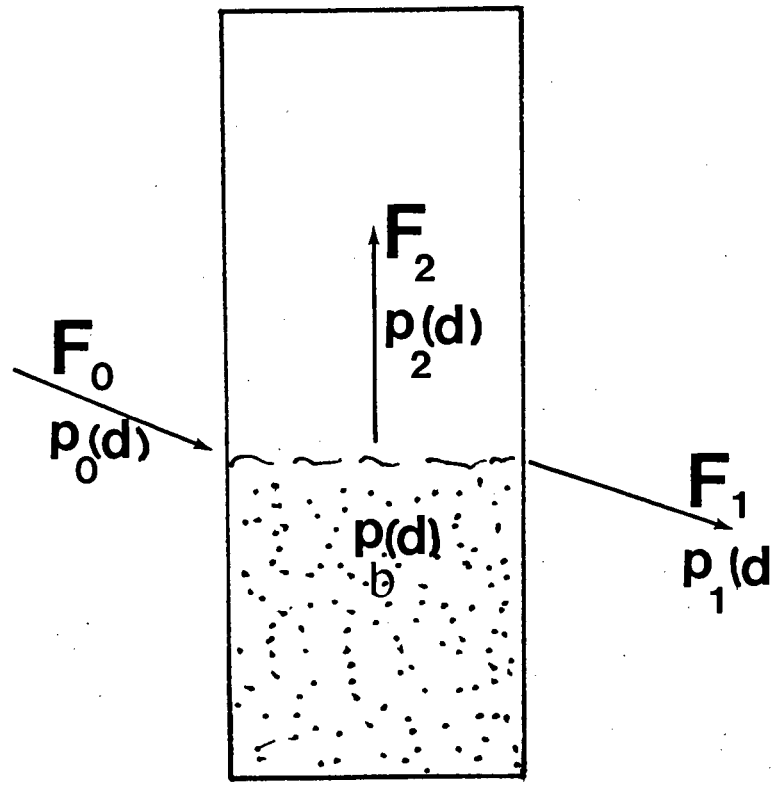

FIGURE 6.1 PROCESS FLOW DIAGRAM FOR COMBUSTOR

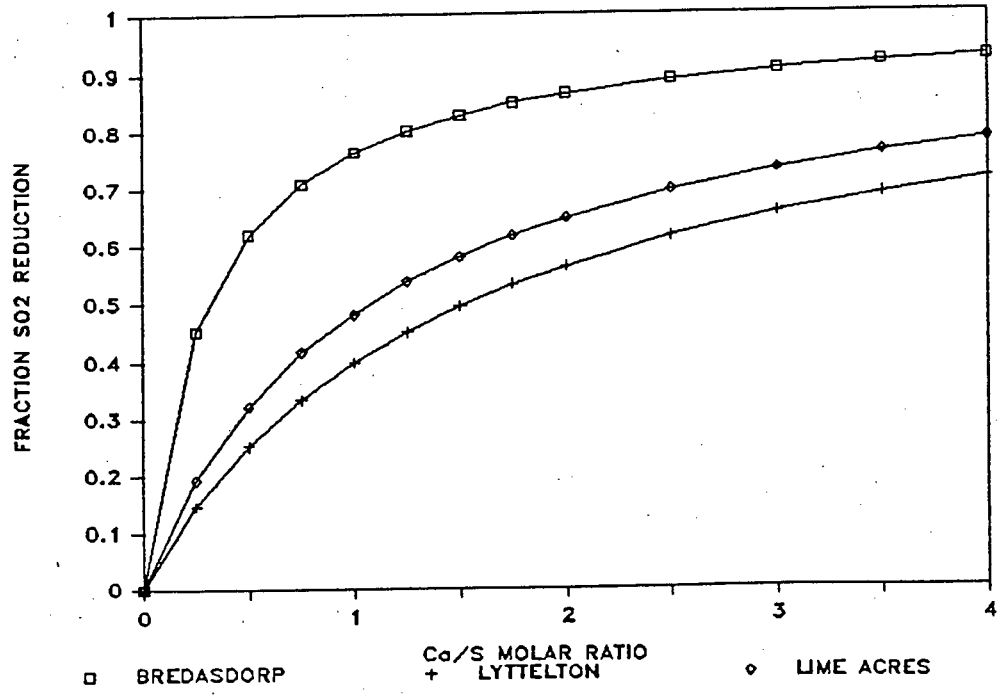

FIGURE 6.2 MODEL PREDICTION OF EFFECT OF SORBENT TYPE ON SO2 CAPTURE

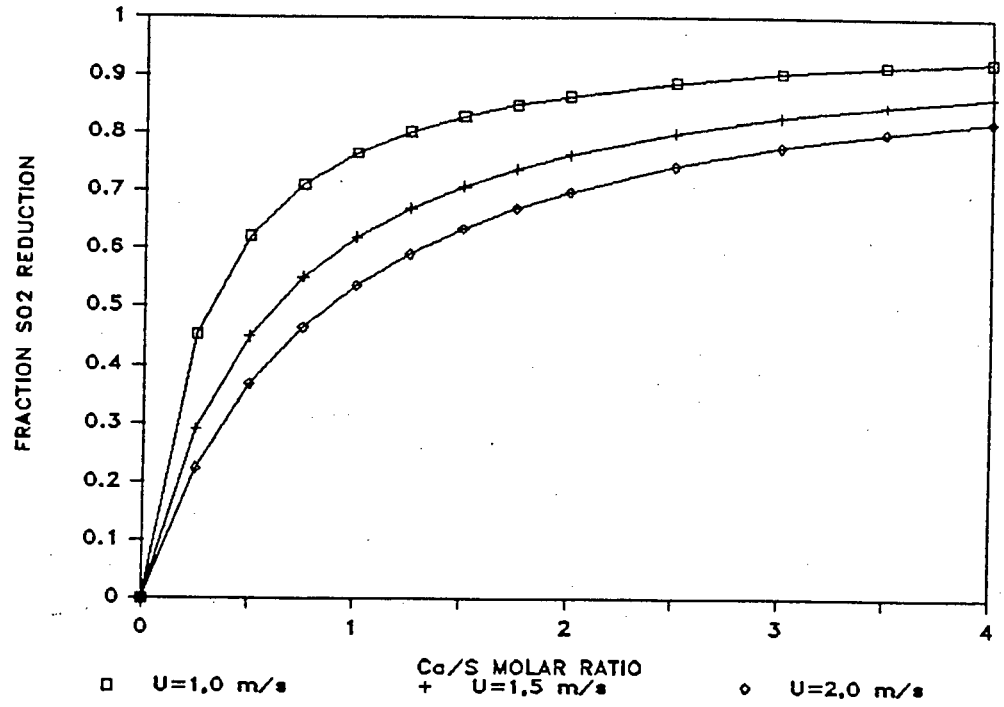

FIGURE 6.3 MODEL PREDICTION OF EFFECT OF FLUIDISING VELOCITY ON SO2 CAPTURE

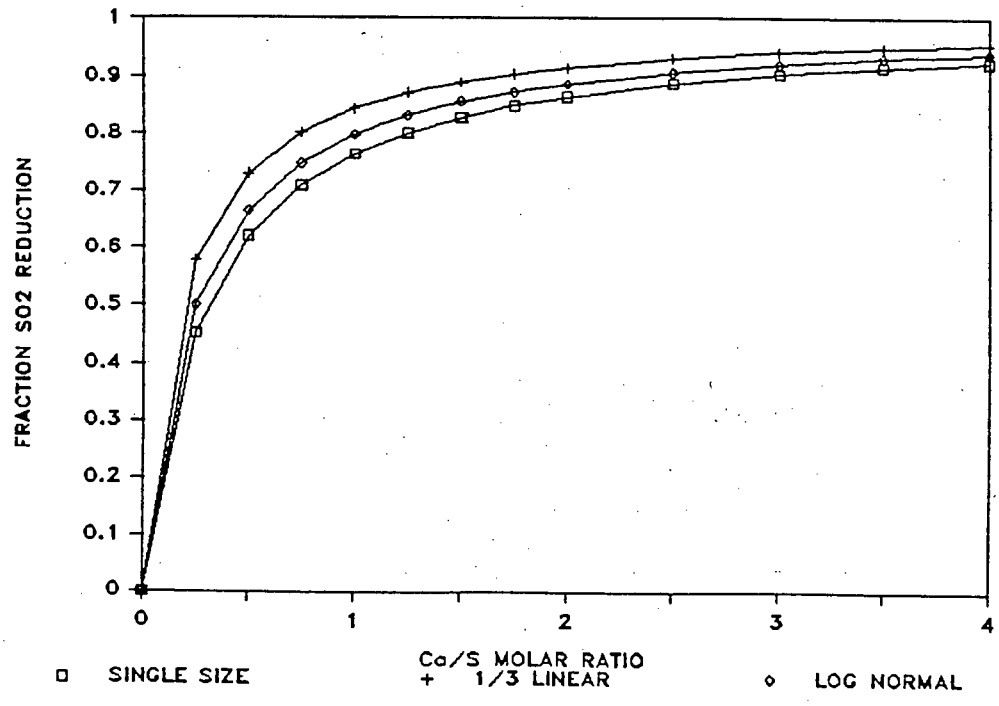

FIGURE 6.4 MODEL PREDICTION OF EFFECT OF SORBENT FEED DISTRIBUTION ON SO2 CAPTURE

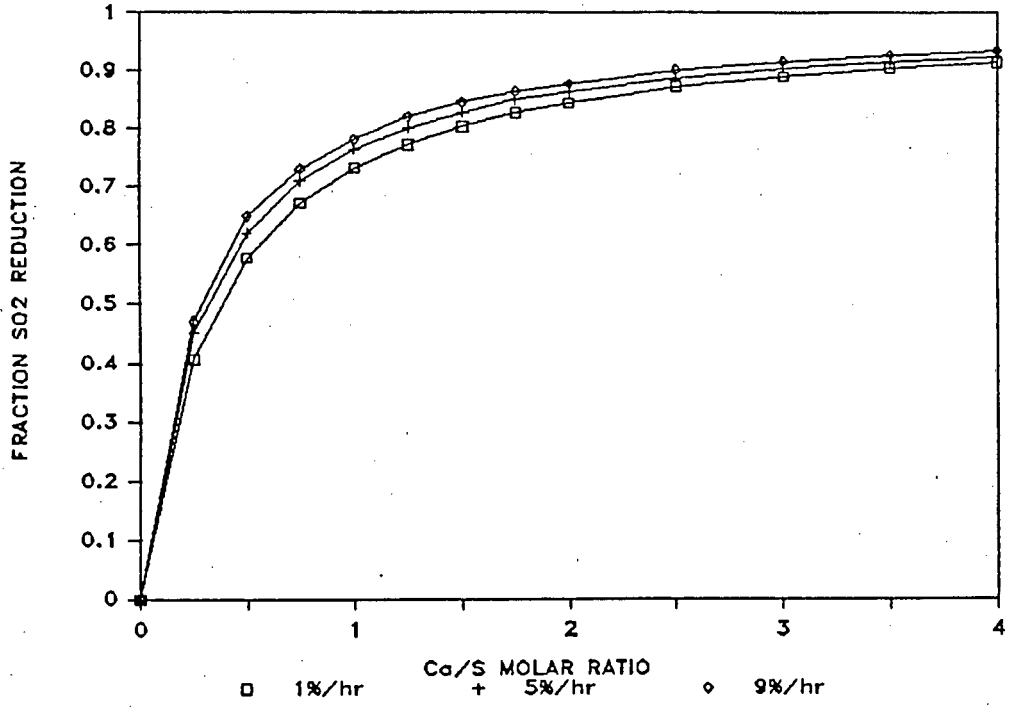

FIGURE 6.5 MODEL PREDICTION OF EFFECT OF ATTRITION RATE ON SO2 CAPTURE

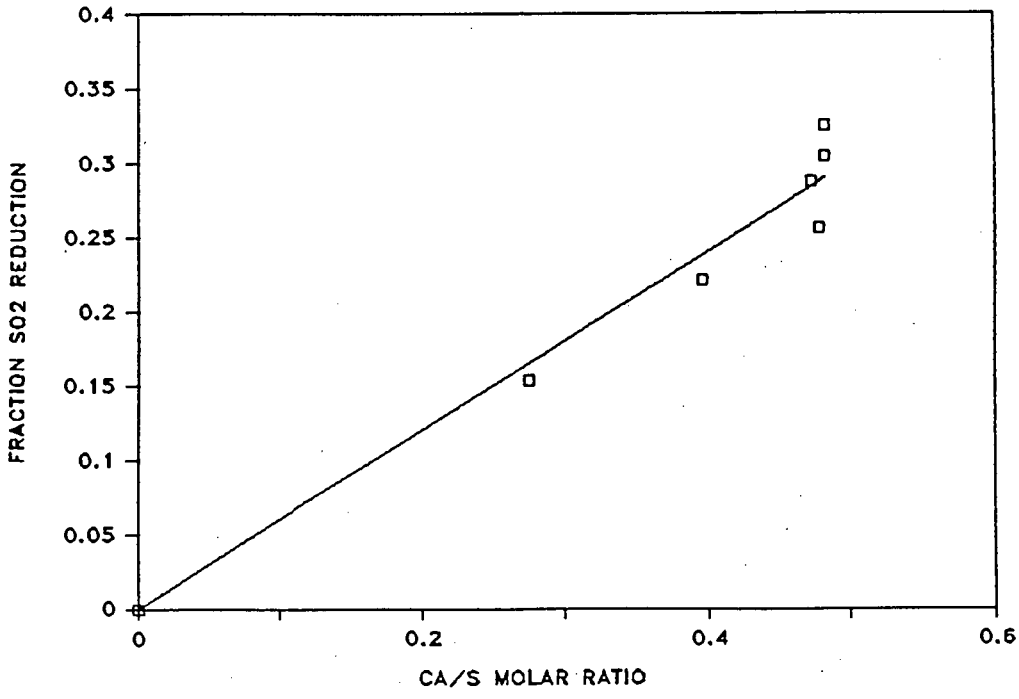

FIGURE 7.1 EFFECT OF CALCIUM IN COAL ASH ON SO2 CAPTURE

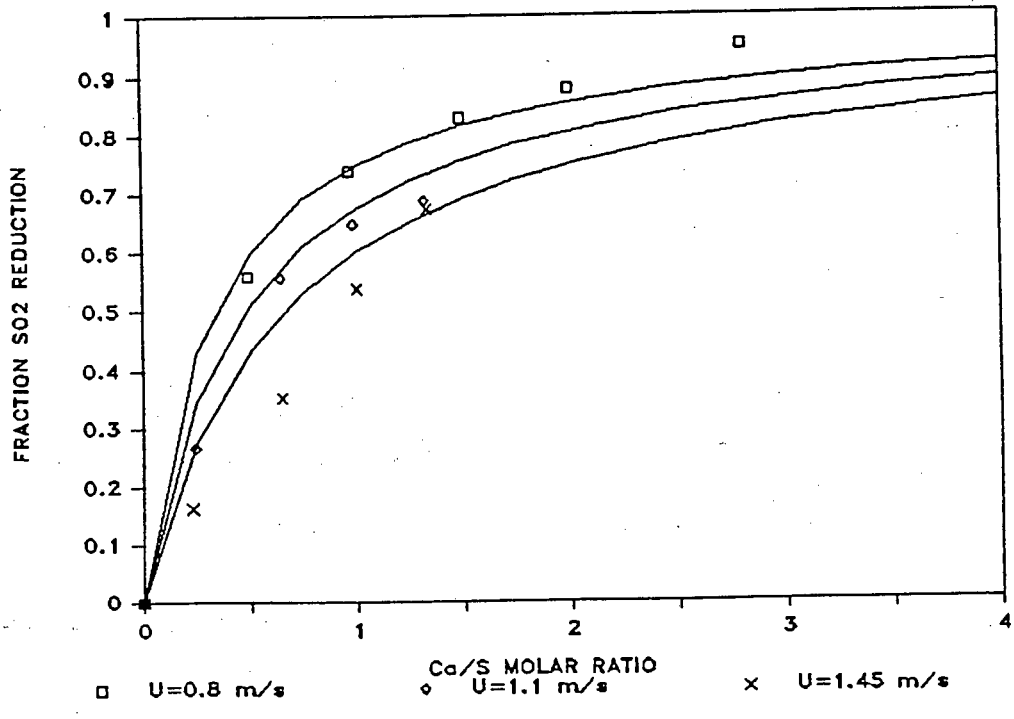

FIGURE 7.2 EFFECT OF FLUIDISING VELOCITY ON SO2 CAPTURE FOR BREDASDORP LIMESTONE

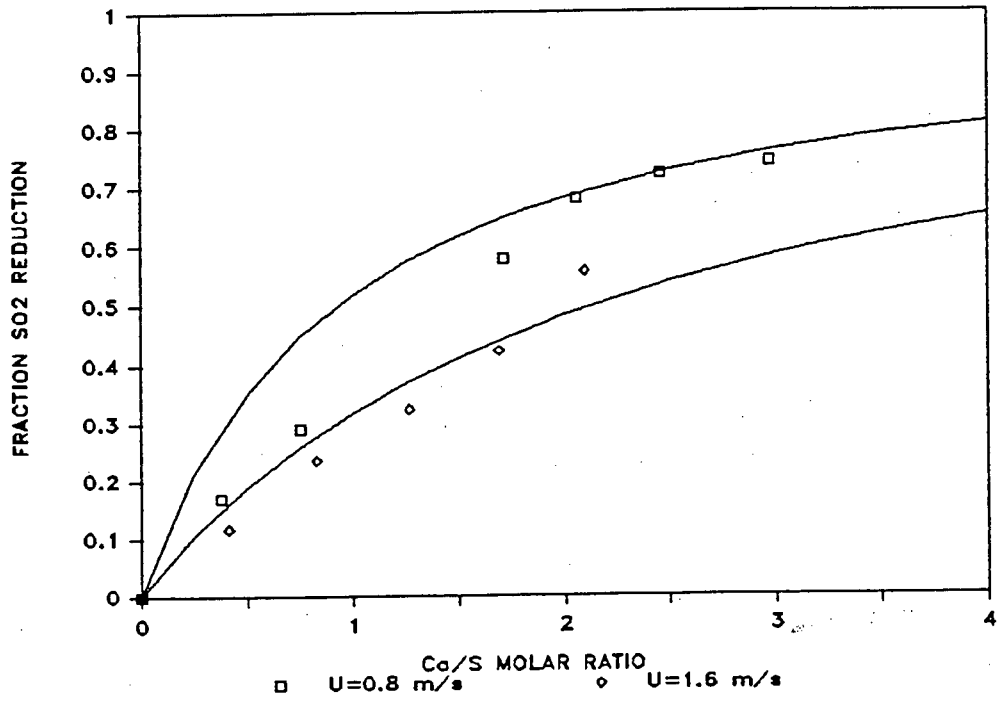

FIGURE 7.3 EFFECT OF FLUIDISING VELOCITY ON SO2 CAPTURE FOR UNION LIMESTONE

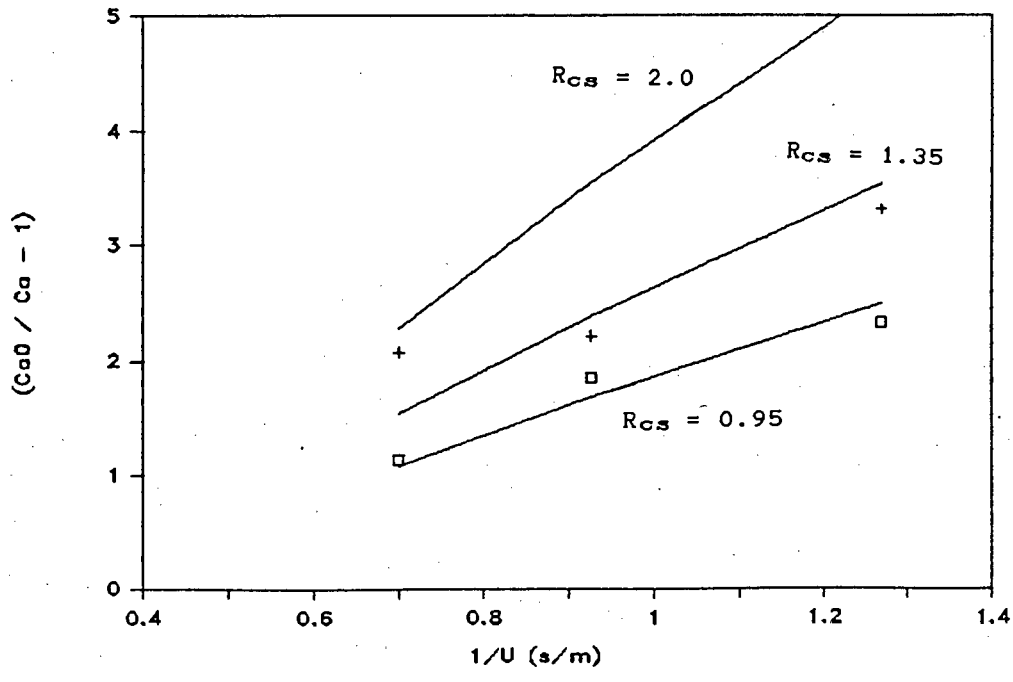

FIGURE 7.4 EXPLICIT MODEL DEPENDENCE ON FLUIDISING VELOCITY

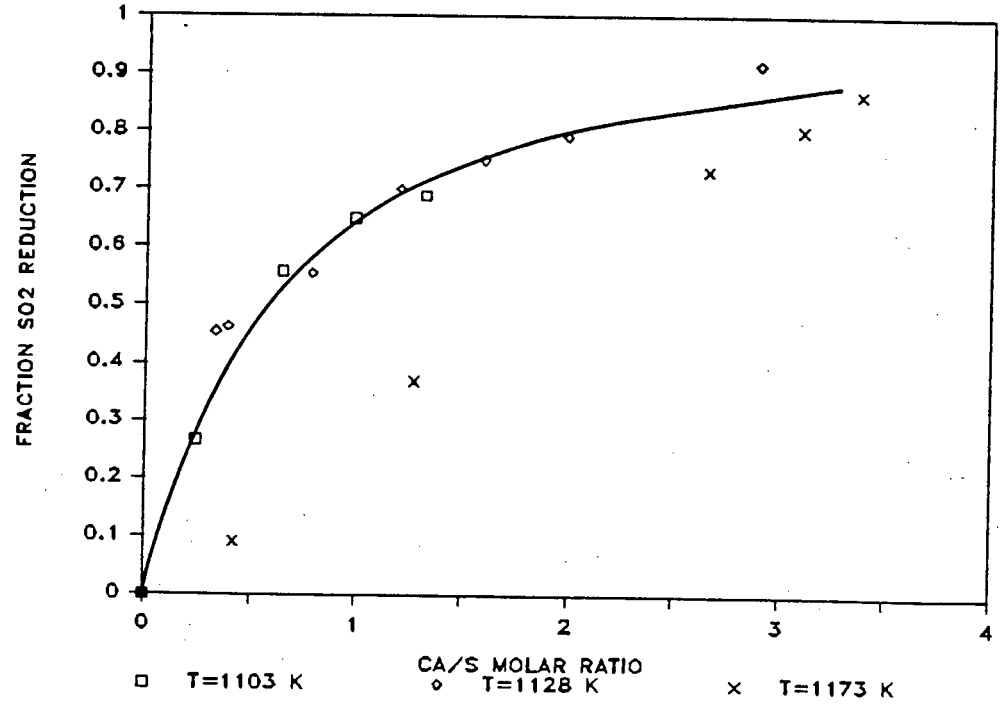

FIGURE 7.5 EFFECT OF COMBUSTOR TEMPERATURE ON SO2 CAPTURE FOR BREDASDORP LIMESTONE

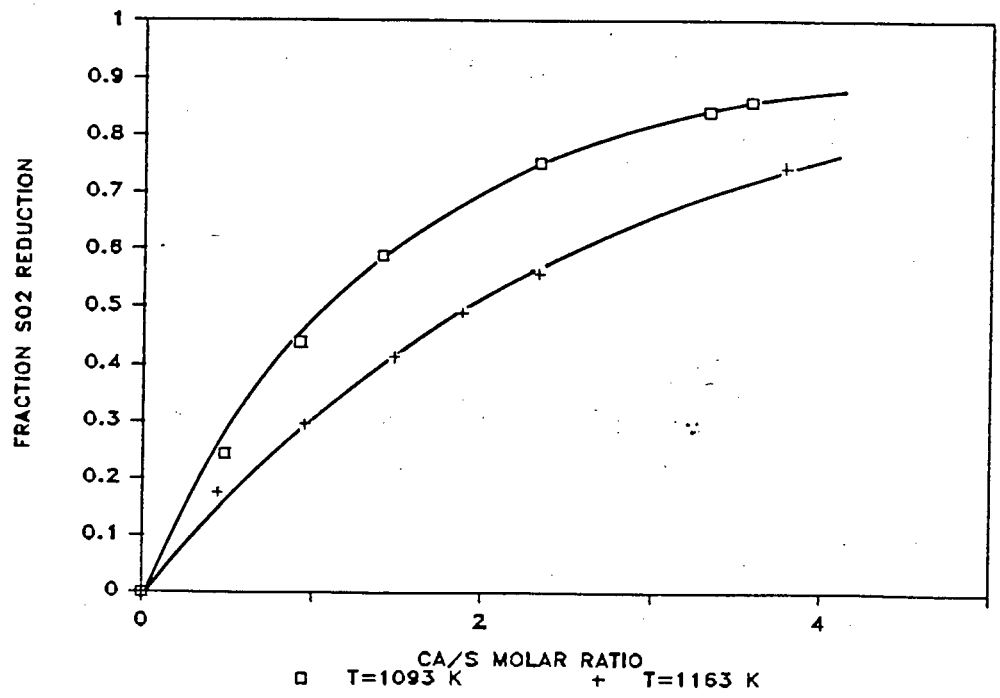

FIGURE 7.6 EFFECT OF COMBUSTOR TEMPERATURE ON SO2 CAPTURE FOR UNION LIMESTONE

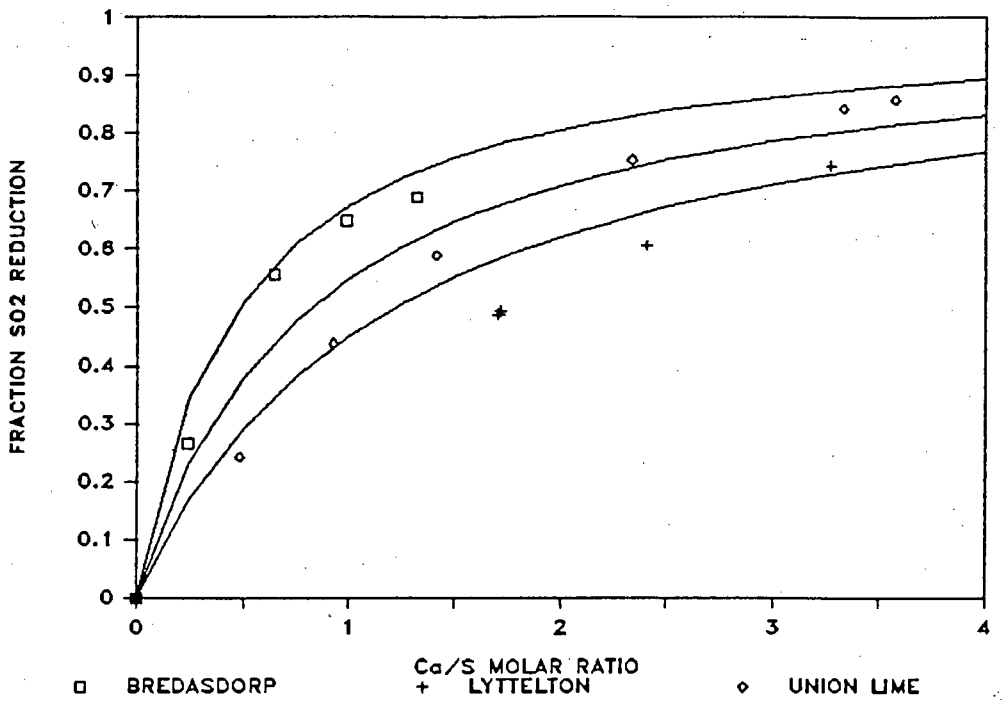

FIGURE 7.7 EFFECT OF SORBENT TYPE ON SO2 CAPTURE IN 10 MW FBC

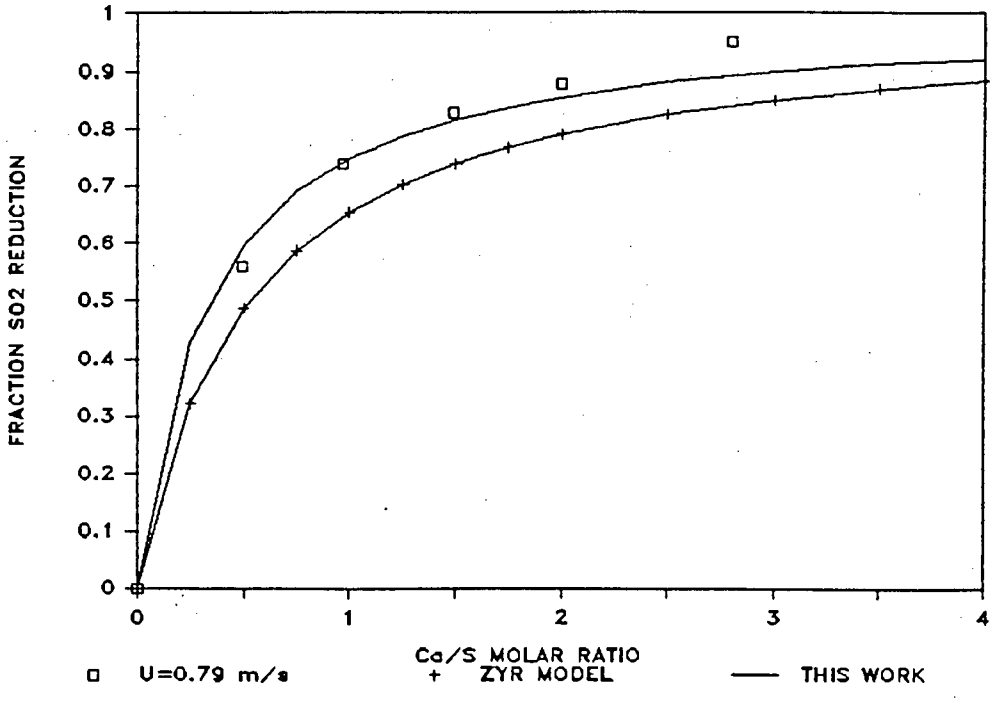

FIGURE 7.8 COMPARISON OF SIMPLIFIED MODEL OF ZHENG et al
WITH THIS WORK FOR BREDASDORP LIME (U=0.79 m/s)

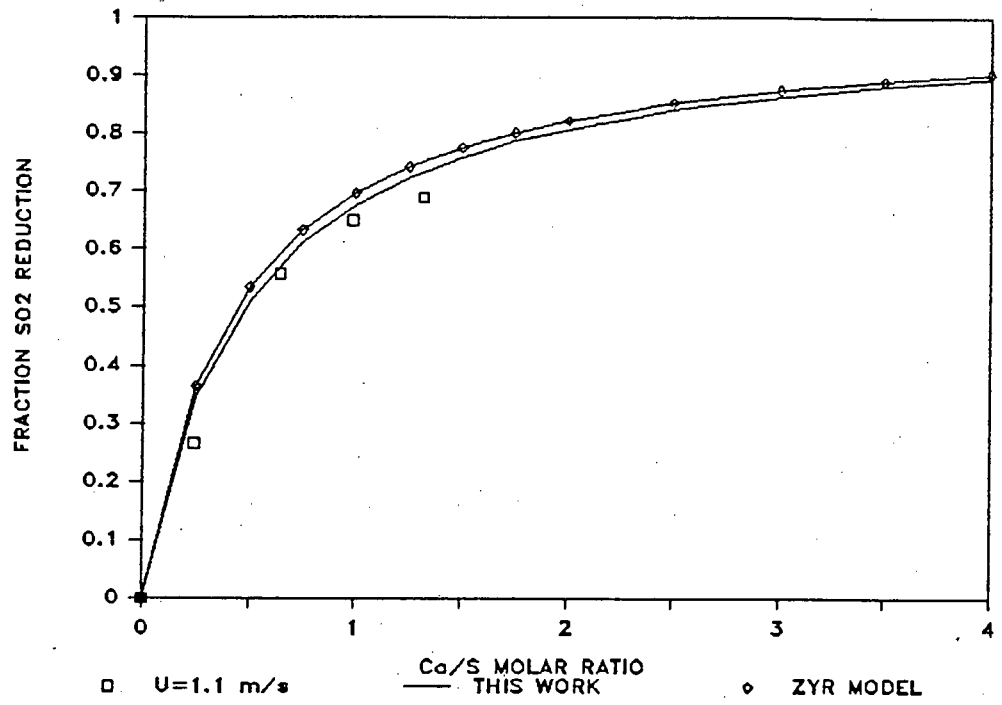

FIGURE 7.9 COMPARISON OF SIMPLIFIED MODEL OF ZHENG et al WITH THIS WORK FOR BREDASDORP LIME (U=1.1 m/s)

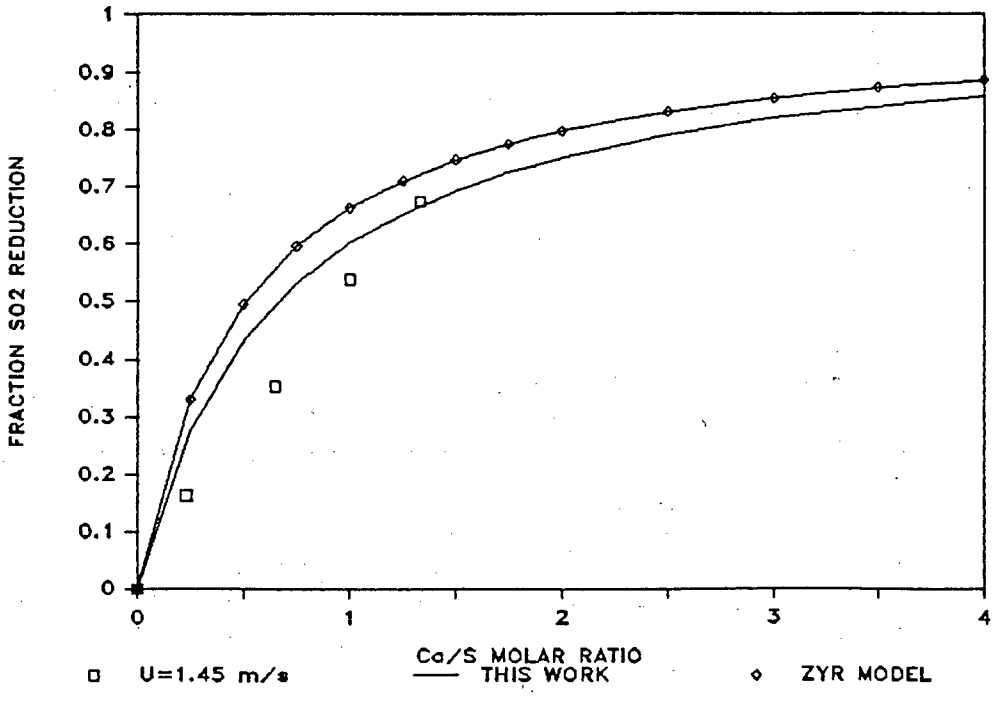

FIGURE 7.10 COMPARISON OF SIMPLIFIED MODEL OF ZHENG et al WITH THIS WORK FOR BREDASDORP LIME (U=1.45 m/s)

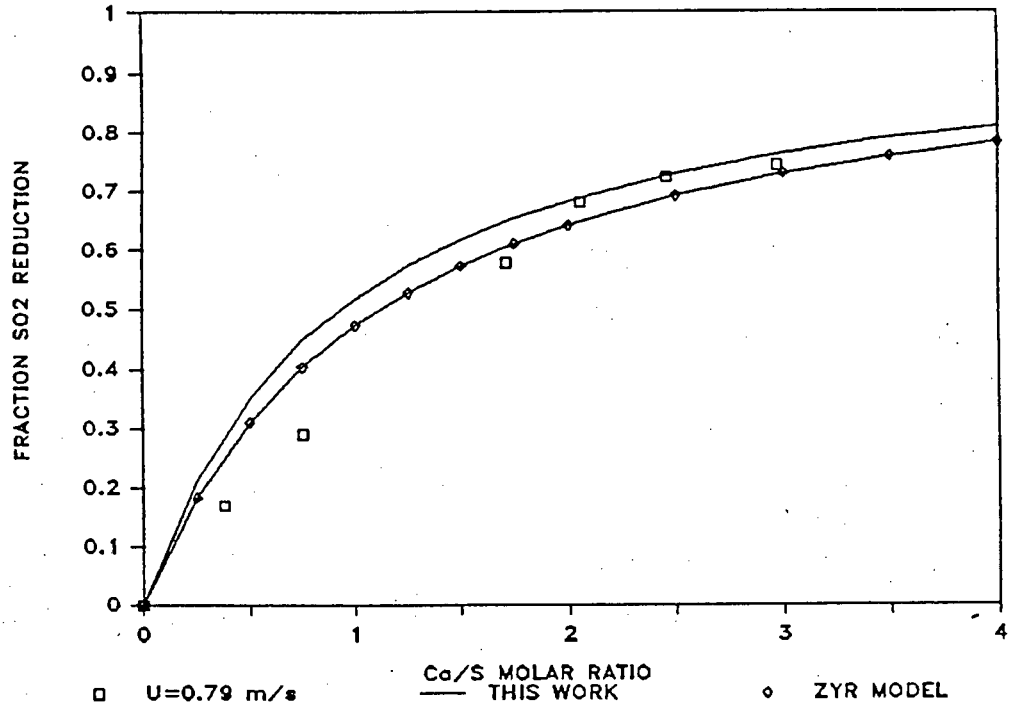

FIGURE 7.11 COMPARISON OF SIMPLIFIED MODEL OF ZHENG et al WITH THIS WORK FOR UNION LIME (U=0.79 m/s)

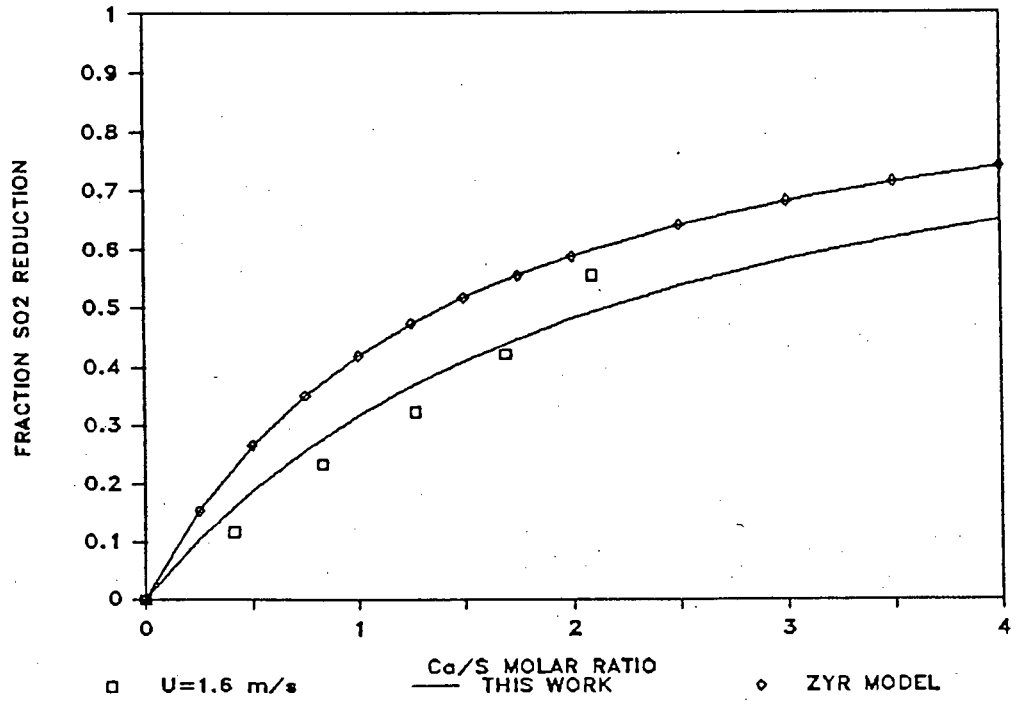

FIGURE 7.12 COMPARISON OF SIMPLIFIED MODEL OF ZHENG et al WITH THIS WORK FOR UNION LIME (U=1.6 m/s)

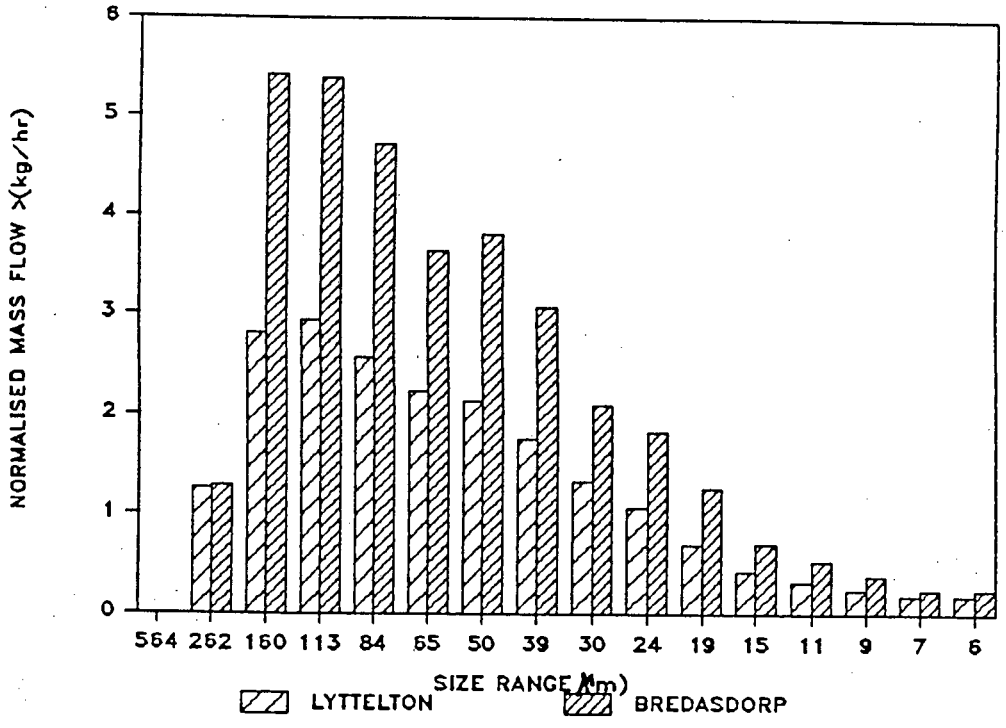

FIGURE 7.13 EFFECT OF SORBENT TYPE ON PRIMARY CYCLONE DUST LOADING

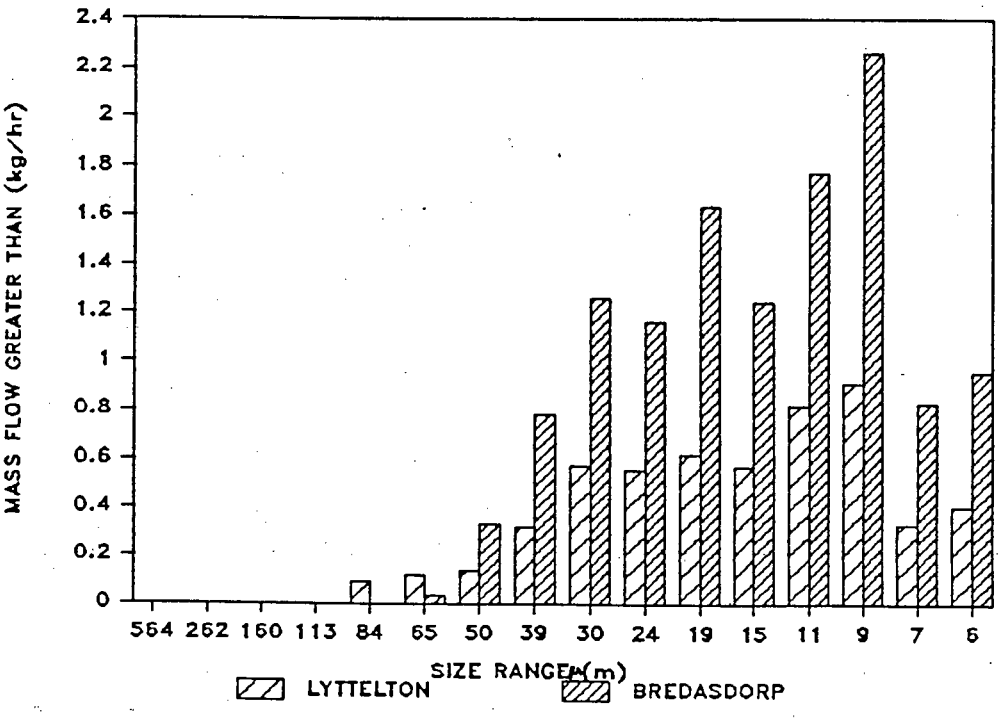

FIGURE 7.14 EFFECT OF SORBENT TYPE ON BAG FILTER DUST LOADING

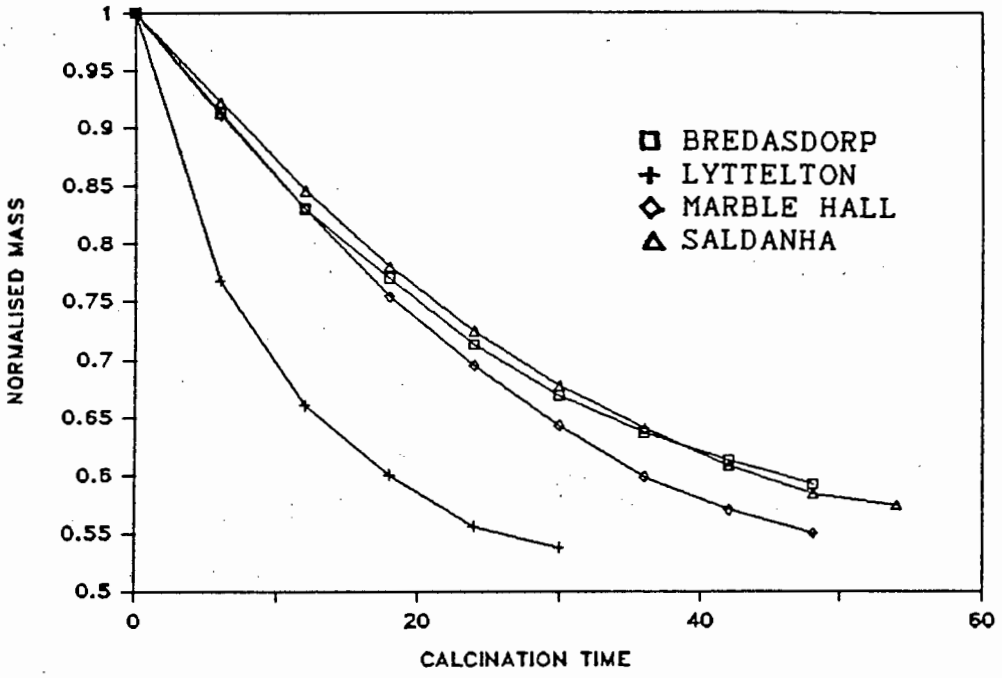

FIGURE A.1 EFFECT OF SORBENT TYPE ON CALCINATION TIME

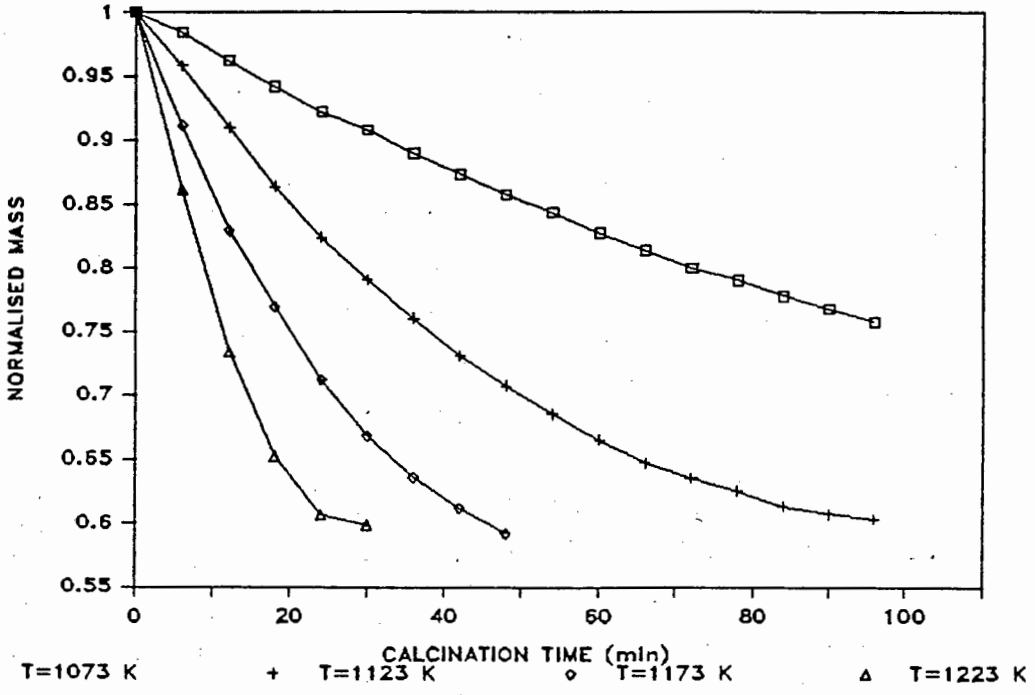

FIGURE A.2 EFFECT OF CALCINATION TEMPERATURE ON CALCINATION TIME

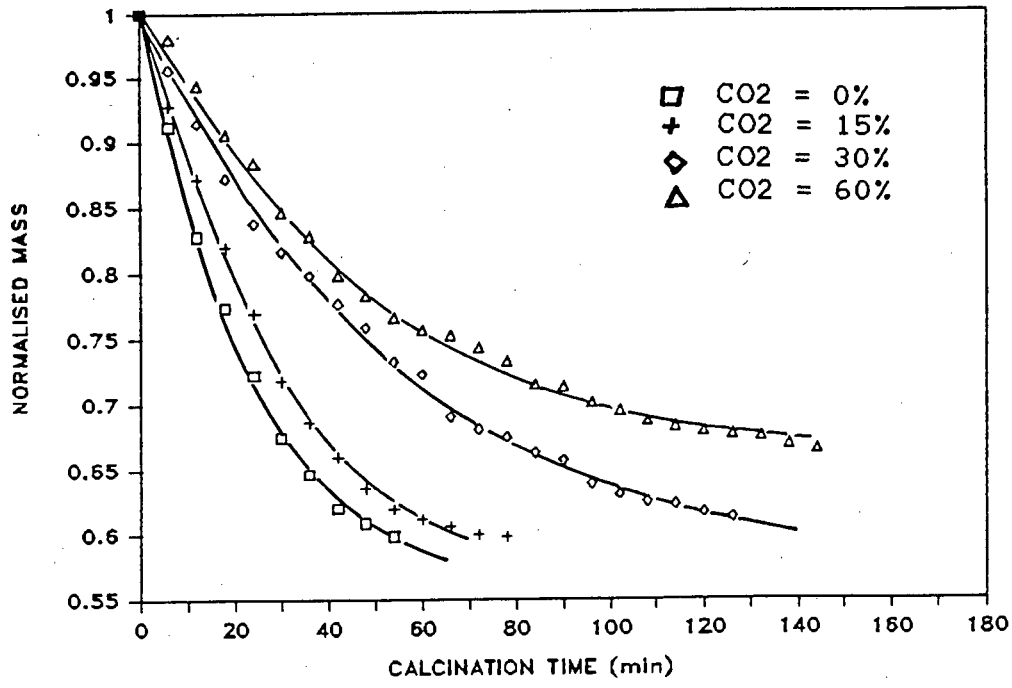

FIGURE A.3 EFFECT OF CO2 CONCENTRATION ON CALCINATION TIME

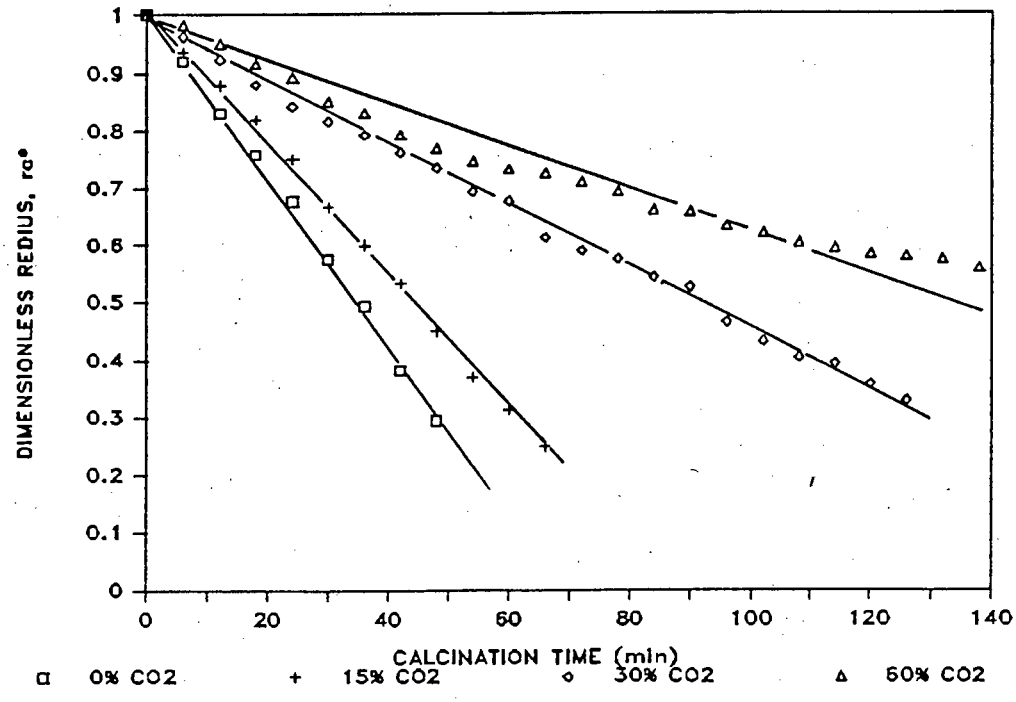

FIGURE A.4 VERIFICATION OF CALCINATION RATE CONTROL BY CHEMICAL REACTION

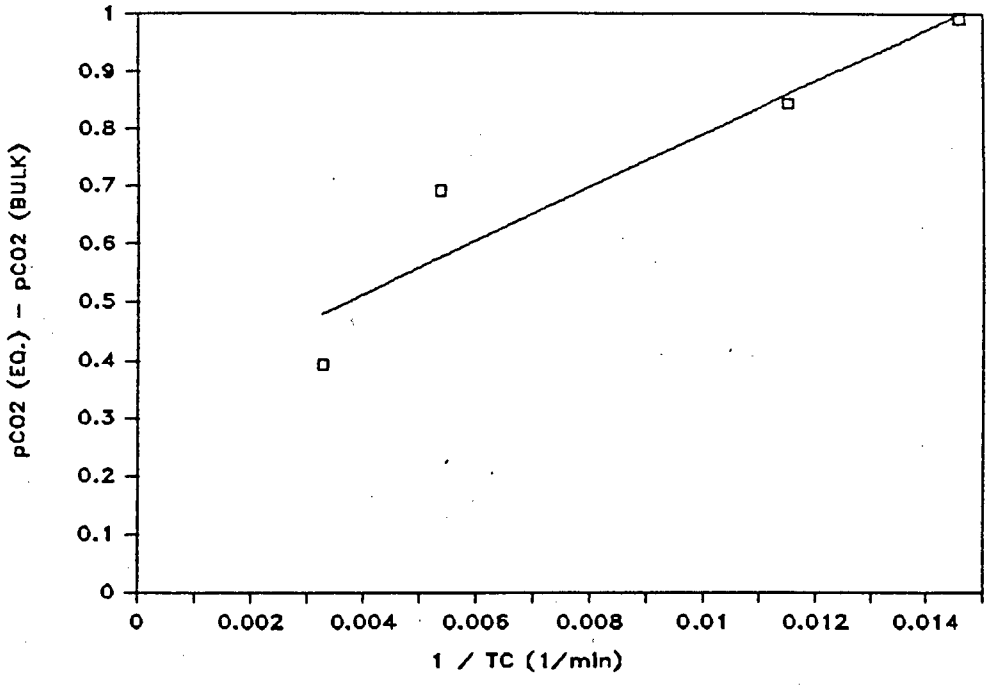

FIGURE A.5 RELATIONSHIP BETWEEN CO2 GRADIENT AND CALCINATION TIME

1. ROBERTSON
2. LICHTENBURG
3. IMMERPAN
4. BREDASDORP
5. SALDANHA
6. MARBLE HALL
7. HOLRIVIER
8. SLURRY
9. MOOREESBURG
10. OLIFANTSFONTEIN
11. LYTTELTON
12. LEO
13. LIME ACRES
14. GLEN DOUGLAS
15. VREDENDAAL
16. UMZIMKULU

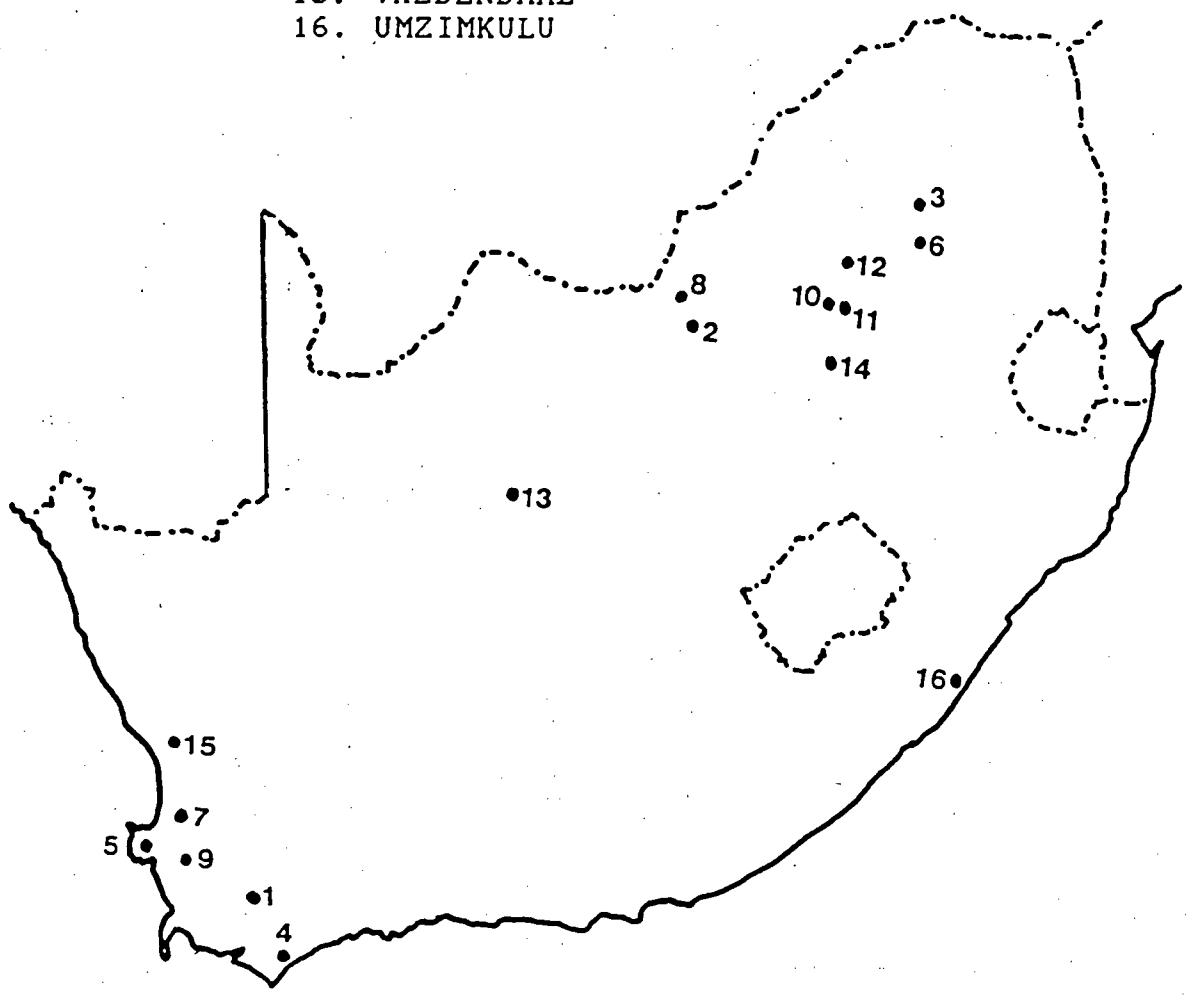

FIGURE C.1 SORBENT LOCATIONS WITHIN SOUTH AFRICA